Functional Luminescent Complex for Cost-Effective Analyte Sensing and Polymer Synthesis for Tunable White-Light Emission

THESIS

Submitted in partial fulfillment

of the requirements for the degree of

DOCTOR OF PHILOSOPHY

by

Raichure Pramod Chandrakant

ID. No. 2017PHXF0440P

Under the supervision of

Prof. Inamur R. Laskar

BITS Pilani

Pilani | Dubai | Goa | Hyderabad

DEPARTMENT OF CHEMISTRY

BIRLA INSTITUTE OF TECHNOLOGY AND SCIENCE

PILANI (RAJASTHAN) INDIA

2023

Birla Institute of Technology and Science Pilani – 333 031 Rajasthan, INDIA

Dr. Inamur Rahaman Laskar,
Ph.D., Department of Chemistry

Email: ir_laskar@pilani.bits-pilani.ac.in
inamur00@gmail.com
Phone: +91 1596-515675
Mob: +91 9602213001

CERTIFICATE

This is to certify that the thesis entitled **'Functional Luminescent Complex for Cost-Effective Analyte Sensing and Polymer Synthesis for Tunable White-Light Emission'** submitted by **Mr. Raichure Pramod Chandrakant** ID No **2017PHXF0440P** for the award of Ph. D. Degree of the Institute embodies the original work done by him under my supervision.

Signature in full of the Supervisor

Dr. Inamur R. Laskar
Designation: Professor

Date:

DEDICATED TO MY MOTHER AND LATE. FATHER WHO ALWAYS MAKE PROUD ON ME, AND MY BELOVED FAMILY MEMBERS

Acknowledgments

I would like to take this opportunity to express my appreciation and thanks to everyone who helped and supported me greatly throughout my Ph.D. studies. As a Ph.D. student, entered an entirely new material world and tried my best to contribute to the field of study. My thesis is a significant achievement in the last five years of work at BITS PILANI. The BITS Pilani campus has given me a scope to gain an incredible experience. I remember enrolling on January 18, 2018, and since then, I have benefited from special opportunities during the thesis work and used the institute's resources. I want to thank all of the people that assisted in my thesis. The thesis is also a result of the numerous discussions I had with the dozens of outstanding professors/Ph.D. students at BITS Pilani.

I start by thanking sincerely Professor Inamur Rahaman Laskar, my supervisor, for letting me work with his team at BITS Pilani. Since the beginning of my time working in the lab, he has guided and supported me. I always remember him saying, “There is nothing a true problem, every problem has its’ solution just think again and again, and the solution will be at your desk!”. These words motivated me to put in more effort. I was able to grasp more and maintain my optimism throughout my studies thanks to his continuous guidance and inspiration. Here, I had the opportunity to learn a lot of new things. His in-depth analysis of my technical writing has had a great effect on my thesis.

I am hugely thankful to the Vice-Chancellor, Directors, Deputy Directors, and Deans of Birla Institute of Technology and Science (BITS) Pilani for allowing me to pursue my doctoral studies by providing the required resources and financial support. My sincere gratitude to Prof. M. B. Srinivas (Dean, Academic-Graduate Studies and Research Division (AGSRD)), Prof. Jitendra Panwar (earlier Associate Dean, AGSRD), and Prof. Shamik Chakraborty (present Associate Dean, AGSRD) BITS Pilani, Pilani Campus. Prof. Saumi Ray and Prof Inamur Rahaman Laskar (earlier Convener, Departmental Research Committee (DRC)), and Prof. Madhushree Sarkar (present Convener, DRC), Department of Chemistry, BITS Pilani, Pilani Campus for their official support and encouragement. I owe my sincere thanks to Prof. Hemanth Jadav, (earlier, nucleus members of AGSRD), also thanks to Prof. Bharti Khungar, Prof. Saumi Ray, and Prof Ram Kinkar Roy (Ex-Head of the Department), Prof. Indresh Kumar (present, Head of the Department) and all other members of DRC, Department of Chemistry for their cooperation and constant support. I, overwhelmingly acknowledge the office staff of AGSRD, whose secretarial assistance helped me in submitting the various evaluation documents on time. I am grateful to the members of my Doctoral

Advisory Committee (DAC), Prof. Saumi Ray and Prof. Surojit Pande, for their excellent cooperation in refining my research proposal and doctoral thesis.

I am so grateful to all the respected teachers: Prof. S. C. Sivasubramanian, Prof. Ajay K. Sah, Prof. Paritosh Shukla, and all other teaching staff members of the Department of Chemistry, BITS Pilani, Pilani Campus for the support and guidance. I am thankful to Prof Inamur Rahaman Laskar, Prof. Mrinmoyee Basu, Prof. Surojit Pande, and Prof. Shamik Chakraborty for their kind support during the difficult phases of this journey. My extended heartfelt thanks to the office, Mr. Soni for their office work support and to all lab and office staff. My sincere thanks to Mr. Giridhar Kunkur (earlier Librarian) and Dr. Ranjan Sinha Thakur (present Librarian) BITS Pilani, and other library staff for their help in utilizing the library resources.

I am thankful to our research collaborators Dr. Pramod Soni and Mr. Tirupati C. Sharma from the Defence R&D Organization, Government of India, for providing the minute sample of nitroaromatic explosive compounds for sensing purposes under the collaborative research project (project no. ARMREB/CDSW/2019/216). I would like to say thanks to Prof Deepak Chitkara, Department of Pharmacy, BITS Pilani, for providing the GPC instrument facility. Also, thankful to Dr. Jagrity Chaudhary and Mr. Ajeet Singh for the computational calculation discussion and work. I am indebted to my senior Dr. Dinesh Kumar Sengottuvelu; his presence and experience made me learn new concepts in polymer research and how to see the problems. Also, extend my thanks to my seniors Dr. Saleem Pasha and Dr. Vishal Kachwal and from them, I learned most of the things related to research. I am very much thankful to my lab mates Mr. Ramprasad Bhatt, Mr. Bharat Kaushik, Mr. Sumit, Mr. Ajeet Singh, Ms. Annu, and Ms. Shilpa Palit for fruitful discussion over most of the concepts and for helping me in my thesis work. I would like to pay my special regards to my batch mates and colleagues Amol Pawar, Mahesha, Dhritbrata Pal, Bintu Kumar, and Santosh for their support in my Ph.D. study coursework and for cheering me up all the time during my journey. And also Prakash Taur, Yadav Nangare, Narsimha, Dhananjay Nipate, Narendra, Prakash Swami, and Vikki Shinde, for their generous assistance in many moments. I am also thankful to all my friends and all other persons whose names are not accommodated here.

I would not be here I am today or the scholar I am, without my great-parents. Sometimes I used to share my work and its applications for future vision with my father. Even though he does not understand completely, he was feeling too proud to tell other relatives about my progress after I joined my Ph.D. But unfortunately, my father is not present today to celebrate my achievement, and he left two years before. Yes, my father Late. Chandrakant

Acknowledgments

Raichure was a very kind person. Words cannot define the love and sacrifice of my mother Mrs. Jayashri Raichure, who still is giving me unconditional support. There was much eternal inspiration, endless patience, and moral support from my elder brother Mr. Prashant Raichure (Assit. Teacher) and he taught me to face any situation in life. Saying that my elder sister Pratibha is everything to me, would not be sufficient, because she nurtured me from my childhood and make me confident in the educational field. And my elder sister Priyanka also supported me in the successful completion of this work. I wish to express my deepest gratitude to all those remarkable individuals. They directly or indirectly helped me in the most memorable journey of my life.

I duly acknowledge valuable financial support in the form of a research fellowship, infrastructure, and financial support during my research work from BITS Pilani, Pilani campus.

Thanks to all.

Date: 09th April 2023

Place: Pilani, India Pramod C. Raichure

Table of Contents

Table of Contents

Table of Contents

Table of Contents

Abstract

The present thesis entitled "**Functional Luminescent Complex for Cost-Effective Analyte Sensing and Polymer Synthesis for Tunable White-Light Emission**" deals with the synthesis of new iridium(III) based metal complexes that exhibited 'Aggregation-induced emission (AIE)' property, structurally characterized and studied their luminescent properties. The synthesized complexes were used in different applications such as dichloromethane (DCM) vapor detection, and creatinine biomolecule detection. We have studied the photophysical properties of oligomeric probe which shows the distinct fluorescence response for multi-stimuli such as solvatochromism, nitro-aromatic TNT detection, acidochromism, and mechanofluorochromism. Furthermore, we developed a synthetic strategy to achieve a phosphorescent white light emission tuning in the form of polymeric materials. The present thesis is divided into six chapters.

The **first chapter** of the thesis describes a literature overview of the fundamental methods for analyte detection techniques by luminescent probes (i.e., volatile organic compounds, biomolecules, solvent polarity, nitro aromatic explosives, mechanical force, etc.) applications. Additionally, the chapter describes the history of AIE property and its probable mechanistic pathways. The background of conventional multi-component and cost-effective techniques for creatinine biomolecule detection has been described in this chapter. Also, the conventional techniques for obtaining the white light emission are discussed.

In the **chapter second**, the details of all the materials, instruments used, and methods utilized during the thesis work are described.

The **third chapter** describes the cyclometalated iridium(III) complexes that are used as molecular sensing probes. This chapter is divided into two parts. Part A describes the unexplored potential in the design of the AIE-active cyclometalated iridium(III) metal complex for selective and sensitive detection of hazardous volatile DCM solvent detection. That detects DCM vapor with a response time of <30 sec and the detection limit is 4.9 ppm with a pristine probe. Moreover, the DCM vapor detection was extended with a low-cost filter paper as the substrate. It was also tested with different solvents which are generally used in laboratories and industries. Part B describes a new cyclometalated oxalyl bridged dinuclear iridium(III) based phosphorescent complex for creatinine detection. Interestingly, the creatinine detection process was made easy with a low-cost filter paper stripe impregnated with a probe and it was tested successfully in the human urine sample. It was screened with most of the components present in human urine and found that it was highly selective for creatinine.

The **fourth chapter** describes electron D-A-based fluorogenic oligomer for multi-stimuli detection including solvatochromism, trinitrotoluene (TNT) nitro explosive detection, acidochromism, and mechanofluorochromism (MFC). The observed detection limit for TNT is femtomolar level (10^{-15} M) in its aqueous solution and 698 ppb in the vapor phase. The oligomeric active protonic sites make them highly sensitive to both Bronsted and Lewis acids in liquid and vapor phases. The observed bathochromic shift is upon exposure with trifluoroacetic acid (TFA) and boron trifluoride etherate by 108 and 94 nm in the liquid phase and 97 nm and 35 nm in the vapor phase, respectively. The oligomer also demonstrates MFC with large hypsochromic shifting (555 to 535 nm) and enhanced emission intensity. Interestingly, the same oligomeric probe exhibits distinct emissive indications in response to various stimuli, including quenching for TNT sensing, bathochromically shifted emission for acidochromism, hypsochromically shifted emission against MFC behavior and polarity-dependent emission for solvatochromism.

In the **fifth chapter**, it was developed a polymer that exhibited the non-luminescent monomeric unit transformed into intensely yellow emissive phosphorescent polymers upon polymerization which is termed polymerization-induced phosphorescent emission (PIPE). Polymer synthesis was performed with a simple free radical polymerization method where the homopolymer shows high photo efficiency with bright yellow emission. It strategically integrated a blue-emitting N-vinyl carbazole with the iridium(III) complex (that exhibited PIPE) and upon polymerization of this integrated monomeric unit produced a polymeric species that emits bright white light. With the varying composition of the monomeric species rationally, several species were developed to obtain the best white light in terms of color purity and quantum efficiency. The resulting white light emissive copolymer (CIE coordinate (0.25, 0.33)) showed a high quantum yield (33.7%) with a long excited-state lifetime (6.54 μs).

Keywords: Aggregation-induced emission, dichloromethane, creatinine, trinitrotoluene, low-cost detection, acidrochromism, mechanofluorochromism, polymerization-induced phosphorescent emission, white light, etc.

List of abbreviations and symbols

Abbreviation/Symbol	Description
Å	Angstrom
AI	Artificial intelligence
ACN	Acetonitrile
a	Onsager cavity radius
^{13}C	Carbon-13
Conc	Concentration
cm	Centimeter
CV	Cyclic voltammetry
^{0}C	Degree centigrade
c	velocity of light
δ	Delta
$CDCl_3$	Deuterated chloroform
d	Doublet
dd	Doublet of doublet
DCM	Dichloromethane
DMF	N,N-Dimethylformamide
DMSO-d_6	Deuterated dimethylsulfoxide
DFT	Density Functional Theory
dL	Deciliter
EI	Electron ionization
ESI	Electron spray ionization
EtOAc	Ethyl acetate
eV	Electron Volt
Equiv.	Equivalent
e.g.	exempli gratia
Ɛ	dielectric constant
ε	molar extinction coefficient
Δf	solvatochromic shift

List of abbreviations and symbols

f_w	Water fractions
FTIR	Fourier Transform Infrared Spectroscopy
FESEM	Field Emission Scanning Electron Microscopy
G	Gram
gm	Gram
h	Hours
HRMS	High-resolution mass spectra
IR	Infrared
Ir	Iridium
ILCT	Intra-ligand charge transfer
Hz	Hertz
J	Coupling constant
Kcal	Kilocalories
Kpa	Kilopascal
LED	light-emitting diodes
L	Liter
LLCT	Ligand -to- ligand charge transfer
LMCT	Ligand -to- metal charge transfer
λ	Wavelength
MS	Mass spectrometry
m	Multiplet
mg	Milligram
MHz	Mega hertz
MLCT	Metal -to- Ligand charge transfer
min	Minutes
mL	Milliliter
µM	Micro molar
M	Molar
mmhg	Millimetres of mercury
mmol	Millimole

List of abbreviations and symbols

M_w	weight average molecular weight
$\bar{\upsilon}$	Wave number
μ	dipole moment
N_2	Nitrogen gas
NMR	Nuclear magnetic resonance
nm	Nanometers
OLED	organic light-emitting diodes
PEG	Polyethylene glycol
PLED	Polymer light-emitting diodes
Pt	Platinum
PXRD	Powder X-ray Diffraction
^{31}P	Phosphorous-31
ϕ	Quantum efficiency
PIE	Polymerization-induced emission
PIPE	Polymerization-induced phosphorescent emission
ppm	Parts per million
ppb	parts per billion
PL	Photoluminescence
ppt	parts per trillion
%	Percentage
rt	Room temperature
η	refractive index
π	Pi
h	Planck's constant
σ	Standard deviation
QY	Quantum yield
TFA	Trifluoroacetic acid
Sec	Seconds
τ	Tau
θ	Diffraction angle

List of abbreviations and symbols

THF	Tetrahydrofuran
TLC	Thin layer chromatography
TPE	Tetraphenylethene
VOC	volatile organic compound
μL	Microliter
μM	Micromolar
μs	Microseconds
v	Volume
λ	Wavelength
W	Watt

List of tables

List of Schemes

List of Schemes

List of Figures

List of Figures

List of Figures

CHAPTER 1

INTRODUCTION

1.1 Luminescent materials

Light is emitted by luminescent materials in response to light exposure, temperature rise, or the application of an electrical current.[1] Light-sensitive materials come under the category of photoluminescent materials. They emit light at a different wavelength (generally visible light) after absorbing light at a particular wavelength, usually UV irradiation. A substance that exhibits luminescence properties is called a luminophore or luminogen. The terms 'fluorescence' and 'phosphorescence' refer to two different types of photoluminescence. When the light source is turned off, fluorescent light instantly stops emitting but phosphorescent light can last up to a few seconds. A fluorophore is a material that shows fluorescence properties. Most of the heavy metal-based organometallic complexes (such as iridium(III) and platinum(II)) emit light through phosphorescence, and the lifetime is in the micro- to millisecond range, but it can be extended even for hours.[2] Hence, it is gaining massive attention for various applications like optoelectronic, metal cation sensing, and explosive sensing,[3] as their long luminescence lifetimes (up to μs), high quantum yield, and large stokes shifts (hundreds of nm).[4-6] Solid-state luminescent materials show diverse applications such as solar cells, organic light-emitting diodes (OLED), metal ion sensing, bacterial imaging, stimuli-responsive materials, etc.[7-11] In addition, remarkable progress and exciting discoveries in luminescence-related research originate a new direction for future application through artificial intelligence (AI) techniques.[12]

1.2 Conventional fluorophores and their limitations

There have been numerous publications on the use of fluorescent probes for sensing various analytes, including anions, cations, pH, and organic solvents. Since fluorescence signals are stronger than those produced by other optical methods, it is particularly sensitive to the presence of analytes at low concentrations. Recently one example is napthalimides-based frameworks, which have been widely used in the design and synthesis of luminous probes (**1**) among the organic fluorophores developed for fluorescent-based approaches (Fig. 1.1).[13, 14]

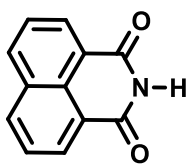

1

Figure 1.1 Molecular structure of the multi-analyte probe (**1**).

Luminophores are typically utilized in thin films or aggregated forms in applications like organic light-emitting diodes (OLEDs), organic field-effect transistors (OFETs), and so on.[15] Also, the luminescent molecule is used in aqueous medium or physiological conditions for biological applications. With increasing concentration, the emission is quenched in many conventional luminophores; this phenomenon is known as "Aggregation-Caused Quenching" (ACQ). The use of fluorophores in aggregated or solid states was restricted for many years due to the dominance of ACQ.[16]

1.3 Aggregation-caused Quenching

When most of the luminophores exhibit an emission quenching effect, either completely or partially, in their aggregated state or solid state leads to an "Aggregation-caused Quenching (ACQ)" effect. As a result, ACQ has drawbacks when used in real-time applications. Most commonly, organic-based conventional luminophores with strong emissivity in diluted solutions, such as perylene (**2**), pyrene (**3**), naphthalene (**4**), fluorescein (**5**), etc. (Fig. 1.2), have been extensively studied in a variety of fields, including light-emitting devices, chemical sensing, and particularly for bio-imaging.[17] However, ordinary fluorophores (e.g., perylene) often have planar aromatic cores, which favor the occurrence of π–π stacking interactions when they come closer or aggregated. As a result, their emission is decreased or quenched in the concentrated or aggregated state.[18]

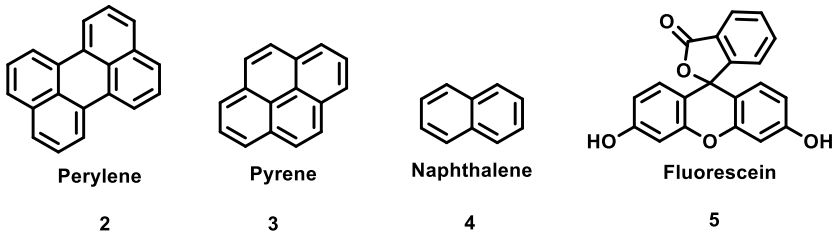

Figure 1.2 Molecular structures for common conventional ACQ fluorophores (**2**-**5**).

To reverse the ACQ, Tang et al. proposed the concept of "Aggregation-induced Emission (AIE)" in 2001.[19] This concept was based on the fact that luminophores with freely rotating groups were substantially emissive in the aggregated state but non-emissive in a dilute solution.

1.4 Aggregation-induced Emission

Aggregation-induced Emission (AIE) is a fascinating photophysical phenomenon in which non-emissive molecules in solutions are made to emit strongly in the aggregated or solid state. AIEgens are luminogens that have the AIE property. When the AIEgens emit stronger in the

aggregated state as compared to their solution state, it is termed as 'Aggregation-induced Enhanced Emission' (AIEE), in marked contrast to ACQ molecules. Generations of new AIE active compounds have been developed over the past ten years. 1-Methyl-1,2,3,4,5-pentaphenyl-1H-silole (**6**), 1,1,2,3,4,5-hexaphenyl-1H-silole (HPS) (**7**), 1,1,2,2-tetraphenylethene (TPE) (**8**), 9-(diphenylmethylene)-9H-fluorene (**9**), and monocyclometalated iridium metal complex (**10**) are indeed utilized as core and prospective AIE property compounds (Fig. 1.3).[20-22]

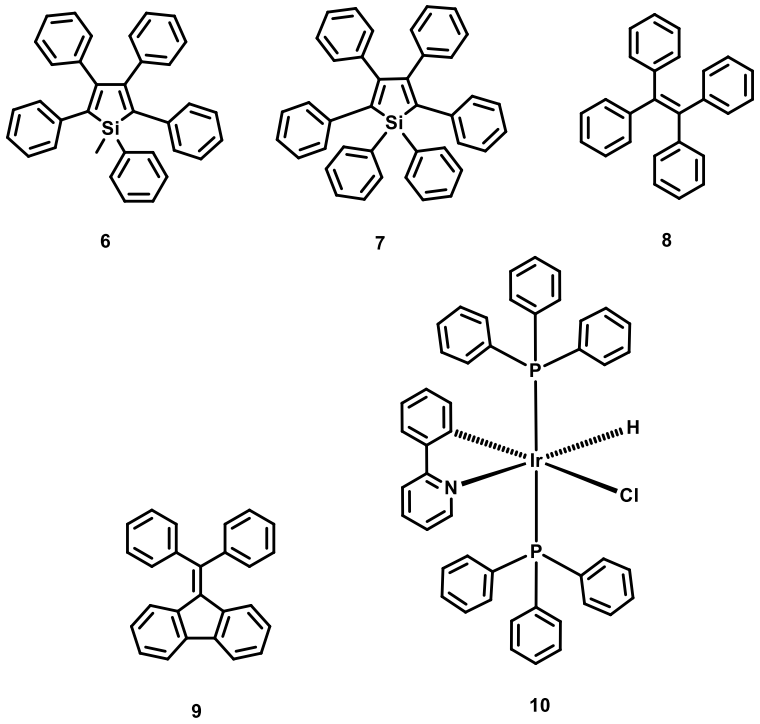

6 7 8 9 10

Figure 1.3 Common AIE fluorophores: 1-Methyl-1,2,3,4,5-pentaphenyl-1H-silole (**6**), 1,1,2,3,4,5-hexaphenyl-1H-silole (HPS) (**7**), 1,1,2,2-tetraphenylethene (TPE) (**8**), 9-(diphenylmethylene)-9H-fluorene (**9**), and monocyclometalated iridium metal complex (**10**).

The mechanism involving the emission in the aggregated state must be understood to develop new AIE molecules. The restriction of intramolecular motion (RIM), which includes the rotation and vibration motion of the molecules, i.e., restriction of intramolecular rotation (RIR) and restriction of intramolecular vibration (RIV) in the aggregated state, is the most widely reported cause in terms of mechanistic studies (Fig. 1.4). If we use the AIE molecule TPE as an example, all four of the phenyl peripheries rotate rapidly in the diluted solution. In a diluted solution, the excitation energy dissipates during the rotation of the ring, which helps to increase the non-radiative decay.[23, 24] However, the rotation of the phenyl rings is restricted in the aggregated state, because of a physical constraint. The non-radiative pathway is blocked by

restricting rotation, allowing the excitons to decay radiatively. In the case of polymeric materials, non-luminescent monomers are frequently used to synthesize polymers. The aggregation of monomeric repeating units is facilitated by polymerization which results in the emission of polymer, and the AIE analysis may assist in studying that. When a non-luminescent monomeric unit is polymerized, it becomes an intensely emissive polymer, known as polymerization-induced emission (PIE). PIE phenomenon homologues to the AIE. A crystallizing aromatic AIEgens is a physical manner to induce emission, while polymerization is a chemical route for generating emissive materials from non-emissive PIEgens.[25] In the PIE mechanism, the chain formations lead to chain entanglement, thus intrachain or interchain interactions have resulted. These interactions lead to conformational rigidity causing more emission via radiative decay.[26]

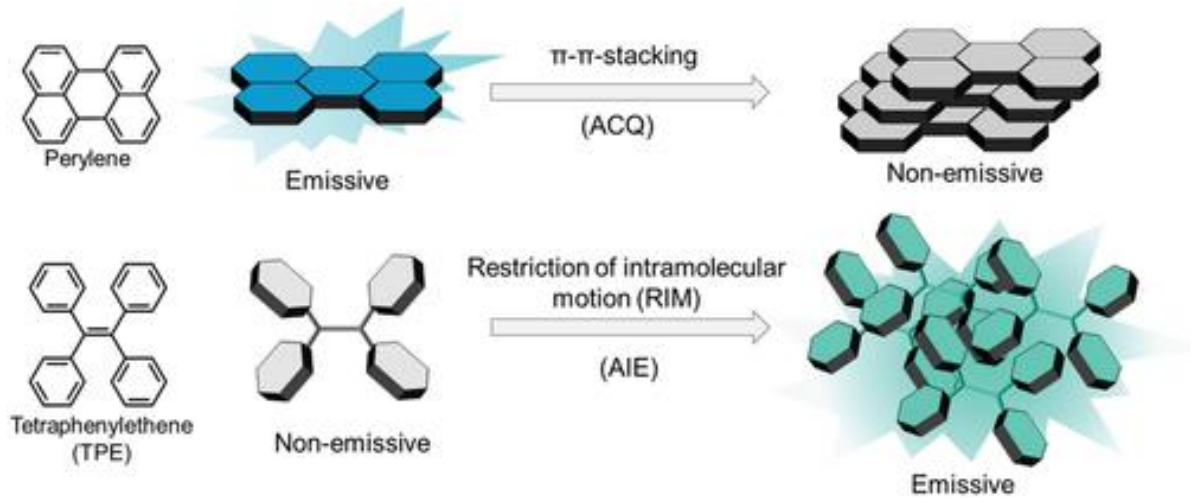

Figure 1.4 Schematic representation of the 'aggregation-caused quenching' (ACQ) mechanism of perylene and the 'aggregation-induced emission' (AIE) phenomena of tetraphenylethene (TPE). Reprinted under the terms and conditions of the Creative Commons Attribution license.[27] Copyright 2021 Wiley-VCH.

1.5 Luminescent-based response for multiple analytes/stimuli

Analytes are chemical substances or subjects of interest whose presence is being detected or measured. The present thesis deals with the luminescent-based probes that respond to various analytes, such as the detection of volatile organic compounds (VOC), creatinine, explosive material, and acid (i.e., acidochromism). It could also be responsive to solvent polarity (i.e., solvatochromism) and mechanical force (i.e., mechanofluorochromism). Additionally, it

demonstrates the beauty of white light emission tuned through the polymerization of distinct emissive monomers.

1.5.1 Volatile organic compound (VOC) detection

Although, numerous gases and volatile organic compounds (VOCs) brought on by human activity and geological hazards have changed the composition of the air over time. VOCs include a variety of substances such as chlorinated hydrocarbons (dichloromethane (DCM), chloroform, etc.), alcohols (methanol, butanol, ethanol, etc.), aldehydes (formaldehyde, acetaldehyde, etc.), ketones (acetone and butanone), N,N-dimethylformamide, aliphatic hydrocarbons (ethylene, acetylene, and ethane), and aromatic hydrocarbons (benzene, toluene, xylene, etc.), and others. The presence of VOCs in indoor and outdoor air is caused by emissions from pesticides, detergents, cosmetics, building materials, chemical processing industries, etc. Organic solvents are widely used in laboratories and industry, and there are still risks to human health from solvent exposure.[28] Metal degreasing, manufacturing paint, painting, and dry cleaning are just a few examples of operations that could be exposed to hazardous solvents.[29] Such volatile solvents are typically exposed via the skin or respiratory tract, which can have a drastic impact on health.[29] Low-level, long-term, or combined chemical exposure may result in liver damage that is challenging to detect, and harmful effects have been observed in the nervous system, renal system, skin, cardiovascular system, and health developmental.[30, 31] The ecosystem and the global climate have been significantly affected by the excessive industrial exhaust fumes, which include greenhouse gases, industrial toxic gases (such as NH_3, CO, SO_2, CS_2, H_2S, etc.), and VOCs.[32] Protection of the environment and human health depend on the development of effective sensor materials with excellent performance for selective, rapid, and sensitive detection of hazardous gases including VOCs. However, the detection of VOCs relies on costly stationary systems such as UV and IR spectrometers, gas chromatographs, and mass spectrometers, as well as common techniques like photoionization detector (PID), flame ionization detector (FID), and others.[33, 34] But fluorescence-based MOF materials are also extensively studied for VOC detection.[35, 36]

Among the above VOCs, chlorinated hydrocarbons are widely employed in many sectors as an essential organic solvent and product intermediate; however, they are frequently mutagenic, carcinogenic, and teratogenic chemicals. The chlorinated hydrocarbons are absorbed through the skin, invading the nervous system or the internal organs, causing poisonous the body. For the first time, an interesting luminescent sensor was developed for chlorinated hydrocarbons that had a guest-lock-induced light-up mechanism. Lang et al.

synthesized a metal-organic framework (MOF) from $[Cu_4I_4(Py_3P)_2]_n$ in which a Cu_4I_4 cluster serves as the node and tris(2-pyridyl) phosphine serves as the linker.[37] The MOF has large channels that trap the guest molecules, then it shows the luminous properties of copper iodide MOF compounds (Fig. 1.5).

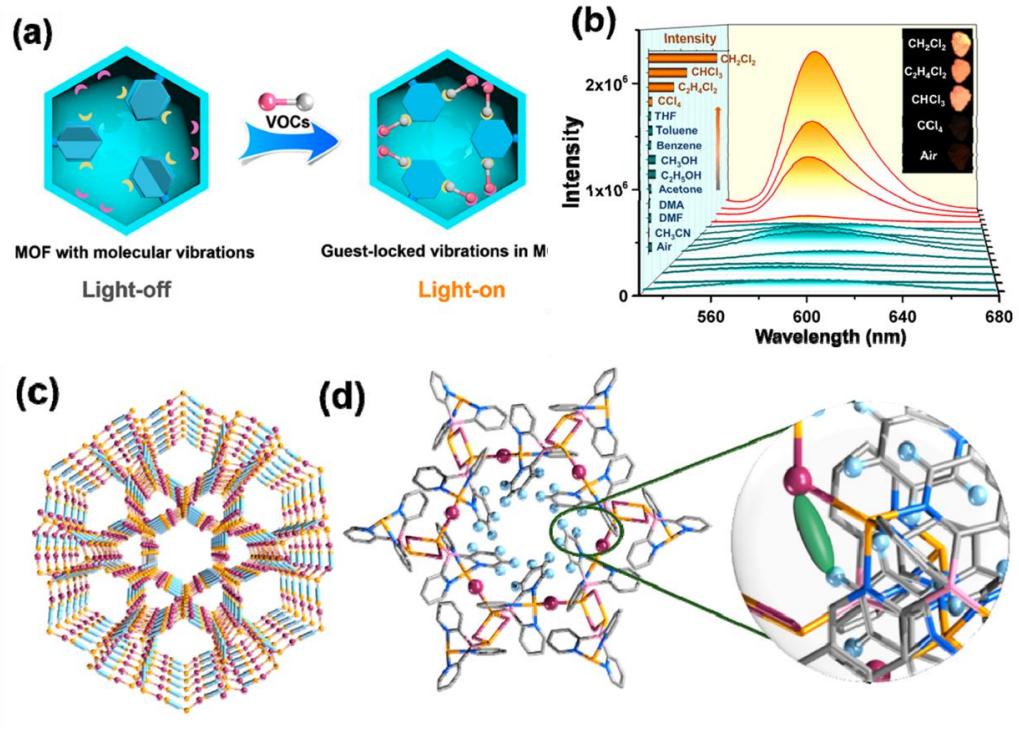

Figure 1.5 (a) Model of Light-Up Luminescent Detection by a Guest-Lock Process. (b) Emission spectra of $[Cu_4I_4(Py_3P)_2]_n$ after incubation for 30 min in various solvent vapors. Inset: The emission intensity of $[Cu_4I_4(Py_3P)_2]_n$ after exposure to various solvent vapors and air at 580 nm and the photographs of $[Cu_4I_4(Py_3P)_2]_n$ after incubation for 30 min with chloroalkane vapors under UV light irradiation. (c) View of the open channels available for guest molecules along the c-axis. (d) Potential binding sites in the open channel. Color code: orange, Cu; purple, I; dark blue, N; pink, P; gray, C; light blue, H. Reprinted from Ref.[37] Copyright 2020, American Chemical Society.

Interestingly, the luminescence was enhanced by chloroalkane molecules (such as DCM or chloroform), and the MOF's luminescence significantly increased following the vapor treatment. The mechanistic study found that the strong hydrogen bonding interactions between the host and guest molecules increased the binding of guests to the framework. In accordance with additional theoretical calculations, it is observed that the vibrations of the organic ligand will be locked by the guest molecules, resulting in a reduction in nonradiative decay and an increase in luminescence. Although the materials were recyclable and had a rapid

response (less than 1 sec), they weren't DCM-selective. Also, it detects chloroform, carbon tetrachloride, $C_2H_4Cl_2$, and PhCl, at the same emissions wavelength (580 nm). Liu et al. reported a sensitive nanoporous fluorescence sensor based on core-shell upconversion nanoparticles (UCNPs) for the detection of dichloromethane.[38] To make a thin film with intense background-free fluorescence and optical sensitive, UCNPs with active shells were deposited on porous anodic alumina oxide (AAO) templates supported by glass slides. An AAO template is used as a porous substrate for UCNPs to improve the absorption capacity for the molecules under test. However, the UCNPs have good optical sensitivity for DCM detection in the vapor phase, but it need a particular kind of substrate (i.e., AAO supported by glass) to analyze DCM detection. Liu et al. studied the methylacryloyl tetraphenylethylene oligomer (**11**) for DCM detection in the vapor phase (Fig 1.6).[39] Here, the oligomer's solution spots on the thin layer chromatography plates, exhibit switched 'off' and 'on' fluorescence continuously and reversibly upon DCM vapor exposure. The oligomer is not selective, despite being more sensitive to VOCs (DCM, acetone, and tetrahydrofuran).

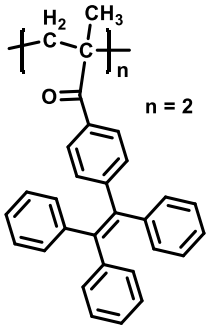

11

Figure 1.6 Molecular structure for oligomer (**11**).

1.5.2 Creatinine detection

The detection of different biomolecules (such as proteins, cholesterol, amino acids, glucose, DNA, uric acid, bovine serum albumin (BSA), human serum albumin (HSA), and creatinine, etc.) and microorganisms has led to the major aspect of disease diagnosis or to recognize the diseases through deficiency /excess of certain biomolecules.[40] Creatinine and BSA are two kidney disease biomarkers that are used in the diagnosis to know the various stages of kidney diseases.[41] Worldwide, 8-16% of people an affected by chronic kidney disease (CKD).[42] Millions of people die each year as a result of the lack of inexpensive treatment options for CKD disease. Since there are no symptoms or signs in the early stages of CKD disease, the

majority of those affected remain unrecognized. With early-stage diagnosis and treatment, CKD is treatable, and kidney disease development can be slowed or stopped. The key sign of kidney health is the amount of creatinine found in the blood and urine, which are the body's waste products.[43] Creatinine levels in urine or blood are higher when kidney function is reduced. As a result, creatinine amount tests on the blood and urine are utilized to monitor the progression of kidney disease. Creatinine is a by-product of the breakdown of creatine in muscle metabolism. It enters the bloodstream to the kidneys where it is filtered by glomerular filtration before being eliminated in the urine. The concentration of creatinine in the serum and urine of normal adults is 45-110 μmol L^{-1} and 5.3-17.7 mmol when both samples were taken within 24 hours, respectively.[44] The creatinine concentration will increase once the kidney filtration function is reduced. Typically, biomolecules including proteins or creatinine can be detected by mass spectrometry, immunoassays, or electrophoresis.[45] Although these approaches have the benefits of good sensitivity and high accuracy, they frequently require sophisticated instruments, and the process can be time-consuming and expensive. The fluorescence-based optical devices have numerous advantages, including biocompatibility, smaller size, lighter weight, flexibility, lower cost, online monitoring, small volume detection, and remote sensing capability.[46-48]

The most popular method for determining creatinine levels in blood and urine right now in clinical laboratories is the colorimetric Jaffe assay.[49] A reddish-orange complex with a maximum absorbance at about 520 nm is formed in a Jaffe reaction between the reactive methylene group of creatinine and sodium picrate in an alkaline medium. This color shift is correlated with the creatinine concentration and can be used to detect creatinine.[50] Although the assay is simple, it is not highly sensitive and selective.[51] A solution-based AIE-active probe for creatinine detection was reported by Tang and co-workers in 2017.[52] The TPE core of this probe was modified with iminodiacetic acid (as seen in Fig. 1.7). The presence of several H-bonding active sites facilitates hydrogen bond interactions between the carboxyl acid groups of the probe (**12**) and the amine groups of creatinine. As a result, the formation of aggregation of probe (**12**) leads to restricted rotation of phenyl rings causing emission enhancement (i.e., RIM mechanism). Thus, probe (**12**) shows the emission enhancement for creatinine sensing. The probe (**13**) was studied for human serum albumin (HSA). However, they studied Crt9 detection with artificial urine (i.e., prepared composition from contents present in human urine). However, this organic tetraphenylethene probe shows fluorescence in both probe solutions in water and artificial urine in the absence of Crt9. It increases the emission intensity

up to 1 mM of Crt9 and then decreases for further increasing concentration, which makes it difficult to monitor the sensing response in real urine samples.

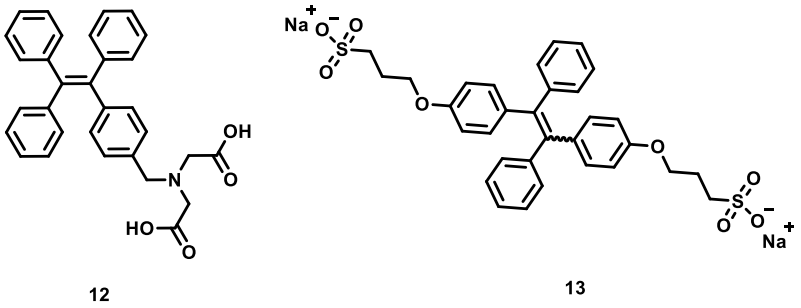

12 13

Figure 1.7 Molecular structures of AIE luminogens (**12**) and (**13**).

Chattopadhyay et al. presented a different approach that made use of a fluorescent light-up probe composed of Pd^{2+}-naphthalimide.[53] The probe (**14**) consists of a naphthalimide moiety which acts as the fluorescent ligand, and an ethylenediamine moiety complexing with Pd^{2+} (Fig. 1.8). Due to the combination of the photoinduced electron transfer (PET) from the naphthalimide fluorophore to the Pd^{2+} unit, and the heavy atom (Pd^{2+}) quenching effect, this probe shows very weak fluorescence. But when probe (**14**) is treated with creatinine, Pd^{2+} combines with creatinine because it has a higher affinity for the Pd^{2+} ion, and free naphthalimide is released to activate the fluorescence. Here the probe responds only after being treated with creatinine in reaction buffer with pH 7.2 at 37 °C.

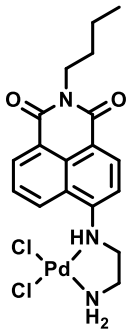

14

Figure 1.8 Molecular structure of fluorogen (**14**).

For the detection of creatinine, several Molecularly imprinted polymer (MIP)-capped nanocomposites were reported.[54, 55] MIP-capping with infrared fluorescent quantum dots have both been used to detect creatinine.[56] Apart from the lengthy synthetic process, MIP strategies have several other drawbacks, such as random distribution of binding sites, leakage or

incomplete template removal, and irregular morphology.[57] In conventional probes for creatinine sensing, selectivity is a challenge in the presence of interferents, such as glucose, proteins, acetoacetate, and ascorbic acid which lead to false readings for creatinine sensing.[58] Therefore, the development of new and more effective techniques for creatinine analysis is necessary.

1.5.3 Solvatochromism

Depending on the polarity of the medium, several compounds are known to exhibit varying responses to their absorption or emission properties, these are known as solvatochromic probes. Solvatochromic compounds are molecules that change their optical characteristics with various polarities of solvent environment. The proteins, nucleic acids, and bio-membranes that are involved in biomolecular interactions can be detected using the solvatochromic probes.[59] Additionally, it can be utilized in chemosensors, bioimaging, and trace amounts of water detection from solvent.[60, 61] Several essential molecular properties, such as degree of polarisation, coplanar π-conjugated bridges, and push-pull charge-transfer (CT) character, must be considered to design and synthesize the solvatochromic fluorophore to achieve maximum sensitivity and response to external stimuli.[62, 63] High polarisation can be attained by introducing polar functionality groups to molecules, such as amino, carbonyl, cyano, nitro, or heteroaryl groups.[64] A key design approach for making a better solvatochromic dye is a high level of conjugated π-electron system with backbone coplanarity.[65] Mandal et al. designed and synthesized two functional covalent organic frameworks (**15a**) and (**15b**), made from three connected triazine-based amine or hydrazine with linear dialdehyde (Fig. 1.9).[66] It reveals their solvatochromic activity in various alcoholic, chlorinated aprotic volatile solvent molecules. Although the covalent organic frameworks show a good response to different polarity of solvents, both have been synthesized with multi-steps, and at high temperatures and longer time (i.e., reflux at 120 °C for 3 days).

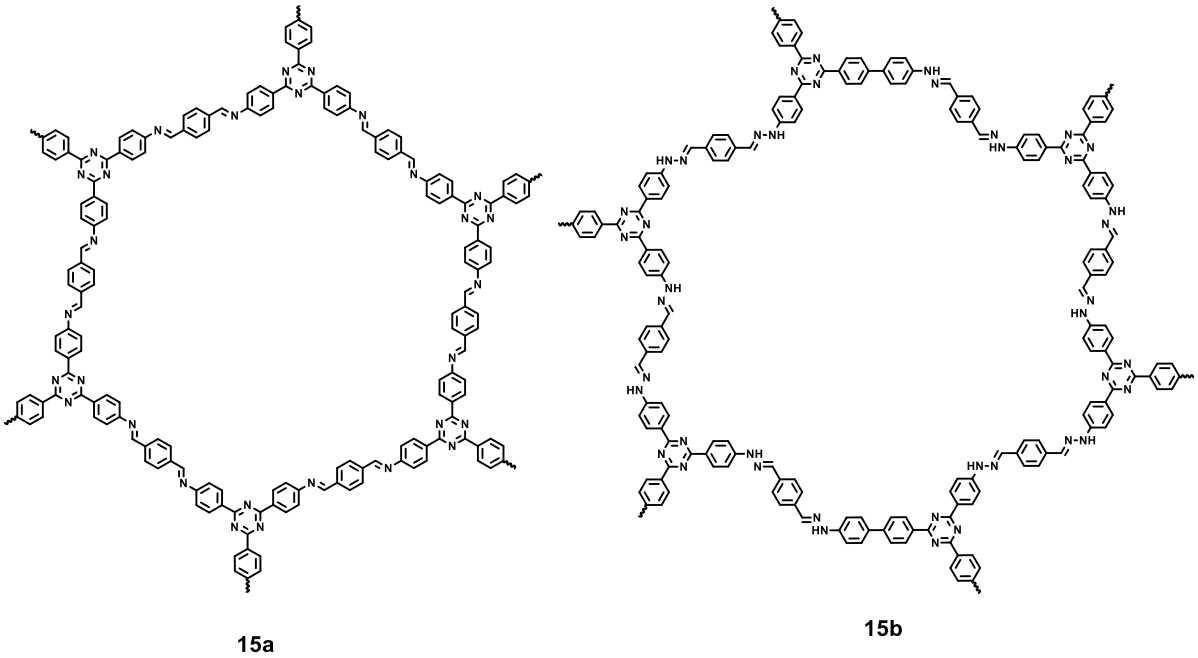

Figure 1.9 Molecular structures of covalent organic frameworks (**15a** and **15b**).

1.5.4 Explosive Sensing

Chemical explosives are now more frequently utilized in terrorist attacks because they are portable and concealable. Such explosives can be of two types: a) primary explosives, which need a fire source, a spark, or enough heat to ignite them. Lead azide and lead styphnate are examples of primary explosives. b) Secondary explosives are chemical compounds that are less sensitive to heat, shock, or friction and require a primary explosive to detonate, such as nitroaromatics or nitramines, which are used mostly in military sites. Nitro aromatics such as trinitrotoluene (TNT), dinitrotoluene (DNT), and cyclotrimethylene trinitramine (RDX), require a primary explosive to detonate. Compared to primary explosives, these compounds can produce a higher explosion. Moreover, nitro explosive can be classified as electron-deficient aromatics compounds such as, picric acid (PA) or trinitrophenol (TNP), trinitrotoluene (TNT), 2,4-dinitrotoluene (DNT), 1,3-dinitrobenzene, etc., and electron-deficient aliphatic such as 2,3-dimethyl-dinitrobutane (DMNB), trinitroglycerin (TNG), 1,3,5-trinitroperhydro-1,3,5-triazine (RDX), octahydro-1,3,5,7-tetranitro-1,3,5,7-tetrazocine (HMX), etc. These explosives are all toxic, but RDX, HMX, TNT, TNP, TNG, and PA explosives are the most hazardous as well.[67-71]

The explosives can be detected using a variety of detection methods, such as gas chromatography[72], Raman spectroscopy[73], sniffing dogs[74], X-ray scanning[75], cyclic voltammetry[76], and ion mobility spectrometry[77]. However, most of the instruments used are

large in size, expensive, and unsuitable for incorporating into a portable system for in-field, remote, or non-contact detection. Being explosives are non-fluorescent in nature, fluorescence-based explosive detection can be possibly made by using fluorescent sensory materials, which can change in fluorescence when in contact with explosives. The ability to detect explosives lies in any phenomenon that causes a change in wavelength, fluorescence intensity (quenching or enhancement), or lifetime in relation to the concentration and exposure duration of explosives. Most of the published research on explosives sensors based on fluorescence still uses fluorescence quenching techniques. Fluorescence quenching can be caused by several different mechanisms, including photo-induced electron transfer (PET), intermolecular charge transfer (ICT), electron exchange, resonance energy transfer, and so forth.[78] Nitroaromatic compounds are electro-deficient in nature, they might bind with electron-rich fluorophores as a donor-acceptor (D-A) interaction.[79] The excited state of fluorophores (D) is likely to donate an electron to the ground state of explosive compounds (A) during the PET, as illustrated in Fig. 1.10a.

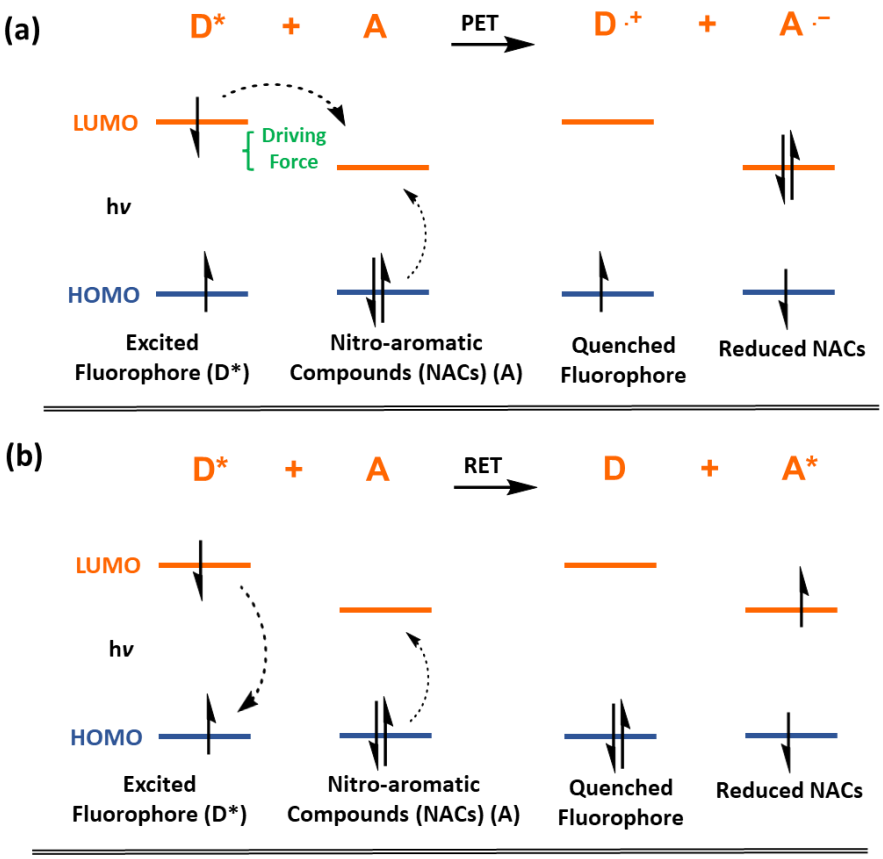

Figure 1.10 Schematic illustration for molecular orbital for different interactions in (**a**) photoinduced electron transfer (PET), (**b**) resonance energy transfer (RET).

Explosive sensors have also been developed using the energy transfer mechanism, which can significantly increase the fluorescence-quenching efficiency and improve sensitivity.[80] The extent of overlap between the fluorescence emission spectrum of the donor (the fluorophore) and the absorbance spectrum of the acceptor (an analyte, i.e., nitroaromatics compounds) determines the amount of resonance energy transfer (RET) (Fig 1.10b).[81-83]

Recently, nitrated explosive TNT detection in an aqueous medium has been effectively carried out using fluorescent conjugated polymers.[84] It has an extended exciton migration pathway than small molecule fluorophores and more effective electronic communication between quenchers along the polymer backbone. Conjugated polymers are efficient electron donors, and the delocalized excited state enhances the polymer's donor capacity, which promotes exciton migration and hence improves the electrostatic interaction between the polymer and electron-deficient nitroaromatic analytes.

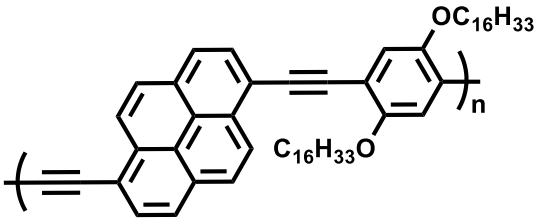

16

Figure 1.11 Schematic molecular structure of (**16**).

Nitrated explosives are extremely sensitive to impact, friction, and shock, so it is preferable to use detection techniques that allow for contact-free analysis. Various organic fluorescent polymers have shown sensitivity to the detection of nitro-aromatic explosives. Zhang et al. reported two organic conjugated polymers (**17** and **18**) constructed of benzene and quinoxaline moieties and connected by C=C double bonds or C≡C triple bonds (Fig. 1.12).[85] Both of the polymers exhibited fluorescence quenching to TNT in solution and vapor phases which are exposed to a thin film. However, the detection limit was not reported, but they could have increased the sensitivity by synthesizing porous structured hyperbranched polymer.

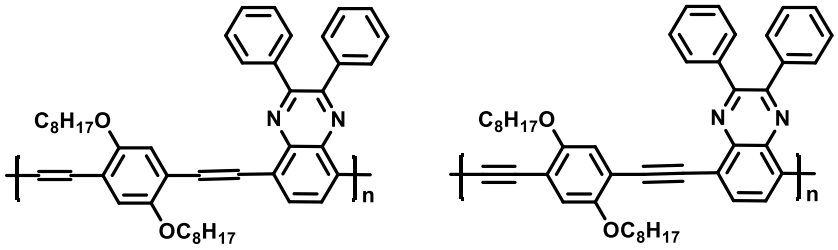

17 18

Figure 1.12 Molecular structures for conjugated polymers (**17** and **18**).

Mothika et al. developed conjugated microporous polymer (CMP) thin films for sensitive and selective vapor-phase TNT detection (Fig. 1.13).[86] Three CMPs thin films were prepared from tetra(carbazolylphenyl) ethylene monomer (**19**), on indium tin oxide (ITO) electrode by electrochemical oxidative polymerization method, and their fluorescence response to TNT vapor was studied. To analyze the optical response of the CMP films toward TNT for the sensing experiments, a dual-chamber setup coupled with a laser diode for excitation is used. The probe (**20**) quenched the fluorescence to about 95% of its original intensity when exposed to 33 ppb of TNT vapors for 3 min and 30% quenching at a lower concentration, 5-10 ppb vapors of TNT. Probe (**21**) showed a negligible response, while probe (**22**) containing the structural units of tetraphenylethylene (TPE) and fluorenone quenched its emission by about 70% in the presence of 0.2 ppm TNT. This means that the existence of an electron-donor TPE core is crucial for effective photoinduced electron transfer from polymer to nitroarenes. It is found that the microporosity and extended π-conjugation of the polymer are beneficial for the highly sensitive detection of explosives. Although it is highly sensitive to TNT, they used an electro-polymerization method for synthesis on a specific substrate and a specific dual-chamber setup for sensing, which is a lengthy procedure.

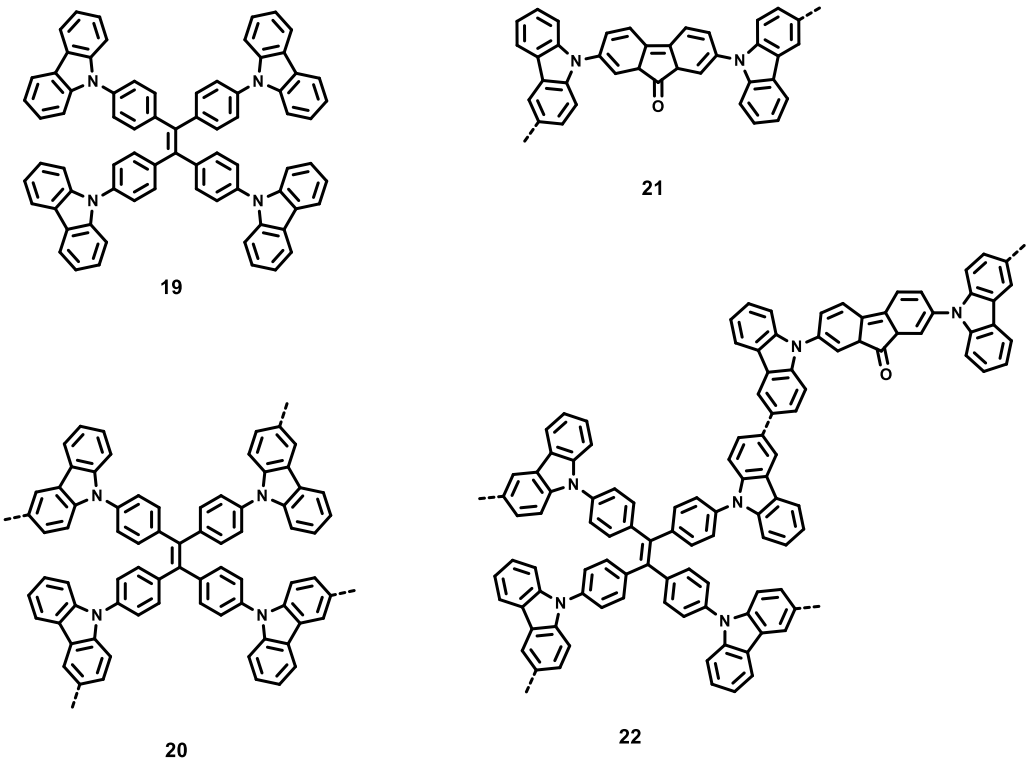

Figure 1.13 Molecular structures for the monomer (**19**) and polymers (**20-22**).

1.5.5 Acidochromism

Acidochromism, the term for chromophores that change color when they interact with acids, has been extensively explored in recent years due to its significance in the industry (such as many chemical industries including food and beverage processing).[87, 88] A dipolar molecule is often synthesized using an aromatic π-electron linker, which helps the donor and acceptor moieties interact.[89, 90] The protonation of nitrogen atoms makes the nitrogen-containing heterocyclic ring sensitive to acid medium.[91] Siva et al. reported two different C3-triazine based star-shaped D-π-A compounds (**23**) and (**24**) (Fig. 1.14).[92] Both compounds' absorption spectra reveal negligible solvatochromic variations. Increasing the solvent polarity tends to increase the wavelength in the emission spectra, which shows significant Stokes shifts. The ICT character is higher in the excited state than the ground state, thus negligible change is observed in the absorption spectrum. Conjugation of a donor-acceptor moiety facilitates the protonation at triazine nitrogen upon the addition of trifluoroacetic acid (TFA). Although a strong D-A character was incorporated here, a hyperbranched porous network polymer with this character would have made more impact on trapping the acid vapor.

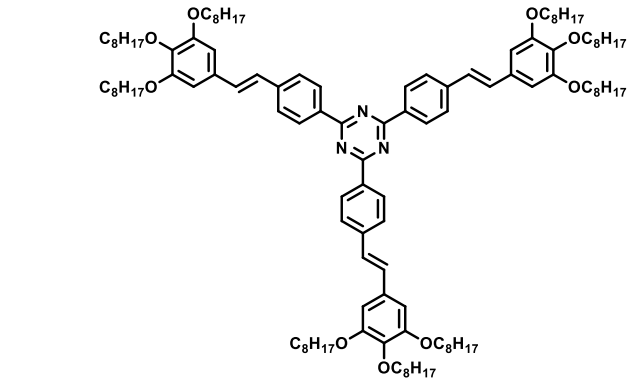

23

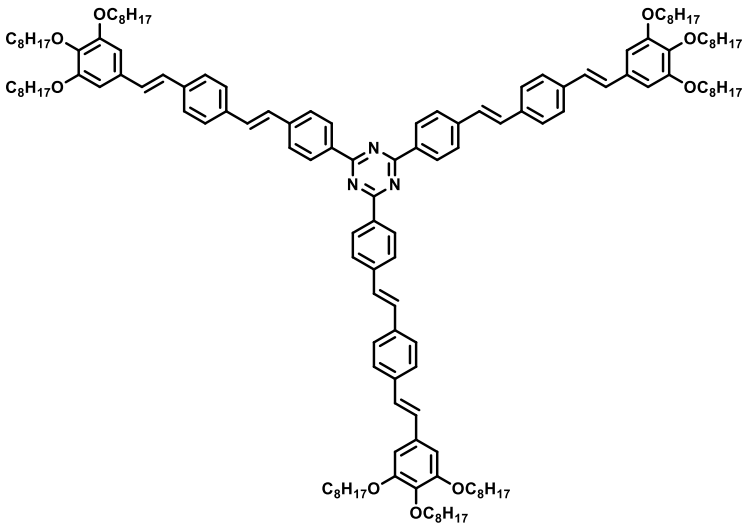

24

Figure 1.14 Molecular structures for triazine based star-shaped D-π-A compounds (**23**) and (**24**).

Mamtimin et al. studied only liquid-phase acidochromicity for pyrimidine-based low-molecular-weight copolymers (**25**) and (**26**) (Fig. 1.15), which was synthesized by a Grignard reaction involving 1,4-dibromo-2,5-didodecyloxybenzene and 2-amino-4,6-dichloropyrimidine in the presence of [1,2 Bis(diphenylphosphino) ethane] dichloronickel(II).[93] The protonation of the nitrogen-containing heterocyclic compounds and the partial charge transfer between the electron-donating phenyl and electron-accepting pyrimidine units could have a significant effect on protonic acid sensitivity.[94] Auras et al. synthesized a series of perylene-based COF (**27**) (Fig. 1.16) and showed that their imine bonds (−N=CH−) of all three COFs (**27a-c**) could be protonated reversibly, leading to considerable protonation show color change. However, sufficiently strong acids can protonate the nitrogen

lone pair of imines, but this process usually results in their decomposition if there is even a trace of water.

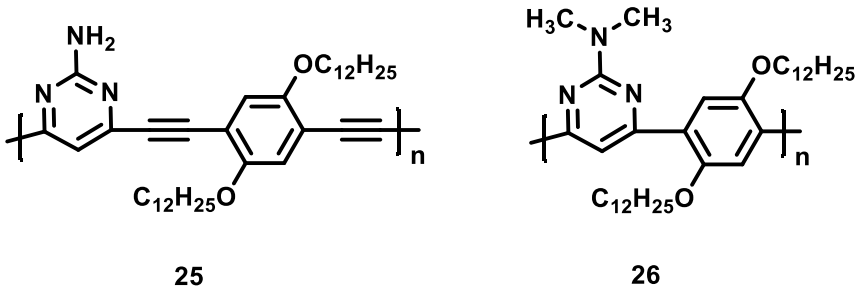

25 26

Figure 1.15 Molecular structures for pyrimidine-based copolymers (**25**) and (**26**).

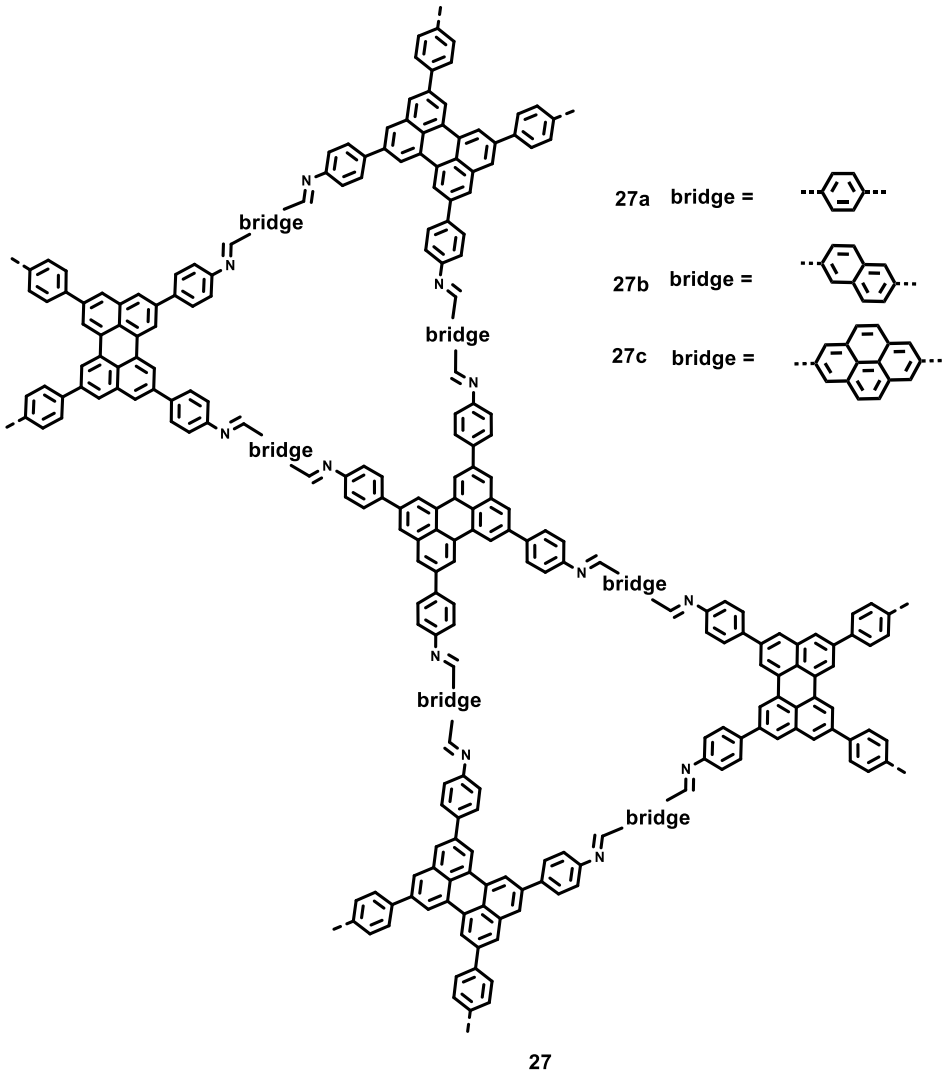

27

Figure 1.16 Molecular structures for perylene-based COF (**27**).

1.5.6 Mechanofluorochromism

Mechanofluorochromism (MFC) is the phenomenon by which materials emit light in response to external mechanical stimuli such as pressure, grinding, stress, rubbing, shearing, and crushing.[95-98] The material's response to these stimuli has achieved significant attention from the scientific community because of their potential applications in mechanosensor, optical storage, and security papers.[99] It is likely that the development of these materials will encourage the creation of cutting-edge technology around the world.[100] When mechanical stimuli are applied, intermolecular interactions such as hydrogen bonds, dipole-dipole interactions, or π-π interactions can change, causing various morphological changes such as transitions from crystalline to amorphous states, from a stable to a metastable liquid crystalline phase, between two different crystalline phases, etc.[101] As per the molecular level mechanism, the observation of MFC characteristics is the result of a minor or significant change in the structure of the molecular packing during grinding or pressing. The majority of materials with MFC properties can be quickly reversed by solvent fuming.[102] Weder et al. presented the initial study on a series of organic compounds (**28a**-**28e**) that exhibit fluorescence response under pressure stimuli i.e., piezochromism (Fig. 1.17).[103] The piezochromic fluorescent properties were observed for (**28c**) and (**28d**), when compared to others in the series. It indicates that balancing π-π electrons and aliphatic chain interactions in cyano-substituted oligo(p-phenylene vinylene) derivatives is possible through the length of peripheral aliphatic tails and the variation of electron density in the central ring. This approach facilitates the development of fluorophores that can take on many polymorphs and show piezochromic properties.

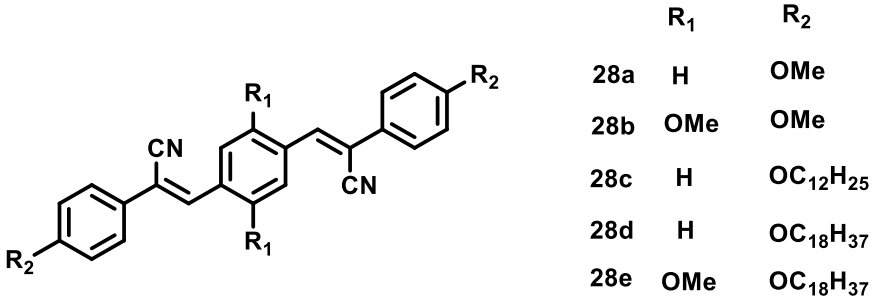

Figure 1.17 Molecular structures for cyano-substituted oligo(p-phenylene vinylene) derivatives (**28a**-**28e**).

One new compound (**29**) with triphenylamine (TPA)-anthrylenevinylene and TPE moieties was successfully synthesized by Xu et al. (Fig. 1.18).[104] It shows the change in emission color which is shifted from orange (561 nm) to red (583 nm) upon grinding. Based on wide-

angle X-ray diffraction data, the mechanism of the MFC property was explained. The diffraction curve of the compound shows a broad, and weak peak after grinding, indicating the phase transformation (ordered structure to amorphous).[104] Recently, Chi et al. synthesized a conjugated polymer (**30**) that exhibited interesting MFC (Fig. 1.18).[105] As shown in Fig. 1.19, the conjugated and rigid backbone is constructed using the building blocks fluorene and 9,10-distyryllanthracene moieties. Tetraphenylethenes act as large pendant groups that are connected to the fluorene segments by alkyl chains to prevent the backbone from π-π stacking and make the polymer 'aggregation-enhanced emission' (AEE)-active. The fluorescence emission color of (**30**) was observed bright yellow at 541 nm, which shows red-shifted emission (from yellow to red) after being ground with a pestle or sheared with a spatula. According to the findings of the powder X-ray diffraction study, the MFC of **30** may be correlated to the external forces that have transformed from a crystalline structure into an amorphous one. Upon mechanical force, planarization of the molecular conformation may take place and an increase in molecular conjugation of the polymers resulted from the transition from a partly crystalline to an amorphous structure. As a result, the emission color was noticeably red-shifted by (61 nm) following grinding. Although red-shifted emission response under the stimulus of mechanical force was explored, blue-shifted MFC material is required to explore because it is associated with a shorter wavelength and higher energy level of emitted light. This means that even small changes in the structure of materials or properties can be detected and measured accurately.

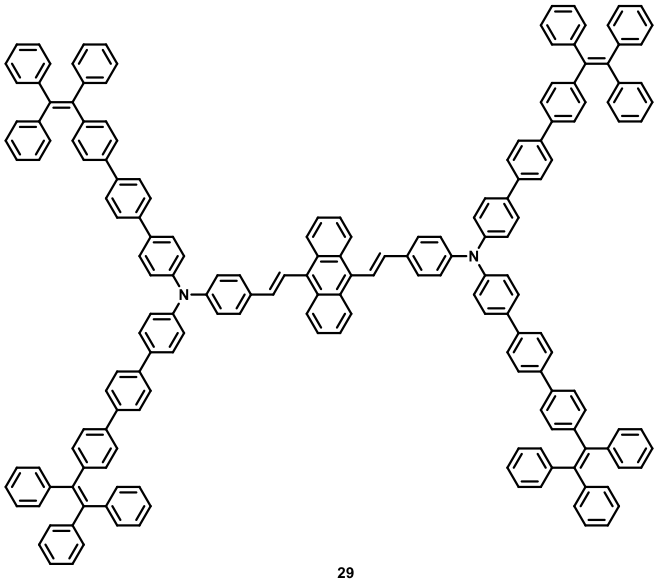

Figure 1.18 Molecular structure for compound (**29**).

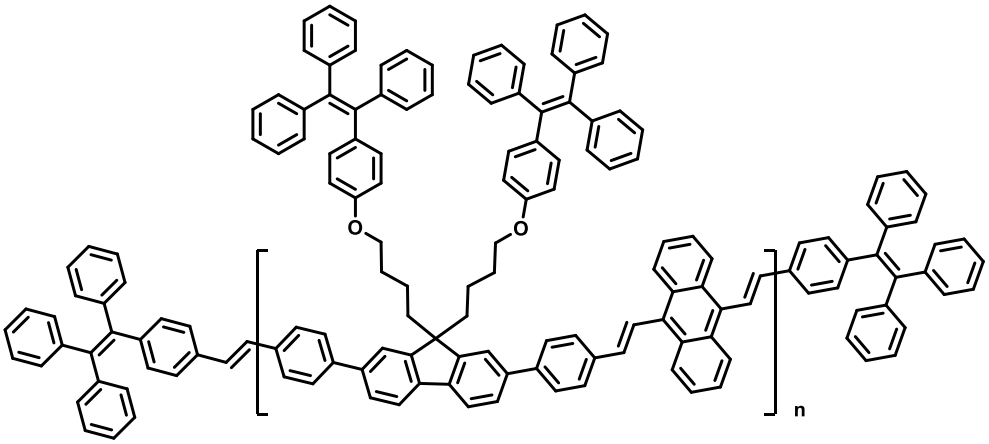

30

Figure 1.19 Molecular structure for polymer (**30**).

1.6 White light tunable emission through polymerization

Light-emitting polymeric materials have been getting more attention recently on emission color tuning as they provide flexibility and diversity due to the wide range of molecular design and material processing possibilities.[80, 106] Such materials can be used in many applications including organic light-emitting diodes,[107] bioimaging,[108] theranostics,[109] and secure printing,[110]. It has been of great interest for the research and practical application to design light-emitting materials that can show tunable emission color, especially in their solid or aggregated states.[111] Traditionally, such materials rely on the blending of multiple compounds that emit light at different wavelengths (i.e., Blue, Green, and Red)[112] or covalently combining various emissive fluorophores in polymer chains to provide desired emission colors.[113, 114] In addition, blue-to-red emission color tuning can be obtained by combining different emissive donor (D)/acceptor (A) fluorophore pairs in a single polymer resulting through-space charge transfer process.[115, 116] The potential use of white light-emissive materials in displays, lighting, low-energy devices, molecular sensors, and switches have drawn increased attention recently.[117] Phosphorescence-based white light emitting materials can be utilized as an efficient light source in a variety of applications, including polychromatic screen printing, multilevel information encryption, and the detection of volatile organic chemicals.[118-120] Due to their long lifespan, high efficiency, and excellent color rendering index, the development of white light-emitting substances based on phosphorescence is receiving a lot of interest for use as a lightning source in displays, LED devices, and sensors.[121] In most cases, the host-guest interactions, solvent polarity, integrating organic or polymeric frameworks, or energy and charge transfer

processes are usually responsible for tuning the white light emission.[26] Hawker and co-authors designed and synthesized single-component host-guest materials (**31**) that have been copolymerized using free radicals polymerization from methacrylate-based heteroleptic iridium(III) complex and substituted carbazole with variable degrees of polymerization and monomer ratio in mol % (in range of 0 to 29 mol %) (Fig. 1.20).[122] Particularly, thermal stability and good hole transport mobility are provided by electron-rich carbazole units. Although it has a high PL quantum yield (∼70−80%) with phosphorescence green and blue emission, but could not reach up to the white light emission tuning.

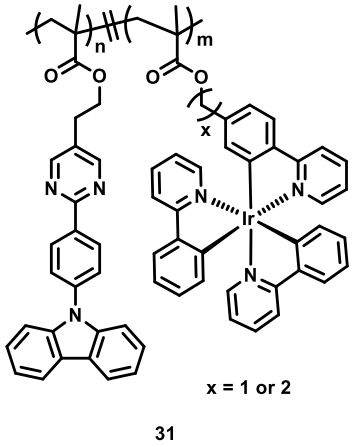

31

Figure 1.20 Molecular structures for copolymer (**31**) with various monomer (mol %) ratio (m-n).

Mandal et al. designed, synthesized and studied spectral properties of a polymerizable luminogenic monomer (2Z,2′Z)-6,6′-(2,7dibromo-9H-fluorene-9,9-diyl)bis(hexane-6,1-diyl)bis(2-cyano-3-(10-hexyl-10H-phenothiazin-3-yl)acrylate (**32a**) with AIEE property and its copolymers (**32b**) (Fig. 1.21).[123] To adjust the quality of white light produced by OLEDs, non-AIE (**32a**)-fluorene copolymers (**32b**) were synthesized using various monomers ratios (**32a**)-9,9-dihexylfluorene (m-n) [0.5-0.5; 0.25-0.75; 0.10-0.90; 0.05-0.95; 0.01-0.99; 0.005-0.995]. By adding a strong AIEE monomer, Somanathan and co-workers developed a successful approach for the rational design of a white light-emitting copolymer (**33**) (Fig. 1.22). A derivative of tetraphenylethene building blocks alternated with a 9,9'-dihexylfluorene core is used to show white light emission. Even if, few more organic fluorophores are reported as a white-light material,[124, 125] but phosphorescent heavy metal complexes such as iridium(III) or platinum(II) based compounds are used as emitters in LED devices because of their high luminous efficiency and excellent stability.

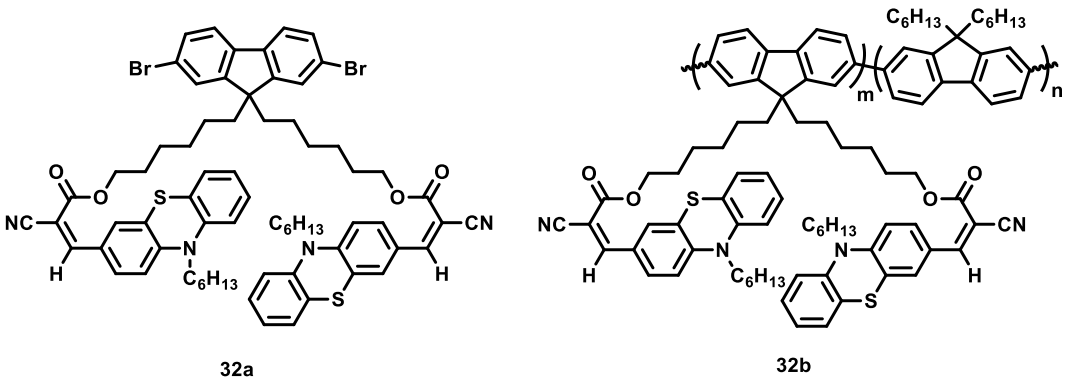

Figure 1.21 Molecular structures for monomer (**32a**), and copolymer (**32b**) using various monomers ratios (**32a**)-fluorene (m-n).

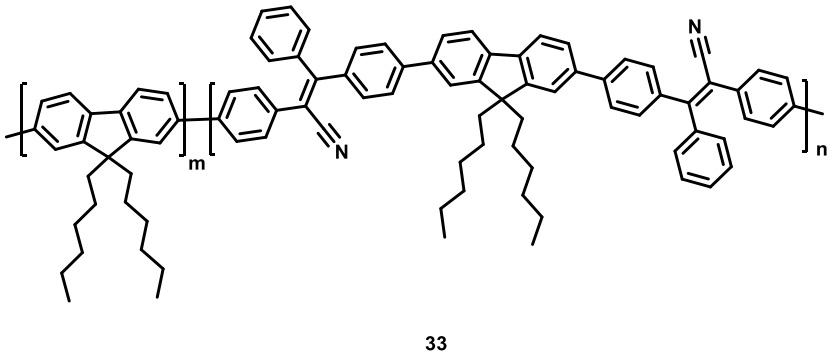

Figure 1.22 Molecular structure for copolymer (**33**).

1.7 Research Gaps

The discovery and development of advanced luminescent materials are both topics covered in the present thesis. We have explored the potential of a primitive material and also developed a new "Aggregation-induced Emission" (AIE) active small and polymeric material. We have employed these for emission property transformation, and sensitive and selective sensing of several analytes. Even though most compounds only showed one or dual distinct response activities, relatively less reports have been given to investigate distinct responsive multi-stimuli probes for multi-sensing applications.[126-128] The cyclometalated ligand can be modified to allow for polymer emission tuning across the whole visible spectrum, and enabling a real response to the analytes. An important task is to describe the method of developing effective new compounds. According to phosphorescence's high theoretical quantum efficiency, it can be used as a reliable light source in a variety of applications such as polychromatic screen printing, volatile organic compound detection, and multilevel information encryption.[118-120] The

development of a sensitive and selective luminescent probe for detecting harmful volatile organic compounds (VOCs) is now gaining attention.[35] Most solvents are frequently used for various purposes in our daily life. Dichloromethane (DCM) is widely used as a paint remover in industry and as a solvent in labs. It is also used as an aerosol propellant, metal degreaser, room deodorizer, herbicide, and pesticide.[129, 130] The serious health issues caused by DCM inhalation are now well known. In general, gas chromatography,[131, 132] mass spectroscopy,[133] or bioluminescent markers[134] are used to detect DCM. All these techniques require high cost, and significant time, are less efficient in sensing, and are operationally laborious. Reports on fluorescent-based sensing materials, though exhibit sensitive detection of a variety of organic solvents, such as acetone, chloroform, DCM, methanol, and tetrahydrofuran (THF). Still, concerns exist regarding a lack of selectivity, a rapid response, or the requirement for particular types of substrates (i.e., porous material like alumina oxide or polymethylmethacrylate (PMMA) or surfaces like glass or TLC sheet, on which sensing compound or probe are placed or deposited to detect vapor-phase analyte).[135-140] A real-time application also requires a technique that is more reliable, portable, targeted, and sensitive. To the best of our knowledge, the pristine probe for a reusable, sensitive, and selective DCM detection with the lowest limit of detection (LOD) has not been explored yet.[38] Another interesting aspect of luminescent probes is in diagnostics or the early-stage identification of diseases by a deficiency/excess of particular biomolecules. It has been made possible by the detection of several biomolecules such as BSA, creatinine, or microorganisms.[141] Creatinine is one of them important biomolecules that can help to identify kidney disease. It determines the level of creatinine from the blood sample or waste product of the body (i.e., urine) excreted by the kidneys. Proteins and creatinine may typically be detected using mass spectrometry, UV-Vis spectroscopy, Raman spectroscopy, and other methods.[142] Various biomolecules capped nanoclusters (such as gluten, glutathione, cholic acid, BSA, etc.) and molecularly imprinted polymer (MIP) techniques have been reported for the purpose of detecting creatinine.[143-146] Still, single-component probes for sensitive and selective creatinine detection with a luminescent-based simple and easy strategy are still needed to explore more.

Polymeric materials also have several advantages when compared to small molecules, including various topologies (linear, hyperbranched, star-shaped), versatility of functionalization, tunable emission, facilitated processing ability, improved mechanical strength, etc.[147, 148] In the field of explosives detection, it is extremely difficult to identify nitro explosives on-site in either of their solid or gaseous phases to prevent terrorism. Getting an

ultra-sensitive sensor to detect nitro explosives is a challenge in the current study. There are numerous probe molecules available for contact mode detection of nitro explosives, however, vapor phase sensing is quite rare. Around hundreds of ppb (parts per billion) levels are maintained for the existence of contact mode-sensitive probe molecules.[149] For real-time military applications and to minimize mass destruction from explosions caused by detonating explosives in a public area, vapor phase sensing of explosives is necessary. Due to the substantially lower vapor pressure of nitro-based explosives, designing extremely sensitive explosive detection in the non-contact mode is a major challenge.[150] Highly sensitive detection of explosive materials would be considerably better facilitated by the use of D-A type fluorescent polymer.[151, 152] Commonly available luminescent materials can be used to detect explosive compounds utilizing a process that primarily relies on photo-induced electron transfer (PET) and energy transfer caused by the quenching of emission intensity.[153] Cyclic voltammetry and UV-VIS spectroscopy methods can be used to determine the HOMO and LUMO energy levels of the probe molecules. The vapors of low volatile explosives (RDX, PETN, and HMX) would be possible to detect using conjugated hyperbranched-based polymer or D-A-based conjugated polymer networks.[149] The sensitivity can be increased even further by strategically selecting a luminescent hyperbranched conjugated polymer with a high quantum yield and porous structure to detect low-volatile explosives.

For the acidochromism study, the push-pull π-electrons mechanism is expected from the π-electron donor group, like triphenylamine, sensitive to acids when it is conjugated to nitrogen-containing heterocyclic molecule.[154-156] Hence, nitrogen-based D-A probes typically become sensitive to the acidic medium.[91] Therefore, incorporating several protonic sites into the polymer might be responsible for the increased sensitivity of such materials towards the acidic medium as compared to small molecules.

Mechanofluorochromic (MFC) compounds are also an interesting luminescent material, which can be used in various applications, such as stress detectors,[157] force distribution sensors,[158] pressure indicators,[159] etc. Effective results in the MFC mechanism depend on planarization of the molecular conformation and an increase in molecular conjugation resulting from the transition from a partly crystalline to an amorphous structure, which is superior for polymeric materials as compared to small molecules.[105] A few D-A-type polymeric materials with MFC properties have been reported.[160-162] Most of the reported materials show a bathochromic shift with decreasing emission intensity upon grinding or pressing force.[163-165] Therefore, the probe with hypsochromic shift (i.e., blue-shifted) with

enhanced emission intensity is needed to get a clear and intense fluorescent response upon mechanical action or stimuli like grinding, crushing, pressing, etc. Furthermore, polymeric compounds respond efficiently over small molecules, because the rigid, extended conjugated backbone of D-A polymers allows for the ICT phenomenon and restricts intramolecular rotation.[166] These features contribute to their remarkable fluorochromic behavior, which includes a sharp color change upon mechanical grinding. Although few reports devoted to the small molecules MFC-active probes showing blue shift with enhanced emission intensities,[159, 167, 168] MFC-active D-A polymer for the response of blue shift with enhanced emission is still challenging. Also, considering the importance of phosphorescent materials, and white light-emissive materials in potential application like display, low-energy consumption devices, lighting devices, molecular sensors, and switches,[117] the current research in emission color tuning rely on doping or color blending of multiple dyes (e.g., blue, green, and red emissive) molecules.[169] There have not yet been any research reports on phosphorescent-based white light-emissive materials with AIE active in a single entity.

1.8 References

1. I. Obodovskiy, in *Radiation*, ed. I. Obodovskiy, Elsevier, 2019, pp. 207-220.
2. P. Alam, C. Climent, P. Alemany and I. R. Laskar, *Journal of Photochemistry and Photobiology C: Photochemistry Reviews*, 2019, **41**, 100317.
3. W. Che, G. Li, X. Liu, K. Shao, D. Zhu, Z. Su and M. R. Bryce, *Chemical Communications*, 2018, **54**, 1730-1733.
4. Q. Zhao, C. Huang and F. Li, *Chemical Society Reviews*, 2011, **40**, 2508-2524.
5. M. Mauro and C. Cebrián, *Israel Journal of Chemistry*, 2018, **58**, 901-914.
6. L. Ravotto and P. Ceroni, *Coordination Chemistry Reviews*, 2017, **346**, 62-76.
7. H. Liu, Q. Bai, L. Yao, H. Zhang, H. Xu, S. Zhang, W. Li, Y. Gao, J. Li, P. Lu, H. Wang, B. Yang and Y. Ma, *Chemical Science*, 2015, **6**, 3797-3804.
8. M. Kramarenko, C. G. Ferreira, G. Martínez-Denegri, C. Sansierra, J. Toudert and J. Martorell, *Solar RRL*, 2020, **4**, 1900554.
9. P. Alam, N. L. C. Leung, J. Zhang, R. T. K. Kwok, J. W. Y. Lam and B. Z. Tang, *Coordination Chemistry Reviews*, 2021, **429**, 213693.
10. X. He, Y. Yang, Y. Guo, S. Lu, Y. Du, J.-J. Li, X. Zhang, N. L. C. Leung, Z. Zhao, G. Niu, S. Yang, Z. Weng, R. T. K. Kwok, J. W. Y. Lam, G. Xie and B. Z. Tang, *Journal of the American Chemical Society*, 2020, **142**, 3959-3969.
11. P. Alam, G. Kaur, S. Chakraborty, A. Roy Choudhury and I. R. Laskar, *Dalton Transactions*, 2015, **44**, 6581-6592.
12. Y. Zhuo and J. Brgoch, *The Journal of Physical Chemistry Letters*, 2021, **12**, 764-772.
13. C.-G. Niu, G.-M. Zeng, L.-X. Chen, G.-L. Shen and R.-Q. Yu, *Analyst*, 2004, **129**, 20-24.
14. N. I. Georgiev, V. B. Bojinov and P. S. Nikolov, *Dyes Pigm.*, 2011, **88**, 350-357.
15. M. A. Auwalu and S. Cheng, *Journal*, 2021, **9**.

16. J. Mei, Y. Hong, J. W. Lam, A. Qin, Y. Tang and B. Z. Tang, *Adv. Mater.*, 2014, **26**, 5429-5479.
17. F. Cicoira and C. Santato, *Advanced Functional Materials*, 2007, **17**, 3421-3434.
18. Y. Huang, J. Xing, Q. Gong, L.-C. Chen, G. Liu, C. Yao, Z. Wang, H.-L. Zhang, Z. Chen and Q. Zhang, *Nat. Commun.*, 2019, **10**, 169.
19. J. Luo, Z. Xie, J. W. Y. Lam, L. Cheng, H. Chen, C. Qiu, H. S. Kwok, X. Zhan, Y. Liu, D. Zhu and B. Z. Tang, *Chemical Communications*, 2001, DOI: 10.1039/B105159H, 1740-1741.
20. Y. Hong, J. W. Lam and B. Z. Tang, *Chem. Comm.*, 2009, 4332-4353.
21. Z. Zhao, B. He and B. Z. Tang, *Chem. Sci.*, 2015, **6**, 5347-5365.
22. P. Alam, G. Kaur, V. Kachwal, A. Gupta, A. Roy Choudhury and I. R. Laskar, *Journal of Materials Chemistry C*, 2015, **3**, 5450-5456.
23. D. Sengottuvelu, V. Kachwal, P. Raichure, T. Raghav and I. R. Laskar, *ACS Applied Materials & Interfaces*, 2020, **12**, 31875-31886.
24. V. Kachwal, P. Alam, H. R. Yadav, S. S. Pasha, A. Roy Choudhury and I. R. Laskar, *New Journal of Chemistry*, 2018, **42**, 1133-1140.
25. B. Liu, H. Zhang, S. Liu, J. Sun, X. Zhang and B. Z. Tang, *Materials Horizons*, 2020, **7**, 987-998.
26. N. N. Mohd Yusof Chan, A. Idris, Z. H. Zainal Abidin, H. A. Tajuddin and Z. Abdullah, *RSC Advances*, 2021, **11**, 13409-13445.
27. J. Voskuhl and M. Giese, *Aggregate*, 2022, **3**, e124.
28. Y. Nagasawa, H. Samoto, H. Ukai, S. Okamoto, K. Itoh, T. Hanada, A. Kanemaru, Y. Fukui, S. Kojima, J. Moriguchi, S. Sakuragi, F. Ohashi, S. Takada, T. Kawakami and M. Ikeda, *Environmental Health and Preventive Medicine*, 2013, **18**, 341-348.
29. A. Kaukiainen, T. Vehmas, K. Rantala, M. Nurminen, R. Martikainen and H. Taskinen, *International Archives of Occupational and Environmental Health*, 2004, **77**, 39-46.
30. N. Brautbar and J. Williams, *International Journal of Hygiene and Environmental Health*, 2002, **205**, 479-491.
31. R. F. White and S. P. Proctor, *The Lancet*, 1997, **349**, 1239-1243.
32. C. He, J. Cheng, X. Zhang, M. Douthwaite, S. Pattisson and Z. Hao, *Chemical Reviews*, 2019, **119**, 4471-4568.
33. J. Wang, Q. Zhou, S. Peng, L. Xu and W. Zeng, *Frontiers in Chemistry*, 2020, **8**.
34. B. Szulczyński and J. Gębicki, *Journal*, 2017, **4**.
35. H.-Y. Li, S.-N. Zhao, S.-Q. Zang and J. Li, *Chemical Society Reviews*, 2020, **49**, 6364-6401.
36. Y. D. Farahani and V. Safarifard, *Journal of Solid State Chemistry*, 2019, **275**, 131-140.
37. C.-Y. Liu, X.-R. Chen, H.-X. Chen, Z. Niu, H. Hirao, P. Braunstein and J.-P. Lang, *Journal of the American Chemical Society*, 2020, **142**, 6690-6697.
38. H. Wang, S. Zhan, X. Wu, L. Wu and Y. Liu, *RSC Advances*, 2021, **11**, 565-571.
39. H. Zhang, X. Niu, S. Zhu, M. Tian and W. Liu, *Journal of Applied Polymer Science*, 2022, **139**, 51699.
40. S. Kumar and R. Singh, *Optics & Laser Technology*, 2021, **134**, 106620.
41. B. Yao, M.-C. Giel and Y. Hong, *Materials Chemistry Frontiers*, 2021, **5**, 2124-2142.
42. V. Jha, G. Garcia-Garcia, K. Iseki, Z. Li, S. Naicker, B. Plattner, R. Saran, A. Y.-M. Wang and C.-W. Yang, *The Lancet*, 2013, **382**, 260-272.
43. W. G. Couser, G. Remuzzi, S. Mendis and M. Tonelli, *Kidney International*, 2011, **80**, 1258-1270.
44. M. Wyss and R. Kaddurah-Daouk, *Physiological reviews*, 2000, **80**, 1107-1213.

45. A. P. de Silva, H. Q. N. Gunaratne, T. Gunnlaugsson, A. J. M. Huxley, C. P. McCoy, J. T. Rademacher and T. E. Rice, *Chemical Reviews*, 1997, **97**, 1515-1566.
46. X.-d. Wang and O. S. Wolfbeis, *Analytical Chemistry*, 2016, **88**, 203-227.
47. M.-j. Yin, B. Gu, Q.-F. An, C. Yang, Y. L. Guan and K.-T. Yong, *Coordination Chemistry Reviews*, 2018, **376**, 348-392.
48. C. Elosua, F. J. Arregui, I. D. Villar, C. Ruiz-Zamarreño, J. M. Corres, C. Bariain, J. Goicoechea, M. Hernaez, P. J. Rivero, A. B. Socorro, A. Urrutia, P. Sanchez, P. Zubiate, D. Lopez-Torres, N. D. Acha, J. Ascorbe, A. Ozcariz and I. R. Matias, *Journal*, 2017, **17**.
49. T. Küme, B. Sağlam, C. Ergon and A. R. Sisman, *Journal of clinical laboratory analysis*, 2018, **32**.
50. J. R. Delanghe and M. M. Speeckaert, *NDT Plus*, 2011, **4**, 83-86.
51. K. Kotaska, B. Jedlicková and R. Průsa, *Casopis lekaru ceskych*, 2008, **147**, 392-395.
52. T. Chen, N. Xie, L. Viglianti, Y. Zhou, H. Tan, B. Z. Tang and Y. Tang, *Faraday Discussions*, 2017, **196**, 351-362.
53. S. Pal, S. Lohar, M. Mukherjee, P. Chattopadhyay and K. Dhara, *Chemical Communications*, 2016, **52**, 13706-13709.
54. R. Narimani, M. Esmaeili, S. H. Rasta, H. T. Khosroshahi and A. Mobed, *Analytical Science Advances*, 2021, **2**, 308-325.
55. R. A. A. U. H. K. J. A. U. V. V. M. A. U. C. S. A. T. I. M. I. P. w. F. Almotiri, *Journal*, 2019, **12**.
56. M. Hassanzadeh, M. Ghaemy, S. M. Amininasab and Z. Shami, *Sensors and Actuators A: Physical*, 2021, **331**, 112936.
57. M. Niu, C. Pham-Huy and H. He, *Microchimica Acta*, 2016, **183**, 2677-2695.
58. G. L. Myers, W. G. Miller, J. Coresh, J. Fleming, N. Greenberg, T. Greene, T. Hostetter, A. S. Levey, M. Panteghini, M. Welch and J. H. Eckfeldt, *Clinical chemistry*, 2006, **52**, 5-18.
59. A. S. Klymchenko, *Accounts of Chemical Research*, 2017, **50**, 366-375.
60. U. Fegade, S. Patil, R. Kaur, S. K. Sahoo, N. Singh, R. Bendre and A. Kuwar, *Sensors and Actuators B: Chemical*, 2015, **210**, 324-327.
61. Z. Huang, F. Tang, A. Ding, F. He, R.-H. Duan, J. Huang, L. Kong and J. Yang, *Molecular Systems Design & Engineering*, 2022, **7**, 963-968.
62. Y. Niko, S. Sasaki, S. Kawauchi, K. Tokumaru and G.-i. Konishi, *Chemistry – An Asian Journal*, 2014, **9**, 1797-1807.
63. K. Takagi, K. Kusafuka, Y. Ito, K. Yamauchi, K. Ito, R. Fukuda and M. Ehara, *The Journal of Organic Chemistry*, 2015, **80**, 7172-7183.
64. J.-K. Fang, D.-L. An, K. Wakamatsu, T. Ishikawa, T. Iwanaga, S. Toyota, S.-i. Akita, D. Matsuo, A. Orita and J. Otera, *Tetrahedron*, 2010, **66**, 5479-5485.
65. X. L. Guan, T. M. Jia, D. H. Zhang, Y. Zhang, H. C. Ma, D. D. Lu, S. J. Lai and Z. Q. Lei, *Dyes and Pigments*, 2017, **136**, 873-880.
66. P. Das, G. Chakraborty, S. Tyagi and S. K. Mandal, *ACS Applied Materials & Interfaces*, 2020, **12**, 52527-52537.
67. A. L. Lehnert and K. J. Kearfott, *Nucl. Technol.*, 2010, **172**, 325-334.
68. J. I. Steinfeld and J. Wormhoudt, 1998, **49**, 203-232.
69. P. W. Cooper and S. R. Kurowski, *Introduction to the Technology of Explosives*, John Wiley & Sons, 1996.
70. J. Oxley, *Explosives detection: potential problems*, SPIE, 1995.
71. M. Marshall and J. C. Oxley, in *Aspects of Explosives Detection*, eds. M. Marshall and J. C. Oxley, Elsevier, Amsterdam, 2009, pp. 11-26.
72. M. E. Walsh, *Talanta*, 2001, **54**, 427-438.

73. M. Gaft and L. Nagli, *Opt. Mater.*, 2008, **30**, 1739-1746.
74. I. Gazit and J. Terkel, *Appl. Anim. Behav. Sci.*, 2003, **81**, 149-161.
75. Z. Ying, R. Naidu, K. Guilbert, D. Schafer and C. R. Crawford, 2007.
76. M. Krausa and K. Schorb, *J. Electroanal. Chem.*, 1999, **461**, 10-13.
77. R. G. Ewing, D. A. Atkinson, G. A. Eiceman and G. J. Ewing, *Talanta*, 2001, **54**, 515-529.
78. in *Principles of Fluorescence Spectroscopy*, ed. J. R. Lakowicz, Springer US, Boston, MA, 2006, DOI: 10.1007/978-0-387-46312-4_8, pp. 277-330.
79. M. S. Meaney and V. L. McGuffin, *Anal Chim Acta*, 2008, **610**, 57-67.
80. S. W. Thomas, G. D. Joly and T. M. Swager, *Chemical Reviews*, 2007, **107**, 1339-1386.
81. S. Rochat and T. M. Swager, *ACS Applied Materials & Interfaces*, 2013, **5**, 4488-4502.
82. J.-S. Yang and T. M. Swager, *Journal of the American Chemical Society*, 1998, **120**, 5321-5322.
83. T. M. Swager, *Accounts of Chemical Research*, 1998, **31**, 201-207.
84. G. He, N. Yan, J. Yang, H. Wang, L. Ding, S. Yin and Y. Fang, *Macromolecules*, 2011, **44**, 4759-4766.
85. S. Chen, Q. Zhang, J. Zhang, J. Gu and L. Zhang, *Sensors and Actuators B: Chemical*, 2010, **149**, 155-160.
86. V. S. Mothika, A. Räupke, K. O. Brinkmann, T. Riedl, G. Brunklaus and U. Scherf, *ACS Applied Nano Materials*, 2018, **1**, 6483-6492.
87. C. Dou, L. Han, S. Zhao, H. Zhang and Y. Wang, *The Journal of Physical Chemistry Letters*, 2011, **2**, 666-670.
88. H. Quitmann, R. Fan and P. Czermak, *Advances in biochemical engineering/biotechnology*, 2014, **143**, 91-141.
89. A. Baheti, P. Tyagi, K. R. J. Thomas, Y.-C. Hsu and J. T. s. Lin, *The Journal of Physical Chemistry C*, 2009, **113**, 8541-8547.
90. K. R. Justin Thomas, J. T. Lin, M. Velusamy, Y. T. Tao and C. H. Chuen, *Advanced Functional Materials*, 2004, **14**, 83-90.
91. P. Singh, A. Baheti and K. R. J. Thomas, *The Journal of Organic Chemistry*, 2011, **76**, 6134-6145.
92. K. Duraimurugan, V. Dhanamoorthy, J. Madhavan and A. Siva, *Journal of Photochemistry and Photobiology A: Chemistry*, 2018, **359**, 164-171.
93. X. Mamtimin, A. Tursun, R. Matsidik, S. Sidik, K. Abdulla, H. Mamut, A. Obulda and I. Nurulla, *Journal of Applied Polymer Science*, 2014, **131**.
94. Y. Shen, P. Xue, J. Liu, J. Ding, J. Sun and R. Lu, *Dyes and Pigments*, 2019, **163**, 71-77.
95. X. Zhang, Z. Chi, Y. Zhang, S. Liu and J. Xu, *Journal of Materials Chemistry C*, 2013, **1**, 3376-3390.
96. Y. Sagara and T. Kato, *Angewandte Chemie International Edition*, 2008, **47**, 5175-5178.
97. X. Zhang, J.-Y. Wang, J. Ni, L.-Y. Zhang and Z.-N. Chen, *Inorganic Chemistry*, 2012, **51**, 5569-5579.
98. D. R. T. Roberts and S. J. Holder, *Journal of Materials Chemistry*, 2011, **21**, 8256-8268.
99. Y.-X. Peng, F.-D. Feng, H.-Q. Liu, Y. Zhang, B. Hu, W. Huang and W. Zheng, *Dyes and Pigments*, 2020, **174**, 108110.
100. C. Wang, D. Peng and C. Pan, *Science Bulletin*, 2020, **65**, 1147-1149.

101. Y. Shao, Z. Xiao, C. Bi, Y. Yuan and J. Huang, *Nature Communications*, 2014, **5**, 5784.
102. Y. Sagara and T. Kato, *Nature Chemistry*, 2009, **1**, 605-610.
103. J. Kunzelman, M. Kinami, B. R. Crenshaw, J. D. Protasiewicz and C. Weder, *Advanced Materials*, 2008, **20**, 119-122.
104. H. Li, Z. Chi, B. Xu, X. Zhang, X. Li, S. Liu, Y. Zhang and J. Xu, *Journal of Materials Chemistry*, 2011, **21**, 3760-3767.
105. J.-r. Chen, J. Zhao, B.-j. Xu, Z.-y. Yang, S.-w. Liu, J.-r. Xu, Y. Zhang, Y.-c. Wu, P.-y. Lv and Z.-g. Chi, *Chinese Journal of Polymer Science*, 2017, **35**, 282-292.
106. W. Tian, J. Zhang, J. Yu, J. Wu, J. Zhang, J. He and F. Wang, *Advanced Functional Materials*, 2018, **28**, 1703548.
107. H. Uoyama, K. Goushi, K. Shizu, H. Nomura and C. Adachi, *Nature*, 2012, **492**, 234-238.
108. Y. Yang, Q. Zhao, W. Feng and F. Li, *Chemical Reviews*, 2013, **113**, 192-270.
109. M. Gao, F. Yu, C. Lv, J. Choo and L. Chen, *Chemical Society Reviews*, 2017, **46**, 2237-2271.
110. Q. Qi, C. Li, X. Liu, S. Jiang, Z. Xu, R. Lee, M. Zhu, B. Xu and W. Tian, *Journal of the American Chemical Society*, 2017, **139**, 16036-16039.
111. Q. Li and Z. Li, *Advanced Science*, 2017, **4**, 1600484.
112. S. Xu, Y. Duan and B. Liu, *Advanced Materials*, 2020, **32**, 1903530.
113. Z. M. Hudson, D. J. Lunn, M. A. Winnik and I. Manners, *Nature Communications*, 2014, **5**, 3372.
114. Y. Bao, H. De Keersmaecker, S. Corneillie, F. Yu, H. Mizuno, G. Zhang, J. Hofkens, B. Mendrek, A. Kowalczuk and M. Smet, *Chemistry of Materials*, 2015, **27**, 3450-3455.
115. S. Shao, J. Hu, X. Wang, L. Wang, X. Jing and F. Wang, *Journal of the American Chemical Society*, 2017, **139**, 17739-17742.
116. J. Hu, Q. Li, X. Wang, S. Shao, L. Wang, X. Jing and F. Wang, *Angewandte Chemie International Edition*, 2019, **58**, 8405-8409.
117. Z. Chen, C.-L. Ho, L. Wang and W.-Y. Wong, *Advanced Materials*, 2020, **32**, 1903269.
118. Y. Zhang, L. Gao, X. Zheng, Z. Wang, C. Yang, H. Tang, L. Qu, Y. Li and Y. Zhao, *Nature Communications*, 2021, **12**, 2297.
119. C. Wang, L. Qu, X. Chen, Q. Zhou, Y. Yang, Y. Zheng, X. Zheng, L. Gao, J. Hao, L. Zhu, B. Pi and C. Yang, *Advanced Materials*, 2022, **34**, 2204415.
120. Y. Zhang, X. Chen, J. Xu, Q. Zhang, L. Gao, Z. Wang, L. Qu, K. Wang, Y. Li, Z. Cai, Y. Zhao and C. Yang, *Journal of the American Chemical Society*, 2022, **144**, 6107-6117.
121. B. Xie, Y. Cheng, X. Yu, W. Shu, X. Luo, J. Hao and K. Wang, 2017.
122. Z. A. Page, C.-Y. Chiu, B. Narupai, D. S. Laitar, S. Mukhopadhyay, A. Sokolov, Z. M. Hudson, R. Bou Zerdan, A. J. McGrath, J. W. Kramer, B. E. Barton and C. J. Hawker, *ACS Photonics*, 2017, **4**, 631-641.
123. S. J. Ananthakrishnan, E. Varathan, V. Subramanian, N. Somanathan and A. B. Mandal, *The Journal of Physical Chemistry C*, 2014, **118**, 28084-28094.
124. S. Sinha, B. Chowdhury, U. K. Ghorai and P. Ghosh, *Chemical Communications*, 2019, **55**, 5127-5130.
125. X.-H. Jin, C. Chen, C.-X. Ren, L.-X. Cai and J. Zhang, *Chemical Communications*, 2014, **50**, 15878-15881.
126. M. Rajeshirke and N. Sekar, *Dyes Pigm.*, 2019, **163**, 675-683.
127. D. Wang, Y. Jin, X. Zhu and D. Yan, *Prog. Polym. Sci.*, 2017, **64**, 114-153.

128. J. A. McCune, S. Mommer, C. C. Parkins and O. A. Scherman, *Adv. Mater.*, 2020, **32**, 1906890.
129. *IARC monographs on the evaluation of carcinogenic risks to humans*, 1999, **71 Pt 1**, 251-315.
130. R. D. Morrison, B. L. Murphy and R. E. Doherty, in *Environmental Forensics*, eds. R. D. Morrison and B. L. Murphy, Academic Press, Burlington, 1964, pp. 259-277.
131. J. Han and S. M. Yoon, *IEEE Journal of Selected Topics in Quantum Electronics*, 2012, **18**, 1547-1552.
132. T. Sakai, Y. Morita and C. Wakui, *Journal of Chromatography B*, 2002, **778**, 245-250.
133. D. Poli, P. Manini, R. Andreoli, I. Franchini and A. Mutti, *Journal of Chromatography B*, 2005, **820**, 95-102.
134. N. Lopes, S. A. Hawkins, P. Jegier, F.-M. Menn, G. S. Sayler and S. Ripp, *Journal of Industrial Microbiology and Biotechnology*, 2012, **39**, 45-53.
135. Y. Jiang, J. Ma, J. Lv, H. Ma, H. Xia, J. Wang, C. Yang, M. Xue, G. Li and N. Zhu, *ACS Sensors*, 2019, **4**, 152-160.
136. A. Husain, *Journal of Science: Advanced Materials and Devices*, 2021.
137. H. Zhang, X. Niu, S. Zhu, M. Tian and W. Liu, *Journal of Applied Polymer Science*, 2021, **n/a**, 51699.
138. Y. Duan, Y. Liu, H. Han, X. Zhang, M. Zhang, Y. Liao and T. Han, *Spectrochimica Acta Part A: Molecular and Biomolecular Spectroscopy*, 2021, **252**, 119515.
139. Y. Liu, Y. Fan, C. Hou, W. Du, D. Zhang, Y. Liu, J. Xu and Y.-L. Bai, *Inorganic Chemistry*, 2021, **60**, 16370-16377.
140. N. Shiraishi, M. Kimura and Y. Ando, *Microelectronic Engineering*, 2014, **119**, 115-121.
141. K. Dhama, S. K. Latheef, M. Dadar, H. A. Samad, A. Munjal, R. Khandia, K. Karthik, R. Tiwari, M. I. Yatoo, P. Bhatt, S. Chakraborty, K. P. Singh, H. M. N. Iqbal, W. Chaicumpa and S. K. Joshi, *Frontiers in molecular biosciences*, 2019, **6**, 91.
142. S. Sargazi, I. Fatima, M. Hassan Kiani, V. Mohammadzadeh, R. Arshad, M. Bilal, A. Rahdar, A. M. Díez-Pascual and R. Behzadmehr, *International Journal of Biological Macromolecules*, 2022, **206**, 115-147.
143. M. S. Mathew and K. Joseph, *ACS Sustainable Chemistry & Engineering*, 2017, **5**, 4837-4845.
144. P. J. Babu, A. M. Raichur and M. Doble, *Sensors and Actuators B: Chemical*, 2018, **258**, 1267-1278.
145. A. Diouf, S. Motia, N. El Alami El Hassani, N. El Bari and B. Bouchikhi, *Journal of Electroanalytical Chemistry*, 2017, **788**, 44-53.
146. R. Jalili and A. Khataee, *Microchimica Acta*, 2018, **186**, 29.
147. A. C. B. Rodrigues and J. S. Seixas de Melo, *Topics in Current Chemistry*, 2021, **379**, 15.
148. Z. Qiu, X. Liu, J. W. Y. Lam and B. Z. Tang, *Macromolecular Rapid Communications*, 2019, **40**, 1800568.
149. Y.-w. Wu, A.-j. Qin and B. Z. Tang, *Chin. J. Polym. Sci.*, 2017, **35**, 141-154.
150. M. J. Lefferts and M. R. Castell, *Analytical Methods*, 2015, **7**, 9005-9017.
151. J.-B. Chen, B. Li, Y. Xiong and J. Sun, *Sens. Actuators B Chem.*, 2018, **255**, 275-282.
152. M. M. Islam, Z. Hu, Q. Wang, C. Redshaw and X. Feng, *Mater. Chem. Front.*, 2019, **3**, 762-781.
153. D. Giri, S. N. Islam and S. K. Patra, *Polymer*, 2018, **134**, 242-253.
154. J. B. Arockiam and S. Ayyanar, *Sensors and Actuators B: Chemical*, 2017, **242**, 535-544.

155. D. Wang, X. Zhang, X. Han, Y. Zhou, Y. Lei, W. Gao, M. Liu, X. Huang and H. Wu, *Journal of Materials Chemistry C*, 2021, **9**, 12868-12876.
156. S. Achelle, J. Rodríguez-López, F. Bureš and F. Robin-le Guen, *The Chemical Record*, 2020, **20**, 440-451.
157. M. Kondo, S. Miura, K. Okumoto, M. Hashimoto and N. Kawatsuki, *Chemistry – An Asian Journal*, 2014, **9**, 3188-3195.
158. C. K. Lee, D. A. Davis, S. R. White, J. S. Moore, N. R. Sottos and P. V. Braun, *Journal of the American Chemical Society*, 2010, **132**, 16107-16111.
159. K. Nagura, S. Saito, H. Yusa, H. Yamawaki, H. Fujihisa, H. Sato, Y. Shimoikeda and S. Yamaguchi, *Journal of the American Chemical Society*, 2013, **135**, 10322-10325.
160. Y. Zhang, K. Wang, G. Zhuang, Z. Xie, C. Zhang, F. Cao, G. Pan, H. Chen, B. Zou and Y. Ma, *Chemistry – A European Journal*, 2015, **21**, 2474-2479.
161. B. Xu, J. He, Y. Mu, Q. Zhu, S. Wu, Y. Wang, Y. Zhang, C. Jin, C. Lo, Z. Chi, A. Lien, S. Liu and J. Xu, *Chemical Science*, 2015, **6**, 3236-3241.
162. C. Y. K. Chan, J. W. Y. Lam, Z. Zhao, S. Chen, P. Lu, H. H. Y. Sung, H. S. Kwok, Y. Ma, I. D. Williams and B. Z. Tang, *Journal of Materials Chemistry C*, 2014, **2**, 4320-4327.
163. S. S. Pasha, H. R. Yadav, A. R. Choudhury and I. R. Laskar, *Journal of Materials Chemistry C*, 2017, **5**, 9651-9658.
164. T. Han, L. Liu, D. Wang, J. Yang and B. Z. Tang, *Macromolecular Rapid Communications*, 2021, **42**, 2000311.
165. Y. Wang, D. Xu, H. Gao, Y. Wang, X. Liu, A. Han, C. Zhang and L. Zang, *The Journal of Physical Chemistry C*, 2018, **122**, 2297-2306.
166. X. Wang, Q. Liu, H. Yan, Z. Liu, M. Yao, Q. Zhang, S. Gong and W. He, *Chemical Communications*, 2015, **51**, 7497-7500.
167. B. Wang, Z. Wu, B. Fang and M. Yin, *Dyes and Pigments*, 2020, **182**, 108618.
168. H. Liu, Y. Gu, Y. Dai, K. Wang, S. Zhang, G. Chen, B. Zou and B. Yang, *Journal of the American Chemical Society*, 2020, **142**, 1153-1158.
169. L. Ying, C.-L. Ho, H. Wu, Y. Cao and W.-Y. Wong, *Advanced Materials*, 2014, **26**, 2459-2473.

CHAPTER 2

MATERIALS, METHODS, AND INSTRUMENTATIONS

Chapter 2. Materials, Methods, and Instrumentations

2.1 Materials

2.1.1 Used Reagents

4-vinylphenylboronic acid, tetrakis(triphenylphosphine)palladium (0), iridium(III) chloride hydrate, 4-(2-Pyridyl) benzaldehyde, triphenylamine (TPA) were purchased from TCI chemicals. 2-bromopyridine, Cyanuric chloride, and iridium(iii) chloride hydrate $IrCl_3(H_2O)_3$ were purchased from Alfa Aesar company.

Sodium carbonate (Na_2CO_3), potassium carbonate (K_2CO_3), triphenylphosphine (PPh_3), Polyethylene glycol (PEG), oxalyl chloride ($C_2O_2Cl_2$), trifluoroacetic acid 99% (TFA), 50% concentrated boron trifluoride etherate [$BF_3(OEt_2)$], triethylamine (NEt_3), anhydrous aluminum chloride ($AlCl_3$), and the UV grades solvents such as THF, ethanol, toluene, hexane, cyclohexane, carbon tetrachloride (CCl_4), acetone, diethyl ether, dichloromethane (DCM), methanol, N, N-dimethylformamide (DMF), and dimethyl sulfoxide (DMSO) procured from Spectrochem. Silver nitrate ($AgNO_3$), 2-ethoxyethanol, sodium hydroxide (NaOH), ethanol (C_2H_5OH), sodium carbonate (Na_2CO_3), and sulfuric acid (H_2SO_4) were purchased from Merck company. Anhydrous solvents such as DCM, hexane, ethyl acetate, THF, and methanol were purchased from CDH (Central Drug House) Fine Chemical Pvt Ltd.

2-ethoxyethanol, Hamilton Sample Lock (gas-tight) syringe of volume 0.5 mL needle size 22 ga (bevel tip) L 51 mm (2 in.), and azobisisobutyronitrile (AIBN) were purchased from Sigma Aldrich chemical company Ltd.

2.2 Methods

2.2.1 Synthesis

In the respective chapters, synthetic methods of each probe and intermediates were included. All the photophysical property studies were performed after the structural characterization of the probes.

2.2.2 Fabrication of thin film on glass substrate for photoluminescence (PL) measurement

The probe solutions of iridium(III) complexes (10^{-3} M) in THF/DMF were prepared. On a 2x2 cm^2 piece of thin glass, 2-3 drops of the solution were placed, and the solvent was let to evaporate gradually. A thin film of polymeric compounds was also made by a drop-casting method using a probe solution in THF (2 mg of a probe in 0.5 ml of THF) and annealed for an hour at 60 °C in the oven.

2.2.3 Sample preparation to investigate the 'Aggregation Induced Emission (AIE)' property

Sample preparation for M1: The AIE experiment for M1 was carried out by taking a mixture of THF and hexane solvents. Firstly, the probe solution (10^{-3} M) of M1 was prepared in THF solvent. The 0.5 ml of probe solution was added in four different glass vials of 5 ml volume. Then it was equally filled with THF: hexane mixture by changing the percentage or ratio of THF and hexane fractions i.e., 5: 0 ml, 2: 3 ml, 3: 2 ml, and 0.5: 4.5 ml THF: hexane respectively that became 0 %, 30 %, 60 %, and 90 % hexane fractions. The photoluminescence (PL) spectra of all the prepared solutions were recorded. To prove the restricted intramolecular motion (RIM) effect, the series of probe solutions in the THF-PEG mixture was prepared in a similar manner as described above (PEG was added in place of hexane).

Sample preparation for polymer: The following experiment was conducted to study the AIE activity of polymer. The stock solution of homopolymer (HP) was made to study the AIE activity of HP (1 mg in 5 ml DMF). The prepared stock solution (0.5 ml) of the polymer HP was taken in four glass vials of 5 ml volume. It was made into a total volume of 5 ml with water-DMF mixture with an increasing concentration of water from 0 %, 30 %, 60 %, and 90 % (e.g., in the case of AIE solution of 90 % water-DMF mixture, 0.5 ml prepared HP solution and 4.5 ml water were taken). In the same way, another four solutions were prepared with PEG instead of water fractions. To study the AIE activity of copolymer CP4, AIE solutions were prepared in the same manner. The first stock solution of CP4 was prepared (1 mg of CP4 in 5 ml of THF), and 0.5 ml of prepared stock solution of CP4 was taken in four glass vials of 5 ml volume. The glass vials contain a 5 ml THF-water mixture with various water fractions (i.e., 0 %, 30 %, 60 %, and 90 %). Same with CP4, four more solutions were prepared using PEG instead of water. For each prepared solution, the PL intensity was recorded.

2.2.4 Experimental procedure for detection limit calculations

The emission intensity of the synthesized compounds on thin film and in solution without an analyte was measured ten times, and the standard deviation of blank readings was calculated, to determine the Signal/Noise ratio. The following equation is used to determine the detection limit.

Detection limit = 3σ/m, where 'σ' is the standard deviation of new measurements, and 'm' is the slope between the plot of PL intensity versus sample concentration.[1-3]

2.2.5 Solvatochromism

The Lippert Mataga Plot is used to understand the solvent effect on the emission spectra of the probe. It explains the Stoke shifts in terms of the excited-state dipole moment. The Lippert-Mataga equation describes the energy related to the refractive index (η), and the dielectric constant (ε) of the solvent as given in the following equation.

$$(\bar{\nu}_{abs} - \bar{\nu}_{emi}) = \left(\frac{2(\mu_e - \mu_g)^2}{hca^3}\right)\Delta f + constant$$

$$\text{Where } \Delta f = \frac{(\varepsilon-1)}{(2\varepsilon+1)} - \frac{(n^2-1)}{(2n^2+1)}$$

$\bar{\nu}_{abs}$ and $\bar{\nu}_{emi}$ are the wavenumbers (cm^{-1}) of the absorption and emission, 'ε' is the dielectric constant and 'n' is the refractive index of the particular solvent, 'h' is Planck's constant, 'c' is the velocity of light, 'a' is the Onsager cavity radius and μ_g and μ_e is the ground state and excited state dipole moment of the fluorophore, respectively. Δf is the orientation polarizability. $\Delta\bar{\nu} = \bar{\nu}_{abs} - \bar{\nu}_{emi}$ is the solvatochromic shift (in cm^{-1}) between the maxima of absorption and fluorescence emission [$\bar{\nu}_{abs} = 1/\lambda_{abs(max)}$, $\bar{\nu}_{emi} = 1/\lambda_{em(max)}$].

2.3 Instrumentation

2.3.1 UV-Visible spectrophotometer

It is a spectroscopic tool that measures the amount of radiation that is absorbed in proportion to its frequency or wavelength when it interacts with a sample. The relative energies of the ground and excited states are changed as a result of environmental factors, and this change results in spectrum changes. The absorbance (A) of an absorber (concentration C) having a molar extinction coefficient ε at wavelength λ is given in the following equation.

$$A = \log\left(\frac{I_o}{I}\right) = \varepsilon_\lambda\, cl$$

where 'A' is absorbance (optical density), I_o, and I represent the intensity of the incident and transmitted light, respectively, c is the concentration of the light-absorbing species, and l is the path length of the light-absorbing medium in a decimeter. A matched pair of 10 cm quartz cuvettes (Hellma, 1 c m light path, capacity 3.5 ml, Model: 100-QS) was used for absorption measurements.

The Shimadzu Spectrophotometer (model UV-1800 and 2550) was used to record UV-VIS absorption spectra. The Shimadzu UV-2450 UV-VIS spectrophotometer was used to record the solid-state UV-VIS absorption spectra in reflectance mode (using the integrated sphere

method) and then converted the reflectance values to absorbance. The block diagram of the instrumentation is shown in Fig. 2.1.

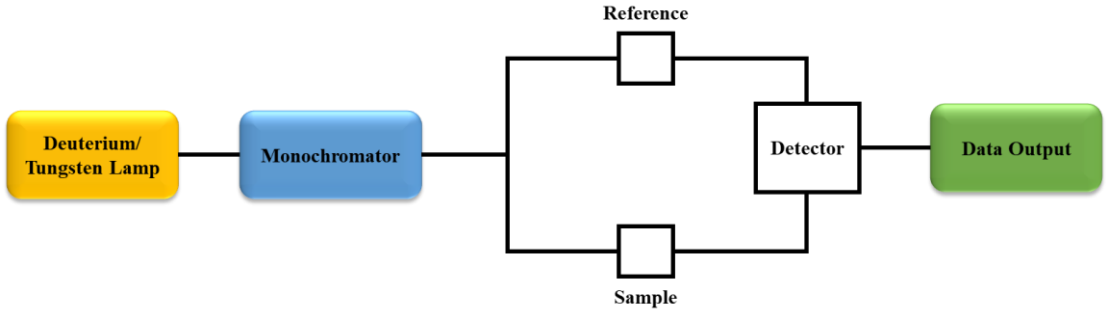

Figure 2.1 Schematic representation of UV-Visible Spectrometer.

2.3.2 Steady-state Spectrofluorimeter

In my present thesis, photoluminescence (PL) spectra were recorded on a Horiba Jobin Yvon Spectrofluorometer (FluoroMax-4) and Horiba 'FluoroLog-3' Spectrofluorimeter. To perform a qualitative or quantitative study, the spectrofluorometer irradiates a sample with a suitable excitation light source and detects the fluorescence emitted from the irradiated sample. The block diagram of the instrument is shown in Fig. 2.2. The brief description of its components is given below:

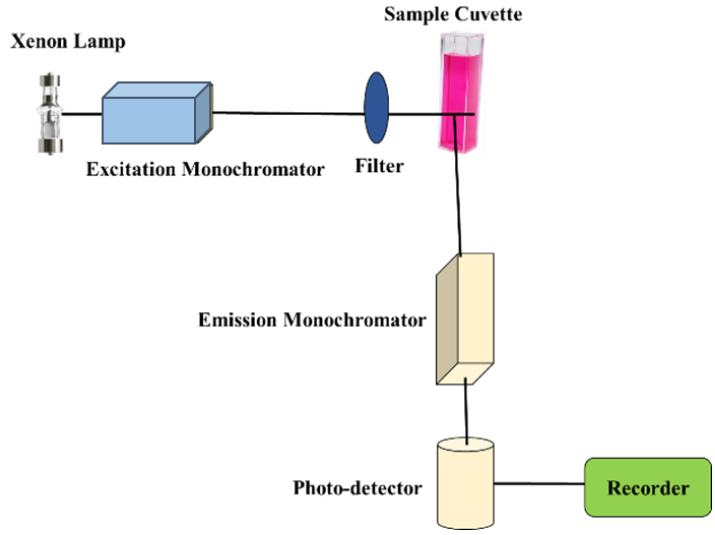

Figure 2.2 Block diagram of a steady-state spectrofluorometer.

This instrument is equipped with a light source of 1905-OFR 150-W Xenon lamp. This instrument has a 240-850 nm scan range. A cell containing the sample is kept in the cell holder. The photomultiplier tube (PMT) measures the fluorescence intensity after the emission monochromator receives the fluorescence that the sample emits. The photomultiplier tube used

in this effective response is the detector for the photometry and monitor sides. This preserves maximum resolution and instant reproducibility. The sample was taken in a Quartz cuvette (Hellma, 1 cm light path, capacity 3.5 ml, Model: 101-QS) with four transparent walls to measure the excitation and emission spectra.

2.3.3 Quantum Yield (QY) Measurement

The quantum yields of solid and liquid forms of the polymer were measured on the Quanta Phi Horiba integrating sphere-based instrument, which has an accessory of quantum yield (QY) and CIE measurement for the fluorometers. The solid powdered compound was placed in the cups provided. Additionally, it has a bottom-loading drawer for solid/powder samples that prevents contamination.[4] The lifetime decay [time-correlated single photon counting (TCSPC)] spectra of the iridium(III) complex and organic compounds in different solvents were obtained with a Spectrofluorometer HORIBA Jobin Yvon FluoroCube at BITS Pilani, Pilani campus, and Spectrofluorometer FLS920- s Edinburgh (AIRF, JNU, New Delhi).

2.3.4 Computational study

The Gaussian 09 and Gaussian 16 software suites were used to perform the Density Functional Theory (DFT) computations.[5] Beckes three-parameter hybrid exchange functional with the Lee-Yang–Parr gradient-corrected correlation (B3LYP functional),[6, 7] for larger correlation (CAM- B3LYP), Perdew–Burke-Ernzerhof (PBE functional), and the basis set 6-31G(+), 6-31G(++)(d,p), LANL2DZ (Los Alamos National Laboratory 2 double-ζ), the level was used in both the DFT and TD-DFT methods. All calculations were performed using the Integral Equation Formalism-Polarizable Continuum Model (IEF-PCM) for the solvents.[8]

2.3.5 Other instruments

^{1}H NMR, ^{13}C NMR, and ^{31}P NMR spectra were recorded by 400 MHz Brucker NMR spectroscope. High-resolution mass spectra were recorded on Agilent 6545 Q-TOF LC/MS. The variation in particle size in the aggregated state was recorded by dynamic light scattering (DLS) experiment, using Anton Paar Litesizer 500 at 25 °C temperature. Raman analysis was studied by the HORIBASCI Raman instrument (model no. LabRAM HR EVO) using excitation lasers with 633 nm wavelength. Microscope version, XT Platform version, XT UI version, Modal- "APREO S" FE-SEM was used to investigate the morphology of the synthesized samples. Thermogravimetric analysis (TGA) was performed by TGA-50,

SHIMADZU equipment at 10 °C/min, under a nitrogen atmosphere. The infrared spectrum was recorded on a Shimadzu FTIR spectrophotometer (IRAffinity-1S).

The weight average molecular weight (M_w) of polymer P1 was estimated by a Gel Permeation Chromatography (GPC) system of Perkin Elmer (model Turbo matrix-40) at the Sophisticated Instrumentation Centre for Applied Research and Testing Lab at Anand, Gujarat. The used column is Pl- Gel Mix B with a flow rate of 1ml/min at 30 °C. Also, the M_w was estimated by another Waters Associates GPC system equipped with RI and UV detectors at the pharmacy department, BITS Pilani, Pilani Campus. Where polystyrene is used as an internal standard and THF as an eluent at a flow rate of 1.0 mL/min. Cyclic voltammetry (CV) measurements were carried out for the sample by using CH Instruments company's model CHI601E (220V AC 0.4A) at the Chemistry department, BITS Pilani, Pilani Campus. Tetrabutylammonium hexafluorophosphate (NBu_4PF_6) was used as the electrolyte in acetonitrile solvent at a scan rate of 100 mVs^{-1}. The working electrode-platinum disc, Ag/AgCl as a pseudo reference electrode, and Pt as a counter electrode were used for the experiment. The solutions were prepared in THF, and tetrabutylammonium hexafluorophosphate (0.1 M) was used as a supporting electrolyte. The grinding force or mechanical stress in mechanofluorochromism was recorded by using the Rheometer instrument, using Anton Paar MCR-92. Powder X-ray analysis was performed by using a Rigaku Mini Flex II diffractometer with incident radiation of Cu-Kα.

2.4 References

1. M.-H. Yang, P. Thirupathi and K.-H. Lee, *Organic Letters*, 2011, **13**, 5028-5031.
2. L. N. Neupane, J. M. Kim, C. R. Lohani and K.-H. Lee, *Journal of Materials Chemistry*, 2012, **22**, 4003-4008.
3. S. Kaur, V. Bhalla, V. Vij and M. Kumar, *Journal of Materials Chemistry C*, 2014, **2**, 3936-3941.
4. N. Hasebe, K. Suzuki, H. Horiuchi, H. Suzuki, T. Yoshihara, T. Okutsu and S. Tobita, *Analytical Chemistry*, 2015, **87**, 2360-2366.
5. A. D. Becke, *The Journal of Chemical Physics*, 1993, **98**, 5648-5652.
6. S. Marković and J. Tošović, *The Journal of Physical Chemistry A*, 2015, **119**, 9352-9362.
7. G. M. Morris, R. Huey, W. Lindstrom, M. F. Sanner, R. K. Belew, D. S. Goodsell and A. J. Olson, *Journal of Computational Chemistry*, 2009, **30**, 2785-2791.
8. H. Li and J. H. Jensen, *Journal of Computational Chemistry*, 2004, **25**, 1449-1462.

CHAPTER 3

CYCLOMETALATED IRIDIUM(III) COMPLEXES AS MOLECULAR SENSING PROBES

Chapter 3. Cyclometalated Iridium(III) Complexes as Molecular Sensing Probes

Part A. 3.1 'Aggregation-Induced Emission' Active Mono-Cyclometalated Iridium(III) Complex Mediated Efficient Vapor-Phase Detection of Dichloromethane

3.1.1 Introduction

The usage of volatile organic compounds (VOCs) is in high demand to solve our daily problems. It is often used for various purposes such as nail polish remover, perfumes, paints, etc., and most of them are hazardous.[1] Dichloromethane (DCM) is one of them which is commonly used as a solvent in laboratories and as a paint remover in industry. Also, it is used as a degreaser agent, an aerosol propellant, room deodorant, insecticide, and herbicide.[2, 3] It is well known that DCM inhalation causes severe health problems. A recent case of an injury in the finger due to DCM injection indicates the gravity of DCM toxicity.[4] High volatility and tremendous use of DCM result in significant contamination of air and water.[5] The development of a sensitive and selective sensing probe for hazardous volatile organic compounds (VOCs) is challenging in real-time applications.[6] DCM detection relies on mass spectroscopy,[7] gas chromatography,[8, 9], and bioluminescent markers.[10] All these techniques require high cost, considerable time, and significant effort. Although fluorescent-based sensing materials are reported for sensitive detection of many organic solvents, such as methanol, DCM, chloroform, tetrahydrofuran (THF), acetone, etc.[11-15] Still, there is a concern over fast response, lack of selectivity, or the need for specific kinds of substrates. In addition, a sensitive, selective, and reliable technique is needed in a real field application. Organic-based solid-state luminescent materials reveal a wide range of applications such as solar cells, organic light-emitting diodes (OLED), stimuli-responsive materials, metal ion sensing, bacterial imaging, etc.[16-20] But, traditional organic luminophores exhibit emission quenching in the aggregated state, known as 'Aggregation-caused Quenching' (ACQ), which limits their applications. Tang et al. and co-workers first proposed a new concept called 'Aggregation-induced Emission' (AIE) in 2001.[21] The luminescent efficiency of AIE-active molecules in the aggregated or solid state is stronger than their dispersed or solution state. The AIE-active compounds came to the fore as a novel advanced material due to their excellent performance in various fields of applications.[22]

Research has drawn more attention to fluorescence-based techniques because of their reliability which can reduce the response time in VOC detection.[23, 24] Liquid phase DCM sensing reported based on quick and easy turn-on fluorescence response, in which Ln(III) complexes sensing probe was synthesized by Schiff base-exchange reaction.[25] A metal-organic framework (MOF) material synthesized from tripyridyl phosphine and CuI was used for chlorinated solvent sensing (CH_2Cl_2, $CHCl_3$, and chlorobenzene).[26] The technique is based on the host-guest chemistry, where the guest solvent molecules are locked in the pores of MOF which induces luminescence enhancement. The MOF compound is non-emissive due to the possible internal vibrations in the absence of solvent molecules. These internal vibrations get restricted in the presence of solvent molecules to result in turn-on emission. Although the recyclability was high and response time was less (<1 s), the MOF sensing probe was not only selective to the DCM but could also sense chloroform and carbon tetrachloride, and the emissions were observed at the same wavelength (580 nm). An excited-state intramolecular proton transfer (ESIPT)-active N-linked salicylaldehyde Schiff base organic compound was utilized to detect DCM and Cs^+ and the turn-off emission fluorescence response was observed upon the ligand to metal charge transfer (LMCT) process.[27] In a solution phase, the DCM detection limit was found at 0.37% (v/v, 3700 ppm). All these studies show that significant insufficiency exists in DCM detection by the developed luminescent-based probes.

In the present work, we reported a new AIE-active mono-cyclometalated Ir(III) complex (M1) for sensitive and selective detection of DCM in a vapor phase. Originally, the synthesized M1 complex was non-emissive, but a turn-on with strong yellow emission was observed upon interaction with the DCM molecule. DCM vapor can be detected by using the M1-impregnated filter paper as well as on thin film. The recorded limit of detection (LOD) was found to be 4.9 ppm for DCM vapor with M1 pristine. To the best of our knowledge, till date, it is the lowest LOD obtained for sensitive and selective DCM detection with the reusable pristine probe.[28]

3.1.2 Results and Discussion

3.1.2.1 Experimental Procedure

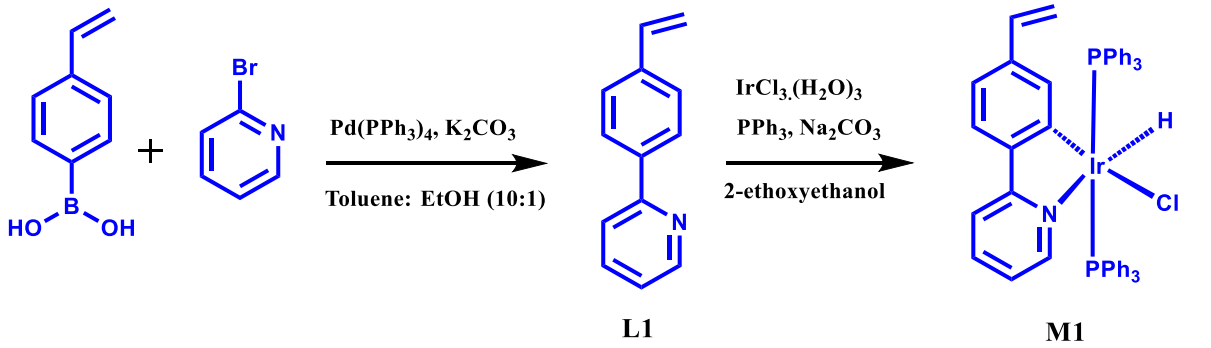

L1 **M1**

Scheme 3.1.1 Synthesis of the ligand L1 (2-(4-vinylphenyl)pyridine) and iridium(III) complex M1 [(ppy-vin)Ir(PPh_3)$_2$(Cl)(H)].

Synthesis of Ligand L1(2-(4-vinylphenyl)pyridine, i.e., ppy-vin): A mixture of 4-vinyl phenylboronic acid (1.31 g, 8.85 mmol), K_2CO_3 (3.29 g, 10.12 mmol), toluene: ethanol (10:1, 22 mL), 2-bromopyridine (1 g, 6.32 mmol) stirred in a 250 mL round bottom flask under N_2 gas for 5 min. Then, the catalyst tetrakis (triphenylphosphine) palladium(0) was added and refluxed for 5 h at 100 °C temperature. After completion of the reaction, it was cooled to room temperature and the reaction was quenched with the addition of water. The reaction mixture was washed with brine solution and then extracted with ethyl acetate. Finally, it dried with anhydrous Na_2SO_4, (the insoluble palladium catalyst residues were removed by filtration over celite). Purified the crude product by column chromatography. Hexane: Ethyl acetate (95:5) used as eluent. The desired vinyl-substituted phenyl pyridine ligand was isolated in the form of a colorless oil (yield, 83.8%). The product was characterized by ^{1}H and ^{13}C spectra. In ^{1}H NMR the peaks at 5.3, 5.8 and 6.8 ppm indicate vinylic protons of L1, and in ^{13}C NMR the peaks at 114.4 and 136.4 ppm indicate the vinylic carbons of L1.

^{1}H-NMR (400 MHz, Chloroform-*d*) δ 8.72 (d, J = 4.6 Hz, 1H), 8.00 (d, J = 8.4 Hz, 2H), 7.81–7.72 (m, 2H), 7.55 (d, J = 8.3 Hz, 2H), 7.25 (ddd, J = 6.0, 4.9, 2.6 Hz, 1H), 6.80 (dd, J = 17.6, 10.9 Hz, 1H), 5.85 (dd, J = 17.6, 0.9 Hz, 1H), 5.33 (dd, J = 10.9, 0.9 Hz, 1H) (Fig 3.1.1).

^{13}C-NMR (101 MHz, Chloroform-*d*) δ 157.01, 149.68, 138.70, 138.20, 136.74, 136.40, 127.04, 126.62, 122.09, 120.42, 114.49 (Fig 3.1.2).

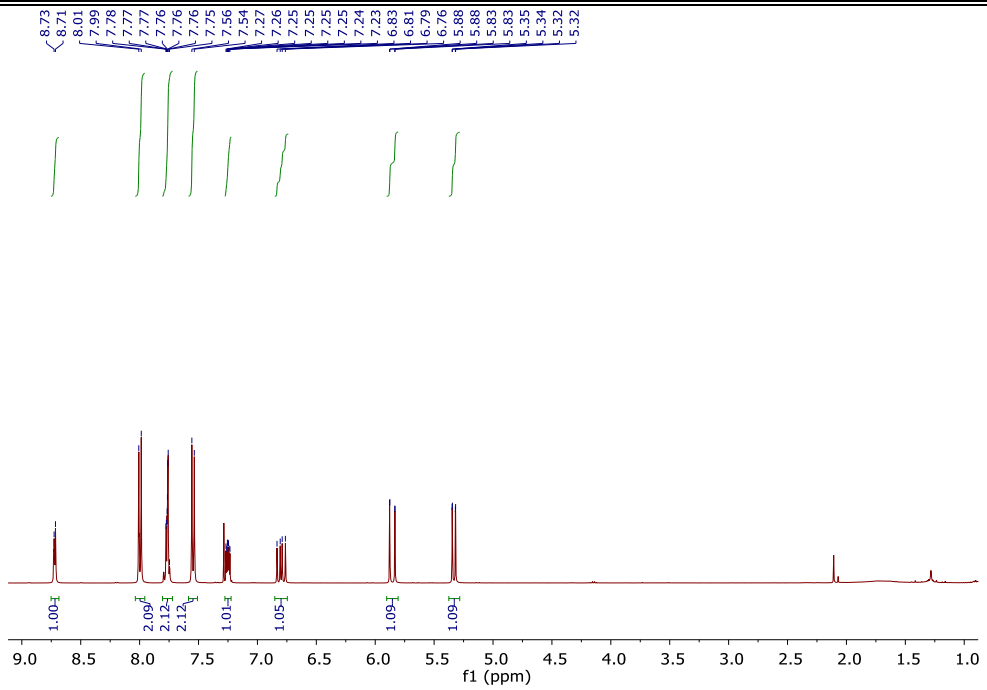

Figure 3.1.1. ^{1}H NMR spectrum of L1 in $CDCl_3$ solvent.

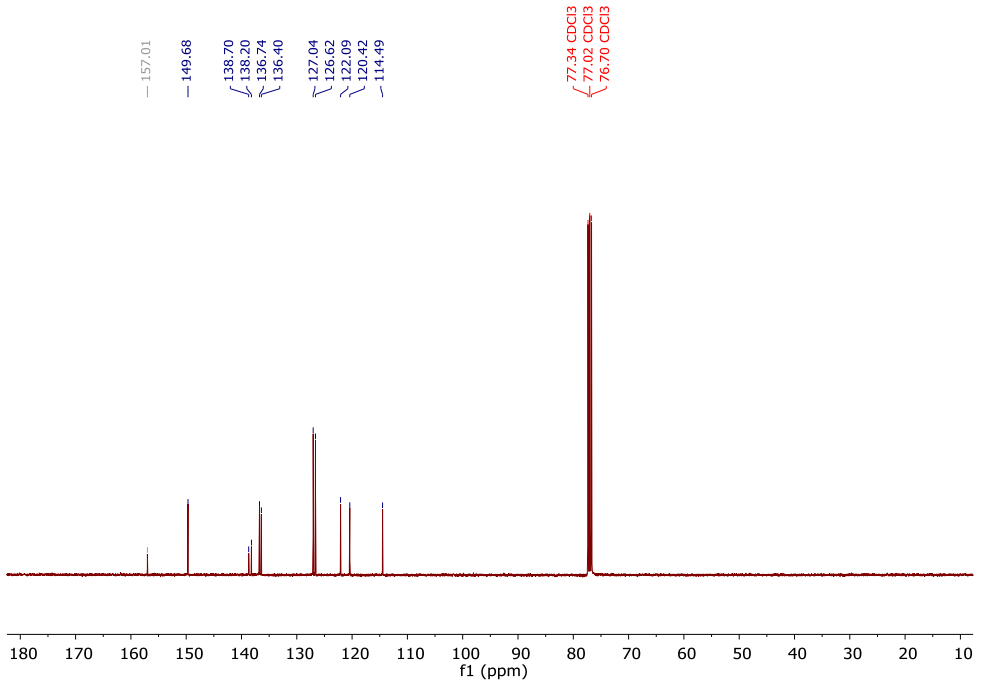

Figure 3.1.2. ^{13}C NMR spectrum of L1 in $CDCl_3$ solvent.

Synthesis of Iridium(III) Complex M1 (ppy-vinIr(PPh$_3$)$_2$ClH): A mixture of iridium(III) chloride hydrate (0.216 g, 1.19 mmol), triphenylphosphine (0.650 g, 2047 mmol), and 4 mL of 2-ethoxyethanol solvent stirred in a 50 mL round bottom flask for 3 h at 125 °C temperature. The reaction mixture turned into a yellow-colored liquid while stirring for 3 h. Then, Na_2CO_3 (0.432 g, 4.07 mmol) and L1 (0.216 g, 1.19 mmol) were added and refluxed for 3 h at 125 °C

temperature under the N_2 gas. The reaction was quenched with the addition of water and then extracted with ethyl acetate. Finally, it dried with anhydrous Na_2SO_4. The crude product was purified by column chromatography, with Hexane: Ethyl acetate (80:20) used as eluent. The desired product (yellow-colored solid) was isolated with a 40% yield. The product was characterized by ^{1}H, ^{13}C, and ^{31}P-NMR spectra. In ^{1}H NMR the characteristic peak at –16.8 ppm is for hydrogen coordinated with iridium metal and in ^{13}C NMR the peaks around 127.1 and 134 ppm aromatic protons in PPh_3 of M1.

^{1}H-NMR (400 MHz, Chloroform-*d*) δ 8.97 (d, J = 5.6 Hz, 1H), 7.42–7.36 (m, 15H), 7.18–7.15 (m, 7H), 7.12 (dt, J = 7.4, 1.2 Hz, 11H), 6.65 (dt, J = 7.1, 1.6 Hz, 2H), 6.29 (s, 1H), 5.95 (dd, J = 17.5, 10.8 Hz, 1H), 5.13 (dd, J = 17.5, 1.4 Hz, 1H), 4.85 (dd, J = 10.8, 1.4 Hz, 1H), -16.82 (s, 1H) (Fig 3.1.3).

^{13}C-NMR (101 MHz, Chloroform-*d*) δ 149.78, 141.77, 137.61, 135.29, 134.14, 134.07, 134.02, 133.96, 131.94, 131.67, 131.41, 129.10, 128.99, 127.21, 127.16, 127.12, 122.30, 120.35, 117.61, 117.19, 112.30 (Fig 3.1.4).

^{31}P-NMR (162 MHz, Chloroform-*d*) δ 9.01 (Fig 3.1.5) and thin peak is for the phosphorous of PPh_3 in M1.

ESI-HRMS calculated: The observed mass for M1 is $[M\text{-}Cl]^+$: m/z = 898.23 and calculated is $[M\text{-}Cl]^+$: m/z = 898.21 (Fig 3.1.6).

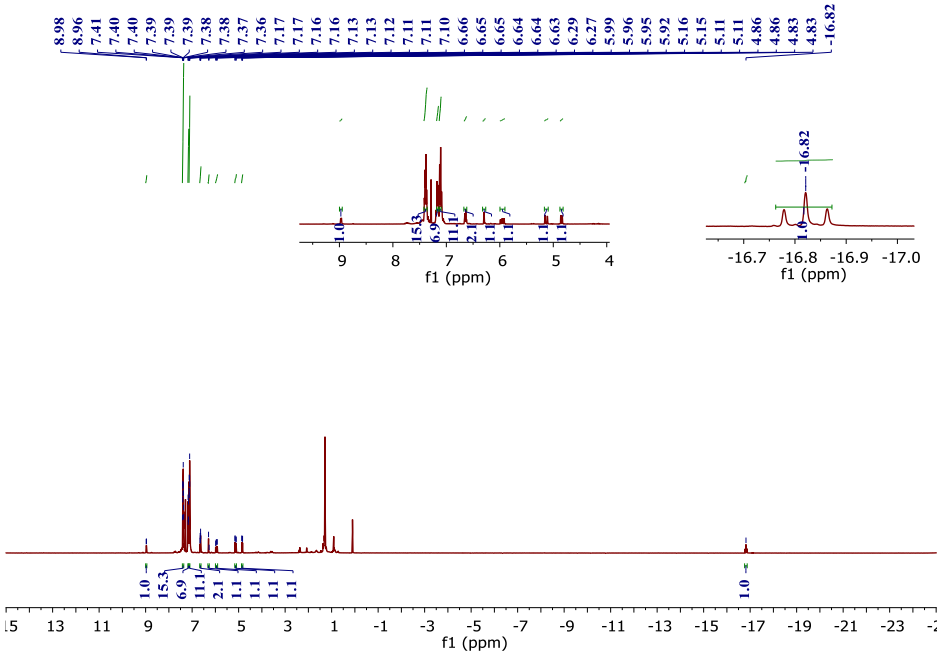

Figure 3.1.3. ^{1}H NMR spectrum of M1 in $CDCl_3$ solvent.

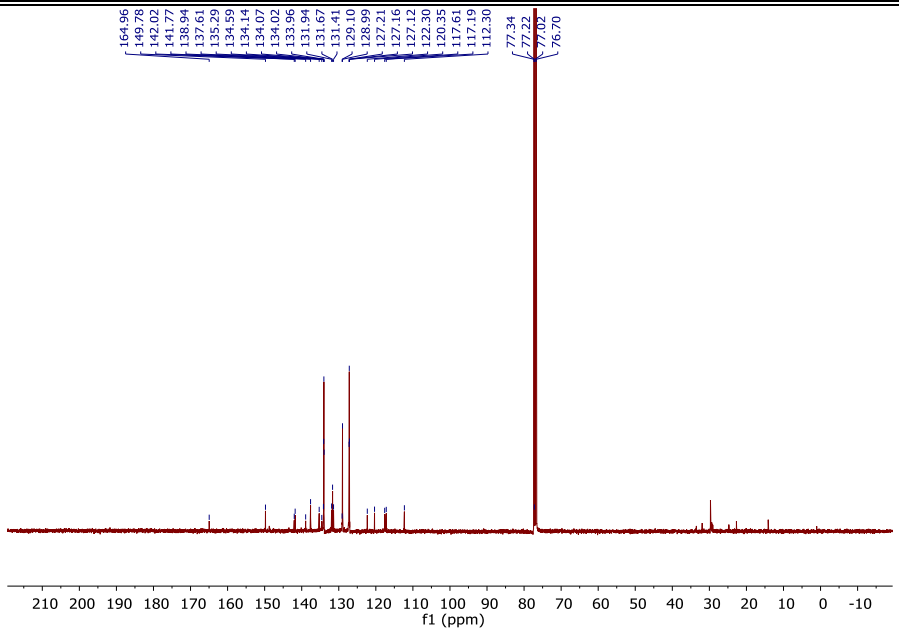

Figure 3.1.4. ^{13}C NMR spectrum of M1 in $CDCl_3$ solvent.

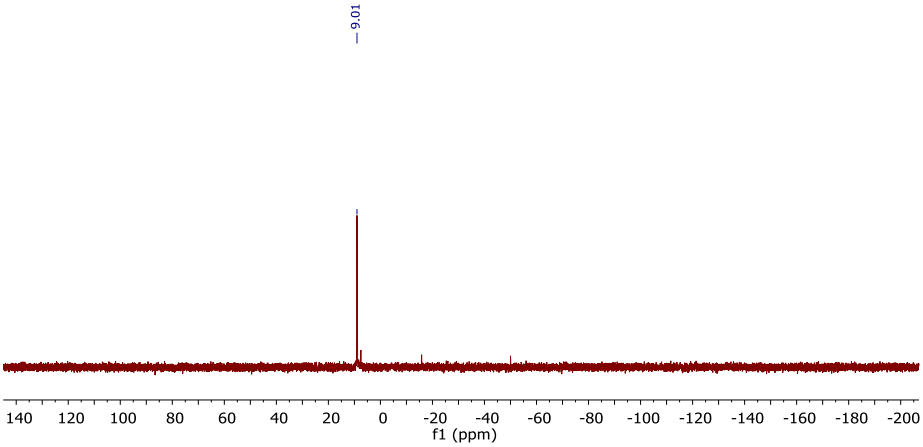

Figure 3.1.5. ^{31}P NMR spectrum of M1 in $CDCl_3$ solvent.

MS zoomed spectra:

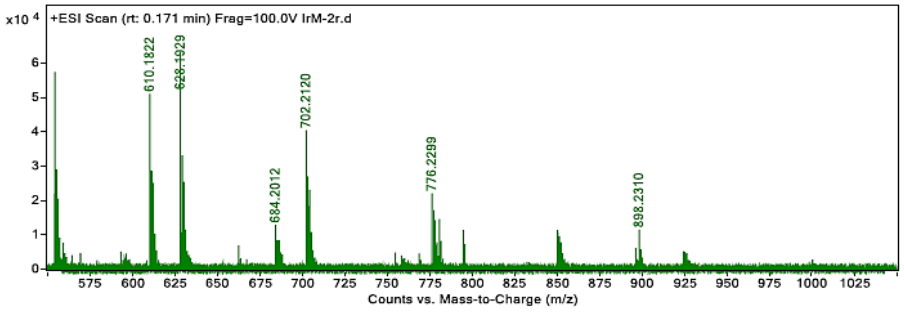

Figure 3.1.6. HRMS mass spectrum of M1.

The synthesized M1 is found as an 'aggregation-induced emission' (AIE)-active compound. The mixture of THF and hexane solvents was used to study the AIE experiment for M1. First

of all, the THF solution (10^{-3}M) of M1 was prepared. The 0.5 ml of prepared probe solution was added to four glass vials of 5 ml volume and then all four vials were equally filled with THF: hexane mixture by changing the percentage of hexane fractions (Fig 3.1.7). The PL spectra of all the prepared solutions were recorded and it indicates the PL intensity steadily increases with increasing hexane fractions. The AIE effect was explained based on the formation of aggregates with increasing concentrations of hexane in THF: hexane mixture which was analyzed by the DLS particle size distribution experiment.[29] The particle size for 0% hexane percentage (f_h) is observed at 52.3 nm (with PDI 0.2) and for 90% hexane percentage (f_h) is at 170.5 nm (with PDI 1.1) (Fig 3.1.8), which supports the formation of aggregates.

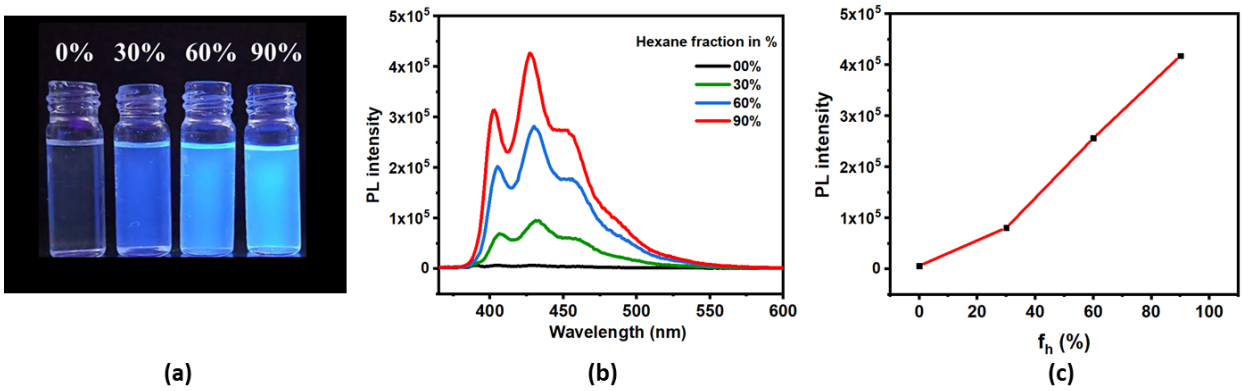

Figure 3.1.7. (a) Image of THF: hexane mixtures of M1 with various hexane fractions (f_h) in percentage (%) under UV lamp (365 nm); (b) PL spectra for the same under excitation of 360 nm wavelength; (c) Line plot for the changes in PL intensity for M1 with gradual increasing hexane percentage (f_h) in THF: hexane mixture.

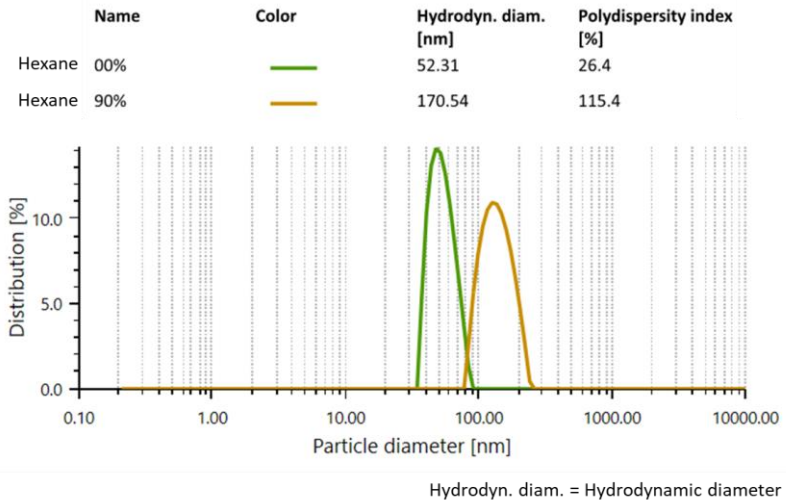

Figure 3.1.8. DLS particle size distribution plot of M1 particle (size) diameter in nm vs distribution (percent); (green colored) for M1 dissolved in THF; (orange colored) for M1 dissolved in 90% hexane.

Here, the AIE effect is speculated due to the RIM mechanism. To prove the RIM effect, a viscous solvent poly(ethylene)glycol (PEG) was chosen for the AIE study. Similarly, the series of THF: PEG mixture was prepared as described above (PEG was added in place of hexane) (Fig 3.1.9). Also, the PL intensity was recorded for the THF: PEG mixture, which shows an increase in the PL intensity steadily with increasing PEG fractions (gradual variation of viscosity of the medium) supporting the RIM mechanism.

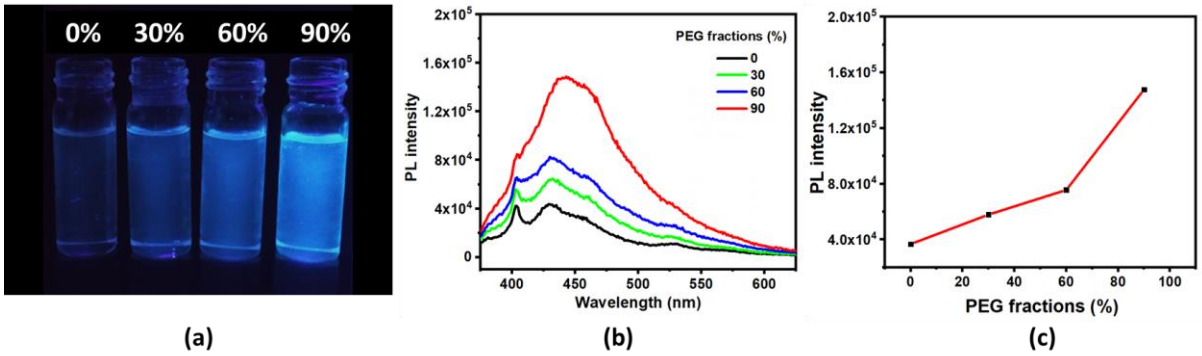

Figure 3.1.9. (a) Photograph of M1 in THF: PEG mixtures with different PEG fractions upon UV light irradiation (at λ_{exc}= 365 nm), (b) PL spectra for the same mixture under excitation 360 nm wavelength. (c) Line plot for the changes in PL intensity for the M1 with different PEG fractions.

The M1 detects DCM in powdered form as well as in thin film. The drop-casting method was used to make the thin film on a glass substrate. The non-emissive M1 shows turn-on yellow emission at 527 nm by putting a drop of DCM on powdered M1 and for thin-film upon 30 s exposure of DCM vapor generated by heating it at 33 °C (Fig 3.1.10). The DCM detection is also possible on M1-impregnated filter paper (Whatman No 1 filter paper) (Fig 3.1.11).

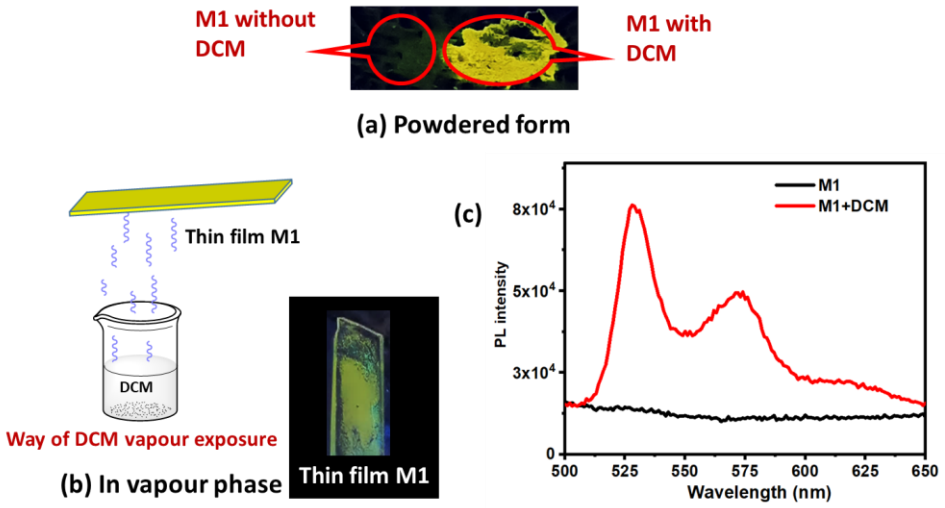

Figure 3.1.10. Photographs for DCM sensing: (a) in powdered form, (b) in the vapor phase with a representation showing the exposure of M1 thin film towards DCM vapors (drawn, left); actual image of emission after exposure to DCM vapor (right), (c) PL spectra for powdered M1 probe for before and after treated DCM (at λ_{exc} = 360 nm and λ_{max} = 527 nm).

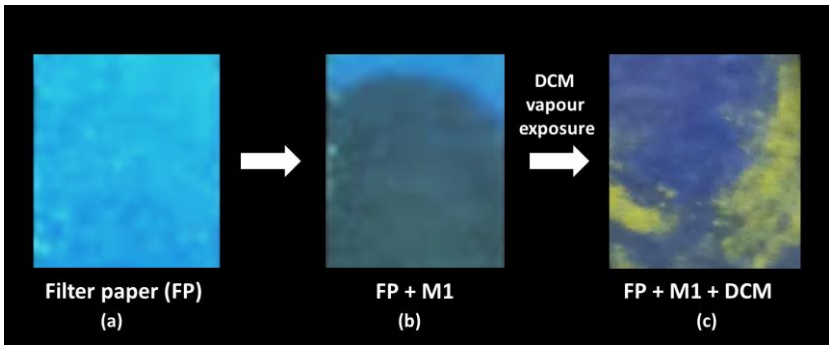

Figure 3.1.11. Photograph of filter paper (FP) under UV lamp (λ_{exc}, 365 nm): (a) filter paper (FP) only; FP impregnated with a toluene solution of M1 (b) without DCM vapor exposure, and (c) in the presence of DCM vapors (turn on emission can be observed in the presence of DCM vapors).

For the selectivity study, M1 was screened with different solvents which are generally used in laboratories and industries.[30] The solution of the M1 probe was prepared (1 mg M1 in 1 mL toluene) for this study. A drop of this prepared probe solution in an equal amount (20 µL) was placed on each of 24 small strips of Whatman No 1 filter paper by the drop-casting technique. The filter paper strips containing M1 were annealed under the oven for about one hour at 70 °C. The emission was observed under a UV lamp after putting a drop of various solvents on different annealed paper strips (Fig 3.1.12). The M1-soaked filter paper shows turn-on yellow emission in the presence of DCM and the same is observed with its' analogue dibromomethane

(DBM) only, while the other solvents-soaked filter paper remains unchanged under the same excitation (vide supra). This study reveals that the M1 selectively detects the DCM and DBM. The probe M1 reveals a similar emission response while testing with DCM and DBM in a powered state (λ_{exc}, 360 nm) (Fig 3.1.13).

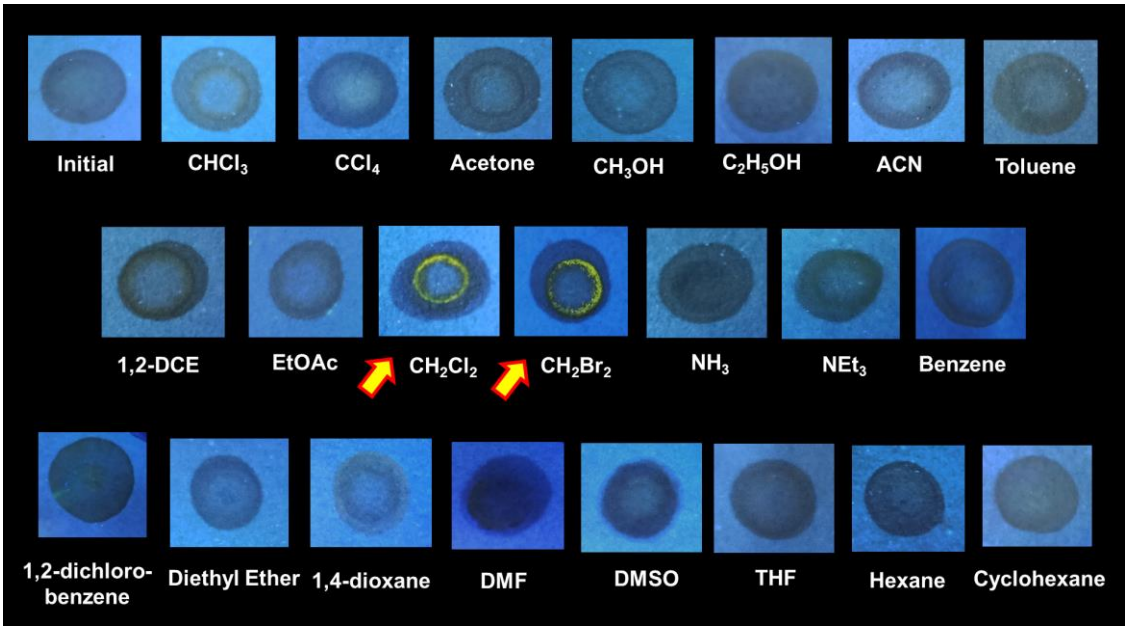

Figure 3.1.12. Image of filter paper strips containing M1 under UV lamp (λ_{exc}, 365 nm), after treated with the various solvents chloroform ($CHCl_3$), carbon tetrachloride (CCl_4), acetone, methanol (CH_3OH), ethanol (C_2H_5OH), acetonitrile (ACN), toluene, 1,2-dichloroethane (1,2-DCE), ethyl acetate (EtOAc), dichloromethane (CH_2Cl_2), dibromomethane (CH_2Br_2), ammonia (NH_3), triethylamine (NEt_3), benzene, 1,2-dichlorobenzene, diethyl ether, 1,4-dioxane, N, N-dimethylformamide (DMF), dimethyl sulfoxide (DMSO), tetrahydrofuran (THF), hexane, and cyclohexane (The arrows indicate the observed turn-on emission response with dichloromethane and dibromomethane only).

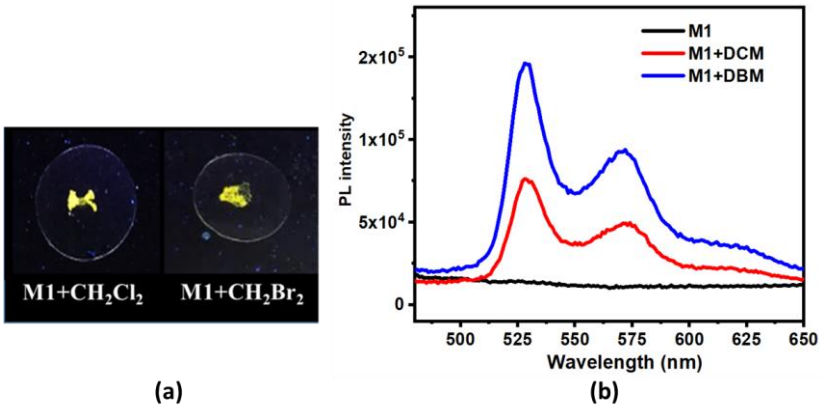

Figure 3.1.13. (a) Photographs of emission of powdered M1 with DCM (CH_2Cl_2) and DBM (CH_2Br_2) on glass film under the UV lamp (λ_{exc}, 365 nm), (b) Recorded PL spectra for the same under 360 nm excitation wavelength.

DBM is a high boiling solvent (97 °C) which rarely used in industries and laboratories compared to its analogue DCM. All the sensing studies were performed with DCM as focal attention. The selectivity of the probe M1 towards DCM was tested successfully after screening with different solvents. The vapor phase DCM detection was performed via a controlled experiment by generating a saturated DCM vapor in a closed pack container at a constant temperature, 33 °C for 48 h (Fig 3.1.14). The container with the outlet was tightly air-packed to eliminate all the possibilities for the leakage of the DCM vapor. The powdered M1 was fixed in the solid sample holder, and it was exposed to the DCM vapor at the outlet.

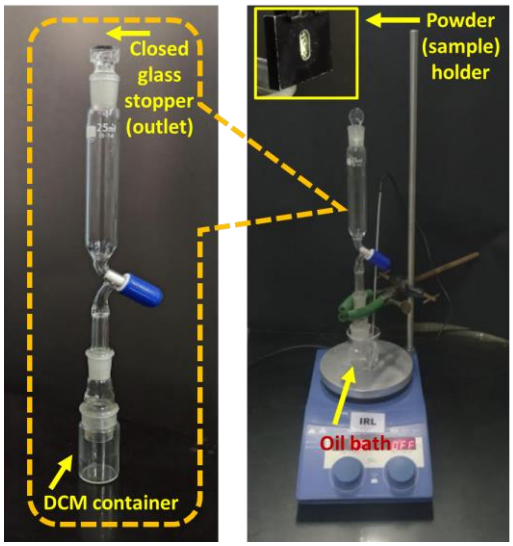

Figure 3.1.14. Photograph of DCM vapor sensing setup; enlarged view of DCM container connected with glass separating funnel (25 ml volume).

The emission spectra were recorded by irradiating the solid sample holder directly under 360 nm excitation (Fig 3.1.15). The DCM container was closed and kept in an oil bath. For each reading, the DCM was heated to 33 °C for two minutes to generate saturated vapors, and the M1 sample holder was exposed to the DCM vapor for 30 seconds at the outlet of the glass funnel for each reading. The saturated vapor pressure of DCM at 33 °C is 86 kPa.[31] Thus, for each reading, 86 kPa vapor of DCM was exposed to probe M1. The emission intensity gradually increased for each exposure of DCM vapor. The emission intensity gradually increased for each exposure of DCM vapor. To find out the optimized time required to form the saturated vapor, the exposure was given to the probe for 2-min and 20-min intervals. The

change of PL intensity for 2 min and 20 min intervals remained unchanged with respect to the initially recorded PL intensity. It shows the saturated vapor of DCM was generated within 2 min intervals (Fig. 3.1.16). A linear relationship can be observed between DCM vapor concentration from 0 to 1204 kPa and the emission intensity of M1 for the same. The limit of detection (LOD) was obtained at 4.9 ppm (0.000497 kPa; calculation shown in Fig 3.1.15) in the vapor phase, which is much less than the saturated vapor pressure of DCM at 33 °C (86 kPa). Also, the obtained LOD crosses the setting inhalation limit (75 to 100 ppm for an hour of inhalation).[32]

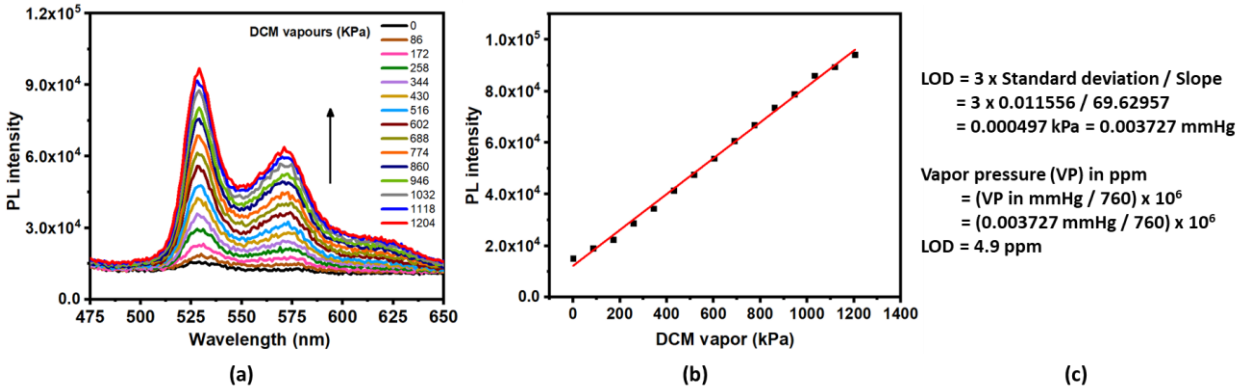

Figure 3.1.15. (a) PL plot for M1 (powdered in solid sample holder) with gradually increasing DCM vapor concentration excited at 360 nm, (b) Plot between PL intensity of M1 vs. DCM vapor concentration (kPa) (Pearson's r value = 0.99), (c) calculation of limit of detection for M1 in the vapor phase with the conversion of vapor pressure from kPa to ppm.

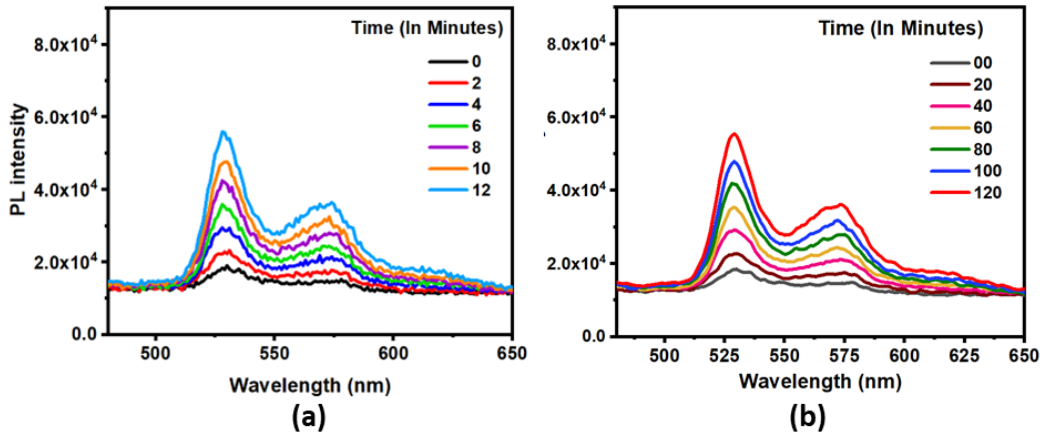

Figure 3.1.16: PL intensities plot for M1 at two different times of DCM vapor pressure saturation, (a) for 2 minutes, (b) for 20 minutes (excited at 360 nm).

The probe M1 can be recycled after being treated with DCM vapor by keeping it in the open air. The emission intensity of the probe was decreased gradually and returned to pristine form after keeping the powder at 25 °C for 40 min. The rate of DCM desorption is accelerated by heating the sample at 80 °C continuously for 30 s. The experiment was repeated several times to study the stability and reusability of the probe in the vapor phase (Fig 3.1.17). The emission intensity of M1 almost remains the same, even if in the seventh cycle. Hence, the same probe M1 can be reused again for further sensing applications.

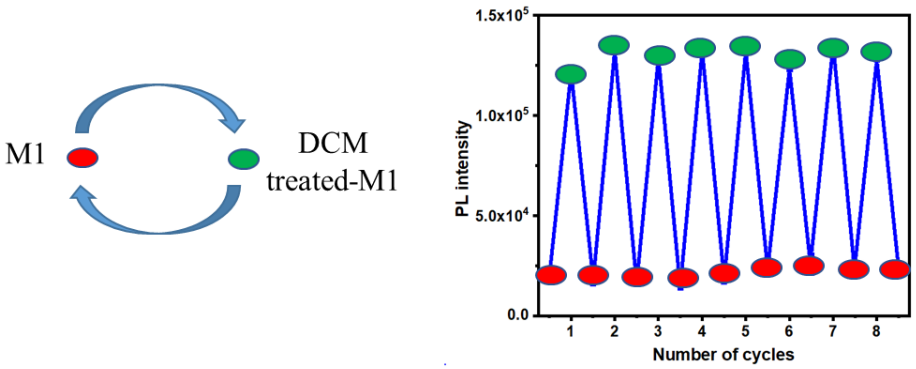

Figure 3.1.17. PL intensity plot for the recyclability study of M1 with DCM vapors.

The halo atom (from DCM or chloroform) behaves as an electron acceptor and interacts with the electron-rich species through halogen bonding.[33-36] Herein, the H-bonding was observed with chlorine, and it was supported by Raman spectroscopy. The mechanism for sensitive and selective sensing of DCM towards M1 was studied by the Raman spectroscopy experiment. The observed Raman peak explains the DCM interaction with M1 shown in the schematic representative structural model with labeled characteristic bonds (Fig 3.1.18).

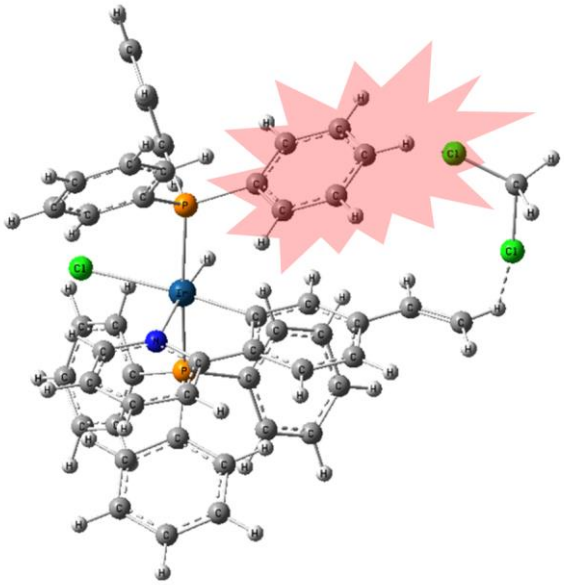

Figure 3.1.18. Schematic representative structural model for the interaction of DCM with M1 labeling with characteristic bonds, 'a' denotes C-Cl and 'b' indicates C-H bonds of a bound DCM; 'c', 'd' and 'e' shows the vinylic C-H bonds of M1, and 'f' is the phenyl ring of triphenylphosphine (PPh_3).

The symmetric Raman stretching peaks for C-Cl and C-H of a bare DCM molecule were reported at 713 and 2996 cm^{-1}, respectively.[37] Some changes in the original stretching peaks of C-Cl and C-H were observed while treating M1 with DCM. The symmetric stretching of C-Cl (a) is reduced to 699 cm^{-1} and C-H (b) is lowered from 2996 cm^{-1} to 2982 cm^{-1} (Fig 3.1.19 and 3.1.19B and Table 3.1.1). After treatment with DCM, the original Raman peak for the vinylic C-H (c) substituent of M1 is also changed. The original Raman peak for C-H (c) bending of substituted vinylic carbon ($=CH_2$), which is trans to phenyl pyridine of M1 was observed at 1025 cm^{-1} for M1 that reduced to 1022 cm^{-1} (Figure 3.1.20A). It was the broader and clearer observation of splitting as compared to bare M1 (considered as monoalkyl vinyl).[38] In the case of C-H stretching of vinylic parts, bending vibrations of vinylic carbon ($=CH_2$) such as cis C-H (d) and a stretching C-H (e) of vinyl carbon (-CH=) observed at 644 cm^{-1} and 3057 cm^{-1}, respectively.[31] These original vibrational Raman peaks for these bonds were retained as compared with the DCM-treated M1 (Fig 3.1.19 and 3.1.20B and Table 3.1.1).

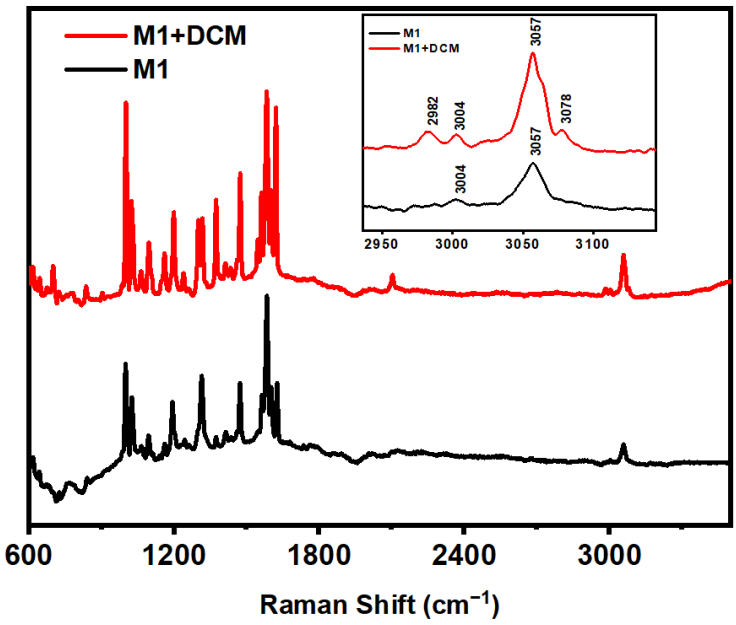

Figure 3.1.19. Raman plot for solid M1 before and after DCM treatment (inset: enlarged view of several peaks).

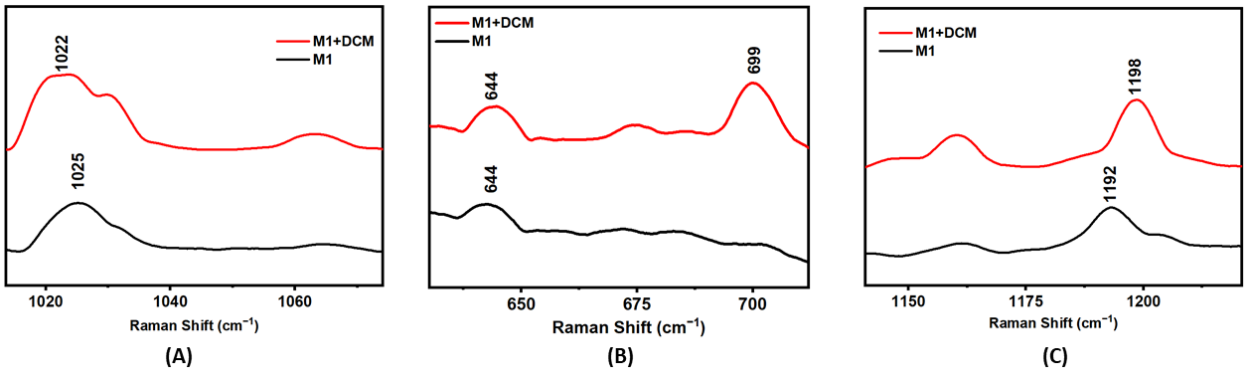

Figure 3.1.20. Enlarged views of RAMAN spectra (partwise): (A) The bending peak for C-H(c) of vinyl (=CH_2), (B) the cis C-H(d) bending vibrations of vinyl (=CH_2) and symmetric stretching C-Cl(a) of treated DCM at 699 cm^{-1}, (C) phenyl ring vibrations; (f) for mono-substituted phenyl of triphenylphosphine (PPh_3) increased from 1192 to 1198 cm^{-1}.

Table 3.1.1. Various vibrational modes for M1 and DCM-treated M1 were recorded by Raman spectroscopy.

	Raman Shifts (cm^{-1})			
Vibrational Modes	**DCM only**	**DCM (in M1+DCM)**	**M1 only**	**M1 (in M1+DCM)**
C-Cl symmetric stretching (a)	713	699	--	--
C-H symmetric stretching (b)	2996	2982	--	--
C-H bending (c)	--	--	1025	1022
C-H bending (d)	--	--	644	644

C-H stretching (e)	--	--	3057	3057
C-H antisymmetric stretching of vinylic carbon (=CH_2) (c, d)	--	--	--	3078
C-H symmetric stretching of vinylic carbon (=CH_2) (c, d)	--	--	3004	3004
Phenyl ring vibrations of triphenylphosphine (PPh_3) (f)	--	--	1192	1198

Furthermore, a new peak at 3078 cm^{-1} was observed which corresponds to the asymmetrical stretching of C-H (c, d) of vinylic carbon (=CH_2) of M1 for the case of DCM treated M1 (the same peak was not observed for the M1 only) (Fig 3.1.19). However, the original symmetrical stretching peak for C-H (c, d) of vinylic carbon (=CH_2) was observed at 3004 cm^{-1} for M1, which becomes stronger, relative to the DCM-treated M1 (Fig 3.1.19). We have performed the Raman analysis for the M1 with dibromomethane (DBM) as well (Fig 3.1.21 and 3.1.22, and Table 3.1.2) and diiodomethane (DIM) (Fig 3.1.23 and 3.1.24, and Table 3.1.3). A change in Raman shift for M1 with DBM was observed nearby similar to DCM interactions with M1, while no change in Raman shift was observed with DIM. After studying the Raman peaks, all the changes are centered on interactions between the C-Cl of DCM and C-H (c) of the vinylic substituent of M1. Overall, it was observed that the C-Cl (a) of DCM loosely interacts with the *trans* C-H (c) of vinyl (=CH_2) of M1 after exposing it to DCM. Thus, the proposed model can be supported by Raman spectroscopy.

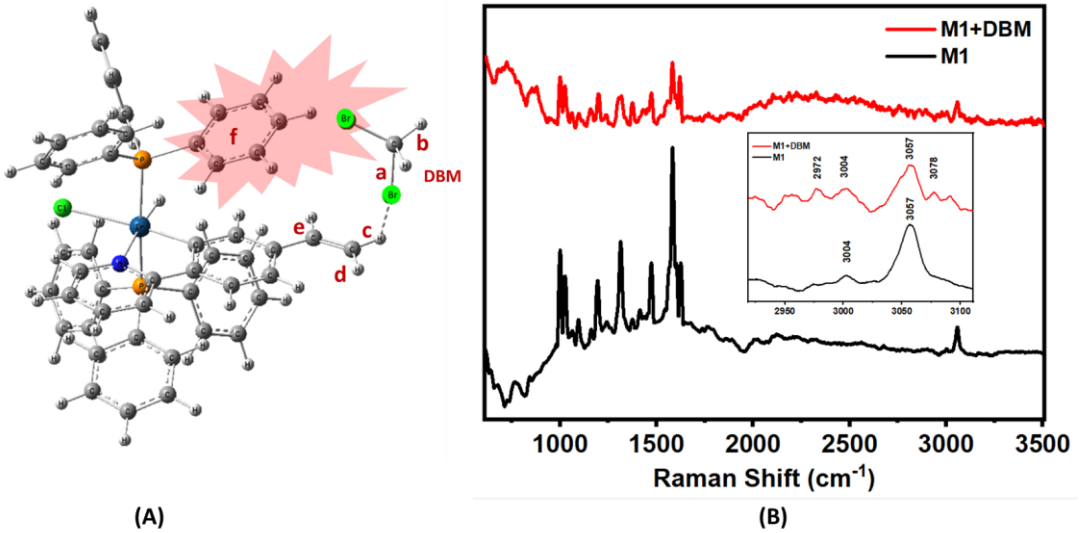

Figure 3.1.21. (A) Schematic representation for the structural model of interaction of DBM with M1 labeling with characteristic bonds: C-Br (a) and C-H (b) bonds of a bound DBM; (c), (d), and (e) are the vinylic C-H bonds of M1; and (f) is the phenyl ring of triphenylphosphine

(PPh_3), (B) Raman spectra for solid M1 before and after DBM treatment (inset: enlarged view of several peaks).

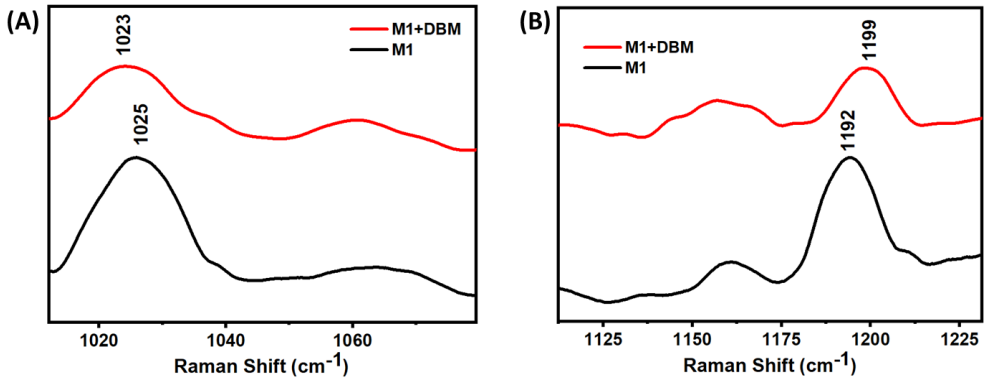

Figure 3.1.22. Enlarged views of Raman spectra for DBM with M1 (partwise): (A) The bending peak for C-H(c) of vinyl (=CH_2), (B) phenyl ring vibrations(f) (for mono-substituted phenyl of triphenylphosphine (PPh_3) increased from 1192 to 1199 cm^{-1}).

Table 3.1.2. Various vibrational modes for M1 and DBM-treated M1.

	Raman Shift (cm^{-1})	
Vibrational modes	M1 only	M1 (in M1+DBM)
C-H bending (c)	1025	1023
C-H stretching (e)	3057	3057
C-H antisymmetric stretching of vinylic carbon (=CH_2) (c, d)	--	3078
C-H symmetric stretching of vinylic carbon (=CH_2) (c, d)	3004	3004
Phenyl ring vibrations of triphenylphosphine (PPh_3) (f)	1192	1199

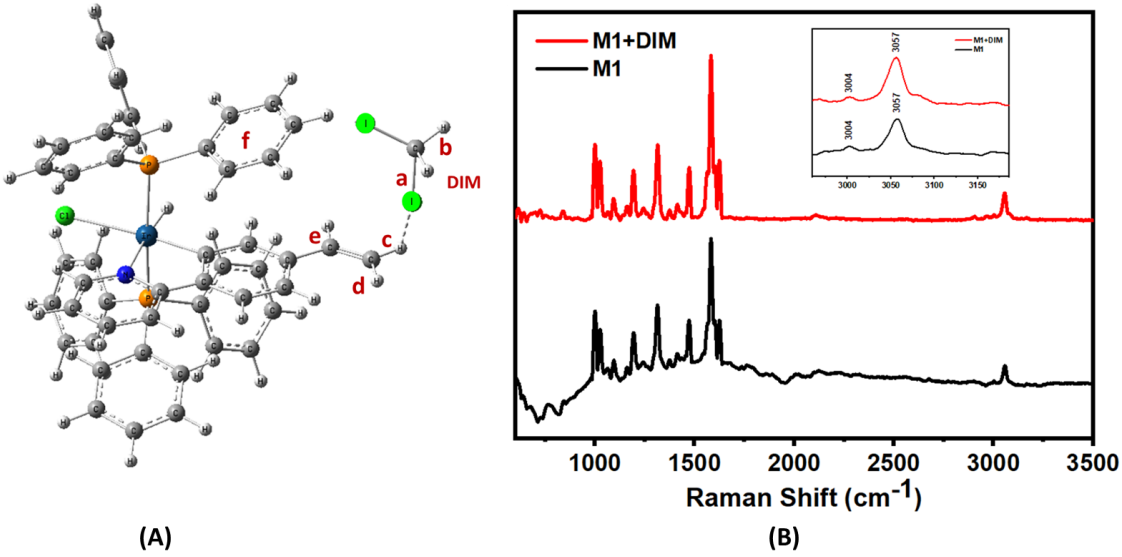

Figure 3.1.23. (A) Schematic representative structural model of interaction of DIM with M1 labeling with characteristic bonds; (a) C-I and (b) C-H bonds of a bound DIM; (c), (d), and (e) are the vinylic C-H bonds of M1; and (f) is the phenyl ring of triphenylphosphine (PPh_3), (B) Raman spectra for solid M1 before and after DIM treatment (inset: enlarged view of several peaks).

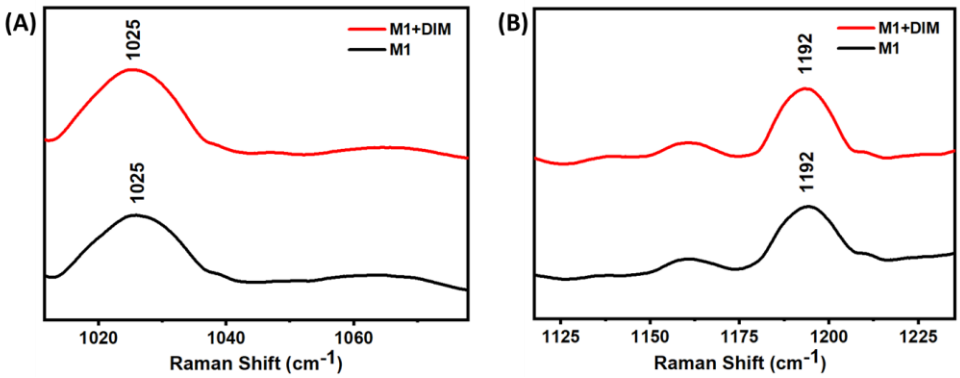

Figure 3.1.24. Enlarged views of Raman spectra for DIM with M1 (partwise): (A) The bending peak for C-H(c) of vinyl (=CH_2), (B) phenyl ring vibrations(f); for mono-substituted phenyl of triphenylphosphine (PPh_3) 1192 cm^{-1}.

Table 3.1.3. Various vibrational modes for M1 and DIM-treated M1.

	Raman Shift (cm^{-1})	
Vibrational modes	M1 only	M1 (in M1+DIM)
C-H bending (c)	1025	1025
C-H stretching (e)	3057	3057

C-H antisymmetric stretching of vinylic carbon (=CH_2) (c, d)	--	--
C-H symmetric stretching of vinylic carbon (=CH_2) (c, d)	3004	3004
Phenyl ring vibrations of triphenylphosphine (PPh_3) (f)	1192	1192

Moreover, the Raman peak of phenyl ring vibrations (i.e., in-plane bending vibrations) (f) for the phenyl group of triphenylphosphine (PPh_3) increased from 1192 to 1198 cm^{-1} (Fig 3.1.19 and 3.1.20C and Table 3.1.1).[39] The fact can be rationalized with the lowering of the vibrations of the phenyl ring due to the restriction imposed by the DCM molecule (Fig 3.1.18 and 3.1.20C). As a result, the turn-on emission was observed.[26, 40] The turn-on emission of M1 is further supported by low-temperature emission analysis (Fig 3.1.25). The non-emissive powdered M1 shows the same kind of yellow emission at low temperatures where turn-on luminescence is possible by restricted intramolecular motion (RIM).[41] From the observation of FESEM images, M1 shows an interlinked nano-rod structure (Fig 3.1.26). A porous with a honey-comb type of structure was observed in a FESEM image for DCM-treated M1. From the thermogravimetric analysis (TGA) analysis of M1, the weight loss was studied for M1, and DCM-treated M1 (Fig 3.1.27).

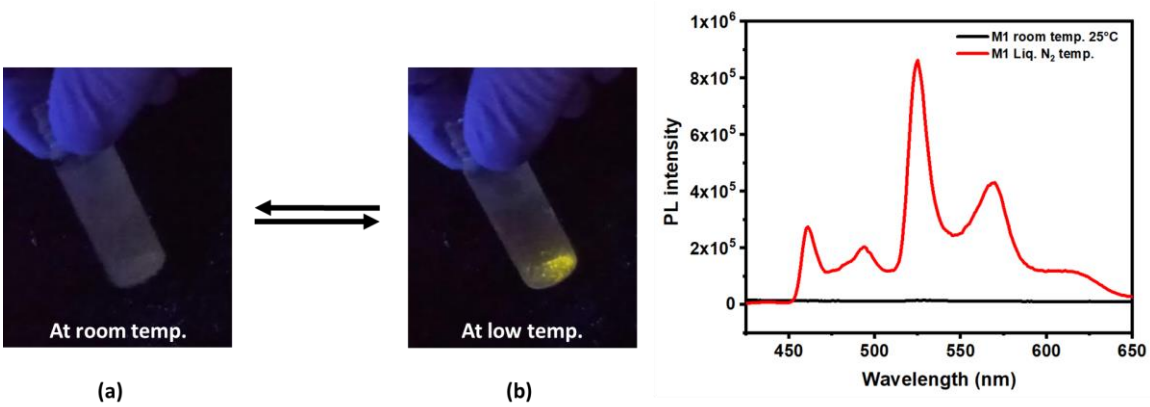

Figure 3.1.25. (a) Photograph of a glass vial containing a little amount of non-emissive powdered M1 at room temperature under the UV lamp (365 nm); same glass vial dipped into the liquid nitrogen for 10 sec. to achieve low temperature, (b) Photograph of same glass vial under the UV lamp (365 nm) immediately after taking out from liquid nitrogen; with corresponding PL spectra for at room temperature (25 °C) and liquid N_2 temperature. It showed the similar emission (λ_{max} = 527) nm as the one observed in presence of DCM at room temperature (in Fig 3.1.15).

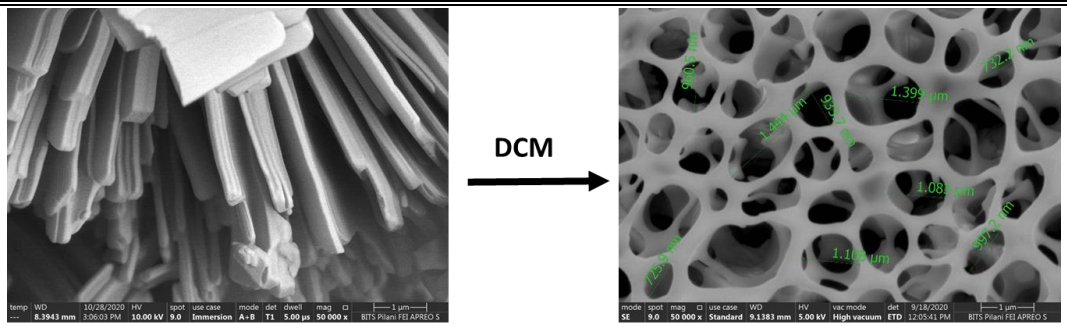

Figure 3.1.26. FESEM images for (a) before and (b) after the addition of DCM to powdered M1.

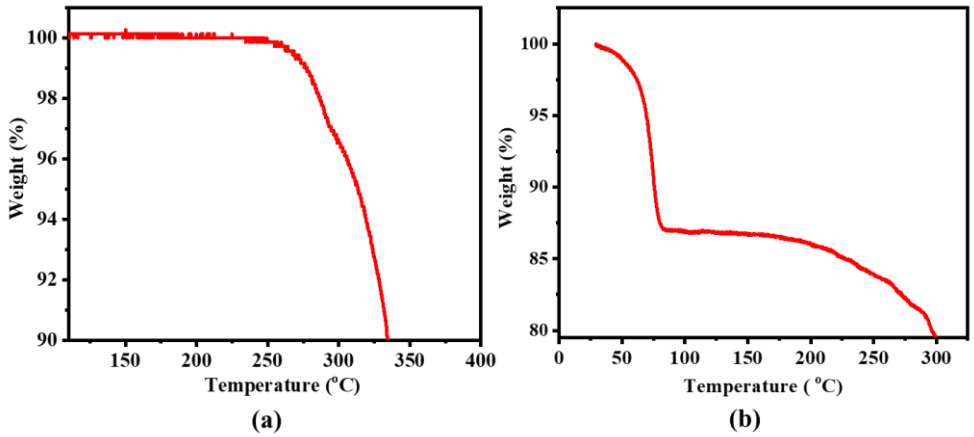

Figure 3.1.27. TGA plot, (a) for compound M1; (b) for DCM-treated M1.

The synthesized M1 is thermally stable up to 250 °C temperature. The sample holder containing powdered M1 was exposed to DCM and excess DCM was evaporated by keeping it in the open air for 5 min. The DCM-treated M1 was analyzed by TGA, and it was observed to have around 13% weight loss at up to 80 °C. It supports the presence of DCM was bound to M1 in DCM-treated M1. This work concludes the M1 is highly sensitive and selective for DCM in a vapor phase. It shows an instant turn-on emission response (a response time <30 sec) in pristine form. The calculated detection limit is 4.9 ppm for DCM vapor and M1 is found to be a stable and reusable efficient probe.

3.1.3 References

1. D. R. Joshi and N. Adhikari, *Journal of Pharmaceutical Research International*, 2019, **28**, 1-18.
2. *IARC monographs on the evaluation of carcinogenic risks to humans*, 1999, **71 Pt 1**, 251-315.

3. R. D. Morrison, B. L. Murphy and R. E. Doherty, in *Environmental Forensics*, eds. R. D. Morrison and B. L. Murphy, Academic Press, Burlington, 1964, pp. 259-277.
4. S. Vidal, *ACS Central Science*, 2020, **6**, 83-86.
5. D. S. MacMillan, J. Murray, H. F. Sneddon, C. Jamieson and A. J. B. Watson, *Green Chemistry*, 2012, **14**, 3016-3019.
6. H.-Y. Li, S.-N. Zhao, S.-Q. Zang and J. Li, *Chemical Society Reviews*, 2020, **49**, 6364-6401.
7. D. Poli, P. Manini, R. Andreoli, I. Franchini and A. Mutti, *Journal of Chromatography B*, 2005, **820**, 95-102.
8. J. Han and S. M. Yoon, *IEEE Journal of Selected Topics in Quantum Electronics*, 2012, **18**, 1547-1552.
9. T. Sakai, Y. Morita and C. Wakui, *Journal of Chromatography B*, 2002, **778**, 245-250.
10. N. Lopes, S. A. Hawkins, P. Jegier, F.-M. Menn, G. S. Sayler and S. Ripp, *Journal of Industrial Microbiology and Biotechnology*, 2012, **39**, 45-53.
11. Y. Jiang, J. Ma, J. Lv, H. Ma, H. Xia, J. Wang, C. Yang, M. Xue, G. Li and N. Zhu, *ACS Sensors*, 2019, **4**, 152-160.
12. A. Husain, *Journal of Science: Advanced Materials and Devices*, 2021.
13. H. Zhang, X. Niu, S. Zhu, M. Tian and W. Liu, *Journal of Applied Polymer Science*, 2021, **n/a**, 51699.
14. Y. Duan, Y. Liu, H. Han, X. Zhang, M. Zhang, Y. Liao and T. Han, *Spectrochimica Acta Part A: Molecular and Biomolecular Spectroscopy*, 2021, **252**, 119515.
15. Y. Liu, Y. Fan, C. Hou, W. Du, D. Zhang, Y. Liu, J. Xu and Y.-L. Bai, *Inorganic Chemistry*, 2021, **60**, 16370-16377.
16. H. Liu, Q. Bai, L. Yao, H. Zhang, H. Xu, S. Zhang, W. Li, Y. Gao, J. Li, P. Lu, H. Wang, B. Yang and Y. Ma, *Chemical Science*, 2015, **6**, 3797-3804.
17. M. Kramarenko, C. G. Ferreira, G. Martínez-Denegri, C. Sansierra, J. Toudert and J. Martorell, *Solar RRL*, 2020, **4**, 1900554.
18. P. Alam, N. L. C. Leung, J. Zhang, R. T. K. Kwok, J. W. Y. Lam and B. Z. Tang, *Coordination Chemistry Reviews*, 2021, **429**, 213693.
19. X. He, Y. Yang, Y. Guo, S. Lu, Y. Du, J.-J. Li, X. Zhang, N. L. C. Leung, Z. Zhao, G. Niu, S. Yang, Z. Weng, R. T. K. Kwok, J. W. Y. Lam, G. Xie and B. Z. Tang, *Journal of the American Chemical Society*, 2020, **142**, 3959-3969.
20. P. Alam, G. Kaur, S. Chakraborty, A. Roy Choudhury and I. R. Laskar, *Dalton Transactions*, 2015, **44**, 6581-6592.
21. J. Luo, Z. Xie, J. W. Y. Lam, L. Cheng, H. Chen, C. Qiu, H. S. Kwok, X. Zhan, Y. Liu, D. Zhu and B. Z. Tang, *Chemical Communications*, 2001, DOI: 10.1039/B105159H, 1740-1741.
22. L. Fageria, V. Pareek, R. V. Dilip, A. Bhargava, S. S. Pasha, I. R. Laskar, H. Saini, S. Dash, R. Chowdhury and J. Panwar, *ACS Omega*, 2017, **2**, 1489-1504.
23. H. Kim, S.-K. Choi, J. Ahn, H. Yu, K. Min, C. Hong, I.-S. Shin, S. Lee, H. Lee, H. Im, J. Ko and E. Kim, *Sensors and Actuators B: Chemical*, 2021, **329**, 129248.
24. J. Hu, Y. Liu, X. Zhang, H. Han, Z. Li and T. Han, *Dyes and Pigments*, 2021, **192**, 109393.
25. K.-Q. Mo, X.-F. Ma, H.-L. Wang, Z.-H. Zhu, Y.-C. Liu, H.-H. Zou and F.-P. Liang, *Scientific Reports*, 2019, **9**, 12231.
26. C.-Y. Liu, X.-R. Chen, H.-X. Chen, Z. Niu, H. Hirao, P. Braunstein and J.-P. Lang, *Journal of the American Chemical Society*, 2020, **142**, 6690-6697.
27. K. Zhang, T.-T. Chen, Y.-J. Shen, Z.-R. Yang, Y. Huang, S. Zhang, J. Xue and B. Li, *Analyst*, 2020, **145**, 5826-5835.

28. H. Wang, S. Zhan, X. Wu, L. Wu and Y. Liu, *RSC Advances*, 2021, **11**, 565-571.
29. P. Alam, G. Kaur, V. Kachwal, A. Gupta, A. Roy Choudhury and I. R. Laskar, *Journal of Materials Chemistry C*, 2015, **3**, 5450-5456.
30. Y. Nagasawa, H. Samoto, H. Ukai, S. Okamoto, K. Itoh, T. Hanada, A. Kanemaru, Y. Fukui, S. Kojima, J. Moriguchi, S. Sakuragi, F. Ohashi, S. Takada, T. Kawakami and M. Ikeda, *Environmental health and preventive medicine*, 2013, **18**, 341-348.
31. F. García-Sánchez, A. Romero-Martínez and A. Trejo, *The Journal of Chemical Thermodynamics*, 1989, **21**, 823-826.
32. M. Schlosser Paul, S. Bale Ambuja, F. Gibbons Catherine, A. Wilkins and S. Cooper Glinda, *Environmental Health Perspectives*, 2015, **123**, 114-119.
33. G. Berger, J. Soubhye, R. Wintjens, K. Robeyns and F. Meyer, *Acta Crystallographica Section B*, 2018, **74**, 618-627.
34. D. M. Ivanov, M. A. Kinzhalov, A. S. Novikov, I. V. Ananyev, A. A. Romanova, V. P. Boyarskiy, M. Haukka and V. Y. Kukushkin, *Crystal Growth & Design*, 2017, **17**, 1353-1362.
35. G. Cavallo, P. Metrangolo, R. Milani, T. Pilati, A. Priimagi, G. Resnati and G. Terraneo, *Chemical Reviews*, 2016, **116**, 2478-2601.
36. G. Berger, P. Frangville and F. Meyer, *Chemical Communications*, 2020, **56**, 4970-4981.
37. D. Kurzydłowski, T. Chumak and J. Rogoża, *Crystals*, 2020, **10**.
38. D. Lin-Vien, N. B. Colthup, W. G. Fateley and J. G. Grasselli, in *The Handbook of Infrared and Raman Characteristic Frequencies of Organic Molecules*, eds. D. Lin-Vien, N. B. Colthup, W. G. Fateley and J. G. Grasselli, Academic Press, San Diego, 1991, pp. 73-94.
39. M. A. S. Garcia, M. Ibrahim, J. C. S. Costa, P. Corio, E. V. Gusevskaya, E. N. dos Santos, K. Philippot and L. M. Rossi, *Applied Catalysis A: General*, 2017, **548**, 136-142.
40. in *The Handbook of Infrared and Raman Characteristic Frequencies of Organic Molecules*, eds. D. Lin-Vien, N. B. Colthup, W. G. Fateley and J. G. Grasselli, Academic Press, San Diego, 1991, pp. 477-490.
41. J. Mei, Y. Hong, J. W. Y. Lam, A. Qin, Y. Tang and B. Z. Tang, *Advanced Materials*, 2014, **26**, 5429-5479.

Chapter 3. Cyclometalated Iridium(III) Complexes as Molecular Sensing Probes

Part B. 3.2 Facile and Selective Low-cost Detection of Creatinine from Human Urine by Cyclometalated Dinuclear Iridium(III) Complex Through Creatinine-triggered Emission

3.2.1 Introduction

Chronic kidney disease (CKD) affects 8-16 percent of people worldwide. The lack of accessible CKD treatments leads to millions of deaths per year.[1] There are no symptoms or signs of CKD in its early stages. As a result, the majority of the affected people are still unknown. With an early-stage diagnosis, CKD is treatable, and renal disease development can be slowed or stopped. The leading indicator of kidney function is a level of creatinine from the blood and waste product (i.e., urine) excreted by the kidneys.[2] If kidney function is reduced, an elevated level of creatinine is found in urine or blood. Therefore, tests on the blood and urine are utilized to monitor the progression of kidney disease. Typically, laboratory tests are performed on blood samples to determine the Glomerular filtration rate, which evaluates the rate at which the kidneys filter blood, and on urine samples to determine albumin and creatinine excretion. The risk of CKD progression is also indicated by the presence of excess protein in the urine. The urinalysis 'dipstick test,' can also be used to identify an excess protein, which has a limited lifespan and is extremely sensitive to air exposure.[3] A kidney disease biomarkers are utilized in both the diagnosis and follow-up of kidney diseases. Typically, biomolecules, including proteins or creatinine detection, rely on mass spectrometry, immunoassays, or electrophoresis.[4] However, these techniques have good sensitivity and high accuracy, but they typically need expensive and sophisticated equipment, and their procedure is time-consuming.

Since fluorescent materials rapidly respond and have excellent photosensitivity, it has found widespread use in a variety of fields,[5-8] including bioimaging,[9, 10] chemical vapor sensing,[11] metal ion sensing,[12] mechanofluorochromism,[13] multi-stimuli responsive polymeric materials,[14] etc. Additionally, fluorescence-based optical sensors have many benefits, such as biocompatibility, smaller size and weight, lower price, small volume detection, and remote sensing capability.[15-17] Because of their long luminescence lifetimes (up

to sec) and high quantum yield, heavy metal-based phosphorescent organometallic complexes (e.g, iridium(III) and platinum(II)) are typically used for greater efficiency.[18] Also, their ability to employ a variety of excited states, including metal-to-ligand charge-transfer (MLCT), ligand-to-metal charge-transfer (LMCT), and ligand-to-ligand charge-transfer (LLCT) states, which distinguishes transition-metal complexes from organic fluorophores.[19] Such a system is gaining significant attention for various applications like optoelectronic, metal cation sensing, explosive sensing, etc.[20]

The solution-based creatinine (Crt9) detection using organic fluorescent moiety was reported based on hydrogen bonding between the $–COO^-$ group of probes and creatinine.[21] However, they studied Crt9 detection with artificial urine (i.e., prepared composition from contents present in human urine). However, this organic tetraphenylethene probe shows fluorescence in both probe solutions in water and artificial urine in the absence of Crt9. It increases the emission intensity up to 1 mM of Crt9 and then decreases for further increasing concentration, which makes it difficult to monitor the sensing response in real urine samples. Unob and co-workers published a paper-based method for colorimetric urine creatinine detection using the Jaffé reaction.[22] In the Jaffé reaction, a cationic form of creatinine was extracted onto paper via the mechanism of an ion exchange where that needed to be washed three times with deionized water and 40 μL of an alkaline picrate solution resulting formation of a yellow-orange colored complex. Although it is a capable method, the approach is not selective.[23]

Metal nanoclusters with biomolecule capped for creatinine detection have been reported.[24] A cholic acid-capped gold nanocluster was produced, and it was utilized as a fluorescence-enhanced probe to detect creatinine in human urine and serum samples.[25] The pH needs to be kept at 12.0 during the high-temperature (180 °C) synthesis of the nanocluster. Joseph et al. reported a gluten-stabilized fluorescent gold quantum cluster and used it for application in fluorescent-based human blood creatinine sensing, where picric acid is used as a binder.[26] To form a picrate complex, picric acid is treated to a gold quantum cluster. Despite having a strong binding affinity for creatinine, picric acid could cause fluorescence quenching due to photoinduced electron transfer (PET). The detection of creatinine based on aggregation in the presence of Al^{3+} ions also uses glutathione-capped copper nanoclusters.[27] The emission quenching of copper nanoclusters was caused by the coordination interaction between creatinine and aluminium cations. Carbon-gold nanocomposites with bovine serum albumin (BSA) capped were produced and used as an optical sensor for creatinine detection.[28] When

creatinine was detected, the emission quenching for the BSA-capped (C-Au) nanocomposite was also observed. Infrared fluorescent quantum dots based on molecularly imprinted polymer (MIP) capping were reported to detect creatinine.[29] For the detection of creatinine, several MIP-capped nanocomposites were reported.[30] In addition to the time-consuming synthesis, MIP techniques have drawbacks such as incomplete or leakage template removal, irregular morphology, and random binding site distribution.[31]

Some colorimetric or electrometric techniques were explored for the detection of creatinine (Crt9), but the fluorescent-based technique showed higher photosensitivity and shorter response time for the detection of creatinine.[32] Although to detect creatinine, various biomolecules capped nanoclusters (such as gluten, glutathione, BSA, cholic acid, and MIP) have been studied,[33] but phosphorescent-based facile and selective low-cost detection of creatinine has not been explored yet. Herein, the ester-functionalized phosphorescent iridium(III) metal complex M3 was developed. It was motivated by the literature that reported creatinine detection through the interaction between creatinine and the methyl methacrylate ester group.[34] Herein, we described an iridium(III) based dinuclear complex as an efficient probe for creatinine detection.

3.2.2 Experimental section

3.2.2.1 Synthesis and Characterization

In scheme 3.2.1, the synthetic route of iridium(III) complex MC1 [(ppy-COOMe)$_2$Ir(μ-Cl)$_2$Ir(ppy-COOMe)$_2$] is shown.

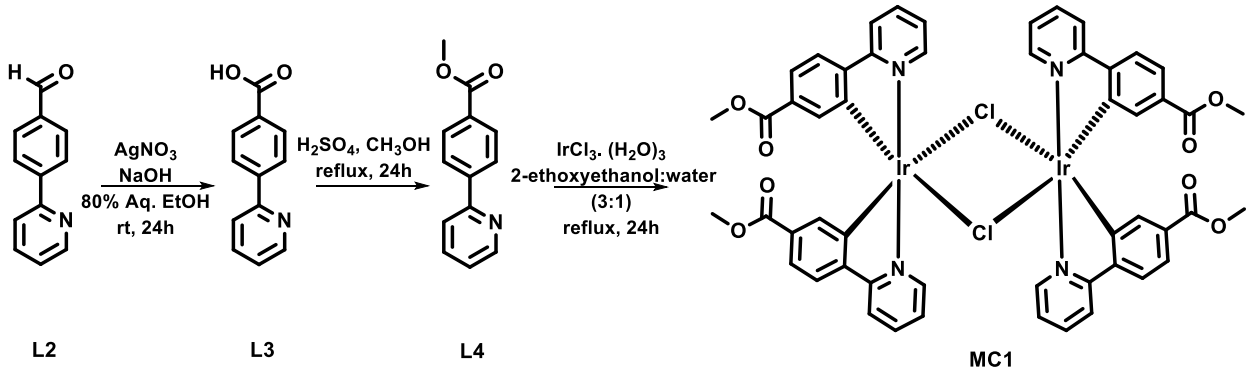

Scheme 3.2.1 Synthesis of ligands L3 (4-(pyridin-2-yl)benzoic acid), L4 (methyl 4-(pyridin-2-yl)benzoate), and bridged dinuclear iridium(III) complex MC1 [(ppy-COOMe)$_2$Ir(μ-Cl)$_2$Ir(ppy-COOMe)$_2$].

Synthesis of L3 (4-(pyridin-2-yl)benzoic acid): A 15 ml of NaOH (1M) and 695 mg (4.09 mmol, 1.5 eq.) of $AgNO_3$ mixed in 80% aq. ethanol (50 ml). After additions of 500 mg of 4-(2-Pyridinyl) benzaldehyde (L2) (2.72 mmol, 1 eq.) were stirred continuously into the reaction mixture. At room temperature (~25°C), the reaction mixture was further stirred for 24 hours. The reaction mixture was filtered, and the filtrate was then acidified with concentrated HCl to obtain solid precipitation. The solid was filtered, then washed with water and dried. We obtained a solid product with a 75-76 % yield. Then the solid product, L3, was characterized by ^{1}H and ^{13}C NMR analysis (Fig. 3.2.1 and 3.2.2). The ^{1}H NMR peak at 13 ppm and ^{13}C NMR peak at 168 ppm indicate the presence of the carboxylic group in L3.

^{1}H NMR (400 MHz, DMSO-d_6): δ 13.07 (s, 1H), 8.74 – 8.69 (m, 1H), 8.25 – 8.19 (m, 2H), 8.10 – 8.02 (m, 3H), 7.93 (td, J = 7.7, 1.9 Hz, 1H), 7.42 (ddd, J = 7.5, 4.7, 1.1 Hz, 1H).

^{13}C NMR (101 MHz, DMSO-d_6): δ 167.58, 155.33, 150.22, 143.04, 137.90, 131.49, 130.25, 127.09, 123.83, 121.37.

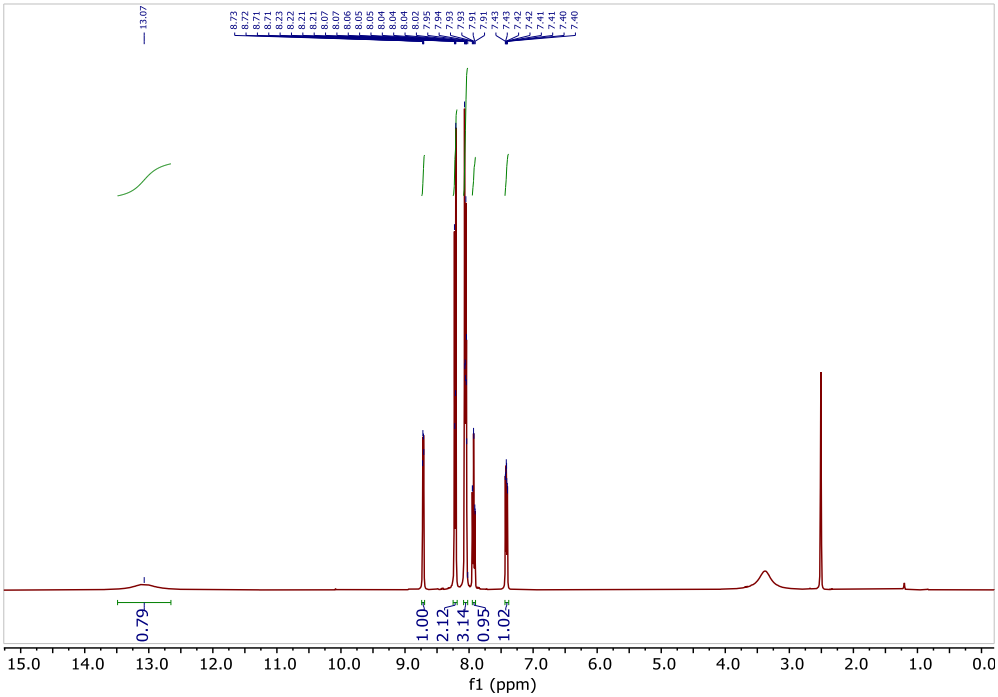

Figure 3.2.1 ^{1}H NMR spectrum of L3 (4-(pyridin-2-yl)benzoic acid) in DMSO-d_6 solvent.

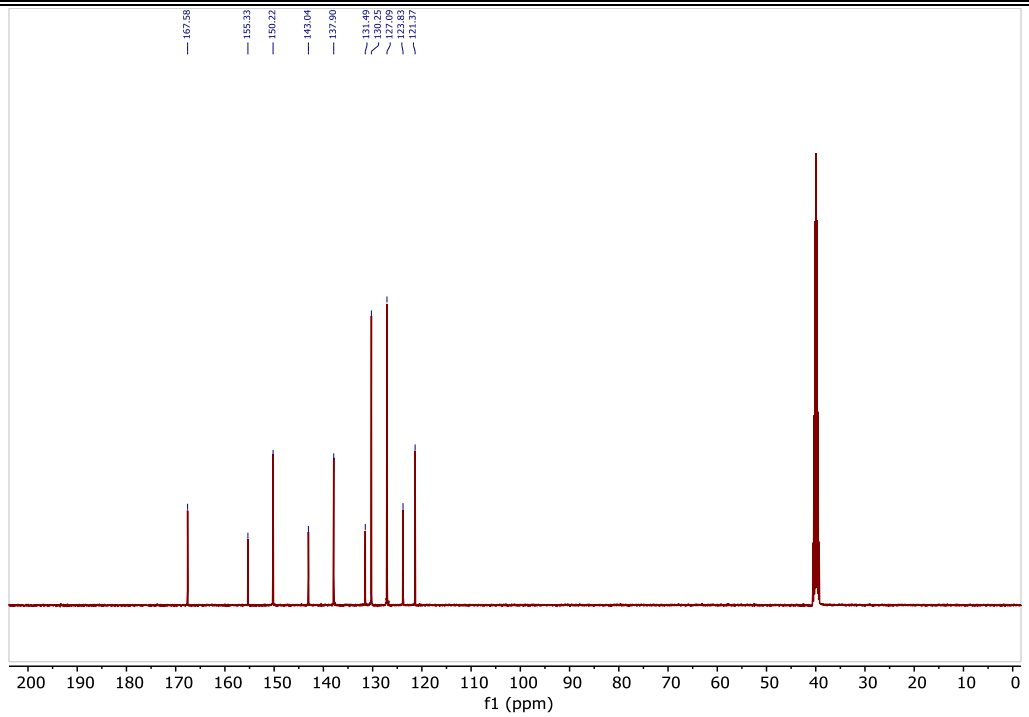

Figure 3.2.2 ^{13}C NMR spectrum of L3 (4-(pyridin-2-yl)benzoic acid) in DMSO-*d*$_6$ solvent.

Synthesis of L4 [methyl 4-(pyridin-2-yl)benzoate (i.e., ppy-COOMe)]: A 15 ml of methanol was added into a clean and dry round-bottom flask which was cooled in an ice bath and then it followed by addition of concentrated H_2SO_4 slowly (1 mL). Then, the compound, L3 was added slowly (400 mg, 2.007 mmol). The mixture was refluxed for 24 hours under an N_2 atmosphere. A saturated Na_2CO_3 solution was used to neutralize the crude product. Ethyl acetate was then used to extract the aqueous phase. The organic phases were dried over Na_2SO_4. A yield of 88-90 % of methyl 4-(2-pyridyl) benzoate was obtained by vacuum solvent extraction. The compound (L4) was characterized by ^{1}H and ^{13}C NMR (Fig. 3.2.3 and 3.2.4). In ^{1}H NMR spectra, a disappearing peak at 13 ppm and the formation of a new peak at 4 ppm, and in ^{13}C NMR, a new peak at 51 ppm indicates the presence of methyl ester in L4.

^{1}H NMR (400 MHz, Chloroform-*d*): δ 8.75 (dt, J = 4.8, 1.4 Hz, 1H), 8.18-8.15 (m, 2H), 8.12-8.07 (m, 2H), 7.83-7.79 (m, 2H), 7.31 (td, J = 4.8, 3.7 Hz, 1H), 3.97 (s, 3H).

^{13}C NMR (101 MHz, Chloroform-*d*): δ 165.90, 155.22, 148.88, 142.51, 135.89, 129.35, 129.03, 125.82, 121.85, 119.99, 51.17.

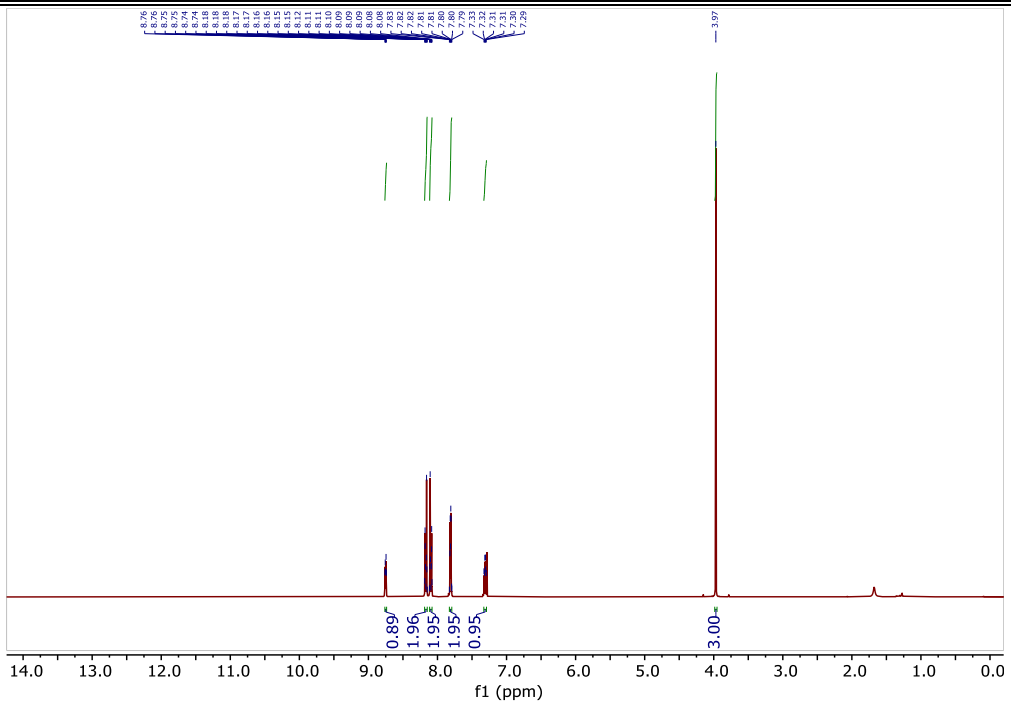

Figure 3.2.3 ^{1}H NMR spectrum of L4 (methyl 4-(pyridin-2-yl)benzoate (i.e., ppy-COOMe)) in $CDCl_3$ solvent.

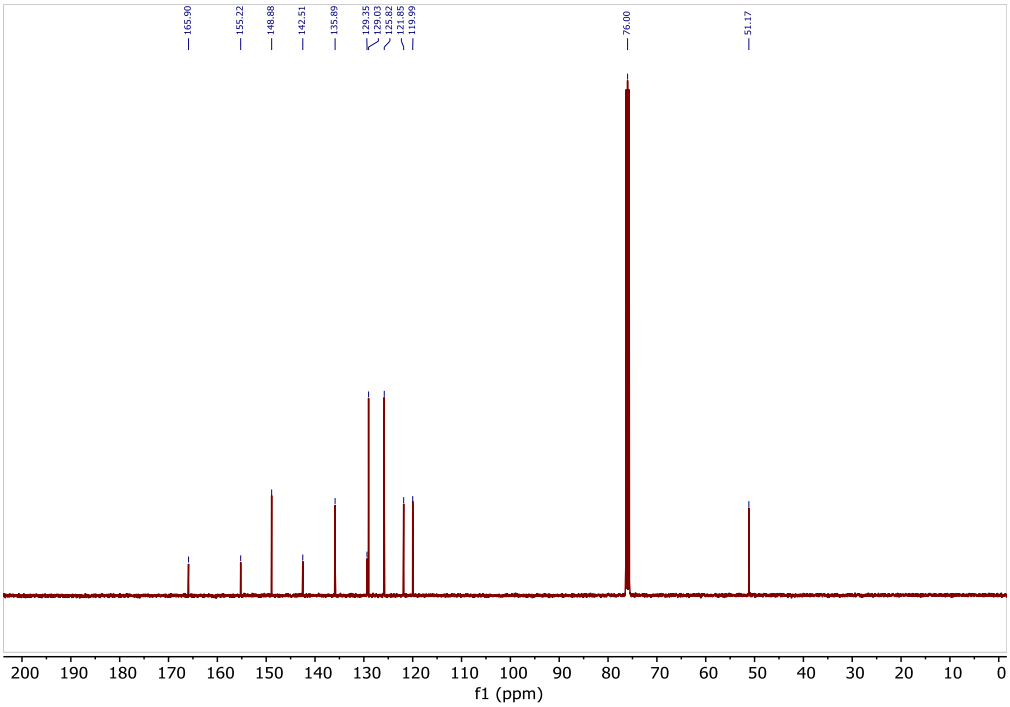

Figure 3.2.4 ^{13}C NMR spectrum of L4 (methyl 4-(pyridin-2-yl)benzoate (i.e., ppy-COOMe)) in $CDCl_3$ solvent.

Synthesis of iridium(III) complex MC1 [(ppy-COOMe)$_2$Ir(μ-Cl)$_2$Ir(ppy-COOMe)$_2$]: A L4 (380 mg, 1.78 mmol) was dissolved in a mixture of 2-ethoxyethanol and water (3:1). Iridium(III) trichloride hydrate [$IrCl_3.(H_2O)_3$] (266 mg, 0.89 mmol) was mixed with the reaction mixture.

The reaction mixture was refluxed for ~22h and then it was cooled to room temperature. Then, enough amount of hexane was added to the reaction mixture to obtain a precipitate. The precipitate was washed with hexane and ether. The resultant crude product was purified by column chromatography (Yield, 35-40%). The MC1 structure was characterized by ^{1}H and ^{13}C NMR spectra. (Fig. 3.2.5 and 3.2.6). The observed ^{1}H NMR peak at 3.6 ppm corresponds to the 12 protons present in four methyl ester groups. Similarly, the ^{13}C NMR peak observed at 52 ppm corresponds to four methyl present in methyl ester.

^{1}H NMR (400 MHz, DMSO-d_6): δ 9.88 (d, J = 5.9 Hz, 1H), 9.59 (d, J = 5.8 Hz, 1H), 8.38 (dd, J = 34.2, 8.2 Hz, 2H), 8.19 (dd, J = 36.0, 7.8 Hz, 2H), 7.93 (dd, J = 24.6, 8.1 Hz, 2H), 7.68 (dt, J = 39.8, 6.7 Hz, 2H), 7.46 (dd, J = 21.0, 8.1 Hz, 2H), 6.88 (s, 1H), 6.30 (s, 1H), 3.65 (d, J = 8.7 Hz, 5H).

^{13}C NMR (101 MHz, DMSO-d_6): δ 166.52, 152.88, 149.09, 145.00, 140.14, 139.18, 132.00, 130.33, 125.20, 124.18, 122.00, 79.65, 52.44.

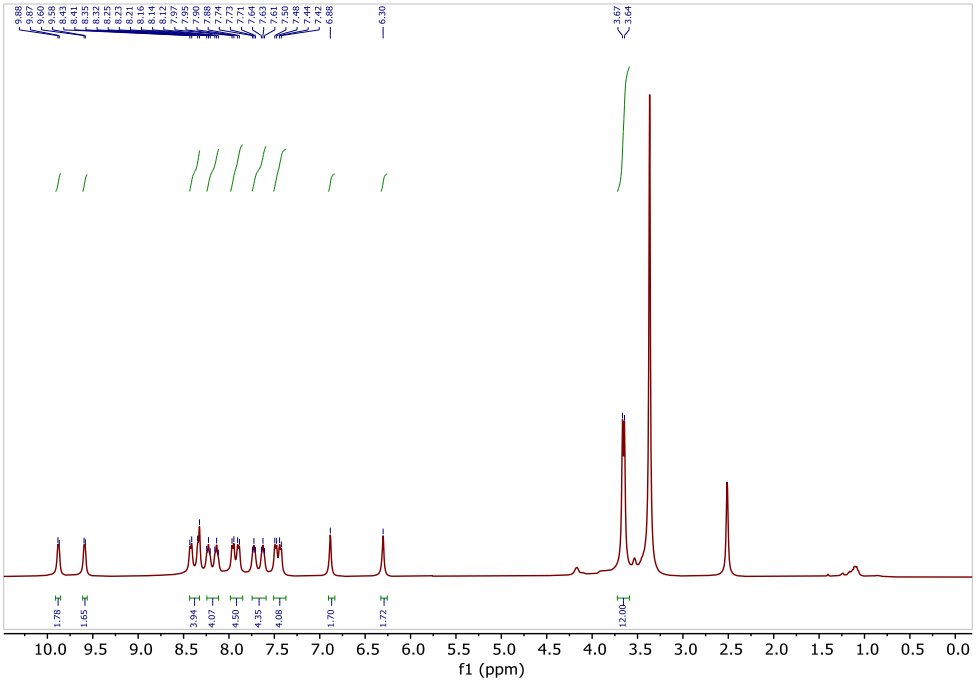

Figure 3.2.5 ^{1}H NMR spectrum of MC1 [(ppy-COOMe)$_2$Ir(μ-Cl)$_2$Ir(ppy-COOMe)$_2$] in DMSO-d_6 solvent.

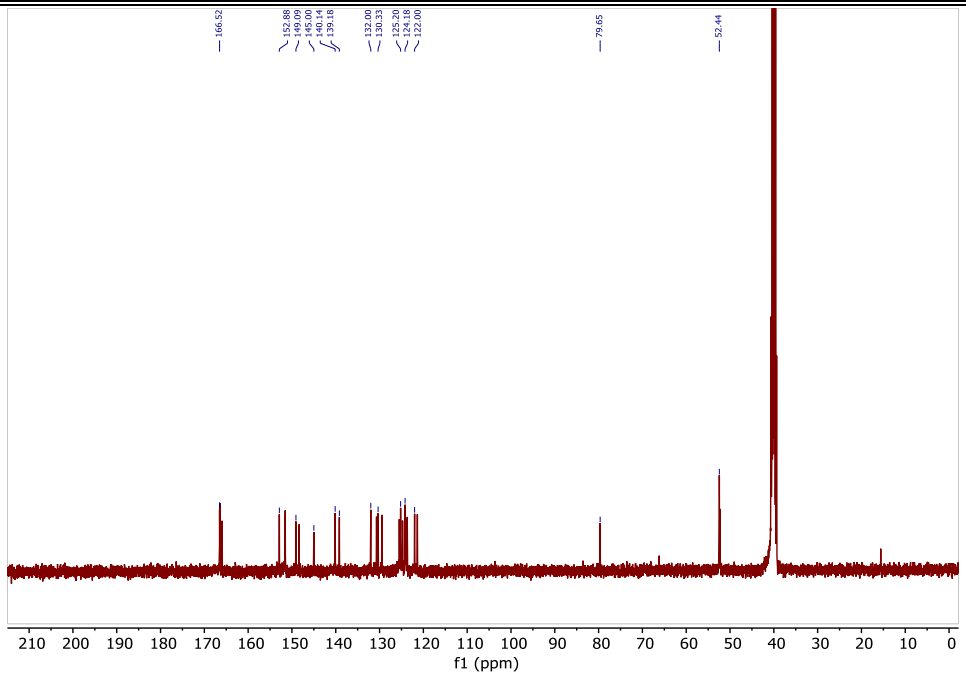

Figure 3.2.6 ^{13}C NMR spectrum of MC1 [(ppy-COOMe)$_2$Ir(μ-Cl)$_2$Ir(ppy-COOMe)$_2$] in DMSO-d_6 solvent.

Synthesis of mononuclear iridium(III) complex [Ir(ppy-COOMe)$_2$(pic)] M2: 0.092 mmol Chloro-bridged dimer complex (MC1) (120 mg), 0.184 mmol (35.5 mg) 3-hydroxypicolinic acid (L5) (*pic*), and 90 mg sodium carbonate were added into a round bottom flask and refluxed it for ~14h in an inert atmosphere. A yellow color precipitate was separated after cooling the reaction mixture to room temperature. The residue was washed using hexane and ether. It was dissolved in dichloromethane and then filtered. Dried it under vacuum, and the product was obtained with a 70 % yield. The synthesized M2 was characterized by ^{1}H, ^{13}C NMR, and HRMS study (Fig. 3.2.7, 3.2.8, and 3.2.9). The ^{1}H NMR peak for the 3-hydroxypicolinate in M2 does not appear due to the deuterated exchange with DMSO-d_6.[35] The ^{1}H NMR peaks at 3.6 and 4.1 ppm for the methyl group in methyl ester. In ^{13}C NMR the peak at 177 ppm for carbonyl carbon in picolinate ester, and at 166.1 and 167 ppm are for carbonyl carbon in methyl ester.

^{1}H NMR (400 MHz, DMSO-d$_6$): δ 8.64 (d, J = 5.7 Hz, 1H), 8.38 – 8.28 (m, 2H), 8.08 – 7.92 (m, 4H), 7.71 (d, J = 5.7 Hz, 1H), 7.51 (dt, J = 10.0, 5.2 Hz, 1H), 7.48 – 7.35 (m, 3H), 6.99 (s, 2H), 6.84 – 6.79 (m, 1H), 6.71 (dt, J = 7.0, 2.3 Hz, 1H), 6.60 (s, 1H), 4.17 (dq, J = 4.3, 2.2 Hz, 2H), 3.65 (d, J = 3.2 Hz, 3H).

^{13}C NMR (101 MHz, DMSO-d$_6$): δ 177.00, 167.00, 166.18, 150.13, 149.65, 149.04, 148.38, 138.76, 132.40, 129.35, 124.91, 120.99, 72.23, 68.13, 66.17, 65.96, 60.70, 52.27, 15.62.

HRMS: observed mass of M2 is m/z $[M+H]^+$ = 756.1308; calculated for $[C_{32}H_{24}IrN_3O_7+H]^+$ = 756.1318.

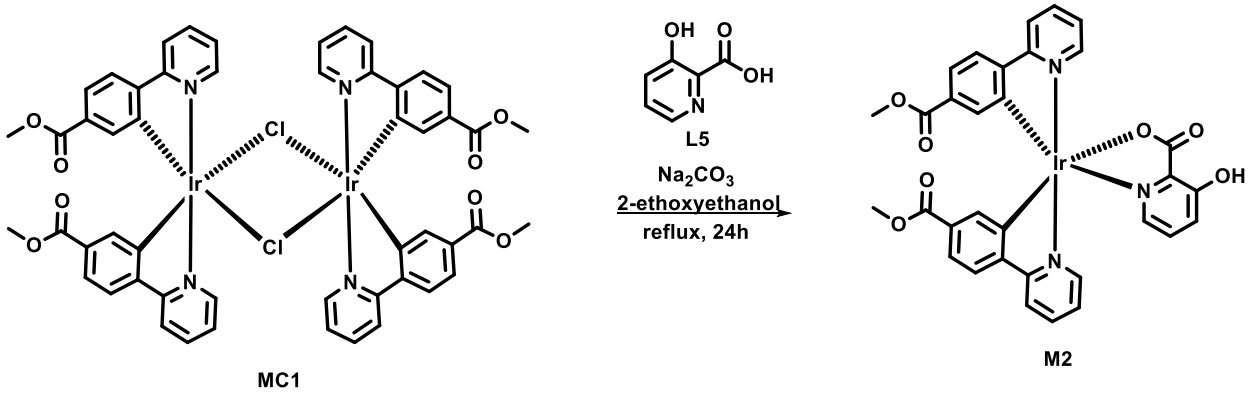

Scheme 3.2.2 Synthesis of mononuclear iridium(III) complex M2 $[Ir(ppy\text{-}COOMe)_2(pic)]$ containing the 3-hydroxypicolinate, from bridged dinuclear iridium(III) complex MC1.

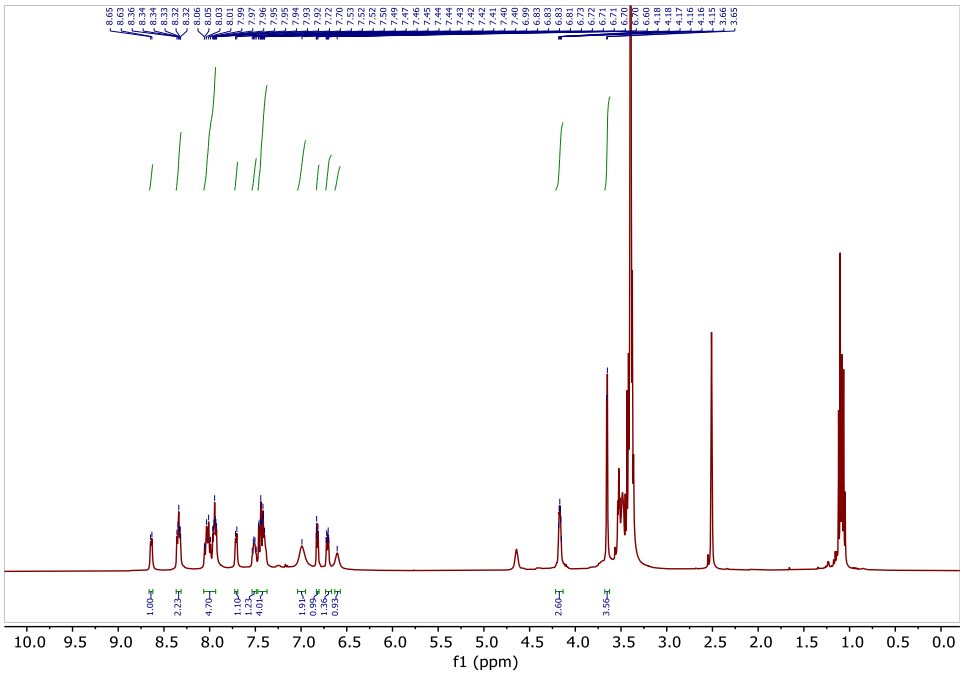

Figure 3.2.7 ^{1}H NMR spectrum of M2 $[Ir(ppy\text{-}COOMe)_2(pic)]$ in DMSO-d_6 solvent.

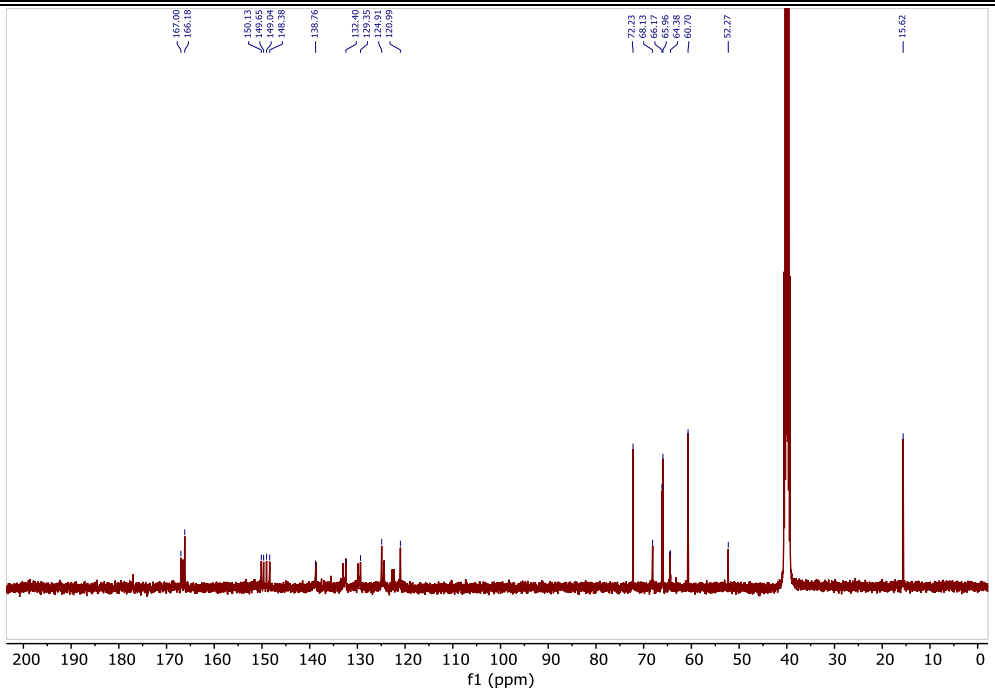

Figure 3.2.8 ^{13}C NMR spectrum of M2 [Ir(ppy-COOMe)$_2$(pic)] in DMSO-d_6 solvent.

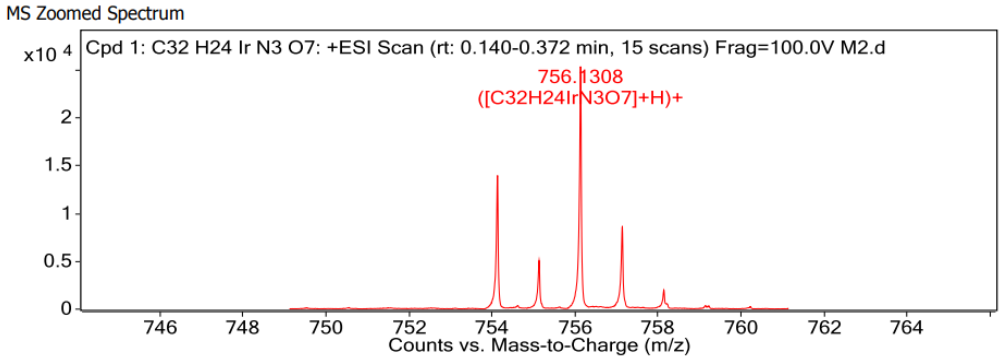

Figure 3.2.9 HRMS mass spectrum of compound M2 [Ir(ppy-COOMe)$_2$(pic)].

Synthesis of iridium(III) complex M3 [(ppy-COOMe)$_4$Ir$_2$(pic)$_2$C$_2$O$_2$], containing bis(2-(oxidaneyl carbonyl)pyridin-3-yl) oxalate:

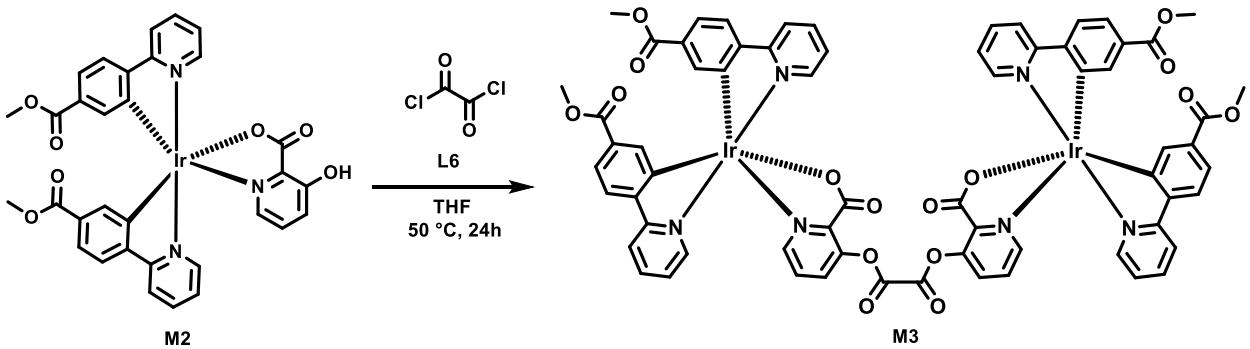

Scheme 3.2.3 Synthesis of dinuclear iridium(III) complex M3 [(ppy-COOMe)$_4$Ir$_2$(pic)$_2$C$_2$O$_2$]

containing bis(2-(oxidaneyl carbonyl)pyridin-3-yl) oxalate, from mononuclear iridium(III) complex M2.

A 2 ml THF was added into a dried round-bottom flask. Then, 80 mg (0.105 mmol) of M2 was added into the same flask with stirring. The oxalyl chloride (4.65ml, 0.052ml) was added to the solution. The reaction mixture was stirred in a nitrogen atmosphere at 50 °C for 24 h. TLC was used to confirm the completion of the reaction, and the reaction mixture was quenched with water, then the organic layer was extracted with dichloromethane. The organic layer was collected, dried over sodium sulphate, and evaporated under reduced pressure. An orange color solid product was separated (with 54 % yield). The ^{1}H, ^{13}C NMR, and HRMS spectral studies were used to characterize the structure of M3 (Figures 3.2.10, 3.2.11, and 3.2.12). M3 was found to have a solid-state absorption wavelength of 375 nm (Fig. 3.1.13) and a lifetime decay of 6 μs, which reveals its distinctive phosphorescence emission (Fig. 3.1.14). The ^{1}H NMR peaks at 3.6 and 4.1 ppm for the methyl group in methyl ester. In ^{13}C NMR the peak at 165.9 ppm for carbonyl carbon in oxalyl ester, and at 166.1.

^{1}H NMR (400 MHz, DMSO-d_6): δ 9.68 (t, J = 4.2 Hz, 1H), 9.35 (s, 1H), 8.48 (dd, J = 30.0, 8.0 Hz, 2H), 8.38 – 8.24 (m, 2H), 8.11 – 7.97 (m, 2H), 7.79 (d, J = 7.5 Hz, 1H), 7.63 (s, 1H), 7.55 (dd, J = 14.0, 8.4 Hz, 2H), 6.89 (s, 1H), 6.41 (d, J = 5.6 Hz, 1H), 4.18 (dd, J = 9.5, 5.0 Hz, 2H), 3.66 (dd, J = 11.6, 3.3 Hz, 3H).

^{13}C NMR (101 MHz, DMSO-d_6): δ 165.97, 165.38, 163.43, 155.39, 152.87, 151.53, 151.47, 149.35, 148.37, 140.14, 131.16, 130.10, 129.44, 125.50, 124.75, 68.06, 66.14, 64.45, 52.41, 15.59.

HRMS: observed mass for M3 is m/z $[M]^+$ = 1563.2428; calculated for $[C_{66}H_{46}Ir_2N_6O_{16}]^+$ 1563.2233.

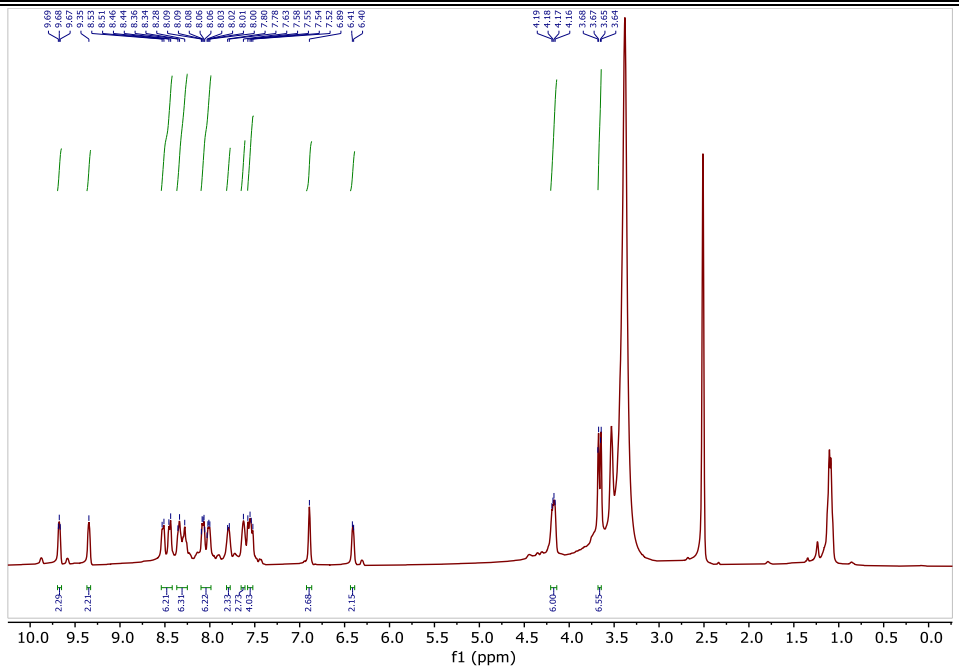

Figure 3.2.10 ^{1}H NMR spectrum of M3 [(ppy-COOMe)$_4$Ir$_2$(pic)$_2$C$_2$O$_2$] in DMSO-*d*$_6$ solvent.

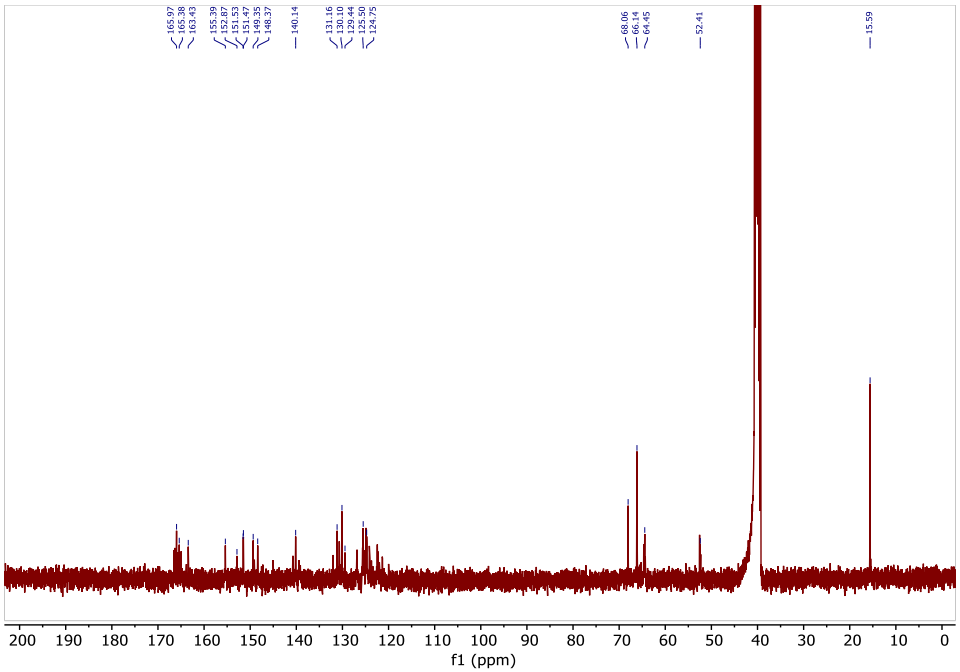

Figure 3.2.11 ^{13}C NMR spectrum of M3 [(ppy-COOMe)$_4$Ir$_2$(pic)$_2$C$_2$O$_2$] in DMSO-*d*$_6$ solvent.

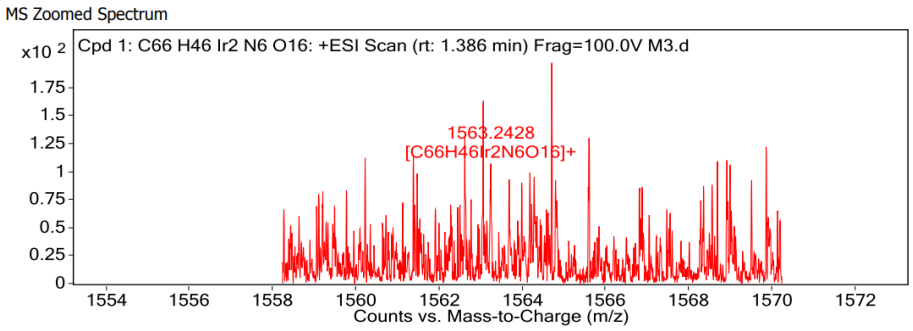

Figure 3.2.12 HRMS mass spectrum of dinuclear iridium(III) complex M3 [(ppy-COOMe)$_4$Ir$_2$(pic)$_2$C$_2$O$_2$] containing bis(2-(oxidaneyl carbonyl)pyridin-3-yl) oxalate.

3.2.2.2 Photophysical study of M3 [(ppy-COOMe)$_4$Ir$_2$(pic)$_2$C$_2$O$_2$]

The M3 was found to have a solid-state absorption wavelength of 375 nm (Fig. 3.1.13) and a lifetime decay of 6 μs, which reveals its distinctive phosphorescence emission (Fig. 3.1.14).

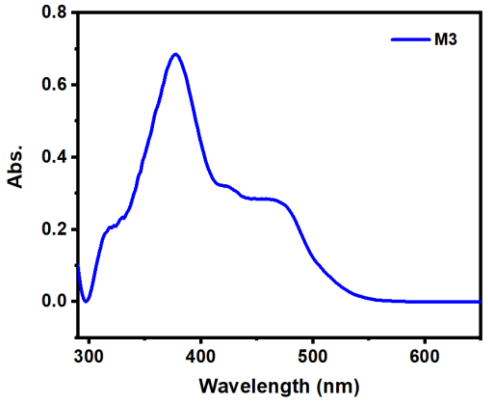

Figure 3.2.13 Absorption plot for solid-state M3 [(ppy-COOMe)$_4$Ir$_2$(pic)$_2$C$_2$O$_2$] performed in reflectance mode and then converted to absorbance value.

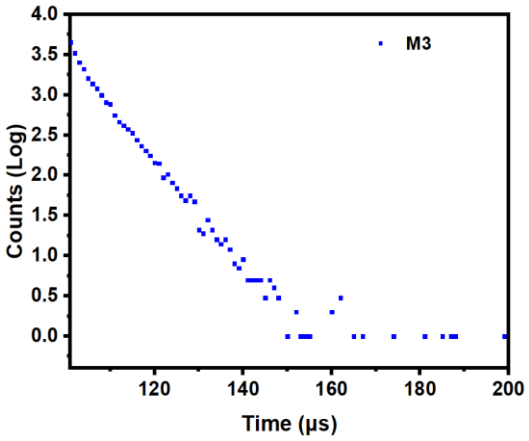

Figure 3.2.14 The characteristic fluorescence lifetime decay curve for THF solution of M3 [(ppy-COOMe)$_4$Ir$_2$(pic)$_2$C$_2$O$_2$] (10^{-5} M) (χ^2 = 1.2).

3.2.3 Results and Discussion

The mode of sample preparation for creatinine detection is given below.

3.2.3.1 Methods of creatinine detection using M3 probe

I. Powder-state creatinine detection: We have added aqueous creatinine to the powdered probe M (100 mg/dL). It was well mixed and dried. Emission intensity with blue shift was observed in the solid state of M3 (the orange color turned into yellow emission) (Fig. 3.2.15a).

II. Paper-based creatinine detection: Here, low-cost Whatman filter paper (FP) strips are used for creatinine (Crt9) detection. It was properly dried after being impregnated with an M3 probe. The dried filter paper was then dipped into an aqueous creatinine solution. After that, the soaked filter paper was dried and examined under a UV lamp. It exhibits an emission enhancement with a blue shift (~ 30 nm) (Fig. 3.2.15b). The same procedure was carried out on a TLC sheet that had been impregnated with an M3 probe, and a similar emission response was noticed under a UV lamp (Fig. 3.2.15c).

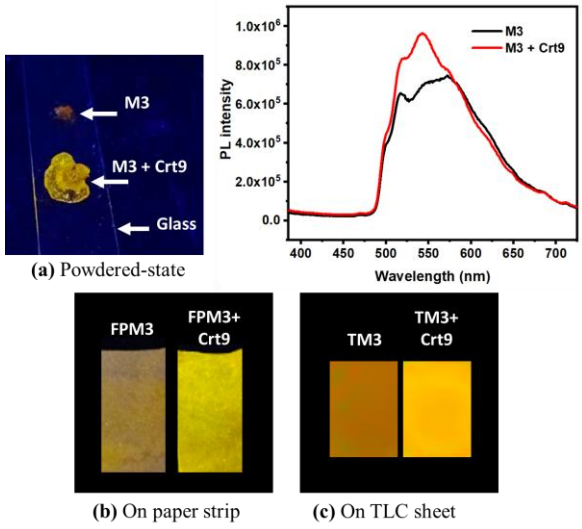

Figure 3.2.15 Images of creatinine (crt9) detection under UV lamp (365 nm); (a) Powdered-state with corresponding PL spectra ($\lambda_{exc.}$=370 nm); (b) On paper strip (filter paper impregnated with M3, i.e., FPM3); (c) On TLC sheet impregnated with M3 (i.e., TM3).

3.2.3.2 Paper-based creatinine detection by PL measurement with increasing concentrations of aqueous Crt9

The creatinine concentration ranges for normal people from 2.8 to 25.9 mg/dL,[36] and it will be elevated in case of CKD. Here, we present the photoluminescence (PL) spectra of M3-impregnated filter paper (FP-M3) at various aqueous creatinine (mg/dL) concentrations (Fig. 3.2.16). We found that the PL intensity increases with blue-shifted emission as the concentration of aqueous crt9 increases.

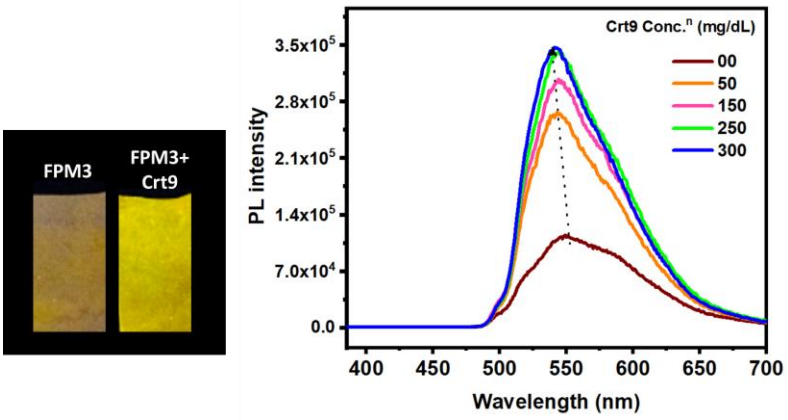

Figure 3.2.16 Images of filter paper impregnated by M3 (FP-M3) before and after being dipped in aq. Crt9 (300 mg/dL) under UV lamp (365 nm) and their corresponding PL intensity plot (FP-M3) showing a gradual variation of PL intensity with increasing concentrations of aq. Crt9 (dotted arrow indicates the blue shift with emission enhancement).

3.2.3.3 Creatinine detection from a human urine sample with M3 probe

The detection of creatinine in human urine is also studied. In this case, the filter paper containing the M3 probe was dipped in a human urine sample and the emission change was observed under a UV lamp (365 nm) (Fig. 3.2.17). Although herein M3 shows emission change with Crt9 in the urine sample of a healthy person, it may also help to assess the Crt9 concentration in CKD patients' samples to determine the albumin-creatinine ratio (ACR).

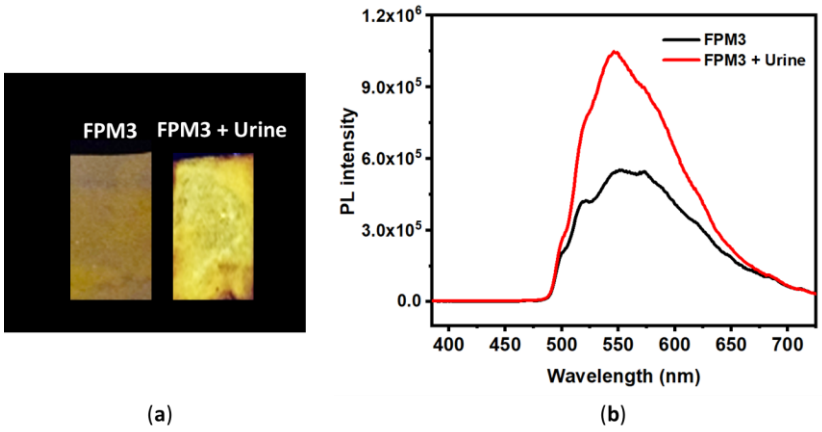

Figure 3.2.17 (a) Images of M3-impregnated filter paper strips (FPM3) under a UV lamp (365 nm) before and after dipping in human urine sample; (b) PL spectra for the same samples described above ($\lambda_{exc.}$= 370 nm).

3.2.3.4 Selectivity

In the presence of various constituents found in human urine, the selectivity study for the M3 probe was performed (Fig. 3.2.18). Under exciting with a UV lamp (λ_{exc}, 365 nm), the probe M3 only exhibits selectively bright yellow emission with creatinine and not with other constituents.

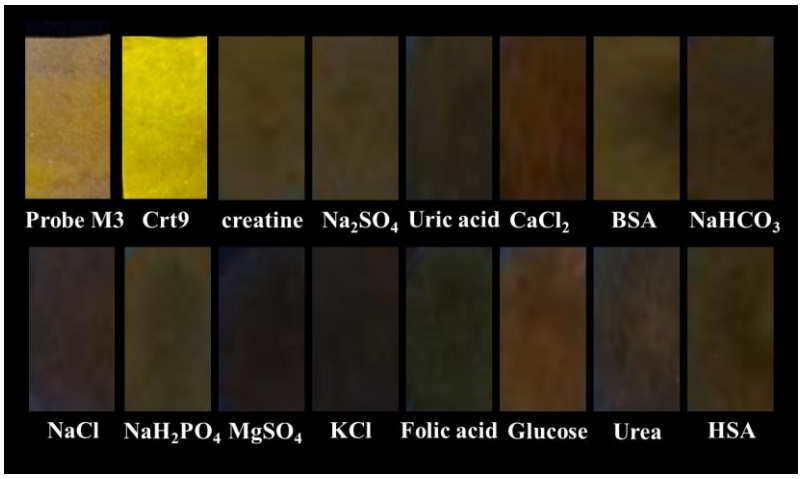

Figure 3.2.18 Images of filter paper strips impregnated M3 under a UV lamp (365 nm) after dipped in aqueous solutions of creatinine (Crt9), creatine, sodium sulphate (Na_2SO_4), uric acid, calcium chloride ($CaCl_2$), bovine serum albumin (BSA), sodium bicarbonate ($NaHCO_3$), sodium chloride (NaCl), monosodium phosphate (NaH_2PO_4), magnesium sulphate ($MgSO_4$), potassium chloride (KCl), folic acid, glucose, urea, human serum albumin (HSA).

To investigate the interaction between M3 and Crt9, the ^{1}H NMR analysis of M3, M3+Crt9, and Crt9 was performed (Fig. 3.2.19). Although there was no significant shifting found for M3' peaks after treatment with Crt9, the observed sharp peaks indicated the possible weak interactions. To understand the role of the terminal ester functional groups on the probe involved in interaction with the creatinine, another analogous iridium(III) complex (M4) without the terminal ester functional groups was synthesized (Fig. 3.2.20) and characterized by ^{1}H NMR analysis (Fig. 3.2.21). The M4 emits greenish-blue emission on a paper strip. The luminescence response of M4 impregnated paper strip was tested with creatinine (Fig. 3.2.20), but there was no change in luminescence observed. Then, to check the possible interaction of creatinine with the carbonyl of the terminal ester group of M3, the M5 probe was designed

(Fig. 3.2.22). It was designed by replacing the terminal ester group with an aldehyde functional group and the synthetic process is similar to M3. It was tested with creatinine and found a luminescence change (Fig. 3.2.22).

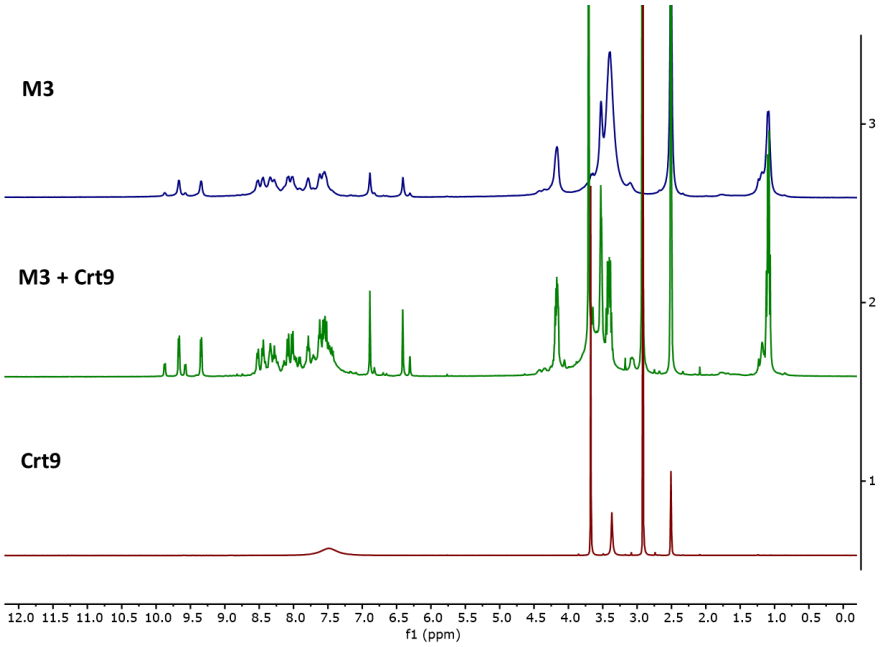

Figure 3.2.19 ^{1}H NMR spectrum of M3, M3+Crt9, and Crt9 in DMSO-d_6 solvent.

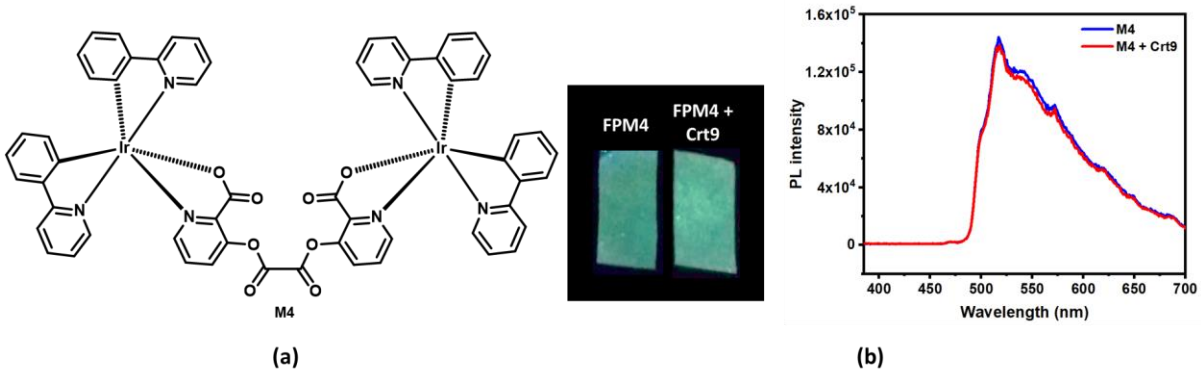

Figure 3.2.20 (a) Chemical structure for synthesized dinuclear iridium(III) complex M4 and (b) luminescent response on filter paper strip impregnated with M4, (i.e., FPM4) under UV lamp (365 nm) with corresponding PL intensity spectra (excitation at $\lambda_{exc.}$= 370 nm).

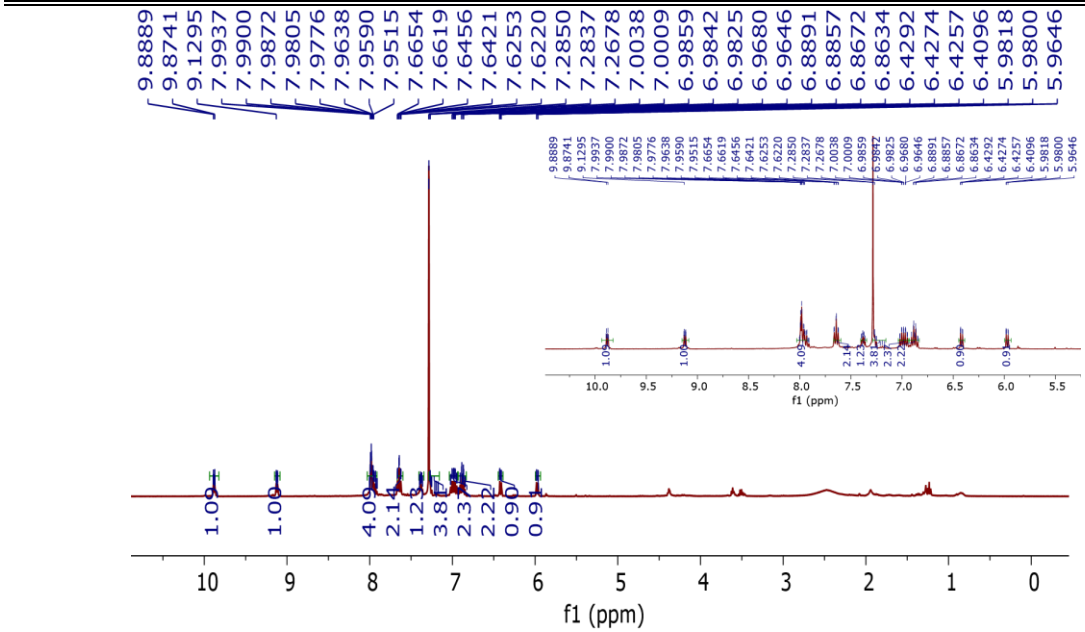

Figure 3.2.21 ^{1}H NMR spectrum of M4 in DMSO-d_6 solvent.

^{1}H NMR for M4: (400 MHz, Chloroform-*d*) δ 9.88 (dd, *J* = 5.9, 1.3 Hz, 1H), 9.32 – 9.02 (m, 1H), 8.18 – 7.81 (m, 4H), 7.64 (td, *J* = 8.0, 1.4 Hz, 2H), 7.45 – 7.34 (m, 1H), 7.28 (m, *J* = 0.5 Hz, 4H), 6.98 (dtd, *J* = 14.7, 7.4, 1.2 Hz, 2H), 6.93 – 6.83 (m, 2H), 6.48 – 6.36 (m, 1H), 6.03 – 5.89 (m, 1H).

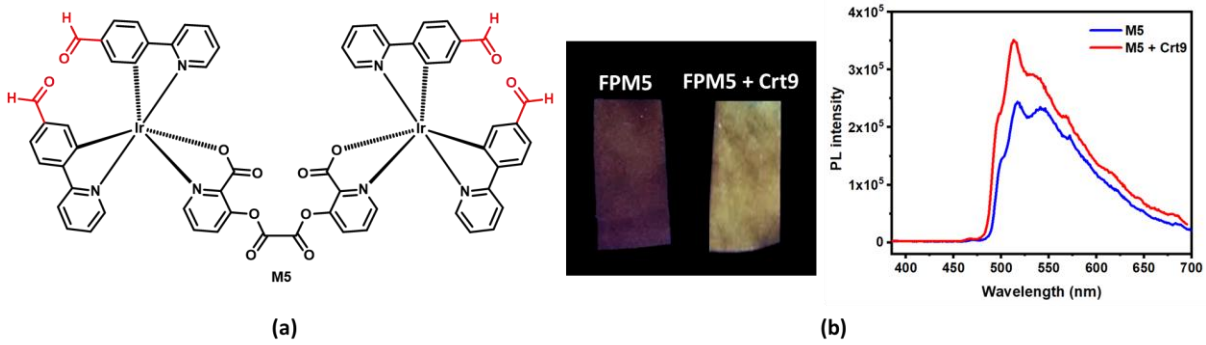

Figure 3.2.22 (a) Chemical structure of the synthesized dinuclear iridium(III) complex (M5) and (b) luminescent response on filter paper strip impregnated with M5, (i.e., FPM5) under UV lamp (365 nm) with corresponding PL intensity spectra (excitation at $\lambda_{exc.}$= 370 nm).

To check the structural arrangement of the M3, M4, and M5 probes, the Gaussian 16 program was used to optimize the structure of all three probes (Fig. 3.2.23). The optimized geometries of M3 and M5 indicate that both are almost similar. In these cases, the picolinate carbonyl groups (A) and (A") come closer [distance between two oxygens of carbonyl (A) and (A") present in picolinate is 4.70 Å and 4.73 Å, respectively] (Fig. 3.2.23). Also, both oxalate

carbonyls (B) and (B”) are observed on the same side for M3 and M5 [dihedral angle between two oxalyl carbonyl (B) and (B”) group is 40.60° and 40.74°, respectively] (Fig. 3.2.23). But for M4, both oxalate carbonyls (B’) are observed on the opposite side [dihedral angle between two oxalyl carbonyl (B’) groups is 154.6°]. From this study, we assume that the V-shaped scaffold network is necessary for showing interaction with creatinine.

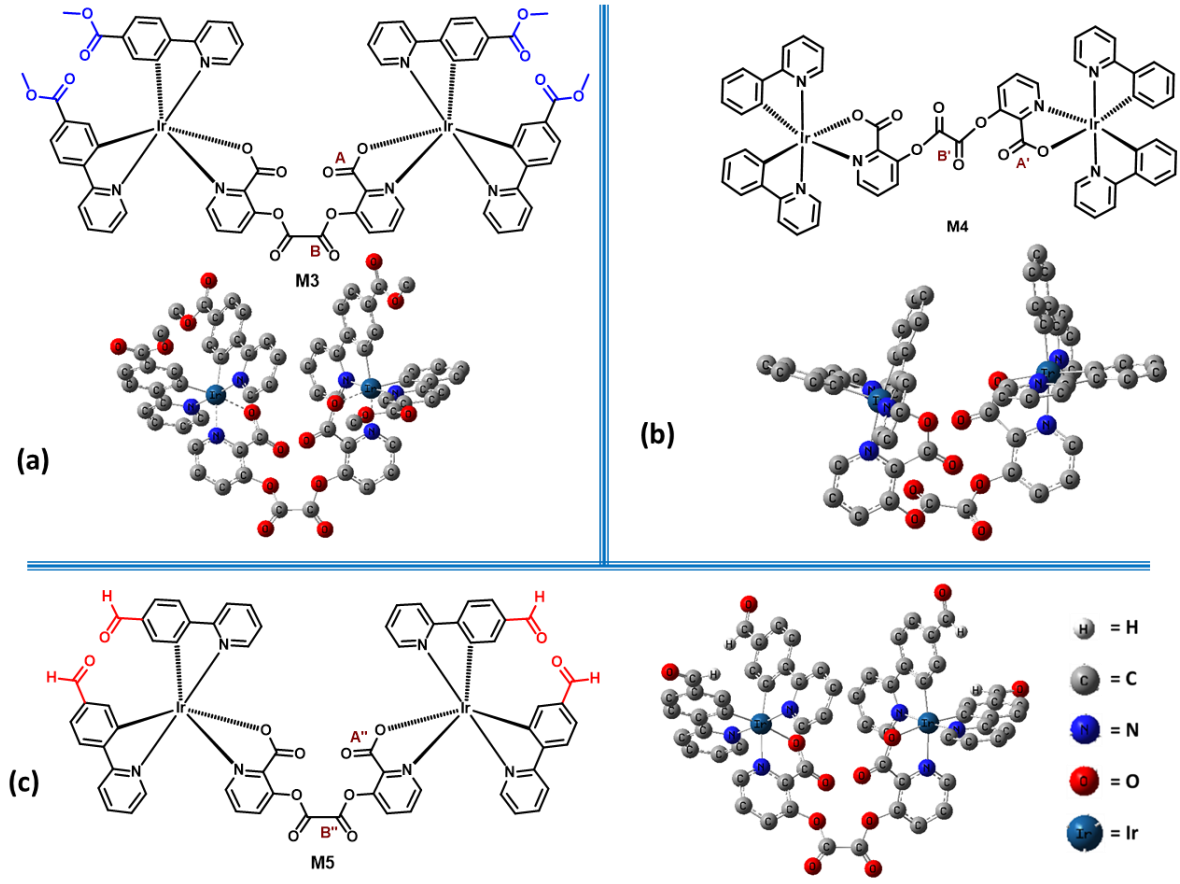

Figure 3.2.23 (a) The basic unit structure and the optimized geometry using DFT via Gaussian 16 with the LanL2DZ basis set and PBEPBE functional; (a) for M3, (b) for M4, and (c) for M5 with labeled characteristic bonds, i.e., picolinate carbonyl (as A, A’, and A”) and oxalate carbonyls as (B, B’, and B”).

The FTIR spectroscopy experiment supports the Crt9 detection mechanism. After treatment with Crt9, the IR frequency for picolinate carbonyl (A) (C=O) stretching of M3 was observed at 1606 cm^{-1},[37] reduced to 1592 cm^{-1} (Fig. 3.2.24). At the same time, the other two carbonyl’s (B) and (C) stretching bands are retained at 1764 and 1712 cm^{-1},[38-40] respectively (Fig. 3.2.24 and Table 3.2.1).[37] Additionally, solid-phase IR spectra of Crt9 were recorded. The stretching of N-H (D) and carbonyl (E) of creatinine was observed at 3242 and 1666 cm^{-1}, respectively (Fig. 3.2.24d).[41, 42] The N-H (D) stretching frequency is changed to 3234 cm^{-1} and carbonyl (E)

of Crt9 was retained at 1666 cm^{-1} after treating with M3. A lowering of the above values for carbonyl (A) of M3 and N-H (D) of Crt9 reveals that N-H (D) bonds of Crt9 might be participating in the hydrogen bonding with picolinate carbonyl (A) of M3, as shown in Fig. 3.2.25.

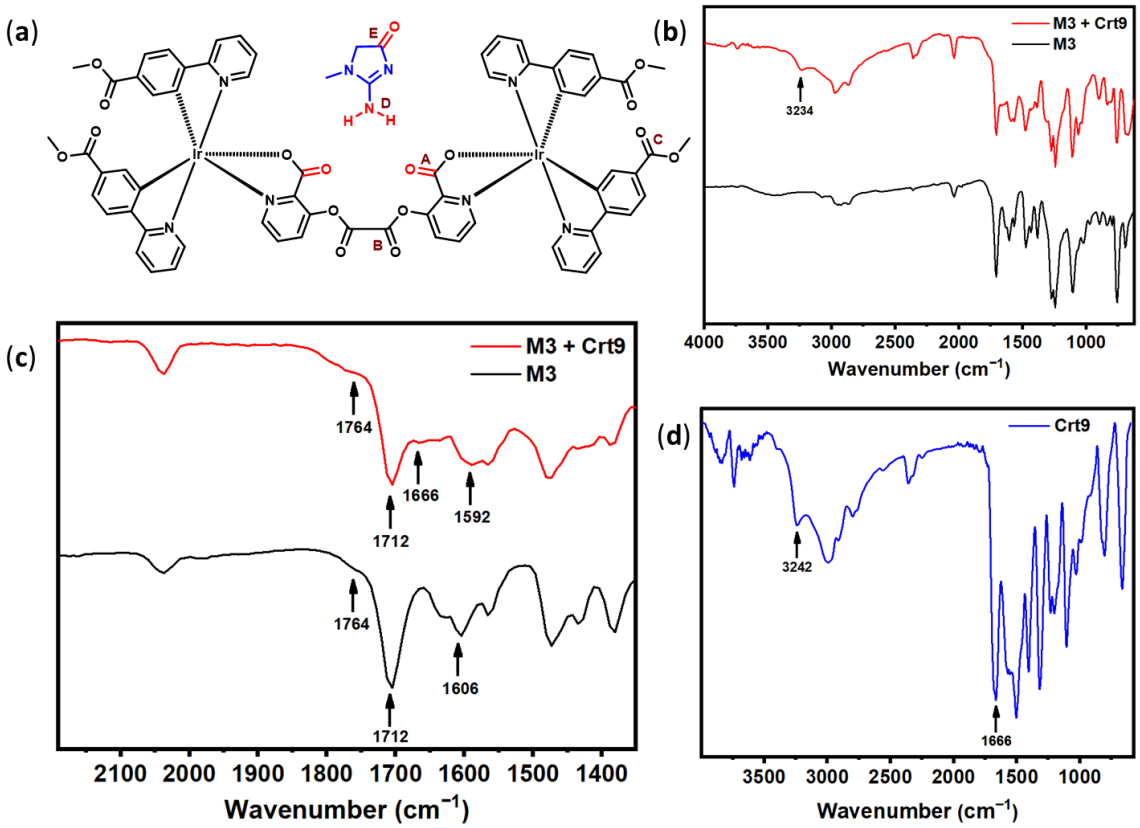

Figure 3.2.24 (a) Chemical structures for M3 and creatinine (Crt9) with labelling the characteristic bonds (as A, B, C, D, and E); (b) FTIR spectra for solid-state M3, and Crt9 treated M3 (M3+Crt9); (c) enlarged view for the same spectra; (d) Crt9 FTIR spectra in solid-state.

Table 3.2.1 Listed the important vibrational modes (frequency, cm^{-1}) recorded by FTIR for M3 and Crt9 treated M3 (M3+Crt9).

	IR frequency (cm^{-1})		
Vibrational modes	M3	M3 + Crt9	Crt9
Carbonyl stretching of M3 (A)	1606	1592	---
Carbonyl stretching of M3 (B)	1764	1764	---
Carbonyl stretching of M3 (C)	1712	1712	---
N-H stretching of Crt9 (D)	---	3234	3242
Carbonyl stretching of Crt9 (E)	---	1666	1666

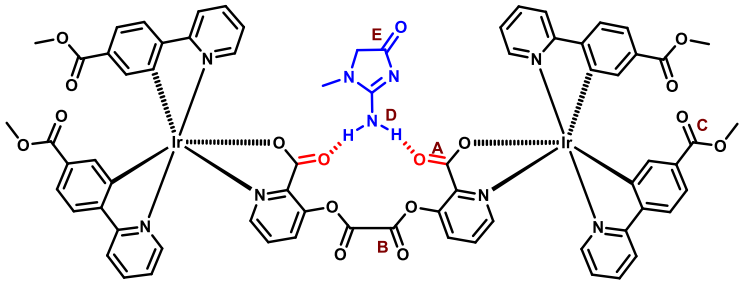

Figure 3.2.25 Schematic representative structural model for the interaction of creatinine (Crt9) with M3, with labeled characteristic bonds (as A, B, C, D, and E).

Moreover, another probe, M6 was designed and synthesized by extending the four-carbon chain between the two bridged carbonyl groups of M3 (Fig. 3.2.26). The probe M6 was synthesized similarly to M3 by using adipoyl chloride instead of oxalyl chloride and it was structurally characterized by ^{1}H NMR (Fig. 3.2.27). The ^{1}H NMR peak at 3.2 and 4.1 ppm indicates the middle two -CH_2- group and two -CH_2- adjacent to oxalyl carbonyl. The M6 was also tested for creatinine detection similar to M3 on a paper strip, and no luminescence response was observed in the presence of creatinine. This study supports the observed change in the luminescence of M3 in the presence of creatinine might result from the interaction of the consecutively placed bridged ester oxygen atom of M3 with creatinine.

^{1}H NMR (400 MHz, DMSO-d_6) δ 9.87 (d, J = 5.7 Hz, 2H), 9.57 (d, J = 5.7 Hz, 2H), 8.42 (dd, J = 7.9, 3.4 Hz, 2H), 8.34 (d, J = 8.1 Hz, 2H), 8.28 – 8.18 (m, 3H), 8.14 (td, J = 7.8, 1.8 Hz, 3H), 7.97 (dd, J = 8.2, 2.8 Hz, 2H), 7.95 – 7.87 (m, 2H), 7.76 – 7.67 (m, 3H), 7.62 (q, J = 6.1 Hz, 3H), 7.52 – 7.45 (m, 2H), 7.47 – 7.39 (m, 2H), 6.87 (dt, J = 5.5, 1.6 Hz, 3H), 6.29 (dt, J = 6.1, 1.8 Hz, 3H), 4.23 – 4.10 (m, 4H), 3.53 (m, J = 2.7, 2.3 Hz, 4H), 2.09 (s, 12H).
HRMS: observed mass of M4 is m/z $[M+H]^+$ = 1621.29; calculated for $[C_{70}H_{54}Ir_2N_6O_{16}+H]^+$ = 1621.3260.

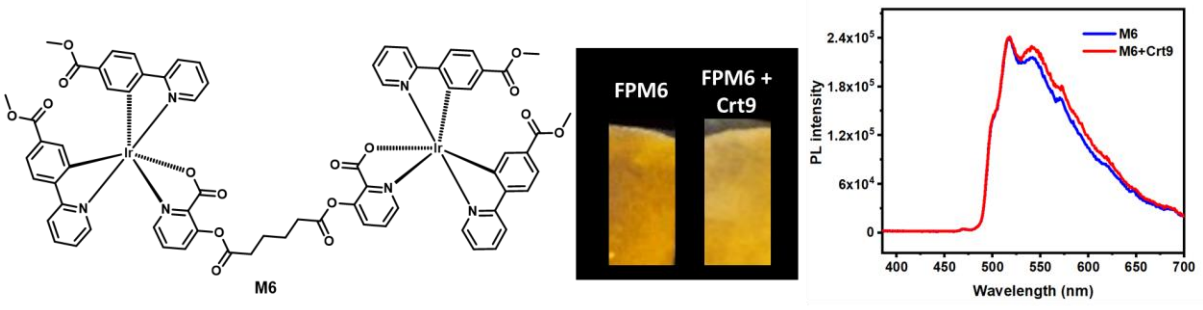

Figure 3.2.26 (a) Chemical structure for synthesized dinuclear iridium(III) complex M6 and (b) luminescent response on filter paper strip impregnated with M6, (i.e., FPM6) under UV lamp (365 nm) with corresponding PL intensity spectra (excitation at $\lambda_{exc.}$= 370 nm).

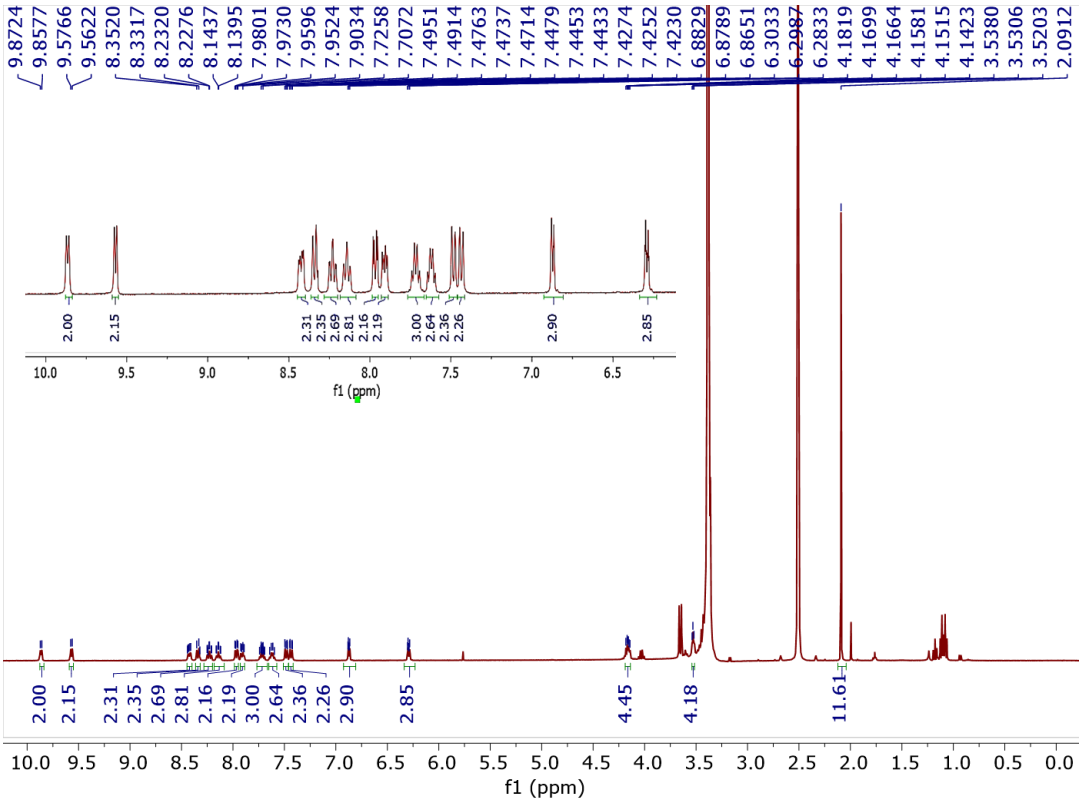

Figure 3.2.27 ^{1}H NMR spectrum of M6 in DMSO-d_6 solvent.

From the FESEM images, there has a very distinct nano-structured morphological difference was observed for solid M3 and M3 mixed with Crt9 (nanowire-based network structure vs continuous uniform nanostructure with scattered porosity) (Fig. 3.2.28). As a result, the absorbance study also provides support for the interactions between creatinine and M3 molecules. As per solid-state UV-VIS analysis, the solid M3 shows a change in absorption in the presence of creatinine (M3+Crt9) because of the formation of a new complex, (Fig. 3.2.29). Hence, this study showed creatinine detection in a low-cost filter paper strip mode. We believe that the current work may assess for ACR study that helps to obtain a prior indication of early-stage kidney disease. Also, such multinuclear iridium(III) based scaffold frameworks may serve as effective luminescent-based probes for sensing important biological analytes.

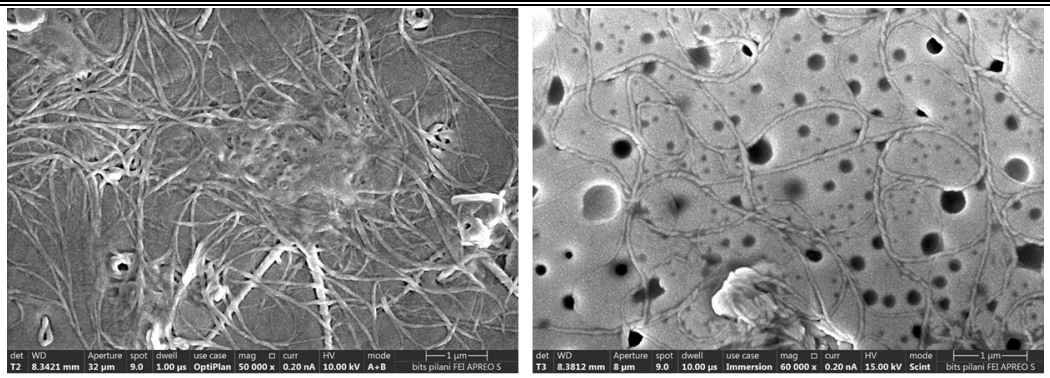

(a) (b)

Figure 3.2.28 FESEM images for; (a) the M3, and (b) Crt9 treated M3.

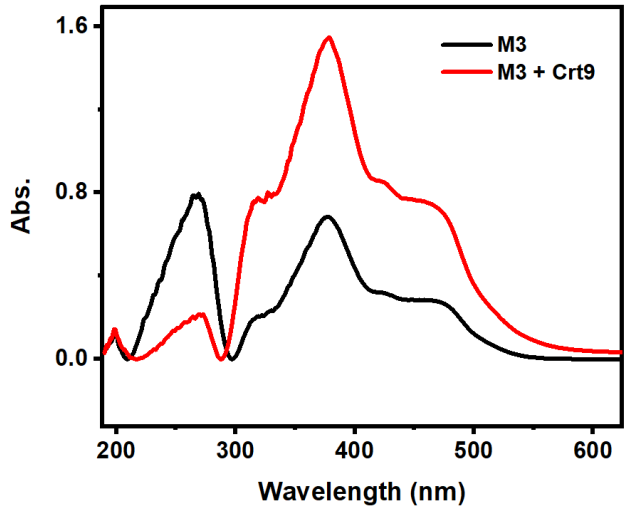

Figure 3.2.29 Solid-state absorption spectra for M3 and M3+Crt9.

3.2.4 References

1. V. Jha, G. Garcia-Garcia, K. Iseki, Z. Li, S. Naicker, B. Plattner, R. Saran, A. Y.-M. Wang and C.-W. Yang, *The Lancet*, 2013, **382**, 260-272.
2. W. G. Couser, G. Remuzzi, S. Mendis and M. Tonelli, *Kidney International*, 2011, **80**, 1258-1270.
3. J. R. Roberts, *Emergency Medicine News*, 2007, **29**.
4. A. P. de Silva, H. Q. N. Gunaratne, T. Gunnlaugsson, A. J. M. Huxley, C. P. McCoy, J. T. Rademacher and T. E. Rice, *Chemical Reviews*, 1997, **97**, 1515-1566.
5. Q. Li and Z. Li, *Advanced Science*, 2017, **4**, 1600484.
6. C. W. T. Leung, Y. Hong, S. Chen, E. Zhao, J. W. Y. Lam and B. Z. Tang, *Journal of the American Chemical Society*, 2013, **135**, 62-65.
7. T. Han, C. Gui, J. W. Y. Lam, M. Jiang, N. Xie, R. T. K. Kwok and B. Z. Tang, *Macromolecules*, 2017, **50**, 5807-5815.
8. C. Zhou, M. Jiang, J. Du, H. Bai, G. Shan, R. T. K. Kwok, J. H. C. Chau, J. Zhang, J. W. Y. Lam, P. Huang and B. Z. Tang, *Chemical Science*, 2020, **11**, 4730-4740.
9. S. S. Pasha, P. Das, N. P. Rath, D. Bandyopadhyay, N. R. Jana and I. R. Laskar, *Inorganic Chemistry Communications*, 2016, **67**, 107-111.

10. P. Alam, P. Das, C. Climent, M. Karanam, D. Casanova, A. R. Choudhury, P. Alemany, N. R. Jana and I. R. Laskar, *Journal of Materials Chemistry C*, 2014, **2**, 5615-5628.
11. P. C. Raichure, V. Kachwal and I. R. Laskar, *Molecules*, 2022, **27**.
12. P. Alam, G. Kaur, C. Climent, S. Pasha, D. Casanova, P. Alemany, A. Roy Choudhury and I. R. Laskar, *Dalton Transactions*, 2014, **43**, 16431-16440.
13. C. Wang, B. Xu, M. Li, Z. Chi, Y. Xie, Q. Li and Z. Li, *Materials Horizons*, 2016, **3**, 220-225.
14. P. C. Raichure, R. Bhatt, V. Kachwal, T. C. Sharma and I. R. Laskar, *New Journal of Chemistry*, 2022, **46**, 6560-6569.
15. X.-d. Wang and O. S. Wolfbeis, *Analytical Chemistry*, 2016, **88**, 203-227.
16. M.-j. Yin, B. Gu, Q.-F. An, C. Yang, Y. L. Guan and K.-T. Yong, *Coordination Chemistry Reviews*, 2018, **376**, 348-392.
17. C. Elosua, F. J. Arregui, I. D. Villar, C. Ruiz-Zamarreño, J. M. Corres, C. Bariain, J. Goicoechea, M. Hernaez, P. J. Rivero, A. B. Socorro, A. Urrutia, P. Sanchez, P. Zubiate, D. Lopez-Torres, N. D. Acha, J. Ascorbe, A. Ozcariz and I. R. Matias, *Sensors*, 2017, **17,** 2312.
18. P. C. Raichure, V. Kachwal, D. Sengottuvelu and I. R. Laskar, *Macromolecules*, 2022, 55, 23, 10377–10384.
19. D.-L. Ma, S. Lin, W. Wang, C. Yang and C.-H. Leung, *Chemical Science*, 2017, **8**, 878-889.
20. W. Che, G. Li, X. Liu, K. Shao, D. Zhu, Z. Su and M. R. Bryce, *Chemical Communications*, 2018, **54**, 1730-1733.
21. T. Chen, N. Xie, L. Viglianti, Y. Zhou, H. Tan, B. Z. Tang and Y. Tang, *Faraday Discussions*, 2017, **196**, 351-362.
22. J. Sittiwong and F. Unob, *Analytical Sciences*, 2016, **32**, 639-643.
23. K. Kotaska, B. Jedlicková and R. Průsa, *Casopis lekaru ceskych*, 2008, **147**, 392-395.
24. M. T. Alula, L. Karamchand, N. R. Hendricks and J. M. Blackburn, *Analytica Chimica Acta*, 2018, **1007**, 40-49.
25. X. Jin, J. Shi, J. Guan, G. Ni and J. Peng, *Nano*, 2017, **12**, 1750070.
26. M. S. Mathew and K. Joseph, *ACS Sustainable Chemistry & Engineering*, 2017, **5**, 4837-4845.
27. R. Jalili and A. Khataee, *Microchimica Acta*, 2018, **186**, 29.
28. P. J. Babu, A. M. Raichur and M. Doble, *Sensors and Actuators B: Chemical*, 2018, **258**, 1267-1278.
29. M. Hassanzadeh, M. Ghaemy, S. M. Amininasab and Z. Shami, *Sensors and Actuators A: Physical*, 2021, **331**, 112936.
30. R. Narimani, M. Esmaeili, S. H. Rasta, H. T. Khosroshahi and A. Mobed, *Analytical Science Advances*, 2021, **2**, 308-325.
31. M. Niu, C. Pham-Huy and H. He, *Microchimica Acta*, 2016, **183**, 2677-2695.
32. S. Sargazi, I. Fatima, M. Hassan Kiani, V. Mohammadzadeh, R. Arshad, M. Bilal, A. Rahdar, A. M. Díez-Pascual and R. Behzadmehr, *International Journal of Biological Macromolecules*, 2022, **206**, 115-147.
33. B. Yao, M.-C. Giel and Y. Hong, *Materials Chemistry Frontiers*, 2021, **5**, 2124-2142.
34. T. S. Anirudhan, J. R. Deepa and N. Stanly, *Applied Surface Science*, 2019, **466**, 28-39.
35. S. M. O. Quintal, H. I. S. Nogueira, V. Félix and M. G. B. Drew, *New Journal of Chemistry*, 2000, **24**, 511-517.
36. E. Liotta, R. Gottardo, L. Bonizzato, J. P. Pascali, A. Bertaso and F. Tagliaro, *Clinica Chimica Acta*, 2009, **409**, 52-55.

37. V. Kachwal, P. K. Sharma, A. Sarmah, S. Chowdhury and I. R. Laskar, *Journal of Materials Chemistry C*, 2020, **8**, 6605-6614.
38. N. B. Colthup, L. H. Daly and S. E. Wiberley, in *Introduction to Infrared and Raman Spectroscopy (Third Edition)*, eds. N. B. Colthup, L. H. Daly and S. E. Wiberley, Academic Press, San Diego, 1990.
39. S.-D. Zhang, Y.-R. Zhang, H.-X. Huang, B.-Y. Yan, X. Zhang and Y. Tang, *Journal of Polymer Research*, 2009, **17**, 43.
40. D. Lin-Vien, N. B. Colthup, W. G. Fateley and J. G. Grasselli, in *The Handbook of Infrared and Raman Characteristic Frequencies of Organic Molecules*, eds. D. Lin-Vien, N. B. Colthup, W. G. Fateley and J. G. Grasselli, Academic Press, San Diego, 1991, pp. 117-154.
41. S. Shariati and G. Khayatian, *Microfluidics and Nanofluidics*, 2022, **26**, 30.
42. D. Gangopadhyay, M. Das, K. K. Singh, R. K. Singh and P. Tandon, *Journal of Raman Spectroscopy*, 2020, **51**, 1056-1066.

CHAPTER 4

MULTI-STIMULI DISTINCT RESPONSIVE D-A BASED FLUOROGEN OLIGOMERIC TOOL AND EFFICIENT DETECTION OF TNT VAPOR

Chapter 4 Multi-Stimuli Distinct Responsive D-A Based Fluorogen Oligomeric Tool and Efficient Detection of TNT Vapor

4.1 Introduction

The design of an electron donor-acceptor (D-A) structure has drawn much interest since it may be used to create a tool for various stimuli-responsive advanced functional materials.[1, 2] The usage of fluorescent materials is widespread and is primarily attributed to their outstanding photosensitivity and quick response times. Examples of these applications include chemical vapor sensing,[3] solvafluorochromism,[4] mechanofluorochromism,[5] bioimaging,[6, 7] metal ion sensing,[8] etc.[9-12] With comparing to small molecules, polymeric/oligomeric materials have distinct advantages, such as higher mechanical strength, processability, ease of functionalization, tunable emission, and various topologies (linear, star-shaped, hyperbranched, etc.).[13, 14] In fact, luminescent polymers broaden the range of applications, including explosive detection,[15] stimuli-responsive materials,[16-18] polymer light-emitting diodes (PLEDs),[19, 20] and others. To fulfill the tremendous potential of practical applications such as light-harvesting photoactive polymeric brushes, theranostics, fluorescent chemosensors and biosensing, drug delivery, etc., the fluorescence properties of the polymers can be modified with composition, structure, and morphology.[21-25]

The significant electron density difference between the electron acceptor and donor in D-A type compounds leads to the strong intramolecular charge transfer (ICT) property. Such compounds with ICT characteristics have been utilized in various applications, including cell imaging,[26, 27] organic light-emitting diodes (OLEDs),[28] and solar cells.[29] Due to a distinct set of advantages, oligomeric/polymeric structures have a growing inclination to incorporate ICT characteristics.[30, 31] Triphenylamine (TPA) is widely known for its high potential to donate π-electrons.[32] While heterocyclic triazines are renowned for their strong ability to accept electrons or for being reactive towards nucleophiles.[33] The unsymmetrical distribution of electrons in the ground or excited state may be influenced by the donating and accepting properties of π-electrons. Strong electron-donating and accepting species (D-A), or a molecular system made up of π-electrons rich coupled with π-electrons poor species, are the conditions in which the greater intramolecular charge transfer (ICT) transitions frequently occur. Solvatochromism is the phenomenon where the emission wavelength of such systems changes when the polarity of the solvent medium changes. The solvatochromic probes can be utilized in chemosensors, bioimaging, water detectors, and other applications,[34, 35] as it is appropriate for detecting biomolecular interactions including proteins, nucleic acids, and bio-membranes.[36] The extent

of the probe molecule's Stokes shift can be affected due to the polarity of the surrounding environment; typically, a more polar solvent produces a more significant Stokes shift with a decrease in emission intensity.[37] The linearity in the Lippert-Mataga plot in different solvents is an indication that the general interaction is desirable for the D-A-based probes' emission property (i.e., solvent polarity).[38]

Nitroaromatic compounds are recognized as harmful pollutants and are being addressed as explosive materials.[39] There are currently various methods available for detecting explosives. These include electrochemical techniques, gas chromatography-mass spectrometry (GC-MS), and ion mobility spectroscopy.[40, 41] The remarkable photosensitivity and quick response time of luminescence-based trace-level explosive detection have recently gained growing attention.[12] The photoinduced electron transfer (PET), energy transfer (ET), or resonance energy transfer (RET) mechanisms are generally used to explain the fluorescence quenching response of the probes with nitroaromatic explosives.[42] It is feasible to transfer the electron to an analyte through the PET mechanism when the LUMO of the sensing probe (donor) is aligned with the LUMO of the analyte (acceptor). To detect nitro explosives, a variety of materials and frameworks have been developed, including metal-organic frameworks,[43] conjugated polymers,[44] dendrimers,[45] nanofibrous materials,[46] calixarenes,[39] cyclodextrins,[47] bioinspired materials,[48] quantum dots.[49] The detection of nitro explosive compounds has often been done in the aqueous phase.[50] It is crucial to detect explosives from vapor in field applications. In recent years, there has been a surge of attention in fluorescence-based vapor phase TNT explosive detection.[15, 51, 52]

Nitrogen-containing D-A probes are often sensitive to an acidic medium.[53] By neutralizing with a base, the possible bathochromic shift in an acidic medium could be reversed.[54] A push-pull π-electron mechanism is expected to cause the π-electron donor group, like TPA, attached through conjugation to the nitrogen-containing heterocyclic compound to be sensitive to acids.[55-57] Hayashi et al. studied the same film of pyridine-based polymer for detecting Bronsted acid and Lewis acid as well as solubility switching via vapor exposure of Lewis acid (BF_3-OEt_2) and base (NEt_3).[58] No additional reports have been found where a single probe can identify both base and acids (Bronsted and Lewis acids) in a vapor phase. If such probes demonstrate the detection of acids and bases from the vapor phase with a significant Stokes shift, that would be more interesting.[59]

Various mechanical stimuli, such as grinding, pressing, crushing, etc., are often used to show mechanofluorochromic (MFC) substances.[60-62] The high potential of MFC materials

satisfies the requirements of numerous applications, including stress detectors,[63] force distribution sensors,[64] micro-environmental change monitoring bioprobes,[65], and pressure indicators.[66] In general, mechanical disturbances could cause crystalline material to lose its ordered form by changes in the intermolecular packing modes.[67-69] Powder X-ray diffraction (PXRD), differential scanning calorimetry (DSC), high-resolution transmission electron microscopy (HRTEM), UV-Vis spectroscopy, infrared and Raman spectroscopy, among other techniques, could be used to investigate the disordered state or change in crystallinity of the MFC sample.[70-75] Although several publications in the literature demonstrate MFC property with bathochromically shifted small molecules and polymers,[62, 76-82] there are noticeably fewer findings on hypsochromic shifted (i.e., blue-shifted) turn-on emission.[83, 84]

Numerous triazine-amine-based donor-acceptor compounds have been reported and used in the reversible and rapid sensing of acids,[33] and sensitive and selective detection of picric acids.[85, 86] Being a strong acceptor, triazine can be combined with an appropriate donor to produce compounds with a strong D-A characteristic. Such compounds can be used not only in sensitive analyte detection but also as sensitive multi-stimuli probes. This feature inspired us to synthesize a donor-acceptor compound based on triazine-amine that can be utilized as a multi-stimulus probe. In this article, we describe the synthesis of an oligomeric network with a D-A type structure made up of a strong heterocyclic electron acceptor based on triazine and an electron donor based on TPA. This synthesized D-A molecule shows the following properties - tracing of TNT from the vapor phase, a sensitive solvatochromic probe, Bronsted and Lewis acid vapor sensing capability (with a significant red-shifted emission for TFA in solution and vapor phases), and blue-shifted turn-on MFC observation, these are examples of distinctive responsive multi-stimuli sensing capabilities.

4.2 Experimental Section

A π-electron donor-acceptor (D-A) based oligomer (P1) has been synthesized, as shown in Scheme 4.1.1. Earlier, a polymeric network similar to P1 was synthesized by refluxing cyanuric chloride, and TPA with anhydrous $AlCl_3$ in degassed o-dichlorobenzene (~190 °C) for 36 h under an argon environment.[87] In the present work, we have achieved the oligomeric network (P1) by following an alternative route with a shorter time (~12 h) and at a lower temperature (60 °C).

4.2.1 Experimental Procedure

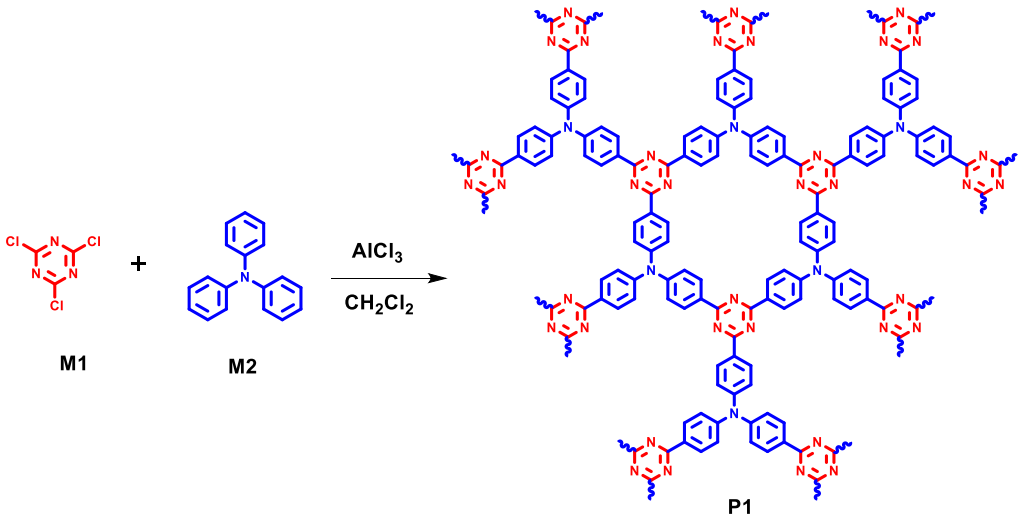

Scheme 4.1 Synthesis of oligomer (P1) from monomers (M1 and M2) via Friedel-Crafts reaction.

Synthesis of oligomer (P1): The P1 was synthesized from the M1 (cyanuric chloride) and M2 (TPA) monomers via Friedel-Crafts reaction by using anhydrous $AlCl_3$ as a catalyst. The monomer M1 (0.375 g, 2.03 mmol), anhydrous $AlCl_3$ (0.813 g, 6.09 mmol), and DCM-solvent (30 ml) were added to a glass-made sealed tube. The mixture in the tube was stirred well for 20 minutes at room temperature. Then, the monomer M2 (0.500 g, 2.03 mmol) was added directly to the same tube and stirred continuously with heating at 60 °C for ~12 h. After that, stirring was stopped and the sealed tube was cooled at room temperature for about an hour. The reaction was quenched with the addition of water and then extracted with DCM. The precipitate was collected by evaporating the solvent. The reprecipitation was done in a large volume of methanol. Then the orange-colored P1 was obtained after centrifugation followed by the washing process with methanol several times (0.700 g). The product was characterized by ^{1}H, and ^{13}C spectra (Fig 4.1 and 4.2, respectively). In ^{1}H NMR, a broad range of aromatic peaks shows many equivalent aromatic protons, whereas in ^{13}C NMR, the number of aromatic carbon peaks indicates the formation of an oligomeric network of P1.

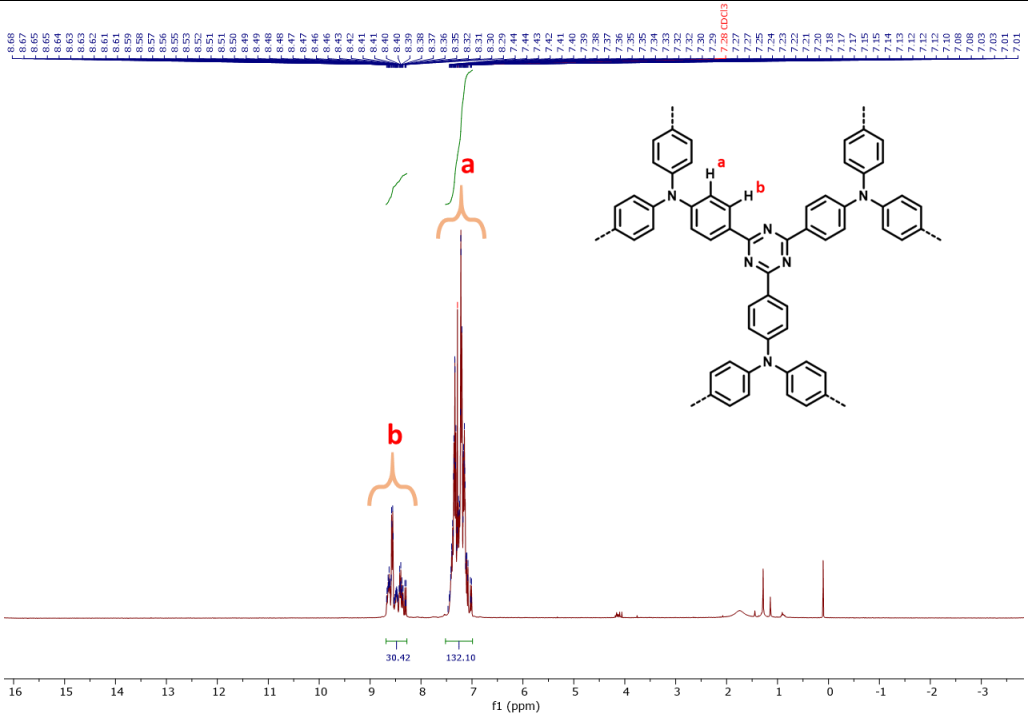

Figure 4.1 ^{1}H NMR spectrum of P1 in $CDCl_3$ solvent.

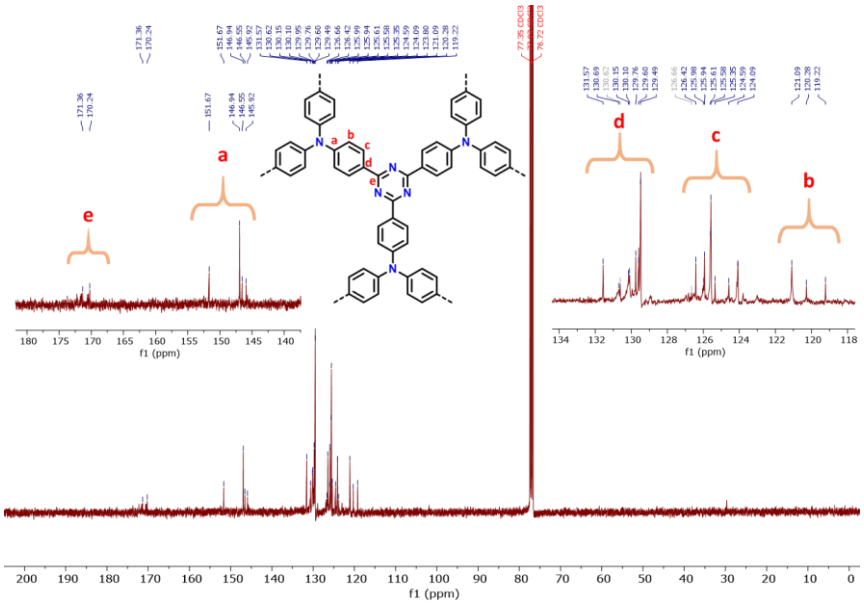

Figure 4.2 ^{13}C NMR spectrum of P1 in $CDCl_3$ solvent.

4.3 Results and Discussion

The weight average molecular weight (M_w) for P1 is 2295 Da, which was obtained from GPC analysis. By the TGA experiment, the P1 is found to be thermally stable up to 200 °C (Fig 4.3). The observed absorption (λ_{abs}) of P1 is 400 nm for both the powdered P1 and THF solution of P1 (Fig 4.4). The observed absolute quantum yield (QY) is 1.4 % and 39.9 % for solid powder

and solution (in DCM), respectively. The characteristic lifetime decay for P1 was recorded and an average lifetime was found at 4.8 ns for solid-state P1 and 3.5 ns for the THF solution of P1 (Fig 4.5).

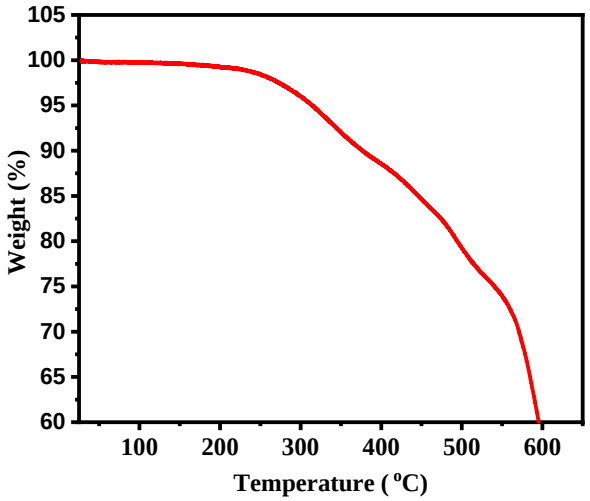

Figure 4.3 Thermogravimetric analysis (TGA) plot for P1.

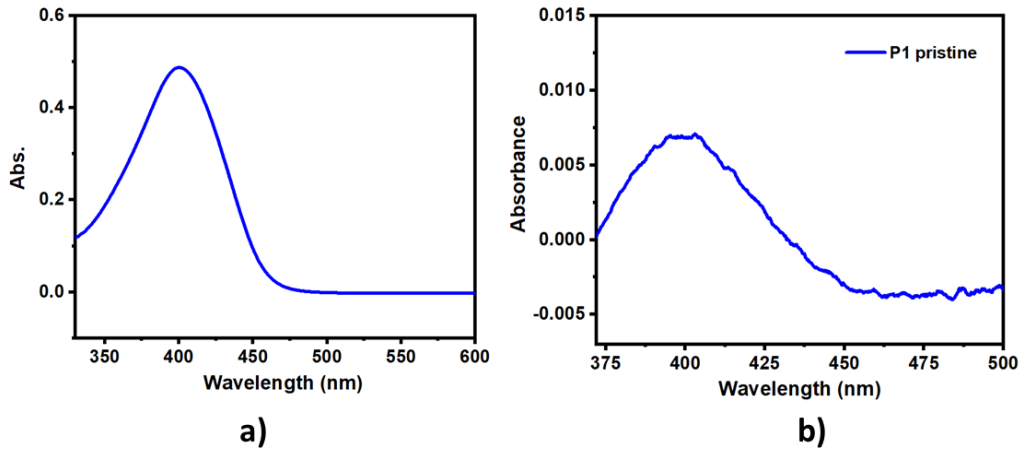

Figure 4.4 Plots of absorbance in a) THF solution of P1 (1 mg P1 in 50 ml THF) (λ_{abs} = 400 nm), b) P1 pristine (powder/solid form) (λ_{abs} = 400 nm) in reflectance mode and then converted it to absorbance value.

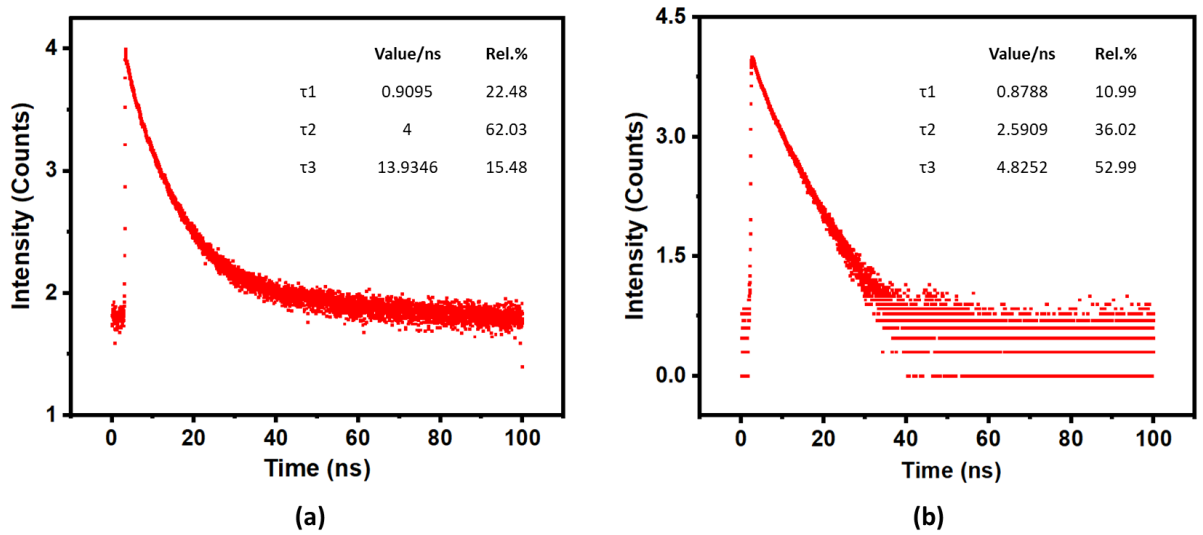

Figure 4.5 The characteristic fluorescence lifetime decay curve [plot: time (ns) vs intensity that is in, $\log_{10}$ (counts)]: a) for P1 in solid state (χ^2 = 1.2), and b) for THF solution of P1 (χ^2 = 1.1).

4.3.1 Solvatochromism

The absorption and emission spectra were recorded to investigate the solvatochromic properties in variable polar solvents. In the hexane solution of P1, strong blue fluorescence was observed at emission wavelength λ_{emi} = 446 nm (Fig 4.6). A bathochromic shift was observed continuously with increasing the polarity of the solvent and the emission peak was observed at λ_{emi} = 514 nm in highly polar DMSO solvent. The Stokes shift was determined for P1 in each given solvent, and it is increasing from hexane (low polar) to DMSO (high polar) solvents (Table 4.1.1). The orientation polarisability values were reported for given solvents in the earlier report.[88] Mostly, the ICT character in the D-A type of molecule is responsible for solvatochromic behavior.[89] The basic unit structure of P1 was optimized using the Gaussian 09 Gauss view program.[90] The LUMO sites were mainly localized on the triazine unit, and the HOMO sites were localized on the TPA unit (Fig 4.7). Such unsymmetrical electronic distribution facilitates the ICT character.[2]

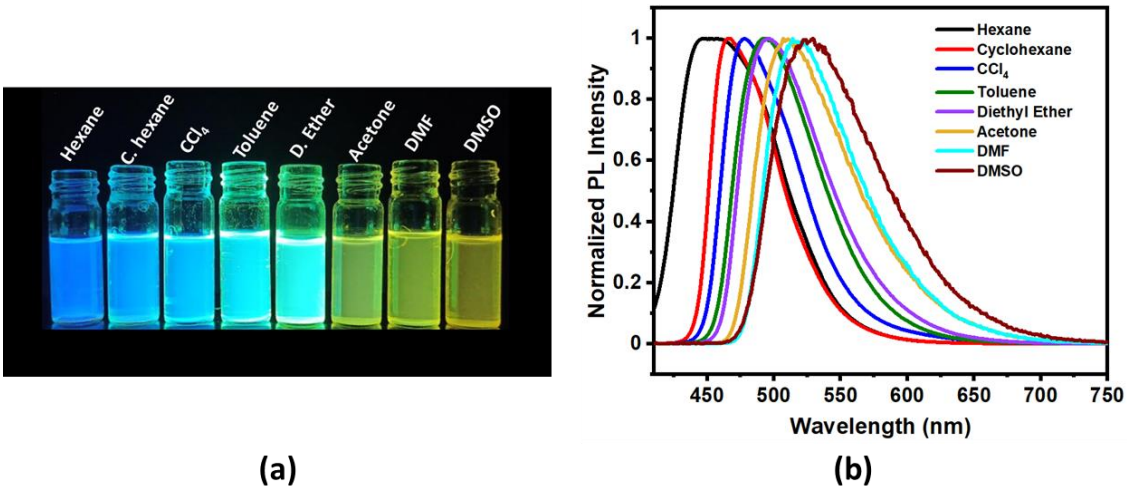

Figure 4.6 (a) Image for the emission color of P1 with various solvents under UV lamp (365 nm): hexane, cyclohexane (C. hexane), carbon tetrachloride (CCl_4), toluene, diethyl ether (D. Ether), acetone, N, N-dimethylformamide (DMF), dimethyl sulfoxide (DMSO); (b) normalized photoluminescence (PL) intensity plot of P1 in the given solvents with various polarities (at excitation 397 nm).

Table 4.1 The absorption and emission maxima of P1 in different solvents along with Stokes shift and orientation polarisability.

Solvents	Abs. wavelength $\lambda_{max.}$ (nm)	Emission wavelength $\lambda_{max.}$ (nm)	Absorption (cm^{-1})	Emission (cm^{-1})	Stokes shift (cm^{-1})	Orientation polarizability (Δf)
Hexane	396	446	25252.5	22421.5	2831	0.002
Cyclohexane	400	467	25000	21413	3586.7	-0.001
CCl_4	404	478	24752.4	20920.5	3831.9	0.008
Toluene	405	491	24691.3	20366.5	4324.7	0.013
Diethyl Ether	401	496	24937.6	20161.2	4776.3	0.167
Acetone	402	507	24875.6	19723.8	5151.7	0.283
DMF	402	514	24875.6	19455.2	5420.3	0.275
DMSO	404	529	24752.4	18903.5	5848.8	0.265

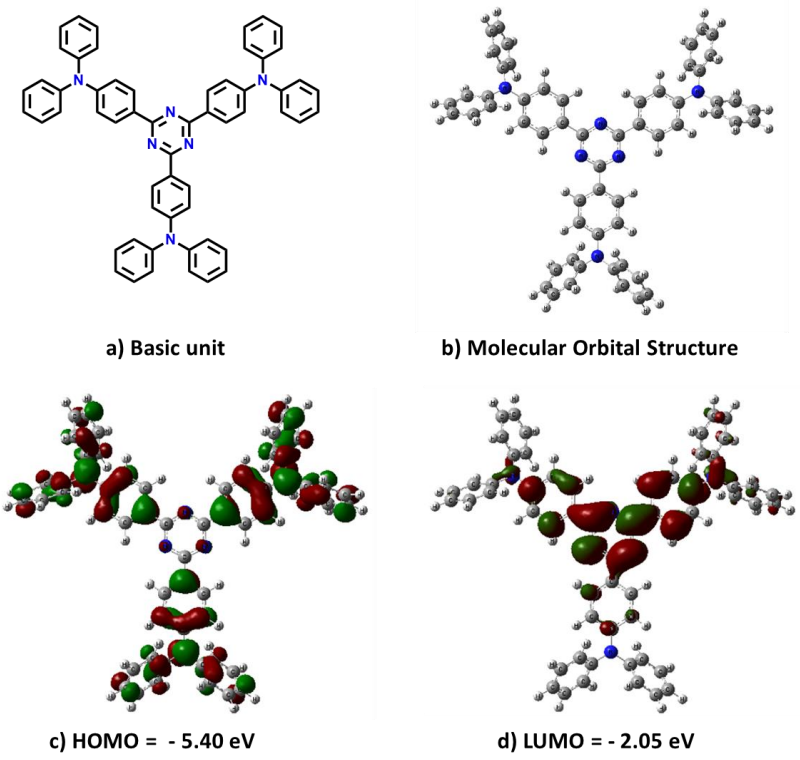

Figure 4.7 It shows a) basic unit (the optimized geometry), b) molecular orbital structure, c) HOMO, and d) LUMO, by DFT-based calculation via Gaussian 09 at the B3LYP/6-31G.

The Lippert-Mataga plot was applied for the orientation polarizability (Δf) of the solvent against the corresponding calculated Stokes shifts (Fig 4.8). It revealed a linear increase of Stokes shift vs. orientation polarisability (Δf) (with the correlation coefficient, Pearson's r value = 0.89). The observed ICT between the donor and acceptor in the excited state is responsible for the observed positive solvatochromism.[91, 92] The probe-solvent dipole interaction controlled the energy of the excited state of P1, which is the cause of the observed bathochromic shift (red-shifted) for emission with increasing solvent polarity.[93]

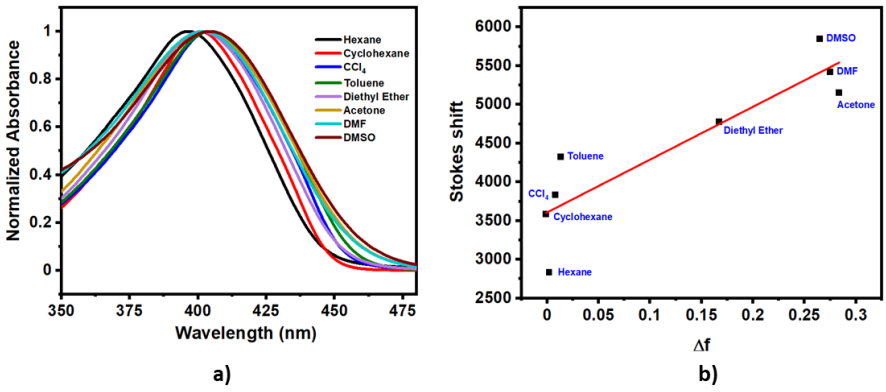

Figure 4.8 a) Plot of normalized absorbance of P1 with various solvents (1 mg P1 in 10 ml solvent) - hexane, cyclohexane, carbon tetrachloride (CCl_4), toluene, diethyl ether, acetone, N,

N-dimethylformamide (DMF), dimethyl sulfoxide (DMSO); b) Lippert–Mataga plot of orientation polarizability (Δf) vs. Stokes shift, shows an approximately linear variation in Stokes shift with the polarity of the solvents.

4.3.2 TNT Detection

The fluorescence quenching response was observed in the presence of TNT explosive. The paper strip (Whatman filter paper No.1) was used successfully to check the TNT sensing response. Paper strips were impregnated with a toluene solution of P1 (1 mg in 5 ml) and then dried well. A drop of an equal amount (i.e., 0.01 ml) of prepared aqueous TNT solution (10^{-3} to 10^{-15} M) was placed on the different impregnated paper strips (Fig 4.9). A marked fluorescence quenching was visualized with 10^{-3} M aqueous TNT solution, and the pale shade of fluorescence quenching was visualized until the dilution reached 10^{-15} M (femtomolar).

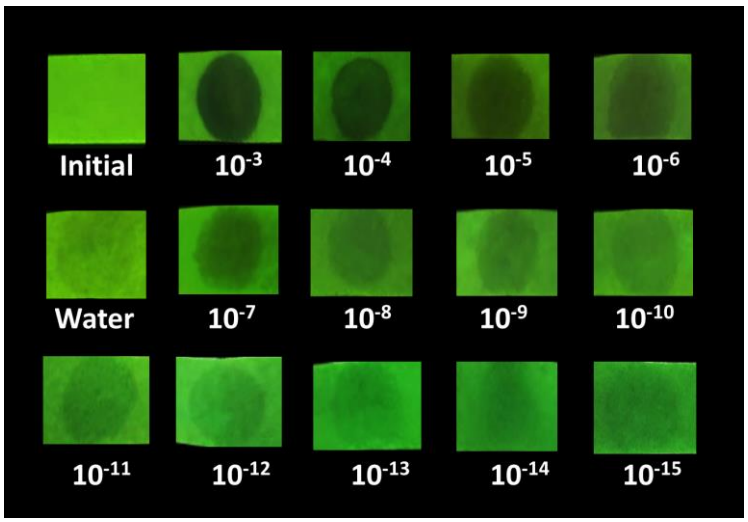

Figure 4.9 Image for filter paper strips impregnated with P1 (under UV lamp 365 nm) after placing a drop of various concentrations of aqueous TNT solution along with initial and with water drop as well.

A vapor phase-based TNT sensing has been studied with probe P1. The glass container of 5 ml volume containing 0.1 g of TNT material was closed with a rubber septum and the container was heated at a constant temperature of 40 °C for 20 minutes to generate saturated vapor pressure. The reported saturated vapor pressure of TNT is 82.8 ppb (8.40×10^{-3} Pa) at 40 °C.[94] An equal amount (0.5 ml) of this vapor was collected by a gas-tight syringe and directly exposed to a P1-impregnated paper strip (Fig 4.10). The fluorescence quenching was observed after an exposed equal amount of TNT vapor for each reading (Fig 4.11). The observed LOD for the TNT in a vapor phase is 698 ppb. Also, solution-based sensitivity has been studied for

TNT. The fluorescence emission quenching was observed for the THF solution of P1 (1 mg P1 in 10 ml THF) after each addition of 0.1 ml aq. TNT solution (10^{-3}M) (Fig 4.12). The calculated LOD for the TNT in the solution phase is 79.2 ppm. The observed excited state lifetime decay for the THF solution of P1 is 3.5 ns and after adding aq. TNT solution decreases to 1.5 ns, which indicates the dynamic quenching takes place at the excited state (Fig. 4.13a).

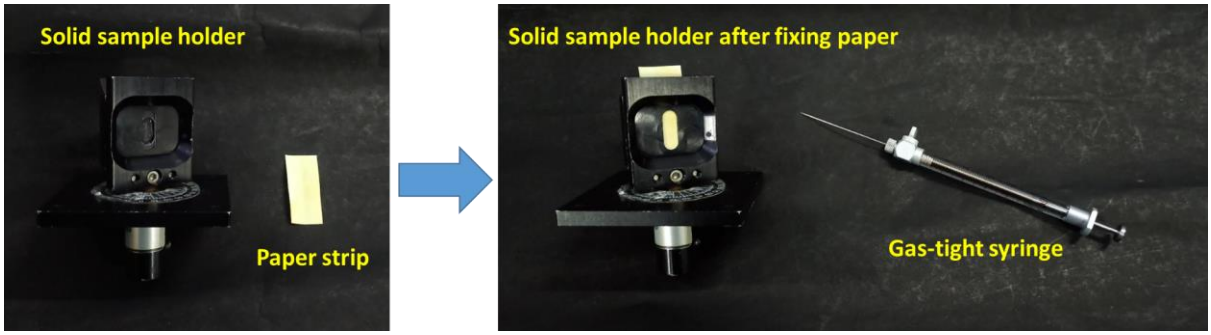

Figure 4.10 Set-up for TNT vapor detection: solid sample holder used in fluorimeter for recording emission spectrum, P1 impregnated filter paper strip, gas-tight syringe.

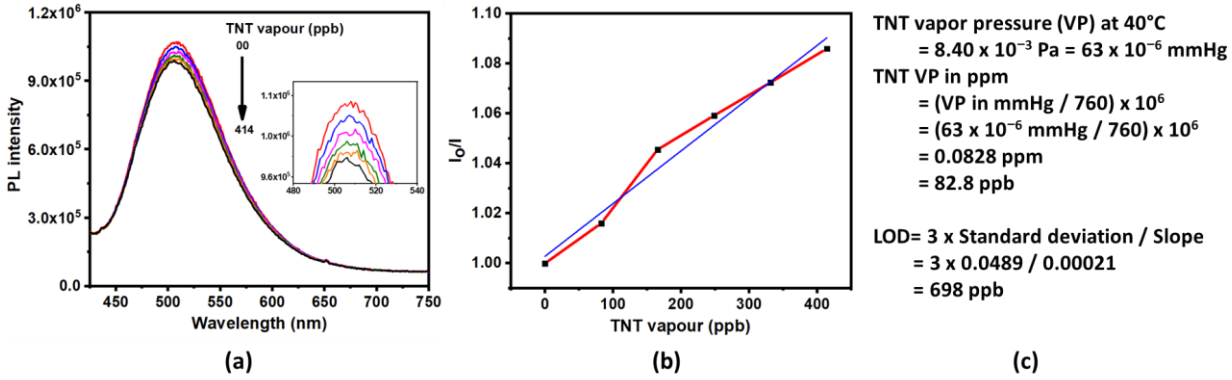

Figure 4.11 (a) PL intensity plot for P1 (emission λ_{emi} = 505 nm at excitation 397 nm) with each exposure of 82.8 ppb TNT vapor; (inset) shown in an enlarged view of PL intensity change; (b) Stern-Volmer plot of (I_o/I) vs. TNT vapor (ppb) exposure (Pearson's r value= 0.98); (c) calculation of limit of detection (LOD) for P1 with TNT vapor.

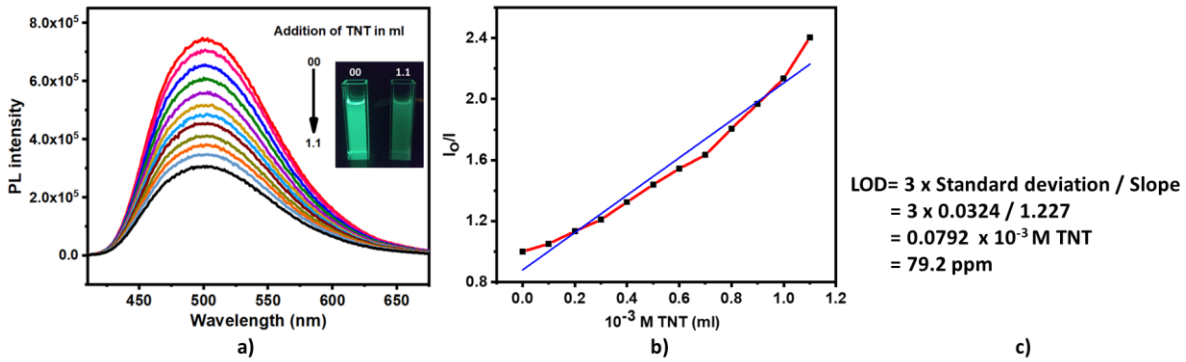

Figure 4.12 a) PL intensity plot for fluorescence emission quenching after each addition of 0.1 ml aq. TNT solution (10^{-3}M) to the THF solution of P1 (1 mg P1 in 10 ml THF) (excitation =397 nm); b) the corresponding Stern-Volmer plot; c) calculation for a limit of detection (LOD) of P1 with TNT solution.

The possible mechanism of energy transfer (ET) and photo-induced electron transfer (PET) for fluorescence quenching was studied. Overlapping was not observed between the emission spectrum of probe P1 and the absorption spectrum of the analyte which excludes the possibility of an ET mechanism (Fig 4.13b). The HOMO and LUMO energy were determined to check the possibility of an electron transfer from electron-rich probe P1 to electron-deficient TNT. The HOMO and LUMO energy levels of P1 were determined from equation $E_{(HOMO)} = E_{(LUMO)} + E_{(gap,\ electronic)}$. The energy gap $E_{(gap,\ electronic)}$ between HOMO and LUMO energy levels was determined from band-edge absorption of the UV-VIS spectrum $E_{(gap,\ electronic)} = h \times c / \lambda_{offset}$ which was found at 2.6 eV (Fig 4.14). Cyclic voltammetry (CV) experiment was performed to calculate HOMO energy $E_{(HOMO)}$ i.e., −5.2 eV (Fig 4.14). The observed LUMO energy for P1 is $E_{(LUMO)} = E_{(HOMO)} - E_{(gap,\ electronic)} = -2.6$ eV which is higher and nearly close to the reported LUMO value of TNT (i.e., −3.5 eV) (Fig 4.15).[95] The fluorescence quenching occurs via photo-induced electron transfer (PET) from the LUMO energy level of excited state P1 to the LUMO energy level of TNT.[96]

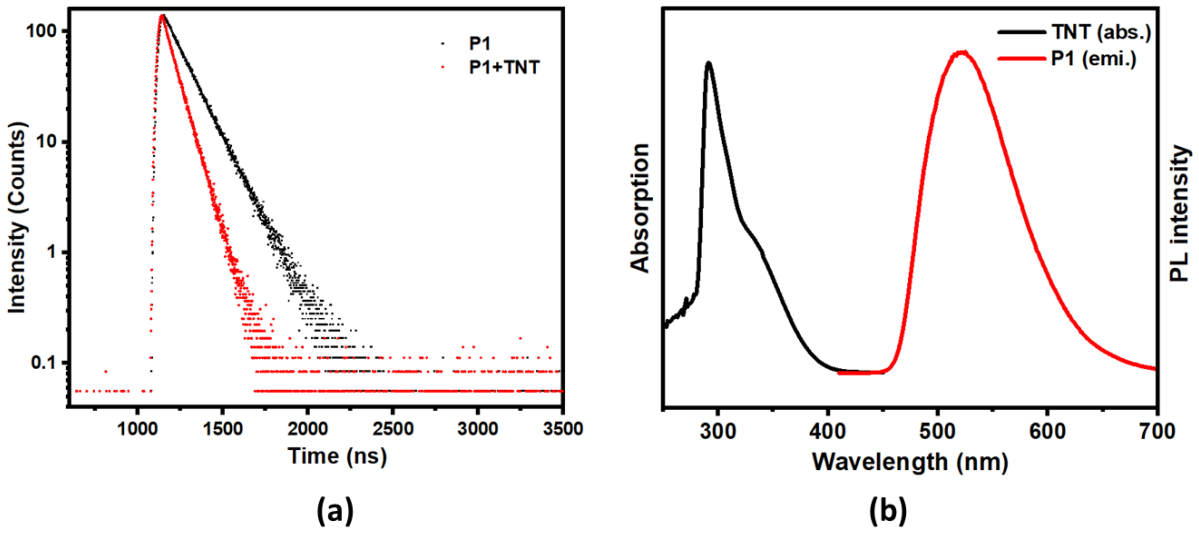

Figure 4.13 (a) The characteristic fluorescence lifetime decay curve for THF solution of P1 and after the addition of 0.1 ml aq. TNT solution (10−3M) to the THF solution of P1 [plot: time (ns) vs intensity that (counts)], (b) Absorption and emission spectra for the solution of

TNT and P1 (in THF); black = TNT (absorption) and red = P1 emission (observed under the 360 nm excitation).

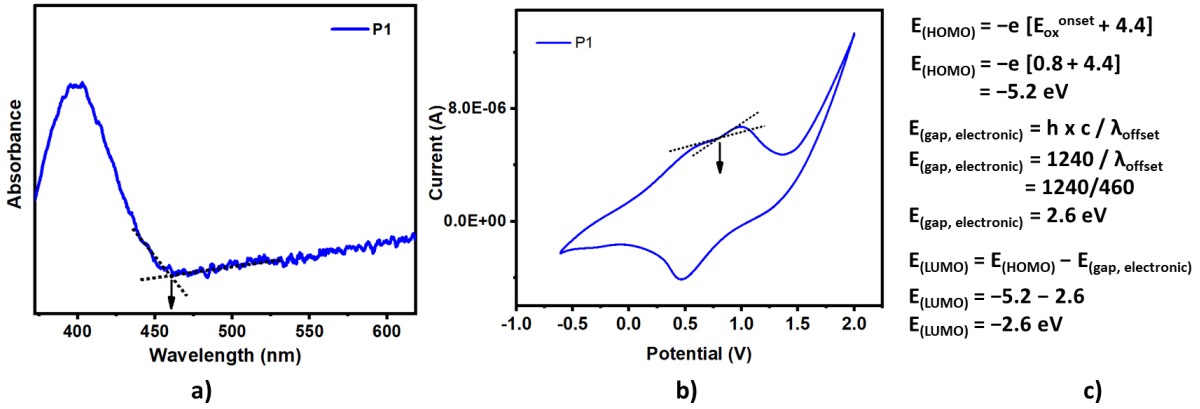

Figure 4.14 a) Absorption spectrum for pristine P1 (arrow sign shows the band edge absorption), **b**) The cyclic voltammetry plot of P1 in acetonitrile (ACN) (1 mg P1 in 5 ml ACN); scan rate: 100 mV s^{-1}, **c**) calculation of HOMO and LUMO energy for P1.

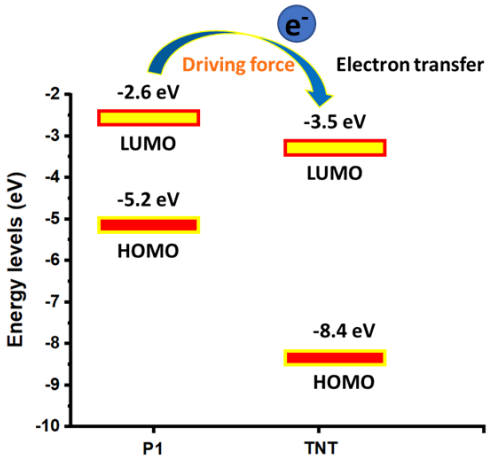

Figure 4.15 Schematic illustrations for electron transfer mechanism of fluorescence quenching by energy level comparison of P1 and TNT.

The observed high detection limit can be explained by the porous microstructure film supported by the FESEM. A thin film of P1 was prepared on glass by a drop-casting method where the solution of P1 in THF (2 mg P1 in 0.5 ml of THF) was used to make a thin film. The prepared thin film was annealed in an oven at atmospheric pressure for an hour at 60 °C. The observed absorbance and emission for the prepared thin film of P1 were almost matched with the pristine P1 (Fig 4.16). From the FESEM analysis, spherical-shaped particles and pores were observed for P1 (Fig 4.17). The porous nature of hyperbranched microstructure P1 assists to trap the TNT, which facilitates the PET mechanism to quench the original emission of P1.

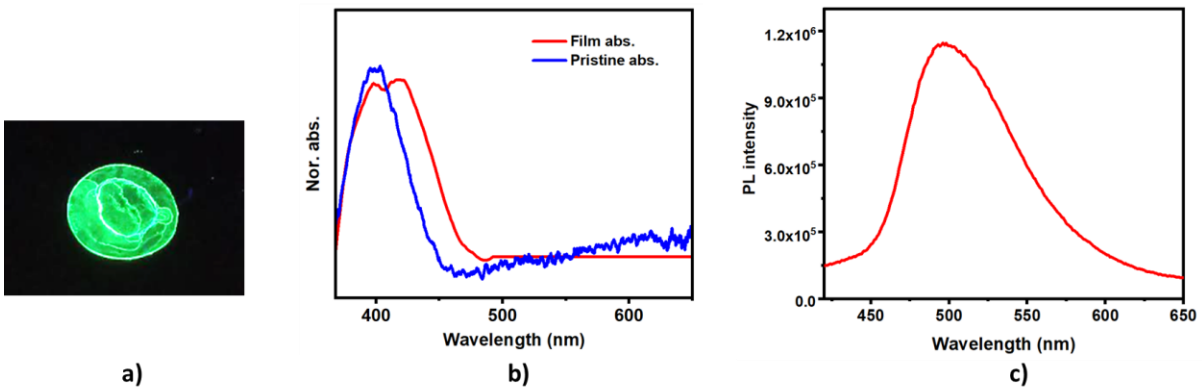

Figure 4.16 a) Photograph of emission for P1 film under UV lamp (λ_{exc}, 365 nm); **b**) absorbance spectrum of P1 was recorded in thin film and powder form indicate the absorbance profile in both cases remain almost same; **c**) PL intensity spectrum in P1 film (excitation = 397 nm) emission at 505 nm that is matching with P1 impregnated paper strip.

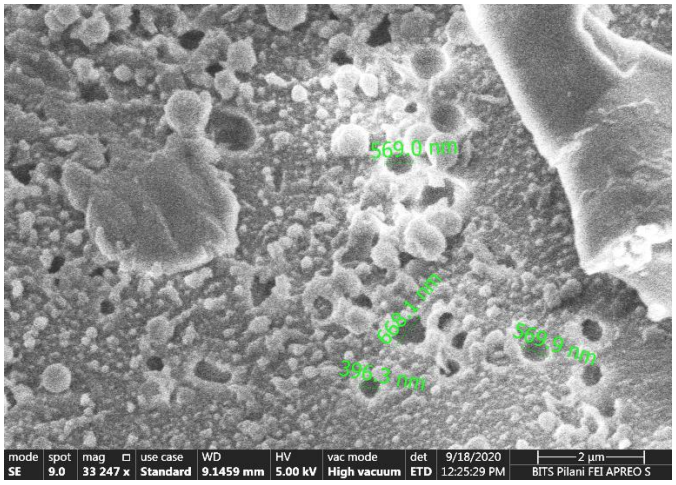

Figure 4.17 FESEM image of the thin film of P1 prepared by drop casting method showing a nanoporosity.

4.3.3 Acidochromism

As per the reports, usually, the D-A-based heterocyclic compounds containing nitrogen atoms are sensitive to the acidic medium.[53, 86] The P1 was treated with trifluoroacetic acid (TFA) (Bronsted acid) to check the protonic acid sensitivity in the liquid phase. Originally, the DCM solution of P1 (1 mg P1 in 10 ml DCM) showed green emission (λ_{emi}= 513 nm). The most significant, red-shifted emission (λ_{max}, 621 nm; which red-shifted by 108 nm) was observed after adding a drop of TFA (0.06 ml) to the above P1 solution. The original green emission could be restored by neutralizing it with base triethylamine (NEt_3) (Fig 4.18). A drastic color change (green to deep red) was also visible under daylight. Again, the same trend was observed

with Lewis acid, boron trifluoride etherate [$BF_3(OEt_2)$], where it reveals a red-shifted emission by 94 nm. The fluorescence emission change was observed due to the interaction of BF_3 with P1 but not with diethyl ether (OEt_2) and that was confirmed by titrating the DCM solution of P1 with diethyl ether (OEt_2) (Fig 4.19). The red-shifted fluorescence emission was also observed on titrating P1 with HCl as well. A constantly red-shifted emission was observed with the gradual addition of HCl (at each addition, 0.01 ml of 12M HCl) (Fig 4.20a). A similar trend was observed with each addition of 0.1 ml of $BF_3(OEt_2)$ (45-50%) into the DCM solution of P1 (Fig 4.20b). In the same way, a drastic change was observed for the DCM solution of P1 emission color after adding 50 µL of different protonic acids, *i.e.*, HCl, TFA, H_2SO_4, HNO_3 under daylight and UV lamp (λ_{exc}, 365 nm), respectively (Fig 4.21). In this case, each of the acids shows a distinct, red-shifted emission color change.

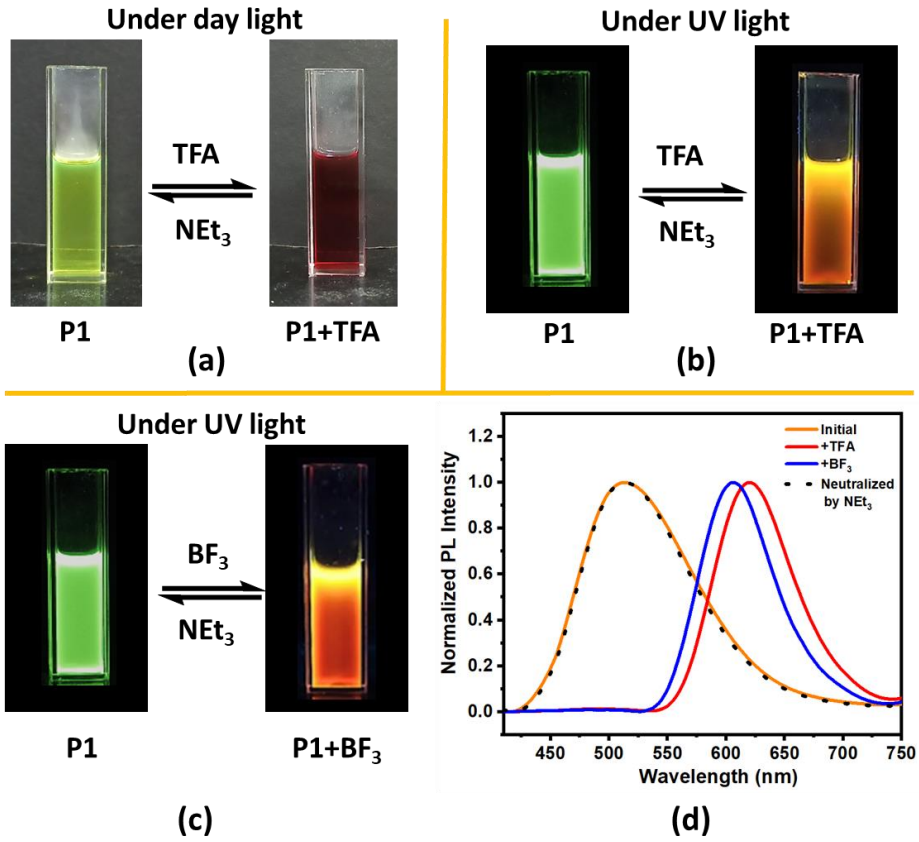

Figure 4.18 Image for the change in the appearance of DCM solution of P1 (green emission λ_{emi} = 513 nm under UV light of 365 nm), (**a**) and (**b**) are on the addition of TFA under daylight and UV light (365 nm), respectively, and (**c**) on the addition of $BF_3(OEt_2)$ under UV lamp (365 nm). (**d**) PL intensity plot (at excitation 397 nm) to show the red-shifted fluorescence emission by 108 and 94 nm by addition of TFA and $BF_3(OEt_2)$, respectively and both could fully reverse to original emission by neutralization with base NEt_3 (dotted line).

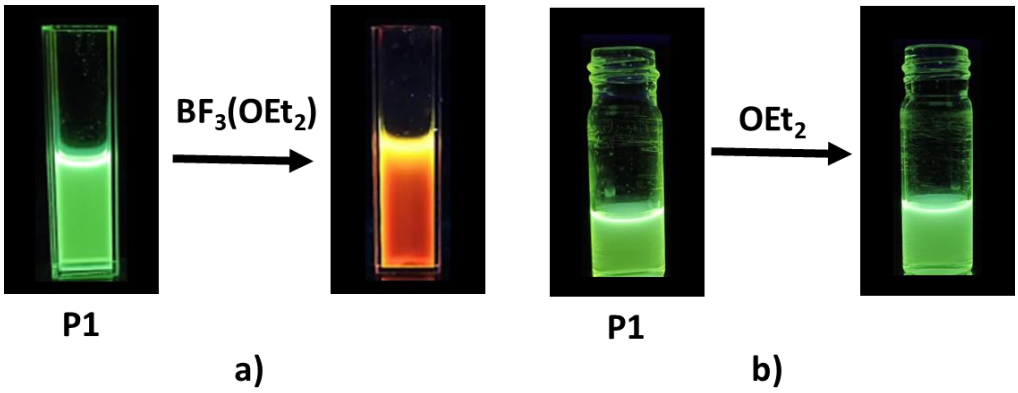

Figure 4.19 Photographs of change in the appearance of a dichloromethane (DCM) solution of P1 (1 mg P1 in 10 ml DCM), **a**) with $BF_3(OEt_2)$ (0.4 ml), and **b**) with OEt_2 (0.4 ml) under UV light of 365 nm.

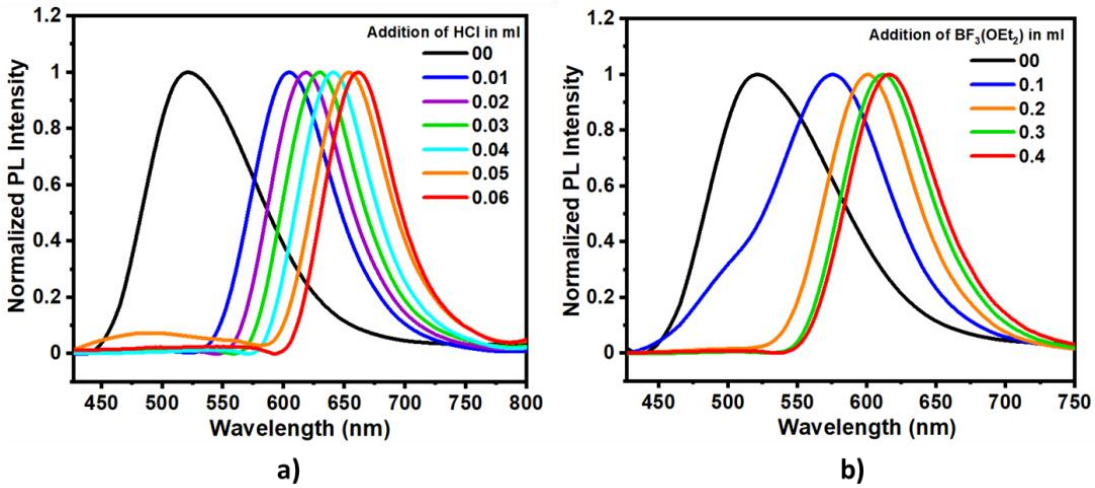

Figure 4.20 Plots for change in emission wavelength of a dichloromethane solution of P1 (at excitation 397 nm), **a**) with each 0.01 ml addition of 12M concentrated HCl, and **b**) with each 0.1 ml addition of boron trifluoride etherate [$BF_3(OEt_2)$] (45-50%).

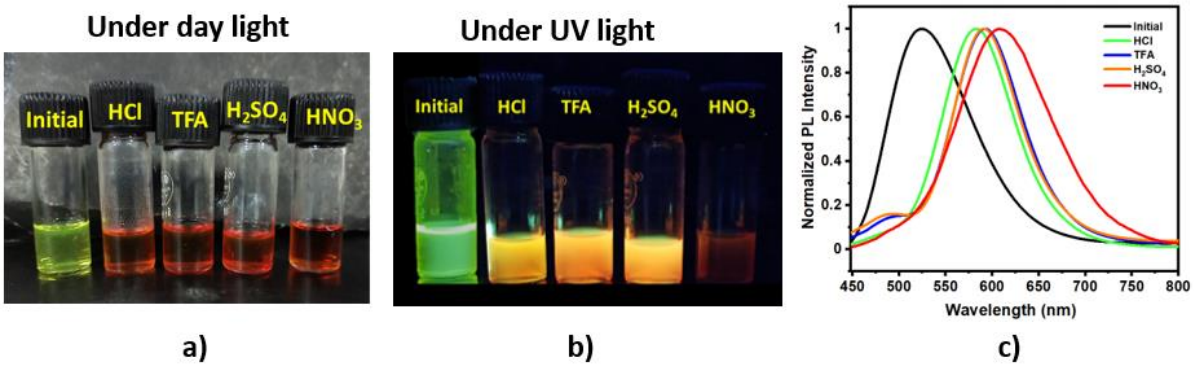

Figure 4.21 Photographs **a**) and **b**) show the change of emission color upon 50 µL addition of each of 10M concentrated different protonic acids [hydrochloric acid (HCl), trifluoroacetic acid (TFA), sulfuric acid (H_2SO_4), nitric acid (HNO_3)] were added into the DCM solution of P1 (2 ml solution; 1 mg P1 in 10 ml DCM) under daylight and UV light (365 nm), respectively, and **c**) is the PL intensity plot for the change in emission (at excitation 397 nm).

For the study of vapor phase protonic acid sensitivity, P1 was exposed to the TFA vapors. After a few seconds of exposure to TFA vapors, the original yellowish-orange colored emission (λ_{emi} = 555 nm) of P1 (pristine) turned to a red emission color (Fig 4.22). The large red-shifted emission wavelength in the presence of Lewis acid (i.e., 94nm) is the second to the best report so far.[97] After neutralizing it with base NEt_3 vapors, the red-colored emission of P1 returns to the original emission, and another way by keeping it as such at room temperature for 24 hours (Fig 4.23). The red-shifted emission for P1 reached a maximum wavelength of λ_{emi} = 652 nm upon the TFA vapors exposure for 6 minutes (Fig 4.23). The same trend was also observed on the exposure of P1 with vapors of $BF_3(OEt_2)$. The gradually red-shifted emission was observed for P1 at each minute vapor exposure of TFA and $BF_3(OEt_2)$ (Fig 4.24). The protonation of the nitrogen in the triazine molecule of P1 may have caused the change in emission.

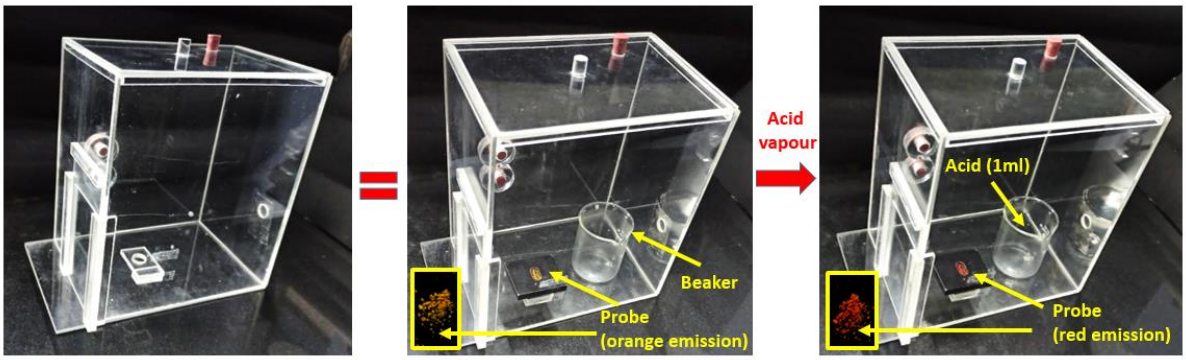

Figure 4.22 Photographs of **a**) closed box with lid made from acrylic sheet, **b**) the box contains one glass-made beaker and powder sample fluorimeter holder with probe P1 (orange emission excited by UV lamp at 365 nm); the door is closed; here the beaker does not contain any acid (blank test), **c**) turned the emission of P1 (red emission excited by UV lamp at 365 nm) within 10 seconds of contact with vapors generated by acid (1 ml of TFA) filled in the beaker.

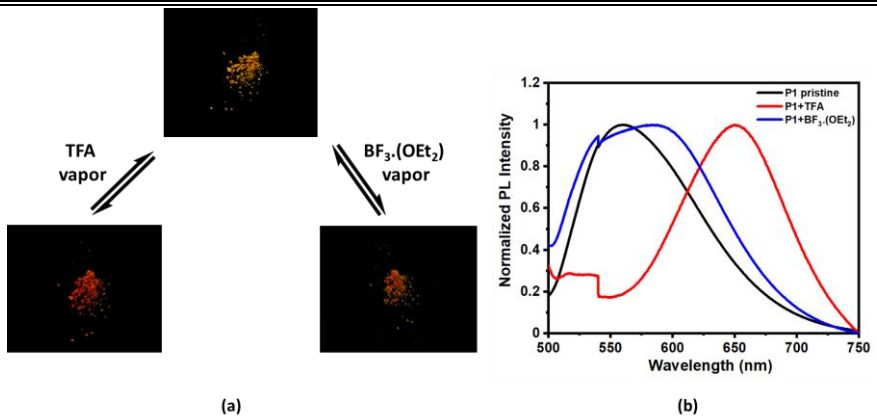

Figure 4.23 (**a**) Images for the solid P1, before and after the TFA vapor exposure and $BF_3(OEt_2)$, under the UV light (365 nm) and (**b**) the corresponding PL intensity plot (at excitation 397 nm).

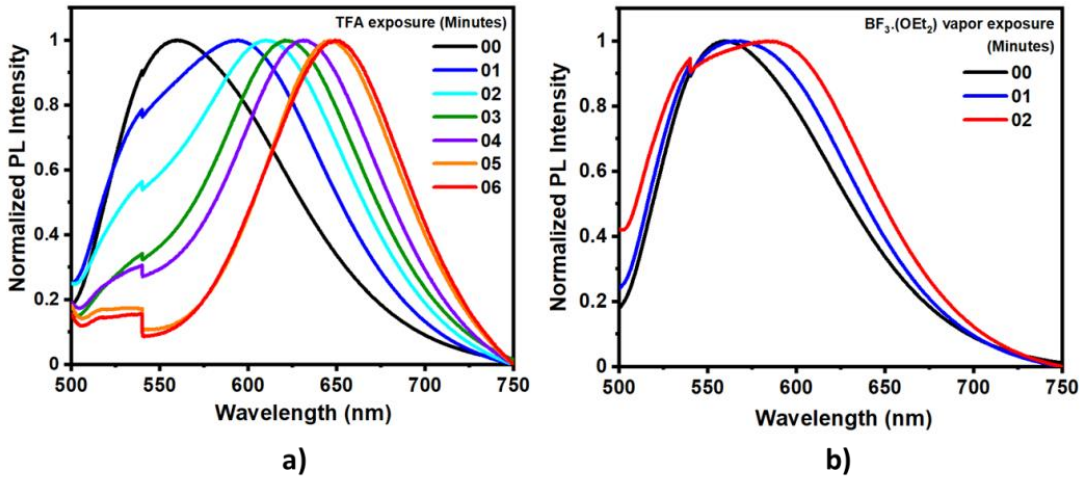

Figure 4.24 Plots for change in emission wavelength of powder form of P1 (at excitation 397 nm), a) with each minute exposure of TFA vapors, and b) with each minute exposure of $BF_3(OEt_2)$ vapors.

To support the study of the interaction of nitrogen atoms in P1 with acids, we have devised a certain experiment which is described here. TFA and $BF_3(OEt_2)$ acids were used to titrate the 1,4-dioxane solution of P1 and the resulting absorption spectra were recorded. The P1 showed the maximum absorption in 1,4-dioxane solution at 400 nm. (Fig 4.25). At each interval, 0.1 ml of TFA was added to the P1 solution. The resulting absorption spectra showed the observation of a new absorption peak emerging at 500 nm, while the existing peak at 400 nm gradually turns weak (Fig 4.25b). Subsequently, triethylamine (NEt_3) a base was added to the solution; the resulting solution was neutralized and produced its initial absorption peak. Similar results were obtained upon each 0.02 ml addition of $BF_3(OEt_2)$ (Fig 4.25c). The

decrease of the original absorption peak at 400 nm and the observation of the new absorption peak appearing at 500 nm reveals the formation of a new complex upon the addition of TFA or $BF_3(OEt_2)$ (Fig 4.25a). In P1, two types of nitrogen are present. To understand the possible protonation site on nitrogen atoms in P1 in the presence of TFA, the ^1H NMR of P1 was studied. ^1H NMR spectrum was recorded for a solution of P1 (5 mg P1 in 0.5 ml $CDCl_3$) containing a few drops of TFA, a new peak was observed at 4.9 ppm in ^1H NMR spectrum which is expected for the protonated nitrogen of triazine (Fig 4.26).[98]

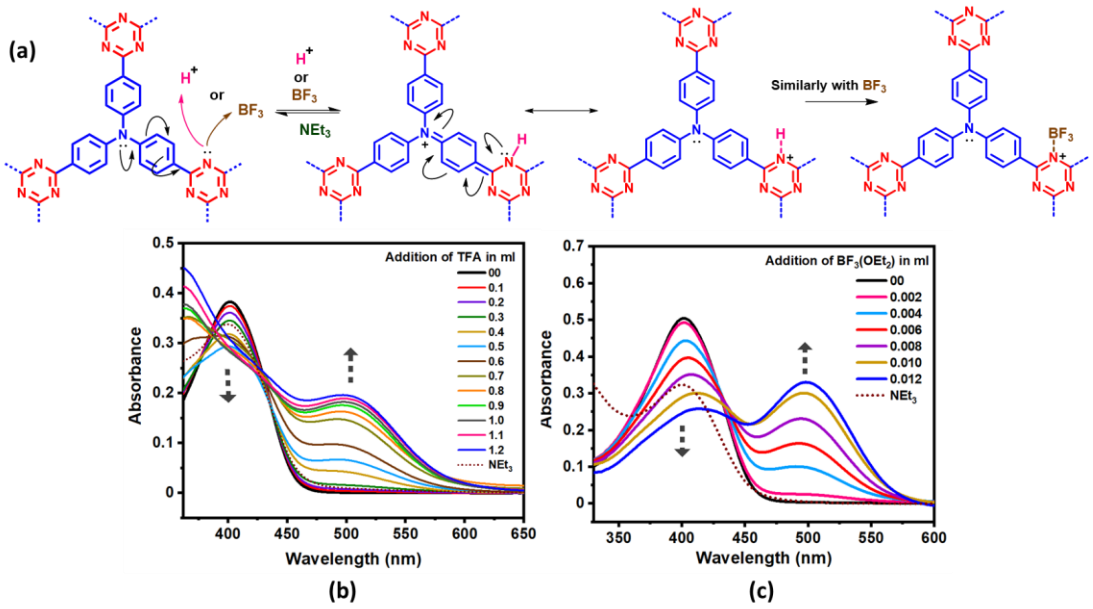

Figure 4.25 (a) Schematic representation for possible interactions of P1 with acidic proton or $BF_3(OEt_2)$, and, (b) and (c) are the absorption changes for the 1,4-dioxane solution of P1 upon gradual addition of various amounts of TFA and $BF_3(OEt_2)$ acids, respectively. Both could completely be reversed by neutralization with base NEt_3 (the dotted arrow shows the corresponding absorption peaks where the changes happen).

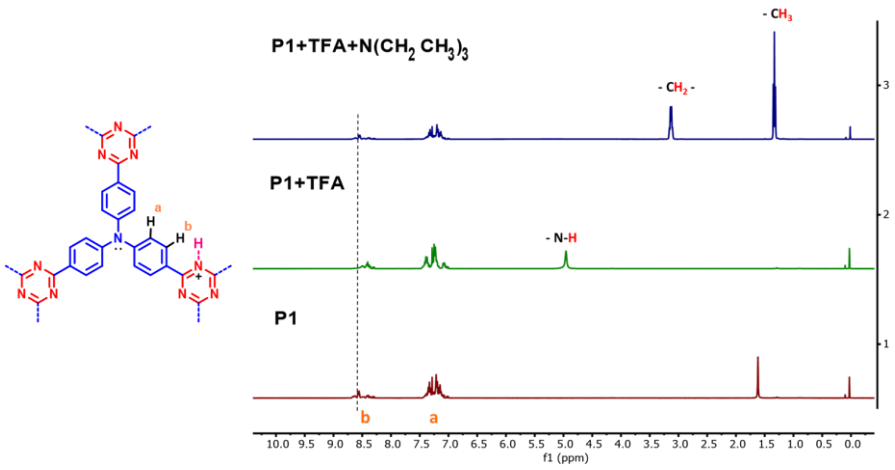

Figure 4.26 ^{1}H NMR spectrum for $CDCl_3$ solution of P1 (5 mg P1 in 0.5 ml $CDCl_3$) (P1) (bottom); after addition of 0.040 ml of TFA (P1+TFA) (middle) and after neutralized with 0.040 ml of $N(CH_2CH_3)_3$ [P1+TFA+$N(CH_2CH_3)_3$] (top); analyzed in $CDCl_3$ solvent (a peak for the TPA aromatic proton next to the triazine unit is indicated by a dotted straight line).

The ^{1}H NMR peak of the TPA aromatic proton adjacent to the triazine unit was initially observed at 8.5 ppm, it has a little shift towards the shielded region (8.4 ppm) in the presence of TFA. When base $N(CH_2CH_3)_3$ is added, this peak returns to 8.5 ppm. Two more peaks, corresponding to $-CH_3$ and $-CH_2$ protons of triethylamine were observed at 1.3 and 3.1 ppm, respectively. Despite TPA nitrogen having a higher basicity than triazine nitrogen,[99] the donor-acceptor character P1 causes protonation to triazine nitrogen rather than TPA nitrogen with the addition of TFA. Additionally, the ^{1}H NMR spectra of the interaction between P1 and $BF_3.[O(CH_2CH_3)_2]$ in $CDCl_3$ solvent was analyzed (Fig 4.27). The aromatic proton next to triazine was initially detected at 8.5 ppm, but due to possible hydrogen bonding between the fluorine of the interacting BF_3, it shifted towards the downfield region around 10.4 ppm. Free diethyl ether $O(CH_2CH_3)_2$ from $BF_3[O(CH_2CH_3)_2]$ has produced two additional peaks, one at 1.3 ppm for $-CH_3$ and the other at 3.9 ppm for $-CH_2$. Each monomeric triazine molecule has three nitrogen atoms. As a result, oligomer P1 has several protonic sites, which may be a possible reason for exhibiting very high sensitivity in an acid medium than small molecular probes.

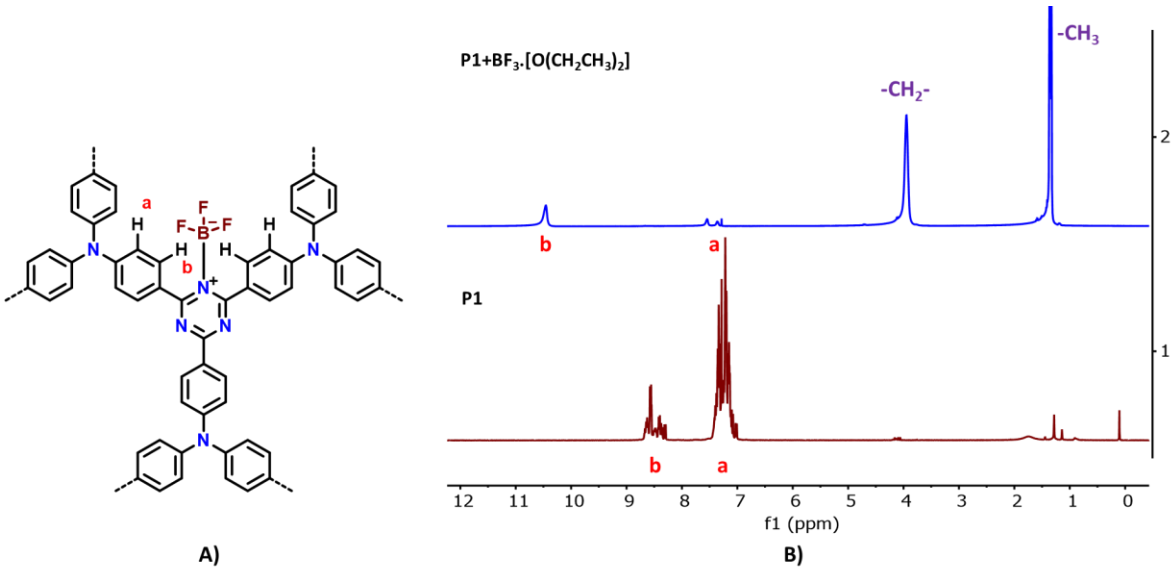

Figure 4.27 A) Schematic representation of possible interactions of P1 with boron trifluoride etherate $BF_3.[O(CH_2CH_3)_2]$; and B) ^{1}H NMR spectrum for $CDCl_3$ solution of P1 (5 mg P1 in 0.5 ml $CDCl_3$) and P1+ $BF_3.[O(CH_2CH_3)_2]$ analyzed in $CDCl_3$ solvent.

4.3.4 Mechanofluorochromism

The D-A-type polymeric materials with mechanofluorochromic (MFC) properties have been studied in some reports.[75, 100, 101] Earlier reports show a red shift with changing emission intensity upon grinding.[60, 102, 103] The change in conformational or phase transformation of the compound during grinding, which was supported by PXRD, HRTEM, etc., is known widely as the cause of such an effect.[60, 83] After grinding P1, we noticed the yellowish-orange emission of P1 in its powder form (λ_{emi} = 555 nm) is blue-shifted with enhanced emission intensity (shifting, 20 nm; λ_{emi} = 535 nm), and quantum yield (QY: 1.9 to 4.1 percent) was observed upon mechanical grinding (Fig 4.28). Moreover, by treating the ground powder with DCM solvent followed by reprecipitating/fuming, the P1 emission was able to regain its original orange color. A continuous, blue-shifted emission was observed as the grinding time for P1 increased (Fig 4.29). The grinding force (shearing) required for the observed mechanofluorochromism is 10kPa determined by a rheometer (Fig 4.30). After a certain time, even with vigorous grinding, there was no change in emission. This suggests that the compounds may undergo a continuous conformational transformation during grinding. It is obvious that P1 in both pristine and its ground form is in an amorphous phase from their PXRD patterns. However, compared to P1 pristine, the observed peak intensity of the ground form (P1) is lesser and broader (FWHM 13.55 and 14.59, for pristine and ground P1, respectively) (Fig 4.31). It indicates that during mechanical grinding, the P1 changes from a less amorphous to a more amorphous phase.[89] The triazine ring and the next phenyl ring have a dihedral angle of ~ 0° from the optimized structure of the repeating unit of P1. It suggests that both, triazine and TPA units might be in a coplanar state (Fig 4.7). The proposed pristine P1 is in a coplanar and more ordered conformation than the ground P1 which was demonstrated by the observed PXRD pattern and optimized geometry.

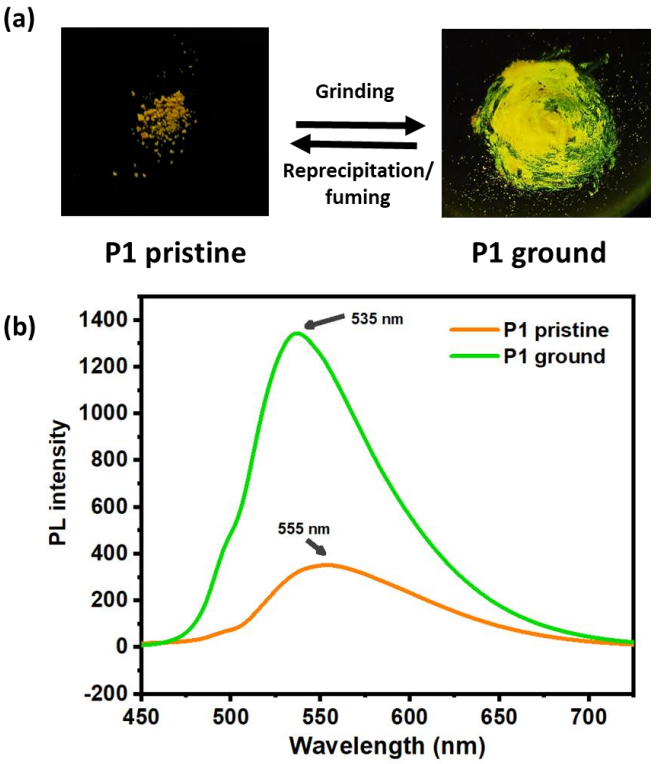

Figure 4.28 (a) Image for P1 pristine and P1 ground under the UV lamp (365 nm). (b) PL intensity plot (at excitation 397 nm); yellowish-orange emission (λ_{emi} = 555 nm) in P1 pristine and the blue-shifted with enhanced emission (λ_{emi} = 535 nm) upon mild grinding under the photoexcitation.

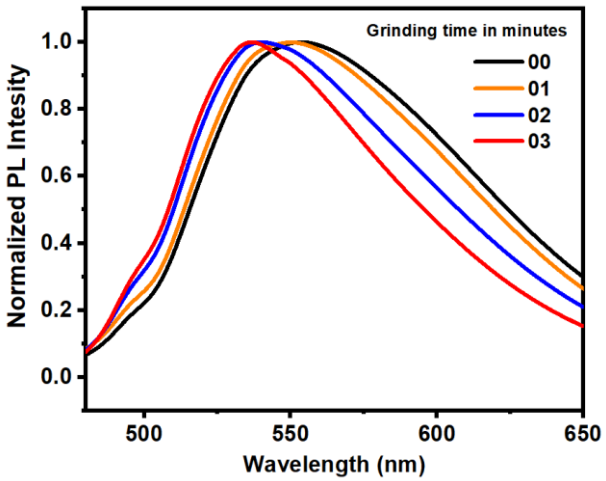

Figure 4.29 Photoluminescence plot for the change in wavelength of P1 (at excitation 397 nm) (i.e., blue-shifted) upon grinding with time.

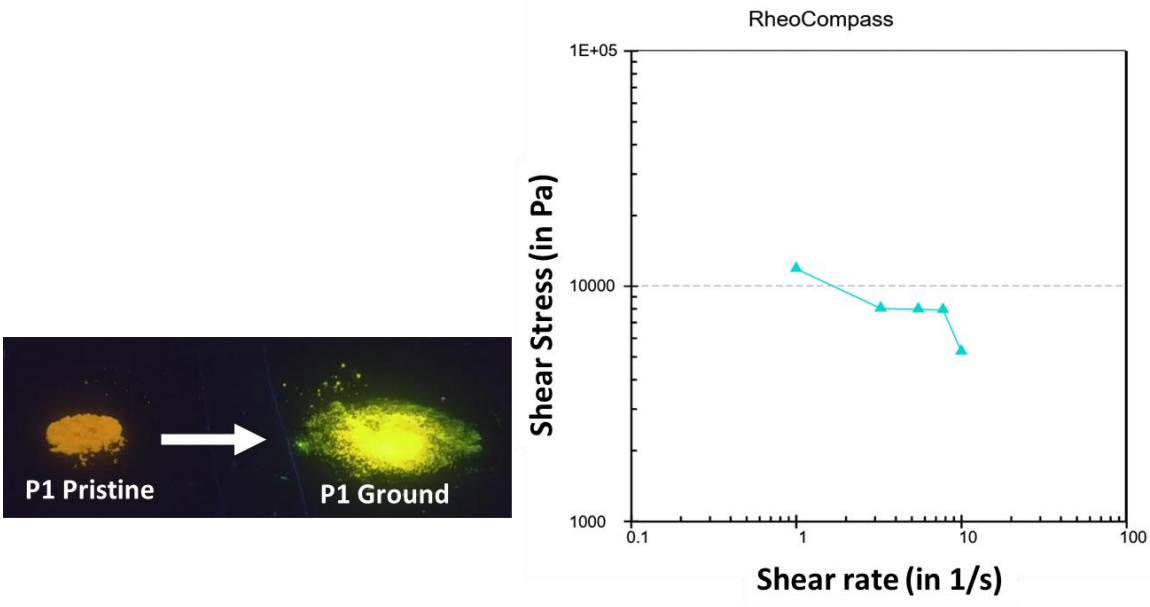

Figure 4.30 Image for P1 pristine and P1 ground under the UV lamp (365 nm), and plot for shear stress (Pa) against shear rate (1/sec).

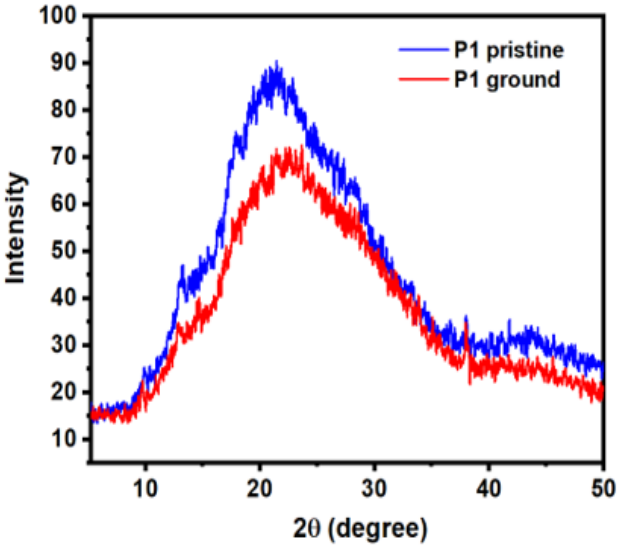

Figure 4.31 PXRD plot for P1 pristine and P1 ground samples.

Most of the triphenylamine derivatives exhibited twisted conformation.[104-107] While grinding P1, the potentially formed π-π stacking in coplanar conformation between two oligomeric layered moieties may be weakened to result in increasing emission intensity (Fig 4.32).[108] It was speculated that the blue-shifted emission may be caused by the D-A-based moiety's twisted conformation (here, D is triarylamine and A is triazine) resulting in less efficient delocalization.[108, 109] The aggregated state of P1 in a THF: water mixture was prepared, and the PL intensity for that, and compared to the diluted P1 solution (Fig 4.33). The solutions

shown in Fig 4.33a were prepared by taking an equal volume (0.5 ml) of P1 probe solution (1 mg P1 in 5 ml THF) in two different glass vials of 5 ml volume (A and B). 'A' vial diluted up to 5 ml by THF (i.e., diluted solution state) and 'B' vial made up to 5 ml by addition of water 4.5 ml (i.e., 90 % aggregated) to form the aggregated state of P1. The possible formation of staked layers of oligomers (aggregates) in the pristine state may reduce the emission intensity, where possibly such aggregates adhere to broken and lead to blue-shifted enhanced emissions in diluted THF solution of P1.

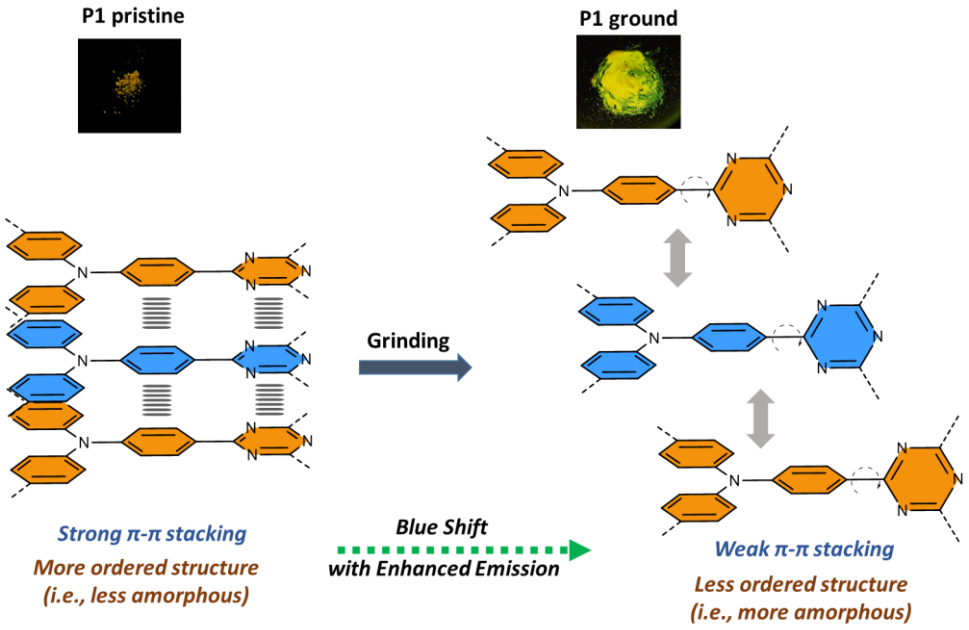

Figure 4.32 Schematic representation for a possible mechanism of blue shift with enhanced emission of P1 upon mechanical grinding.

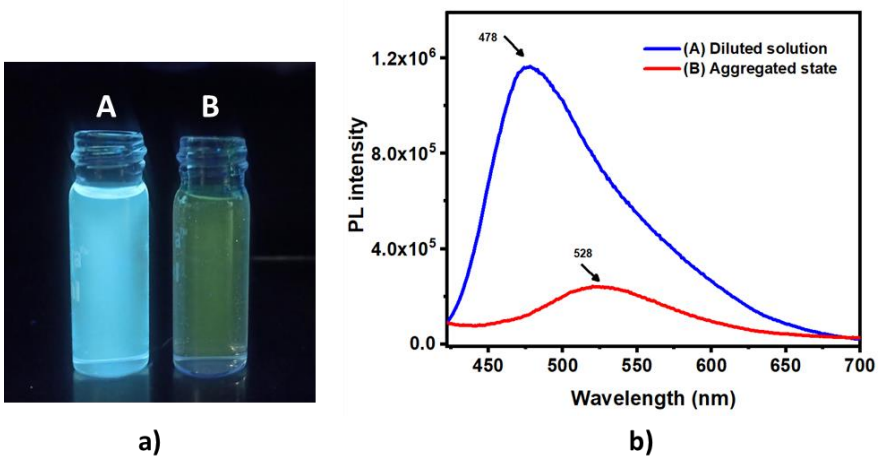

Figure 4.33 a) It shows the comparative photographs of emission in dilute THF solution of P1 (A) and aggregated compound of P1 in THF-water (0.5 ml THF- 4.5 ml water) (B), b) It shows the comparative emission intensity of the solutions as described (λ_{exc} = 397 nm).

Based on the aforementioned information, we have developed a D-A-based probe that exhibited a hypsochromic shift with enhanced emission intensity upon grinding. The mechanism for such processes has been explored.[110] This work describes electron D-A-based fluorogenic oligomer for multi-stimuli detection including solvatochromism, trinitrotoluene (TNT) nitro explosive detection, acidochromism, and mechanofluorochromism (MFC). Interestingly, the same oligomeric probe exhibits a distinct emissive response in the presence of various stimuli, including quenching for TNT sensing, bathochromically shifted emission for acidochromism, hypsochromically shifted emission against MFC behavior, and polarity-dependent emission for solvatochromism.

4.4 References

1. J. Zhang, A. Li, H. Zou, J. Peng, J. Guo, W. Wu, H. Zhang, J. Zhang, X. Gu, W. Xu, S. Xu, S. H. Liu, A. Qin, J. W. Y. Lam and B. Z. Tang, *Materials Horizons*, 2020, **7**, 135-142.
2. S. B. Yadav, S. Kothavale and N. Sekar, *Journal of Photochemistry and Photobiology A: Chemistry*, 2019, **382**, 111937.
3. P. Alam, M. Karanam, D. Bandyopadhyay, A. R. Choudhury and I. R. Laskar, *European Journal of Inorganic Chemistry*, 2014, **2014**, 3710-3719.
4. Y. Xie, J. T. Husband, M. Torrent-Sucarrat, H. Yang, W. Liu and R. K. O'Reilly, *Chemical Communications*, 2018, **54**, 3339-3342.
5. C. Wang, B. Xu, M. Li, Z. Chi, Y. Xie, Q. Li and Z. Li, *Materials Horizons*, 2016, **3**, 220-225.
6. S. S. Pasha, P. Das, N. P. Rath, D. Bandyopadhyay, N. R. Jana and I. R. Laskar, *Inorganic Chemistry Communications*, 2016, **67**, 107-111.
7. P. Alam, P. Das, C. Climent, M. Karanam, D. Casanova, A. R. Choudhury, P. Alemany, N. R. Jana and I. R. Laskar, *Journal of Materials Chemistry C*, 2014, **2**, 5615-5628.
8. P. Alam, G. Kaur, C. Climent, S. Pasha, D. Casanova, P. Alemany, A. Roy Choudhury and I. R. Laskar, *Dalton Transactions*, 2014, **43**, 16431-16440.
9. Q. Li and Z. Li, *Advanced Science*, 2017, **4**, 1600484.
10. C. W. T. Leung, Y. Hong, S. Chen, E. Zhao, J. W. Y. Lam and B. Z. Tang, *Journal of the American Chemical Society*, 2013, **135**, 62-65.
11. T. Han, C. Gui, J. W. Y. Lam, M. Jiang, N. Xie, R. T. K. Kwok and B. Z. Tang, *Macromolecules*, 2017, **50**, 5807-5815.
12. C. Zhou, M. Jiang, J. Du, H. Bai, G. Shan, R. T. K. Kwok, J. H. C. Chau, J. Zhang, J. W. Y. Lam, P. Huang and B. Z. Tang, *Chemical Science*, 2020, **11**, 4730-4740.
13. A. C. B. Rodrigues and J. S. Seixas de Melo, *Topics in Current Chemistry*, 2021, **379**, 15.

14. Z. Qiu, X. Liu, J. W. Y. Lam and B. Z. Tang, *Macromolecular Rapid Communications*, 2019, **40**, 1800568.
15. X. Sun, Y. Wang and Y. Lei, *Chemical Society Reviews*, 2015, **44**, 8019-8061.
16. E. S. Gil and S. M. Hudson, *Progress in Polymer Science*, 2004, **29**, 1173-1222.
17. M. Wei, Y. Gao, X. Li and M. J. Serpe, *Polymer Chemistry*, 2017, **8**, 127-143.
18. P. Schattling, F. D. Jochum and P. Theato, *Polymer Chemistry*, 2014, **5**, 25-36.
19. G. Fu, J. Guan, B. Li, L. Liu, Y. He, C. Yu, Z. Zhang and X. Lü, *Journal of Materials Chemistry C*, 2018, **6**, 4114-4121.
20. S. Khalifeh, in *Polymers in Organic Electronics*, ed. S. Khalifeh, ChemTec Publishing, 2020, pp. 251-339.
21. M. Kopeć, M. Pikiel and G. J. Vancso, *Polymer Chemistry*, 2020, **11**, 669-674.
22. R. Hu, X. Yang, A. Qin and B. Z. Tang, *Materials Chemistry Frontiers*, 2021, **5**, 4073-4088.
23. H. Qin, J. Huang, H. Liang and J. Lu, *ACS Applied Materials & Interfaces*, 2021, **13**, 5668-5677.
24. T. Han, X. Wang, D. Wang and B. Z. Tang, *Topics in Current Chemistry*, 2021, **379**, 7.
25. Z. Wang, C. Wang, Q. Gan, Y. Cao, H. Yuan and D. Hua, *ACS Applied Materials & Interfaces*, 2019, **11**, 41853-41861.
26. F. Qian, C. Zhang, Y. Zhang, W. He, X. Gao, P. Hu and Z. Guo, *Journal of the American Chemical Society*, 2009, **131**, 1460-1468.
27. L. Fageria, V. Pareek, R. V. Dilip, A. Bhargava, S. S. Pasha, I. R. Laskar, H. Saini, S. Dash, R. Chowdhury and J. Panwar, *ACS Omega*, 2017, **2**, 1489-1504.
28. H. Liu, Q. Bai, L. Yao, H. Zhang, H. Xu, S. Zhang, W. Li, Y. Gao, J. Li, P. Lu, H. Wang, B. Yang and Y. Ma, *Chemical Science*, 2015, **6**, 3797-3804.
29. S. Roquet, A. Cravino, P. Leriche, O. Alévêque, P. Frère and J. Roncali, *Journal of the American Chemical Society*, 2006, **128**, 3459-3466.
30. W. Zhang, T. Huang, J. Li, P. Sun, Y. Wang, W. Shi, W. Han, W. Wang, Q. Fan and W. Huang, *ACS Applied Materials & Interfaces*, 2019, **11**, 16311-16319.
31. X. Y. Shen, Y. J. Wang, E. Zhao, W. Z. Yuan, Y. Liu, P. Lu, A. Qin, Y. Ma, J. Z. Sun and B. Z. Tang, *The Journal of Physical Chemistry C*, 2013, **117**, 7334-7347.
32. L. Wang, L. Yang, L. Li and D. Cao, *New Journal of Chemistry*, 2016, **40**, 6706-6713.
33. G. Sathiyan, B. Balasubramaniam, S. Ranjan, S. Chatterjee, P. Sen, A. Garg, R. K. Gupta and A. Singh, *Materials Today Chemistry*, 2019, **12**, 178-186.
34. Y. Zhang, D. Li, Y. Li and J. Yu, *Chemical Science*, 2014, **5**, 2710-2716.
35. X. L. Guan, T. M. Jia, D. H. Zhang, Y. Zhang, H. C. Ma, D. D. Lu, S. J. Lai and Z. Q. Lei, *Dyes and Pigments*, 2017, **136**, 873-880.
36. A. S. Klymchenko, *Accounts of Chemical Research*, 2017, **50**, 366-375.
37. J. Ma, Y. Zhang, H. Zhang and X. He, *RSC Advances*, 2020, **10**, 35840-35847.
38. S. Kothavale and N. Sekar, *ChemistrySelect*, 2017, **2**, 7691-7700.
39. Y. H. Lee, H. Liu, J. Y. Lee, S. H. Kim, S. K. Kim, J. L. Sessler, Y. Kim and J. S. Kim, *Chemistry – A European Journal*, 2010, **16**, 5895-5901.
40. R. G. Ewing, D. A. Atkinson, G. A. Eiceman and G. J. Ewing, *Talanta*, 2001, **54**, 515-529.
41. J. R. C. Junqueira, W. R. de Araujo, M. O. Salles and T. R. L. C. Paixão, *Talanta*, 2013, **104**, 162-168.
42. H. Zhou, M. H. Chua, B. Z. Tang and J. Xu, *Polymer Chemistry*, 2019, **10**, 3822-3840.

43. S. Pramanik, Z. Hu, X. Zhang, C. Zheng, S. Kelly and J. Li, *Chemistry – A European Journal*, 2013, **19**, 15964-15971.
44. F. Chu, G. Tsiminis, N. A. Spooner and T. M. Monro, *Sensors and Actuators B: Chemical*, 2014, **199**, 22-26.
45. G. Vamvounis, P. E. Shaw and P. L. Burn, *Journal of Materials Chemistry C*, 2013, **1**, 1322-1329.
46. Y. Wang, A. La, Y. Ding, Y. Liu and Y. Lei, *Advanced Functional Materials*, 2012, **22**, 3547-3555.
47. H.-T. Feng, J.-H. Wang and Y.-S. Zheng, *ACS Applied Materials & Interfaces*, 2014, **6**, 20067-20074.
48. A. Mathew, P. R. Sajanlal and T. Pradeep, *Angewandte Chemie International Edition*, 2012, **51**, 9596-9600.
49. W. J. Peveler, A. Roldan, N. Hollingsworth, M. J. Porter and I. P. Parkin, *ACS Nano*, 2016, **10**, 1139-1146.
50. S. W. Thomas, G. D. Joly and T. M. Swager, *Chemical Reviews*, 2007, **107**, 1339-1386.
51. E. V. Verbitskiy, Y. A. Kvashnin, A. A. Baranova, K. O. Khokhlov, R. D. Chuvashov, I. y. E. Schapov, Y. A. Yakovleva, E. F. Zhilina, A. V. Shchepochkin, N. I. Makarova, E. V. Vetrova, A. V. Metelitsa, G. L. Rusinov, O. N. Chupakhin and V. N. Charushin, *Dyes and Pigments*, 2020, **178**, 108344.
52. T. Rasheed, F. Nabeel, K. Rizwan, M. Bilal, T. Hussain and S. A. Shehzad, *TrAC Trends in Analytical Chemistry*, 2020, **129**, 115958.
53. P. Singh, A. Baheti and K. R. J. Thomas, *The Journal of Organic Chemistry*, 2011, **76**, 6134-6145.
54. P. Alam, G. Kaur, S. Chakraborty, A. Roy Choudhury and I. R. Laskar, *Dalton Transactions*, 2015, **44**, 6581-6592.
55. J. B. Arockiam and S. Ayyanar, *Sensors and Actuators B: Chemical*, 2017, **242**, 535-544.
56. D. Wang, X. Zhang, X. Han, Y. Zhou, Y. Lei, W. Gao, M. Liu, X. Huang and H. Wu, *Journal of Materials Chemistry C*, 2021, **9**, 12868-12876.
57. S. Achelle, J. Rodríguez-López, F. Bureš and F. Robin-le Guen, *The Chemical Record*, 2020, **20**, 440-451.
58. S. Hayashi and T. Koizumi, *Journal of Polymer Science Part A: Polymer Chemistry*, 2014, **52**, 3142-3145.
59. Y. Shen, P. Xue, J. Liu, J. Ding, J. Sun and R. Lu, *Dyes and Pigments*, 2019, **163**, 71-77.
60. S. S. Pasha, H. R. Yadav, A. R. Choudhury and I. R. Laskar, *Journal of Materials Chemistry C*, 2017, **5**, 9651-9658.
61. X. Meng, G. Qi, C. Zhang, K. Wang, B. Zou and Y. Ma, *Chemical Communications*, 2015, **51**, 9320-9323.
62. G. Zhang, J. Lu, M. Sabat and C. L. Fraser, *Journal of the American Chemical Society*, 2010, **132**, 2160-2162.
63. M. Kondo, S. Miura, K. Okumoto, M. Hashimoto and N. Kawatsuki, *Chemistry – An Asian Journal*, 2014, **9**, 3188-3195.
64. C. K. Lee, D. A. Davis, S. R. White, J. S. Moore, N. R. Sottos and P. V. Braun, *Journal of the American Chemical Society*, 2010, **132**, 16107-16111.
65. M. Dal Molin, Q. Verolet, A. Colom, R. Letrun, E. Derivery, M. Gonzalez-Gaitan, E. Vauthey, A. Roux, N. Sakai and S. Matile, *Journal of the American Chemical Society*, 2015, **137**, 568-571.

66. K. Nagura, S. Saito, H. Yusa, H. Yamawaki, H. Fujihisa, H. Sato, Y. Shimoikeda and S. Yamaguchi, *Journal of the American Chemical Society*, 2013, **135**, 10322-10325.
67. Y. Han, T. Zhang, Q. Chen, X. Chen and P. Xue, *Crystal Growth & Design*, 2021, **21**, 1342-1350.
68. V. Gokul, D. Devadiga and T. N. Ahipa, *Dyes and Pigments*, 2021, **195**, 109692.
69. J. Jia and L. Wu, *Organic Electronics*, 2020, **76**, 105466.
70. K. Suenaga, K. Tanaka and Y. Chujo, *Chemistry – A European Journal*, 2017, **23**, 1409-1414.
71. Z. Ma, J. Zhou, J. Zhang, S. Zeng, H. Zhou, A. T. Smith, W. Wang, L. Sun and Z. Wang, *Materials Horizons*, 2019, **6**, 2003-2008.
72. J. Zhou, Y. Gu, J. Lu, L. Xu, J. Zhang, D. Wang and W. Wang, *Chemical Engineering Journal*, 2020, **390**, 124473.
73. H. Zhang, Z. Xu, F. Tao, Y. Li, Y. Cui and X. Li, *Analyst*, 2020, **145**, 5325-5332.
74. Y. Wang, X. Tan, Y.-M. Zhang, S. Zhu, I. Zhang, B. Yu, K. Wang, B. Yang, M. Li, B. Zou and S. X.-A. Zhang, *Journal of the American Chemical Society*, 2015, **137**, 931-939.
75. C. Y. K. Chan, J. W. Y. Lam, Z. Zhao, S. Chen, P. Lu, H. H. Y. Sung, H. S. Kwok, Y. Ma, I. D. Williams and B. Z. Tang, *Journal of Materials Chemistry C*, 2014, **2**, 4320-4327.
76. T. Yu, D. Ou, Z. Yang, Q. Huang, Z. Mao, J. Chen, Y. Zhang, S. Liu, J. Xu, M. R. Bryce and Z. Chi, *Chemical Science*, 2017, **8**, 1163-1168.
77. Q. Qi, J. Qian, X. Tan, J. Zhang, L. Wang, B. Xu, B. Zou and W. Tian, *Advanced Functional Materials*, 2015, **25**, 4005-4010.
78. H. Li, X. Zhang, Z. Chi, B. Xu, W. Zhou, S. Liu, Y. Zhang and J. Xu, *Organic Letters*, 2011, **13**, 556-559.
79. X. Zhang, Z. Chi, H. Li, B. Xu, X. Li, W. Zhou, S. Liu, Y. Zhang and J. Xu, *Chemistry – An Asian Journal*, 2011, **6**, 808-811.
80. X. Luo, J. Li, C. Li, L. Heng, Y. Q. Dong, Z. Liu, Z. Bo and B. Z. Tang, *Advanced Materials*, 2011, **23**, 3261-3265.
81. Y. Wang, D. Xu, H. Gao, Y. Wang, X. Liu, A. Han, C. Zhang and L. Zang, *Dyes and Pigments*, 2018, **156**, 291-298.
82. W. Yang, Y. Yang, Y. Qiu, X. Cao, Z. Huang, S. Gong and C. Yang, *Materials Chemistry Frontiers*, 2020, **4**, 2047-2053.
83. S. Dineshkumar and I. R. Laskar, *Polymer Chemistry*, 2018, **9**, 5123-5132.
84. M. Chen, R. Chen, Y. Shi, J. Wang, Y. Cheng, Y. Li, X. Gao, Y. Yan, J. Z. Sun, A. Qin, R. T. K. Kwok, J. W. Y. Lam and B. Z. Tang, *Advanced Functional Materials*, 2018, **28**, 1704689.
85. T. Murase and M. Fujita, *The Journal of Organic Chemistry*, 2005, **70**, 9269-9278.
86. Subodh, K. Prakash and D. T. Masram, *Dalton Transactions*, 2020, **49**, 1007-1010.
87. S. K. Das, X. Wang and Z. Lai, *Microporous and Mesoporous Materials*, 2018, **255**, 76-83.
88. in *Molecular Fluorescence*, 2001, pp. 200-225.
89. S. Sasaki, Y. Niko, A. S. Klymchenko and G.-i. Konishi, *Tetrahedron*, 2014, **70**, 7551-7559.
90. M. Buvaneswari, R. Santhakumari, C. Usha, R. Jayasree and S. Sagadevan, *Journal of Molecular Structure*, 2021, **1243**, 130856.
91. A. Abbas, J. J. Pillai, K. Sreekumar, R. Joseph and C. S. Kartha, *Optical Materials*, 2018, **84**, 813-820.
92. Z.-Q. Liang, X.-M. Wang, G.-L. Dai, C.-Q. Ye, Y.-Y. Zhou and X.-T. Tao, *New Journal of Chemistry*, 2015, **39**, 8874-8880.

93. Q. Qiu, P. Xu, Y. Zhu, J. Yu, M. Wei, W. Xi, H. Feng, J. Chen and Z. Qian, *Chemistry – A European Journal*, 2019, **25**, 15983-15987.
94. J. C. Oxley, J. L. Smith, W. Luo and J. Brady, *Propellants, Explosives, Pyrotechnics*, 2009, **34**, 539-543.
95. B. Ju, Y. Wang, Y.-M. Zhang, T. Zhang, Z. Liu, M. Li and S. Xiao-An Zhang, *ACS Applied Materials & Interfaces*, 2018, **10**, 13040-13047.
96. M. Lu, P. Zhou, Y. Ma, Z. Tang, Y. Yang and K. Han, *The Journal of Physical Chemistry A*, 2018, **122**, 1400-1405.
97. S. Cui, B. Wang, Y. Teng, Z. Wan, Y. Zan, L. Chen, Y. Li and X. Yan, *Sensors and Actuators B: Chemical*, 2021, **344**, 130120.
98. K. Duraimurugan, V. Dhanamoorthy, J. Madhavan and A. Siva, *Journal of Photochemistry and Photobiology A: Chemistry*, 2018, **359**, 164-171.
99. Y. Zhan, P. Yang, G. Li, Y. Zhang and Y. Bao, *New Journal of Chemistry*, 2017, **41**, 263-270.
100. Y. Zhang, K. Wang, G. Zhuang, Z. Xie, C. Zhang, F. Cao, G. Pan, H. Chen, B. Zou and Y. Ma, *Chemistry – A European Journal*, 2015, **21**, 2474-2479.
101. B. Xu, J. He, Y. Mu, Q. Zhu, S. Wu, Y. Wang, Y. Zhang, C. Jin, C. Lo, Z. Chi, A. Lien, S. Liu and J. Xu, *Chemical Science*, 2015, **6**, 3236-3241.
102. T. Han, L. Liu, D. Wang, J. Yang and B. Z. Tang, *Macromolecular Rapid Communications*, 2021, **42**, 2000311.
103. Y. Wang, D. Xu, H. Gao, Y. Wang, X. Liu, A. Han, C. Zhang and L. Zang, *The Journal of Physical Chemistry C*, 2018, **122**, 2297-2306.
104. Z. Yang, Z. Chi, Z. Mao, Y. Zhang, S. Liu, J. Zhao, M. P. Aldred and Z. Chi, *Materials Chemistry Frontiers*, 2018, **2**, 861-890.
105. X.-J. Liu, G.-L. Gao, H. Jiang, Y.-R. Jia and M. Xia, *RSC Advances*, 2020, **10**, 23187-23195.
106. Y. Zhang, Y.-Q. Feng, J.-H. Wang, G. Han, M.-Y. Li, Y. Xiao and Z.-D. Feng, *RSC Advances*, 2017, **7**, 35672-35680.
107. Y. Zhan, Q. Wei, J. Zhao and X. Zhang, *RSC Advances*, 2017, **7**, 48777-48784.
108. X. Wang, Q. Liu, H. Yan, Z. Liu, M. Yao, Q. Zhang, S. Gong and W. He, *Chemical Communications*, 2015, **51**, 7497-7500.
109. Q. Wu, T. Zhang, Q. Peng, D. Wang and Z. Shuai, *Physical Chemistry Chemical Physics*, 2014, **16**, 5545-5552.
110. Z. Ruan, L. Li, C. Wang, Y. Xie, Q. Hu, Q. Peng, S. Ye, Q. Li and Z. Li, *Small*, 2016, **12**, 6623-6632.

CHAPTER 5

ACHIEVING SINGLE COMPONENT SOLID-STATE WHITE LIGHT EMISSION THROUGH POLYMERIZATION-INDUCED PHOSPHORESCENT EMISSION (PIPE)

Chapter 5. Achieving Single Component Solid-state White Light Emission Through Polymerization-induced Phosphorescent Emission (PIPE)

5.1 Introduction

Solid-state organic materials with luminescent properties are employed for various applications, including organic light-emitting diodes (OLED), chemical vapor sensing, solar cells, mechanofluorochromism, stimuli-responsive materials, etc.[1-3] Luminophores' emission may be decreased, retained, or even increased when aggregated or in a solid. Aggregation-caused Quenching (ACQ) is the term used to describe when most luminophores exhibit an emission quenching effect, either entirely or partially when aggregated. As a result, ACQ shows limitations in real-time applications.[4] To get around the ACQ, Tang et al. in 2001 developed the "Aggregation-induced Emission (AIE)" phenomenon based on the observation of luminophores with freely rotating groups that were substantially emissive in the aggregated state but non-emissive in a dilute solution.[5] Restricted intramolecular motion (RIM) may often cause radiative decay in the AIE effect, which raises the initial emission intensity in the aggregated state.[6, 7] Compared to small molecules, polymeric materials have a lot of benefits, including tunable emission, various topologies (linear, hyperbranched, star-shaped), ease of functionalization, ease of processing, increased mechanical strength, etc.[8, 9] Compared to conjugated polymers, non-conjugated polymers are typically simpler to synthesize, purify, and have better solubility in common organic solvents.[10] There is potential for practical applications as they have variety in composition, structure, and morphology of copolymers and their dependence on having to adjust luminous wavelength. Thin films or aggregated/solid-state AIE polymer leads to various applications, including drug delivery, biosensing, theranostics, fluorescent chemosensors, and multi-stimuli responsive polymeric materials.[11-15] These thin films also have excellent photosensitivity, faster response time, and significant contrast.[11-15]

Typically, non-luminescent monomers are used to synthesize polymers. Due to the inhibition of π-π electron interaction during aggregation, polymerization improves the AIE characteristics. When a non-luminescent monomeric unit is polymerized, it becomes an intensely emissive polymer, known as polymerization-induced emission (PIE). Over the past few years, research into the underlying principle behind the luminous mechanism has driven a rise in the development of luminescent polymers.[16, 17] By polymerizing non-luminescent monomers, Bin Liu et al. in 2019 described a study on PIE-active non-conjugated luminescent

polymers with and without phenyl rings.[18] These polymers are a particular class of AIE materials that fall within the PIE category. In the PIE mechanism, the chain formations go through chain entanglement. The resultant interactions and conformational rigidity cause the emission, potentially resulting from intrachain and interchain interactions.[18, 19] Jing et al. effectively produced a hyperbranched organic polymer that is PIE-active and used in white light-emitting diodes (WLEDs) and light-harvesting films.[20] It is feasible to increase the light emission efficiency of light-emitting diode (LED) devices by utilizing a phosphorescent copolymer made up of an iridium(III) metal complex and a carbazole unit.[21, 22] Due to their outstanding hole-transporting mobility and substantial absorption in the UV spectral region, carbazole-based polymers are also the most desirable materials for LEDs.[23, 24]

The potential use of white light-emissive materials in displays, lighting, low-energy consumption devices, molecular sensors, and switches has drawn increased attention.[25] A phosphorescence emissive material can be employed as a reliable light source for various applications, such as the detection of volatile organic compounds (VOC), polychromatic screen printing, and multilevel information encryption.[26-28] High efficiency, long-lasting, and excellent color rendering index may cause the development of white light-emitting substances based on phosphorescence. It is receiving much interest for use as a lightning source in LED devices, displays, and sensors.[29] The published typical techniques for producing white light-emitting materials rely on doping or color blending of several dye molecules (for example, blue, green, and red emissive).[30] Hawker et al. described the polymers produced from pendant monomers methacrylate-based heteroleptic iridium(III) complex and carbazole-pyrimidine-based building block.[31] By altering the mole proportion of monomers, the approach can change the emission color from deep blue (for homopolymer) to a green-yellow color (for copolymer). Also, a non-AIE small organic molecule was synthesized, and its solid-state bright white light emission of 1-(1H-phenanthro[9,10-d]imidazol-2-yl)naphthalen-2ol has been described.[32] Rhodamine B is utilized as a guest dye to produce white light emission in a Metal-Organic Framework (MOF) that Pan and co-authors reported on.[33] By copolymerizing fluorescent dianhydride and brominated phosphorescent dianhydride with an alicyclic diamine, white light emission tuning has also been described based on Förster resonance energy transfer (FRET) and room-temperature phosphorescence.[34] It was formed white-light emitting materials with CIE coordinates of (0.34, 0.33) and (0.32, 0.33) from a single polymer unit by incorporating carbazole and 2-phenylquinoline iridium(III) species.[35] Weck et al. also studied modifying the emission wavelength of polymers incorporating functionalized styrene that includes

the iridium(III) complex and N-vinyl carbazole.[36] By changing the Iridium(III) complex linkage to the polymer backbones, polymers' emission wavelengths can be tuned.

However, according to the literature, there is no report on single-component AIE materials that produce white light from solid-state phosphorescent. In the present work, the non-luminescent monomeric unit M1 transforms into intensely yellow emissive phosphorescent polymers upon polymerization, termed Polymerization-induced Phosphorescent Emission (PIPE). A novel PIPE-active polymer (HP) with yellow emission was synthesized. The general concept is to combine two emissive compounds with different emission wavelengths (i.e., yellow and blue) to produce white light emission at a particular composition. This concept motivates us to continue working on the copolymer synthesis by combining M1 with the blue-emitting N-vinyl carbazole M2, which is well-known for being an efficient hole-transporting moiety. To tune the emission, various copolymers (CP1, CP2, CP3, CP4, and CP5) have been synthesized. The CP4 exhibits the solid-state emission of white light. All copolymers and the synthesized HP were shown to be AIE-active and had long lifetime decays, whereas CP4 exhibits remarkable quantum efficiency (33.7 %).

5.2 Experimental details

5.2.1 Synthesis of vinyl ligand L1 (2-(4-vinylphenyl)pyridine, i.e., ppy-vin) and monomer M1 (ppy-vinIr(PPh_3)$_2$ClH)

As per the discussion in Chapter 3A, the ligand L1 and monomer M1 were synthesized and structurally characterized.[37]

5.2.2 Synthesis of homopolymer HP

In a dry THF solvent, M1 (0.1 g, 0.1 mmol) and AIBN (0.006 g, 0.03 mmol) were dissolved in a 25 ml round bottom flask. Under a nitrogen environment, the mixture was stirred for 24 hours at a temperature of 80 ºC. The product was added to a large amount of methanol, and the precipitate was then filtered using Whatman filter paper and collected. The obtained yellow-colored precipitate was dissolved in THF and reprecipitated into methanol. Centrifugation was used to isolate the resulting polymer precipitate, which was then dried at 80 ºC in a vacuum oven to produce a yellow-colored polymer powder with an 80-85 % yield. ^{1}H NMR analysis was used to analyze the synthesized HP (Fig. 5.1). In the ^{1}H NMR, the broad range of peaks at the aromatic region indicates the presence of repeating units of PPh_3 and phenyl pyridene in HP. Polymer HP has a 59115 Da observed molecular weight from GPC analysis.

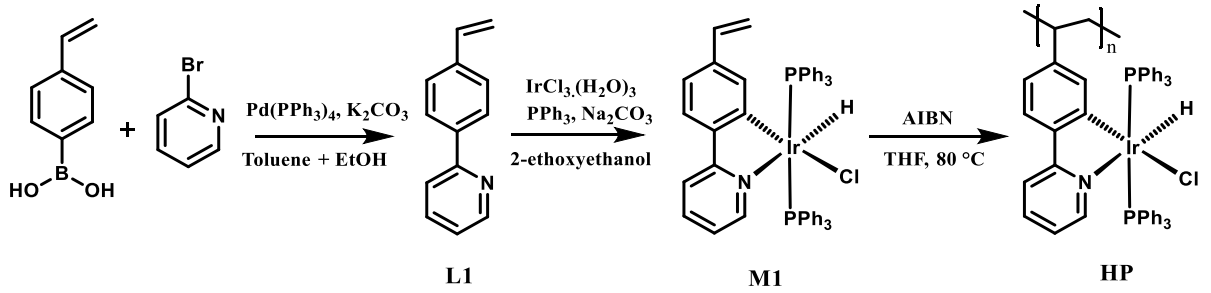

Scheme 5.1 Synthetic route: Vinyl ligand L1 is synthesized using the Suzuki coupling reaction. Synthesis of the vinyl iridium(III) monomer M1(ppy-vinIr(PPh_3)$_2$ClH). Homopolymer (HP) synthesized from the monomer M1, using the free radical polymerization method and the AIBN initiator.

5.2.3 Synthesis of copolymers CP

In a round bottom flask (25 ml), 1 equivalent M1 (0.1 g, 0.1 mmol), various equivalents (i.e., 20/60/100/220/300 equivalents) of M2 (Scheme 5.2) and AIBN (0.006 g, 0.03 mmol) were dissolved in dry THF solvent. With nitrogen gas, the mixture was stirred for 24 hours at 80 ºC. The product was added to a large amount of methanol, and the precipitate was then collected by filtration on Whatman filter paper. THF was used to dissolve the white precipitate, which then reprecipitated back into methanol. A white-colored polymer powder was obtained in a 70-80 % yield by centrifuging the resulting polymer precipitate and drying it at 80 ºC in a vacuum oven. Similar to this, all copolymers with varying compositions have been synthesized from various equivalent monomers, M1 and M2. Among the all-synthesized copolymers, CP4 shows white light emission. Therefore, we have studied the CP4 as focal attention. The growth of an alkane chain derived from vinyl monomers is used to obtain polymers. ^{1}H NMR analysis was conducted to analyze synthesized CP4 (Fig. 5.2). In the ^{1}H NMR, the broad range of peaks at the aromatic region indicates the presence of repeating units of PPh_3 and phenyl pyridine in CP4. All copolymers CPs have observed molecular weights that range from about 3 to 6k Da.

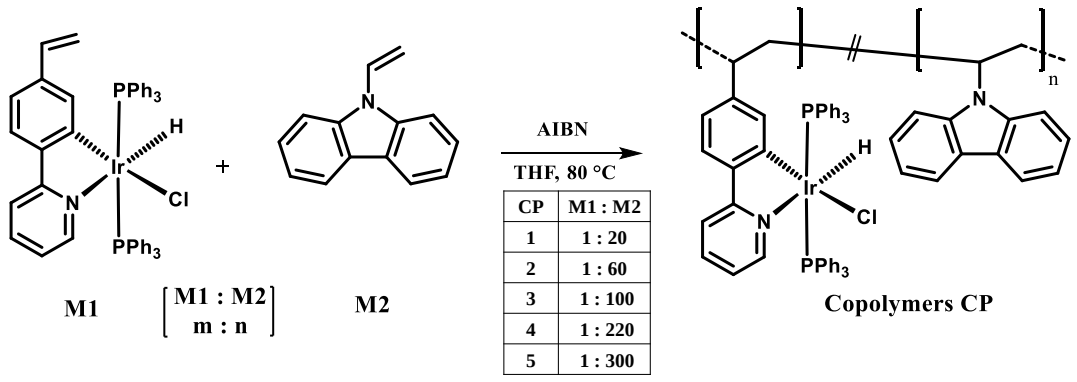

CP	M1 : M2
1	1 : 20
2	1 : 60
3	1 : 100
4	1 : 220
5	1 : 300

Scheme 5.2 Synthesis of all copolymers CPs from different equivalent monomers M1 and M2 via free radical polymerization method and AIBN initiator.

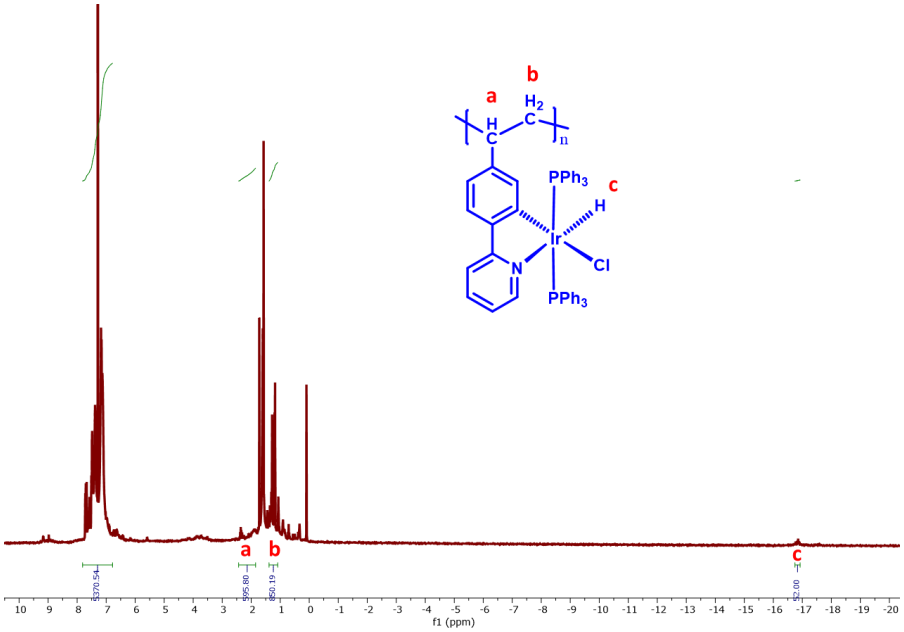

Figure 5.1 ^{1}H NMR spectrum of HP in $CDCl_3$ solvent.

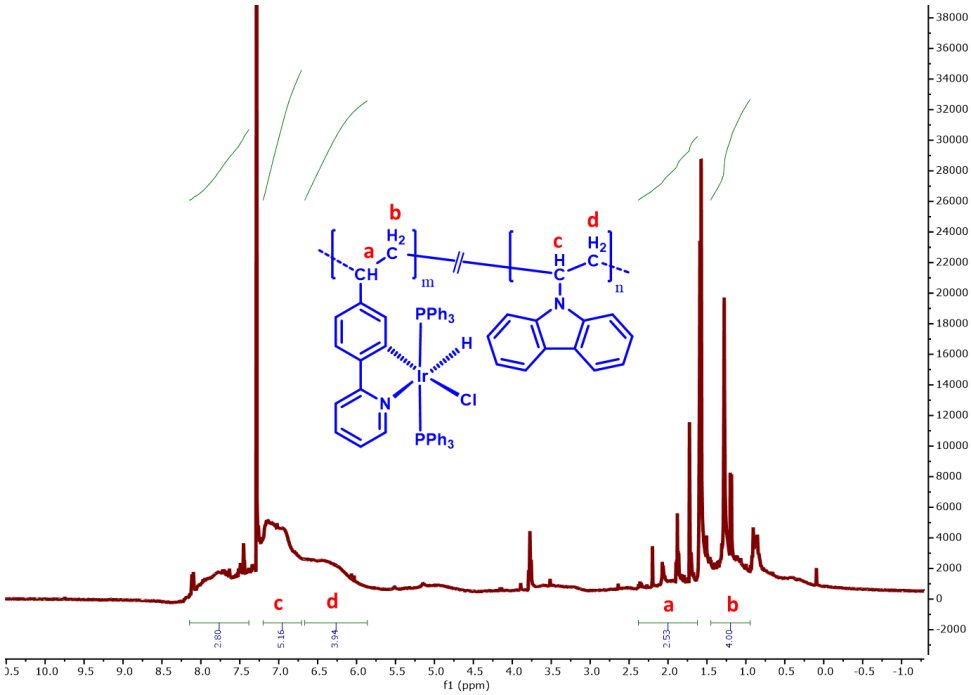

Figure 5.2 ^{1}H NMR spectrum of CP4 in $CDCl_3$ solvent.

5.2.4 Samples Preparation

The following experiment was studied to show the AIE activity of polymers. The stock solution of HP was prepared (1 mg in 5 ml DMF), to study the AIE activity of HP. The prepared HP

stock solution (0.5 ml) was filled in four glass vials of 5 ml volume. It was made into a 5 ml water-DMF mixture with an increasing concentration of water from 0, 30, 60, and 90 % (e.g., in the case of AIE solution of 90 % water-DMF mixture, 0.5 ml prepared HP solution and 4.5 ml water taken). Four other solutions were prepared using PEG in place of water fractions in the same manner. In the same way, AIE solutions for copolymer CP4's were prepared to study AIE activity. The first stock solution of CP4 was prepared (1 mg of CP4 in 5 ml of THF) and 0.5 ml of prepared stock solution of CP4 was filled in four glass vials of 5 ml volume. The glass vials have 5 ml of a THF-water mixture with different water fractions (i.e., 0, 30, 60, and 90 %). As with CP4, four more solutions were prepared using PEG instead of water. For each prepared solution, the PL intensity was recorded.

5.3 Results and Discussion

5.3.1 Synthesis and Characterizations

The polymers HP and CPs were synthesized using a simple free radical polymerization approach in the present work. The yellow color emitting HP has been synthesized from the iridium(III)-based monomer M1 due to the increased need for phosphorescent metal complex polymers in LED devices (Scheme 5.1). In addition, the effectiveness of white light-emissive polymers for LED applications motivates us to tune the iridium(III)-based polymer with blue emitting M2. According to this, the copolymers (CP1 to CP5) were synthesized from the monomers M1 and M2 via free radical polymerization by altering the equivalent ratio of M2 to M1 (Scheme 2). For homopolymer (HP), the typical absorbance is observed at 360 nm, while for all CPs, it is observed at 300 nm (Fig. 5.3) (360 and 300 nm are the suitable excitation wavelengths for HP and CP, respectively). For M1, HP, and the all-copolymers CPs, the observed excited-state lifetime in the solid phase ranged from 0.6 to 10.3 μs. (Fig. 5.4). This shows the characteristic phosphorescence nature of iridium(III) based polymer emission since all of the polymers have lifetime decay falling in the microsecond regime.[38]

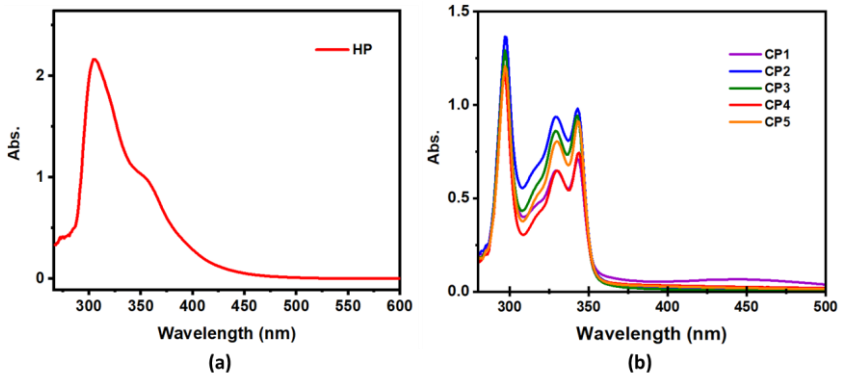

Figure 5.3 Absorption spectra in solid-state for (**a**) HP and (**b**) CP1, CP2, CP3, CP4, and CP5. It is performed in reflectance mode and then converted to absorbance value.

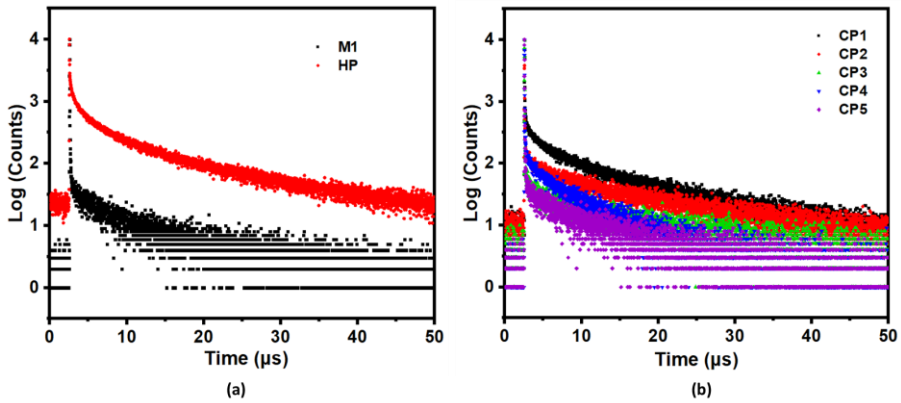

Figure 5.4 The characteristic fluorescence lifetime decay curves: (**a**) for M1 (χ^2 = 1.1) and HP (χ^2 =1); (**b**) for CP1, CP2, CP3, CP4, and CP5 (χ^2 = 1 to 1.1) in a solid state.

5.3.2 Polymerization-induced Phosphorescent Emission (PIPE)

PIE is the phenomenon that homologues to the AIE. Polymerization is a chemical method of producing emissive materials from non-emissive AIEgens (in diluted solutions) or PIEgens (for example electron-rich monomers), while inducing emission by crystallizing aromatic AIEgens is a physical method.[18] The non-luminescent monomer M1 was polymerized to produce non-conjugated luminescent polymers HP. Both the M1 and HP photoluminescence (PL) spectra have been recorded (Fig. 5.5). The Gaussian 09 program was used to optimize the ground state geometries of monomer M1 using density functional theory (DFT) (Fig. 5.6). Calculations were done to determine the electron densities occupied and unoccupied molecular orbitals of M1. The possible intrachain interactions in the resulting polymer are revealed by the optimized HP structure (with possible short contacts) (Fig. 5.7). The phenyl rings of adjacent repeating units of PPh_3 have H...H interactions with each other through short contacts in the range of 2.4 to 2.9 Å.[39, 40] Here, the phenyl rings of triphenylphosphine unit interact within the polymeric chain of HP (i.e., intrachain interactions).

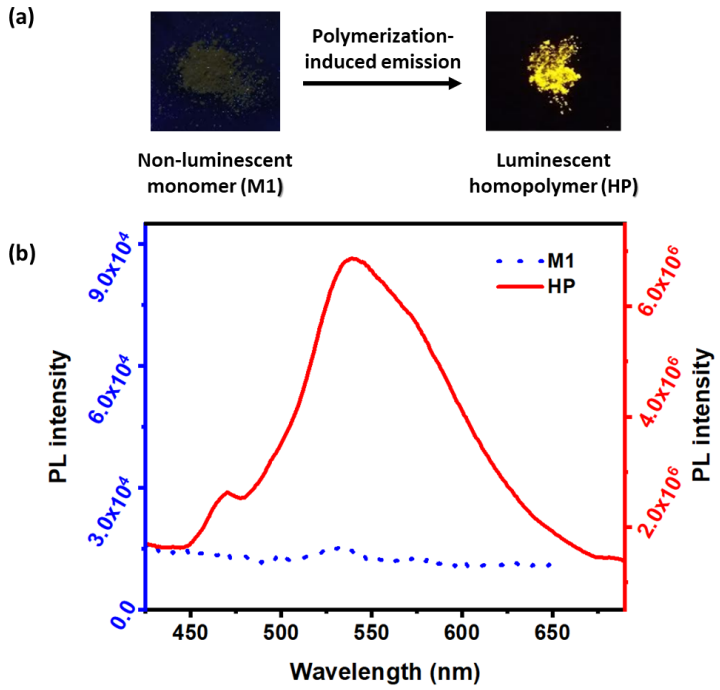

Figure 5.5 (a) Photos of the luminescent homopolymer HP and the non-luminescent monomer M1 taken with a UV lamp (365 nm); (b) corresponding PL spectra with excitation at 360 nm.

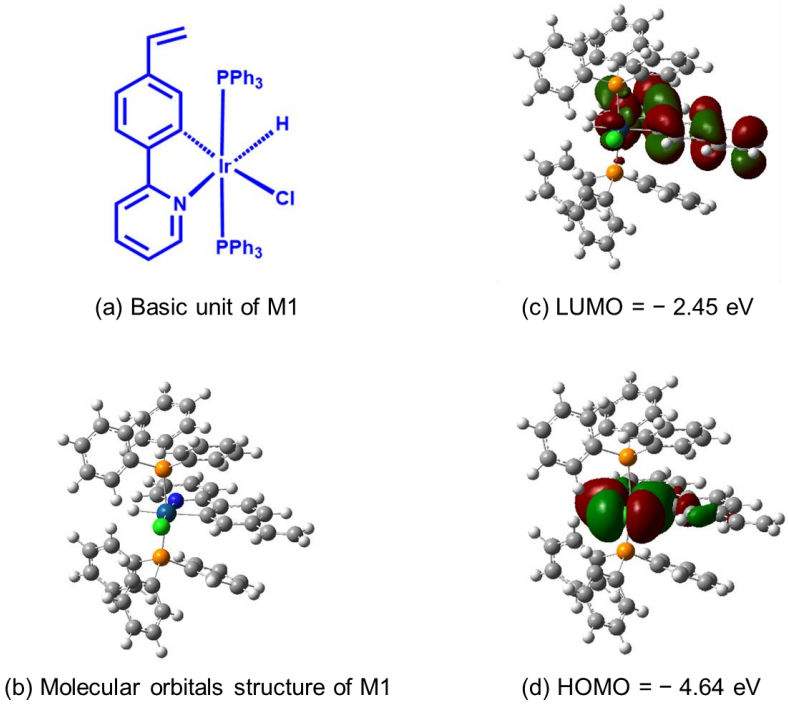

Figure 5.6 The optimized geometry of M1 with HOMO and LUMO molecular orbitals by DFT-based calculation using Gaussian 09 with the basis set LanL2DZ; (a) basic unit of M1; (b) molecular orbitals structure of M1; (c) LUMO; (d) HOMO.

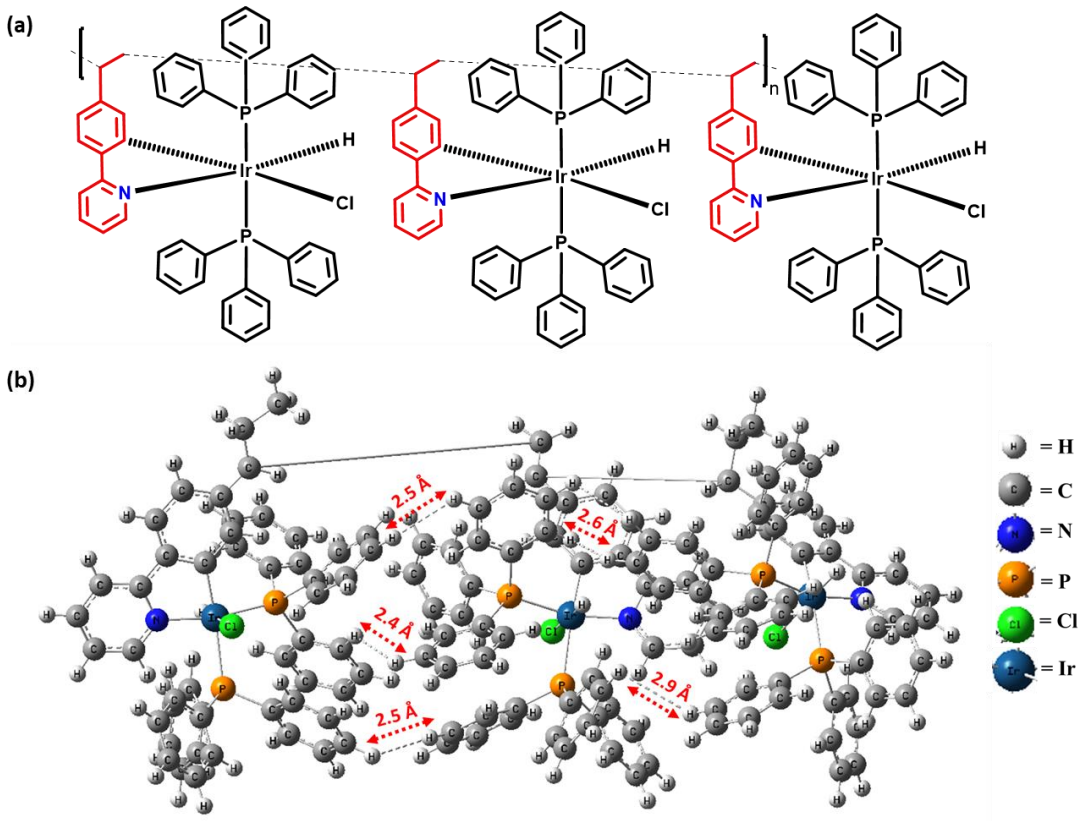

Figure 5.7 (a) HP polymer structure with three repeating units, (b) optimized geometry for the same was calculated using DFT through Gaussian 09 and the LanL2DZ basis set (with an indication of short contacts among the PPh_3 phenyl rings i.e., intrachain interactions) [Interactions: H…H interactions among adjacent repeating units of PPh_3 phenyl rings with short contacts are in the range of 2.4 to 2.9 Å].

The experiments on the concentration-dependent emission spectra of HP and M1 have been performed (Fig. 5.8 and 5.9 respectively). With increasing concentrations from low to high, the intensity of PL emission peaks of HP gradually increased, whereas the intensity of PL emission peaks of M1 gradually decreased. It suggests that, unlike M1, a rising concentration of HP, inter-chain interaction is also a possibility in addition to the intra-chain interaction among the polymeric chains of HP. Strong emission results from restricting the potential motion of the PPh_3 peripheral phenyl rings as well as their conformational rigidity. FESEM data further confirm morphological structure; M1 exhibits an interconnected nano-rod microstructure, while the polymers (HP and CP4) have a dense layered structure (Fig. 5.10).

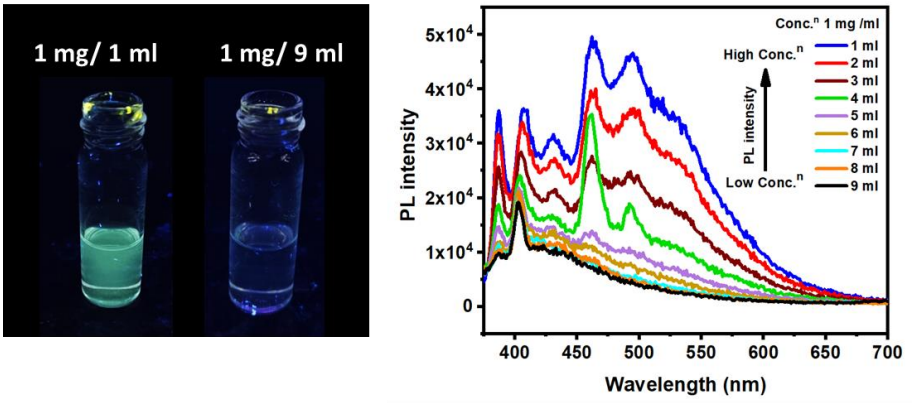

Figure 5.8 (a) Photographs for concentration-dependent emission for concentrated (1 mg/ 1 ml) and diluted (1 mg/ 9 ml) solution of HP in THF solvent, taken under UV lamp (365 nm); (b) PL spectra with a gradual variation in concentration of HP in THF (from 1 mg/ 1 ml to 1 mg/ 9 ml) with excitation at 360 nm.

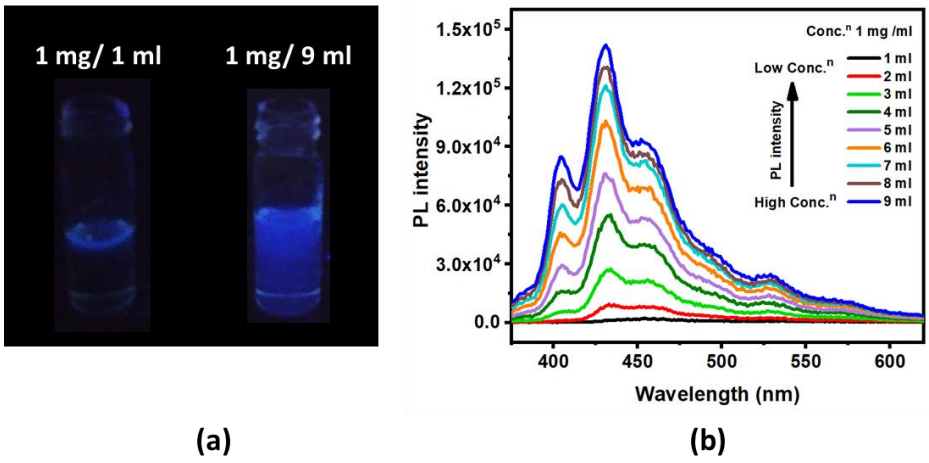

Figure 5.9 (a) Photographs for concentration-dependent emission for concentrated (1 mg/ 1 ml) and diluted (1 mg/ 9 ml) solution of M1 in THF solvent, taken under UV lamp (365 nm); (b) PL spectra with a gradual variation in concentration of M1 in THF (from 1 mg/ 1 ml to 1 mg/ 9 ml) with excitation at 360 nm.

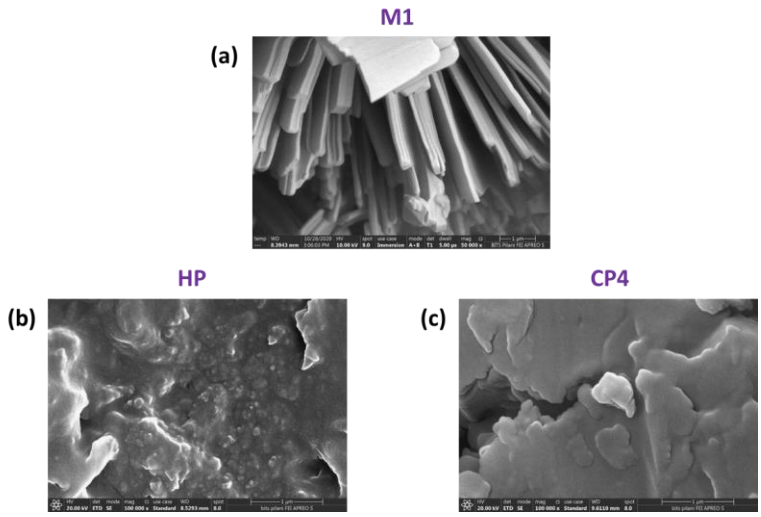

Figure 5.10 FESEM images for (a) monomer (M1), (b) homopolymer (HP), and (c) copolymer (CP4) in the solid state.

The aggregation, which results in the emission of polymer, is made easier by the polymerization of M1, and the AIE study makes it easier to understand this process. Triphenylphosphine ligands, which have triphenyl units that have a peripheral phenyl rotor group, are used in the mono-cyclometalated iridium(III) complexes. Triphenylphosphine is an example of a typical AIE chromophore, in which the restriction of the peripheral phenyl ring's motion promotes radiative decay and causes an increase in luminescence intensity.[41-43] The AIE studies were conducted in both a solution and aggregated state. For HP, PL intensity was measured for all of the made DMF-water mixtures of HP (Fig 5.11). In this case, a 90 % water fraction (i.e., aggregated state) showed an increase in PL intensity compared to a 0 % water fraction. The emission of aggregated state for HP and M1 are observed at 535 nm and 430 nm, respectively.[37] In this instance, the vinyl-substituted ligand of M1, which is converted into the long-chain polymer (HP), may be an attributable change in emission wavelength from M1 to HP in the aggregated state. From 0 to 90 % water fractions, a red-shifted emission was seen for the DMF solution of HP. This was most likely caused by the presence of charge transfer character, which is increasingly influenced by increasing polarity.[44] Recording the PL spectra of HP for various mixtures of DMF and high-viscosity solvent polyethylene glycol (PEG) supports the assumption that the emission enhancement is caused by a potential restricted intramolecular motion (RIM) mechanism (Fig. 5.12). With an increase in the concentration of viscous PEG fractions, the PL intensity was steadily raised.[37] The AIE effect was similarly examined for the CP4, and the PL intensities have been recorded for their prepared AIE solutions of THF-water mixtures of CP4 (Fig. 5.13). For AIE solutions of CP4, PL intensity

increased in 90 % of the water fraction (i.e., the aggregated state) as compared to 0 %. Additionally, the PL intensity of CP4 was recorded for all the different mixtures of THF-PEG (Fig. 5.14). With increasing viscous PEG fractions in the prepared AIE solutions, the emission intensity gradually increased. A DMSO-water mixture was also used to study the AIE effect for HP and CP4 (Fig. 15 and 16). In general, most of the reported cyclometalated iridium(III) complexes show a vibrationally structured emission based on the nature of electronic transitions (i.e., ligand-centered),[45] We also observed the structured emission for M1. Whereas the CP4 shows a broad emission spectrum because of integrating blue- and yellow-light-emitting moieties, preventing energy transfer between them. Thus, the combination exhibits broad white light.[46] From the DLS particle size distribution analysis for both HP and CP4, it was observed that the particle size was increasing with aggregate formation by increasing water concentrations (Figures 5.17 and 5.18).

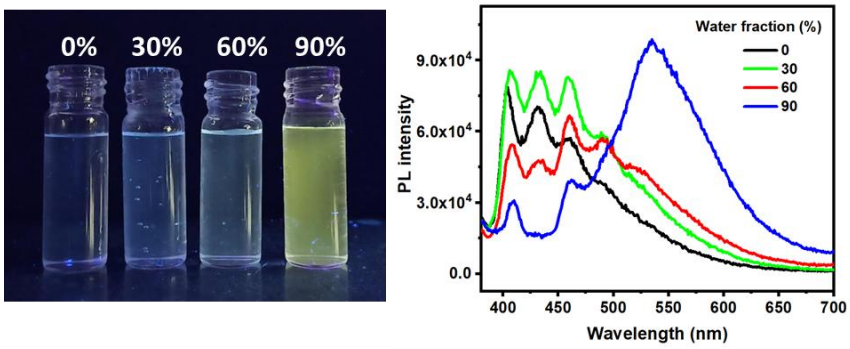

Figure 5.11 (a) Photographs of HP in DMF: water mixtures with different water fractions (0%, 30%, 60%, and 90%) taken under a UV lamp (365 nm); (b) corresponding PL spectra with excitation at 360 nm.

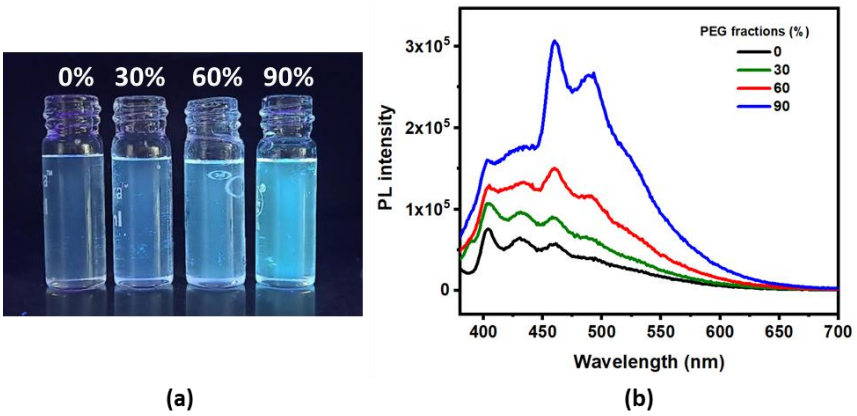

Figure 5.12 (a) Photographs of HP in DMF: PEG mixtures with various PEG fractions (0%, 30%, 60%, and 90%) taken under a UV lamp (365 nm); (b) corresponding PL spectra with excitation at 360 nm.

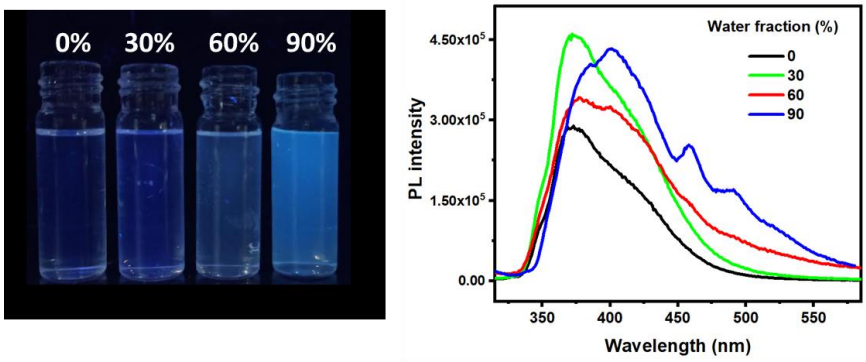

Figure 5.13 (a) Photographs of CP4 in THF: water mixtures with various water fractions (0%, 30%, 60%, and 90%) taken under a UV lamp (365 nm); (b) corresponding PL spectra with excitation at 300 nm.

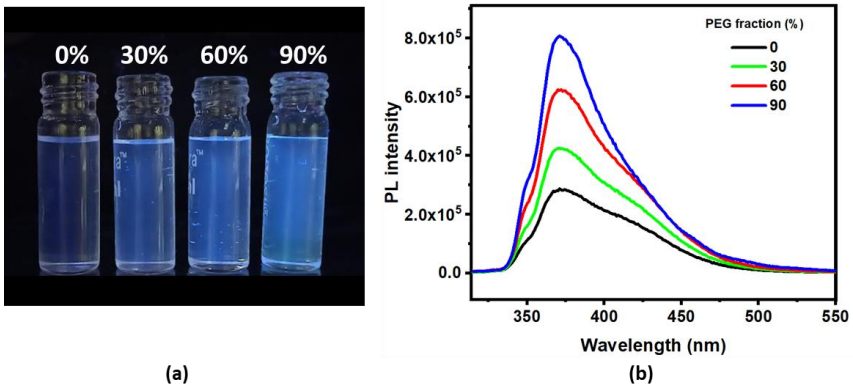

Figure 5.14 (a) Photographs of CP4 in THF: PEG mixtures with various PEG fractions (0%, 30%, 60%, and 90%) taken under a UV lamp (365 nm); (b) corresponding PL spectra with excitation at 300 nm.

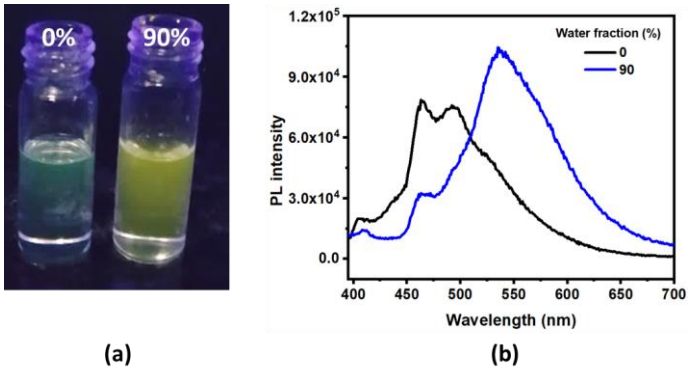

Figure 5.15 (a) Photographs of HP in DMSO-water mixtures with different water fractions (0% and 90%) taken under a UV lamp (365 nm); (b) corresponding PL spectra with excitation at 360 nm.

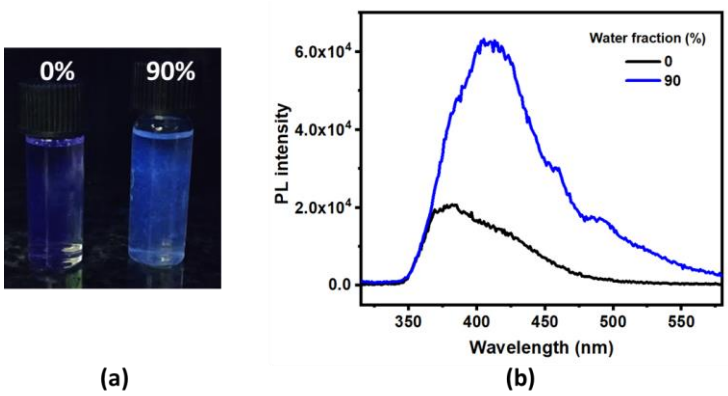

Figure 5.16 (a) Photographs of CP4 in DMSO-water mixtures with various water fractions (0% and 90%) taken under a UV lamp (365 nm); (b) corresponding PL spectra with excitation at 300 nm.

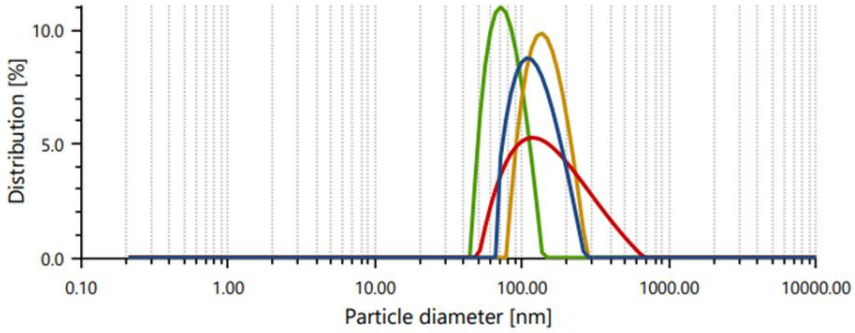

Name	Color	Hydrodyn. diam. [nm]	Polydispersity index [%]
HP-00%		73.27	5.4
HP-30%		195.14	175.5
HP-60%		247.1	529.0
HP-90%		211.2	530.1

Figure 5.17 DLS particle size distribution plot of particle (size) diameter in nm vs. distribution of HP solution in DMF from 0% to 90% water.

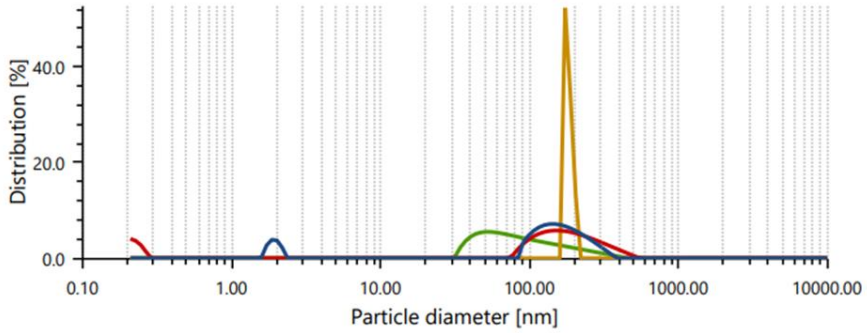

Name	Color	Hydrodyn. diam. [nm]	Polydispersity index [%]
CP4-00%		74.83	18.8
CP4-90%		343.9	672.7
CP4-60%		182.60	80.7
CP4-30%		173.63	250.7

Figure 5.18 DLS particle size distribution plot of particle (size) diameter in nm vs. distribution of HP solution in DMF from 0% to 90% water.

5.3.3 White light emission

The iridium(III) mono-cyclometalated metal complexes exhibit a phosphorescence emission characteristic.[47] The HP emits a yellow color, while the polyvinyl carbazole (PVK) emits a blue color (Fig. 5.19). This fact encourages us to link the monomers M1 of HP and M2 of PVK by a covalent linkage to tune the emission toward the white light. Copolymers (CPs) are produced when M1 and M2 monomeric units are polymerized. Therefore, by gradually altering the amount of blue-emitting M2 monomer, we were able to tune the emission from yellow to white and ultimately achieved nearly white light for CP4 (Table 5.1 and Fig. 5.20).

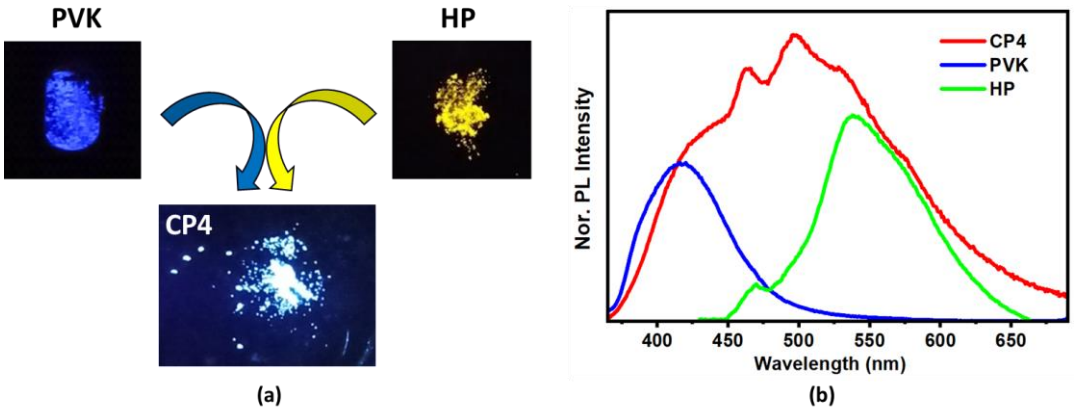

Figure 5.19 (a) Schematic of white light-emitting material tuning with images of polyvinyl carbazole (PVK), HP, and CP4 emission under UV lamp (365 nm); (b) corresponding PL spectra with normalized PL intensity.

Table 5.1 CIE chromaticity coordinates for copolymers (CP).

Copolymers	[M1:M2] equivalents	CIE coordinates (X, Y)
CP1	1:20	(0.39, 0.52)
CP2	1:60	(0.39, 0.52)
CP3	1:100	(0.34, 0.49)
CP4	1:220	(0.25, 0.33)
CP5	1:300	(0.18, 0.18)

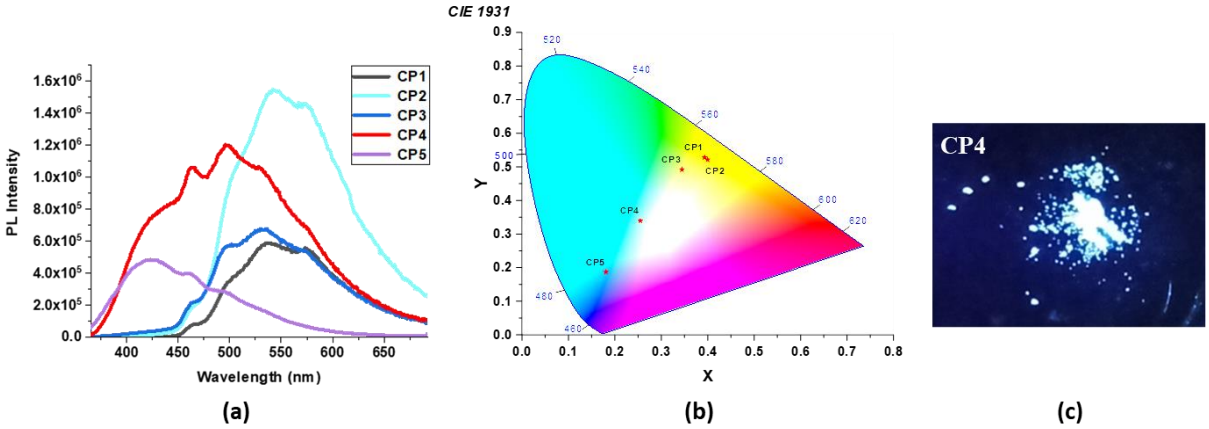

Figure 5.20 (a) PL spectra for CP1, CP2, CP3, CP4, and CP5 synthesized copolymers (at excitation = 300 nm); (b) corresponding CIE chromaticity diagram; (c) photo of CP4 emitting solid-state white light taken with a UV lamp (365 nm).

The copolymer (CP4) produces white light with photoexcitation as a single component without the use of any doping. The PL spectrum shows that CP4's emission wavelength covered the wavelength range, 360-700 nm with a phosphorescence quantum yield Φ_P = 33.7 % (Fig. 5.20). Thermogravimetric analysis (TGA) was used to examine the thermal stability of all synthesized polymers (CP1 to CP5) (Fig. 5.21). Among all the polymers, the white light-emitting copolymer CP4 has good thermal stability and relatively a higher decomposition temperature (T_d) of about 300 °C. For WLED applications, the high thermal stability of CP4 would be desirable.

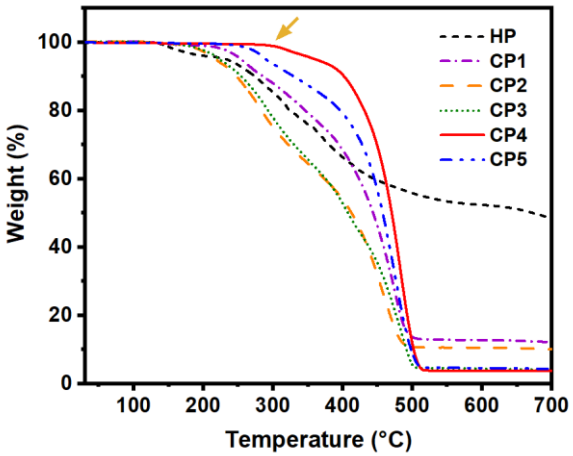

Figure 5.21 Thermogravimetric curves for HP, CP1, CP2, CP3, CP4, and CP5.

This work concludes the covalent integration strategy between PIPE-active (yellow emitting) HP and blue-emitting carbazole must encourage the development of more advanced and effective WLED materials. Such characteristics are white light-emissive polymeric materials, which may promise a breakthrough high-tech display media application for WLED devices.

5.4 References

1. H. Liu, Q. Bai, L. Yao, H. Zhang, H. Xu, S. Zhang, W. Li, Y. Gao, J. Li, P. Lu, H. Wang, B. Yang and Y. Ma, *Chemical Science*, 2015, **6**, 3797-3804.
2. P. C. Raichure, R. Bhatt, V. Kachwal, T. C. Sharma and I. R. Laskar, *New Journal of Chemistry*, 2022, **46**, 6560-6569.
3. Z. Wang, L. Gao, Y. Zheng, Y. Zhu, Y. Zhang, X. Zheng, C. Wang, Y. Li, Y. Zhao and C. Yang, *Angewandte Chemie International Edition*, 2022, **61**, e202203254.
4. Y. Hong, J. W. Y. Lam and B. Z. Tang, *Chemical Communications*, 2009, DOI: 10.1039/B904665H, 4332-4353.
5. J. Luo, Z. Xie, J. W. Y. Lam, L. Cheng, H. Chen, C. Qiu, H. S. Kwok, X. Zhan, Y. Liu, D. Zhu and B. Z. Tang, *Chemical Communications*, 2001, DOI: 10.1039/B105159H, 1740-1741.
6. D. Sengottuvelu, V. Kachwal, P. Raichure, T. Raghav and I. R. Laskar, *ACS Applied Materials & Interfaces*, 2020, **12**, 31875-31886.
7. V. Kachwal, P. Alam, H. R. Yadav, S. S. Pasha, A. Roy Choudhury and I. R. Laskar, *New Journal of Chemistry*, 2018, **42**, 1133-1140.
8. A. C. B. Rodrigues and J. S. Seixas de Melo, *Topics in Current Chemistry*, 2021, **379**, 15.
9. Z. Qiu, X. Liu, J. W. Y. Lam and B. Z. Tang, *Macromolecular Rapid Communications*, 2019, **40**, 1800568.
10. Z. Qiu, B. A. G. Hammer and K. Müllen, *Progress in Polymer Science*, 2020, **100**, 101179.
11. M. Kopeć, M. Pikiel and G. J. Vancso, *Polymer Chemistry*, 2020, **11**, 669-674.
12. R. Hu, X. Yang, A. Qin and B. Z. Tang, *Materials Chemistry Frontiers*, 2021, **5**, 4073-4088.
13. H. Qin, J. Huang, H. Liang and J. Lu, *ACS Applied Materials & Interfaces*, 2021, **13**, 5668-5677.

14. T. Han, X. Wang, D. Wang and B. Z. Tang, *Topics in Current Chemistry*, 2021, **379**, 7.
15. Z. Wang, C. Wang, Q. Gan, Y. Cao, H. Yuan and D. Hua, *ACS Applied Materials & Interfaces*, 2019, **11**, 41853-41861.
16. P. Alam, C. Climent, G. Kaur, D. Casanova, A. Roy Choudhury, A. Gupta, P. Alemany and I. R. Laskar, *Crystal Growth & Design*, 2016, **16**, 5738-5752.
17. T. Han, H. Deng, Z. Qiu, Z. Zhao, H. Zhang, H. Zou, N. L. C. Leung, G. Shan, M. R. J. Elsegood, J. W. Y. Lam and B. Z. Tang, *Journal of the American Chemical Society*, 2018, **140**, 5588-5598.
18. B. Liu, H. Zhang, S. Liu, J. Sun, X. Zhang and B. Z. Tang, *Materials Horizons*, 2020, **7**, 987-998.
19. S.-S. Li, Y.-N. Jing, H. Bao and W.-M. Wan, *Cell Reports Physical Science*, 2020, **1**, 100116.
20. Y.-N. Jing, S.-S. Li, M. Su, H. Bao and W.-M. Wan, *Journal of the American Chemical Society*, 2019, **141**, 16839-16848.
21. S. Tokito, M. Suzuki and F. Sato, *Thin Solid Films*, 2003, **445**, 353-357.
22. Y. Zhang, Y. Su, H. Wu, Z. Wang, C. Wang, Y. Zheng, X. Zheng, L. Gao, Q. Zhou, Y. Yang, X. Chen, C. Yang and Y. Zhao, *Journal of the American Chemical Society*, 2021, **143**, 13675-13685.
23. F. Bekkar, F. Bettahar, I. Moreno, R. Meghabar, M. Hamadouche, E. Hernáez, J. L. Vilas-Vilela and L. Ruiz-Rubio, *Polymers*, 2020, **12**.
24. D. Li, J. Li, D. Liu, W. Li, C.-L. Ko, W.-Y. Hung and C. Duan, *ACS Applied Materials & Interfaces*, 2021, **13**, 13459-13469.
25. Z. Chen, C.-L. Ho, L. Wang and W.-Y. Wong, *Advanced Materials*, 2020, **32**, 1903269.
26. Y. Zhang, L. Gao, X. Zheng, Z. Wang, C. Yang, H. Tang, L. Qu, Y. Li and Y. Zhao, *Nature Communications*, 2021, **12**, 2297.
27. C. Wang, L. Qu, X. Chen, Q. Zhou, Y. Yang, Y. Zheng, X. Zheng, L. Gao, J. Hao, L. Zhu, B. Pi and C. Yang, *Advanced Materials*, 2022, **34**, 2204415.
28. Y. Zhang, X. Chen, J. Xu, Q. Zhang, L. Gao, Z. Wang, L. Qu, K. Wang, Y. Li, Z. Cai, Y. Zhao and C. Yang, *Journal of the American Chemical Society*, 2022, **144**, 6107-6117.
29. B. Xie, Y. Cheng, X. Yu, W. Shu, X. Luo, J. Hao and K. Wang, 2017.
30. L. Ying, C.-L. Ho, H. Wu, Y. Cao and W.-Y. Wong, *Advanced Materials*, 2014, **26**, 2459-2473.
31. Z. A. Page, C.-Y. Chiu, B. Narupai, D. S. Laitar, S. Mukhopadhyay, A. Sokolov, Z. M. Hudson, R. Bou Zerdan, A. J. McGrath, J. W. Kramer, B. E. Barton and C. J. Hawker, *ACS Photonics*, 2017, **4**, 631-641.
32. S. Sinha, B. Chowdhury, U. K. Ghorai and P. Ghosh, *Chemical Communications*, 2019, **55**, 5127-5130.
33. Z. Wang, C.-Y. Zhu, J.-T. Mo, P.-Y. Fu, Y.-W. Zhao, S.-Y. Yin, J.-J. Jiang, M. Pan and C.-Y. Su, *Angewandte Chemie International Edition*, 2019, **58**, 9752-9757.
34. M. Nara, R. Orita, R. Ishige and S. Ando, *ACS Omega*, 2020, **5**, 14831-14841.
35. J. X. Jiang, Y. H. Xu, W. Yang, R. Guan, Z. Q. Liu, H. Y. Zhen and Y. Cao, *Advanced Materials*, 2006, **18**, 1769-1773.
36. X.-Y. Wang, R. N. Prabhu, R. H. Schmehl and M. Weck, *Macromolecules*, 2006, **39**, 3140-3146.
37. P. C. Raichure, V. Kachwal and I. R. Laskar, *Molecules*, 2022, **27**.

38. Z. Feng, P. Tao, L. Zou, P. Gao, Y. Liu, X. Liu, H. Wang, S. Liu, Q. Dong, J. Li, B. Xu, W. Huang, W.-Y. Wong and Q. Zhao, *ACS Applied Materials & Interfaces*, 2017, **9**, 28319-28330.
39. J.-J. Yan, Z.-K. Wang, X.-S. Lin, C.-Y. Hong, H.-J. Liang, C.-Y. Pan and Y.-Z. You, *Advanced Materials*, 2012, **24**, 5617-5624.
40. W. Zou, X. Zhang, H. Dai, H. Yan, D. Cremer and E. Kraka, *Journal of Organometallic Chemistry*, 2018, **865**, 114-127.
41. P. Alam, C. Climent, P. Alemany and I. R. Laskar, *Journal of Photochemistry and Photobiology C: Photochemistry Reviews*, 2019, **41**, 100317.
42. C. Wang, Y. Zhang, Z. Wang, Y. Zheng, X. Zheng, L. Gao, Q. Zhou, J. Hao, B. Pi, Q. Li, C. Yang, Y. Li, K. Wang and Y. Zhao, *Advanced Functional Materials*, 2022, **32**, 2111941.
43. S. Biswas, B. Das, P. Alam, A. Ghatak, U. K. Ghorai, A. Ghosh, B. B. Das, I. R. Laskar and S. Acharya, *The Journal of Physical Chemistry C*, 2021, **125**, 4730-4742.
44. S. D. Padghan, L.-C. Wang, W.-C. Lin, J.-W. Hu, W.-C. Liu and K.-Y. Chen, *ACS Omega*, 2021, **6**, 5287-5296.
45. S. Ilic, D. R. Cairnie, C. M. Bridgewater and A. J. Morris, Journal of Photochemistry and Photobiology, 2021, 8, 100084; J. C. Deaton, C. M. Taliaferro, C. L. Pitman, R. Czerwieniec, E. Jakubikova, A. J. M. Miller and F. N. Castellano, Inorganic Chemistry, 2018, 57, 15445-15461.
46. S. Park, J. E. Kwon, S. H. Kim, J. Seo, K. Chung, S.-Y. Park, D.-J. Jang, B. M. Medina, J. Gierschner and S. Y. Park, Journal of the American Chemical Society, 2009, 131, 14043-14049.
47. P. Alam, G. Kaur, V. Kachwal, A. Gupta, A. Roy Choudhury and I. R. Laskar, *Journal of Materials Chemistry C*, 2015, **3**, 5450-5456; Z. Feng, P. Tao, L. Zou, P. Gao, Y. Liu, X. Liu, H. Wang, S. Liu, Q. Dong, J. Li, B. Xu, W. Huang, W.-Y. Wong and Q. Zhao, ACS Applied Materials & Interfaces, 2017, 9, 28319-28330.

CHAPTER 6

CONCLUSION AND FUTURE SCOPE

Chapter 6. Conclusion and Future Scope

6.1 The thesis primarily focuses on;

I. Strategical construction of iridium(III) complex and polymers-based luminescent probes to provide sensitive detection of important analytes (volatile organic compounds, biomolecules, polarity, acids vapor, etc.).

II. Electron donor-acceptor (D-A) hyperbranched polymeric sensitive probes for examining nitro-explosive compounds.

III. The development of a strategy to construct the covalent integration of yellow and blue-emitting monomers by polymerization will inspire improved and efficient LED applications.

The following things are proposed as the future scope.

6.2 Design and synthesis of new AIE-active mono-cyclometalated Iridium(III) metal complexes for DCM detection in a vapor phase.

In our present work, vinyl substituted mono-cyclometalated iridium(III) complex M1 shows DCM vapor detection with a detection limit is 4.9 ppm,[1] where the detection limit is necessary to improve more. As DCM molecules get trapped between the vinyl group and the phenyl ring of triphenylphosphine PPh_3, owing to the interaction with vinylic hydrogen (*trans* to the phenyl pyridine) results in the restriction of the vibration of that phenyl ring of PPh_3 leads to turn-on emission. Adding such an active vinyl group site to both sides of the cyclometalated ligand of iridium(III) complex (F**1**) makes it possible to increase the effectiveness of vapor phase DCM detection.[2, 3]

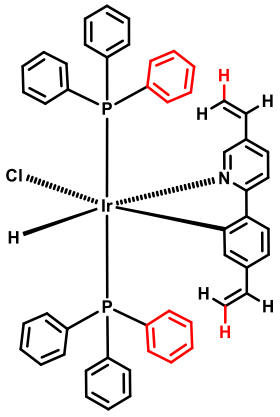

F1

Scheme 6.1 Chemical structures for modified mono-cyclometalated iridium(III) complex (**1**).

6.3 Design and synthesis of D-A-based extended π-electron conjugated polymer for multi-stimuli application.

For nitro-aromatic explosive detection, typically, the D-A-based extended π-conjugation and polymer's porosity enable appropriate host-guest interactions with nitro explosives.[4] To detect nitro explosives from the vapor phase, highly sensitive probe molecules are necessary. The AIE-active probe has effectively worked for explosive sensing because the AIE polymer aggregates the presence of explosives which triggers the fluorescence.[5] In our earlier research report, hyperbranched polymers with tetraphenylethene (TPE) or triphenylamine (TPA) as a core moiety detects nitro explosives picric acid and TNT in the solution phase based on photoinduced electron transfer (PET) mechanism.[6] But due to the lack of electron D-A character, it may not work in a vapor phase. Therefore, a hyperbranched conjugated network with an electron D-A character probe is necessary for vapor phase explosive detection. Hence, the hyperbranched probes (**F2**) and (**F3**) could provide a significant result for nitro-aromatic explosive detection in a vapor phase. Due to the possible phase transformation, it would also work for pressure-sensing applications via the mechanofluorochromism property.

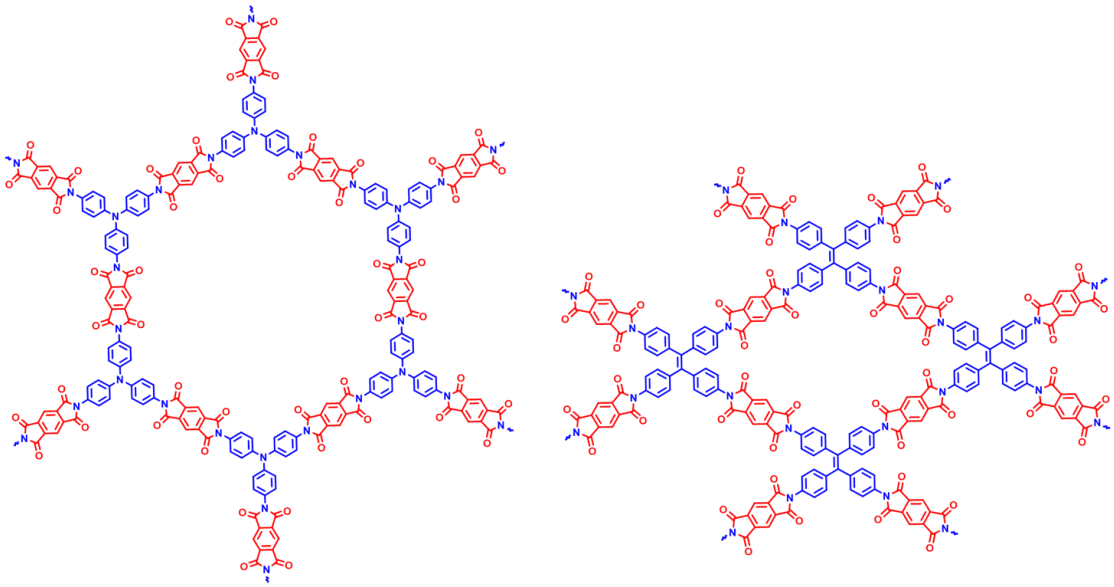

F2 **F3**

Scheme 6.2 Chemical structures for hyperbranched D-A-based polymers (**F2, F3**).

6.4 Introduce multiple Donor-Acceptor (D-A) characters in polymer for vapor phase acid detection and nitro-explosive application.

Considering the feasibility of porous network polymer containing a heterocyclic unit, it is used for analyte detection (e.g., carbon dioxide (CO_2), iodine vapor).[7] For the acidochromism

mechanism, having several active protonic sites in the probes can improve their capacity to detect protonic acids or Lewis acids in the vapor phase.[8] Polymeric probes (F**4**, F**5**) can be used to increase such active protonic sites, and they also present a promising potential for improving acidochromism. It also works for nitro-aromatic explosive detection in the vapor phase efficiently.

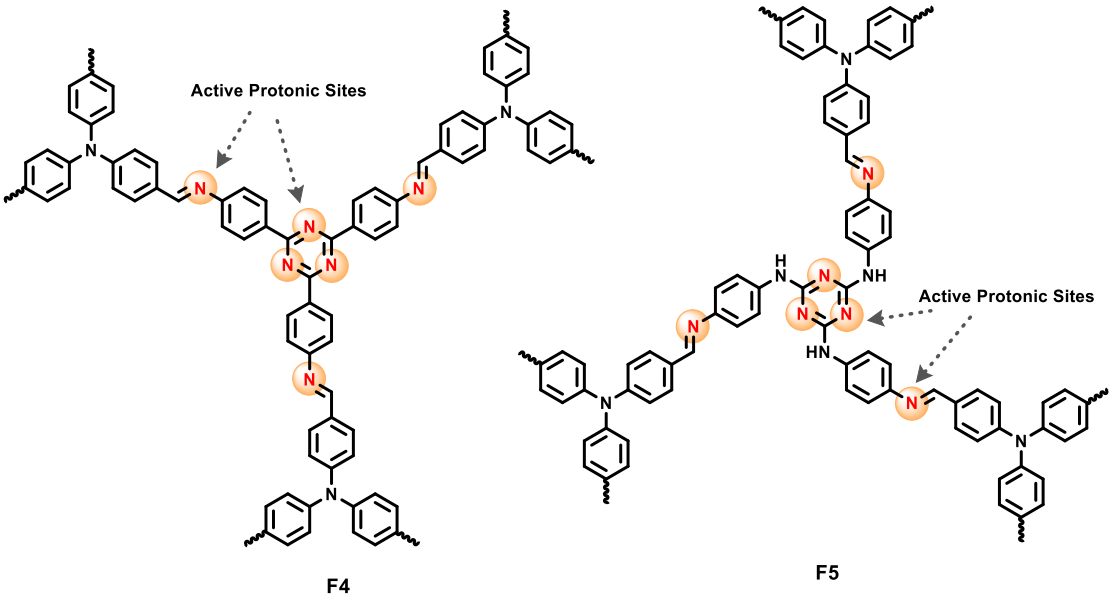

Scheme 6.3 Chemical structures for modified hyperbranched D-A-based polymers (F**4**, F**5**).

6.5 Design and synthesis of new AIE-active single-component polymers with the strategy of tunable white light emission

The AIE phenomena and the phosphorescent emission of iridium-based compounds in LED applications have been getting more attention. In our present report, could not achieve pure white light emission with CIE coordinate (0.33,0.33) owing to the weak blue emissive carbazole monomeric unit.[9] Instead of carbazole, we can use the TPE-substituted monomeric unit (6b) as a strong blue emission to achieve pure white light emissive polymeric material (**6**). In our present report, the effect of functionalization on phenyl pyridine ligands in mono-cyclometalated iridium(III) complexes for emission tuning has been studied systematically.[10] It reveals the non-conjugated functionalization on phenyl pyridine ligand in mono-cyclometalated iridium(III) complex shows blue color emission in the solid state. Using two iridium(III) complexes (**7a** and **7b**) as a blue and yellow emissive monomeric unit could help to increase the quantum yield of phosphorescent emission through polymerization (in the form of polymer **7**). Which would be more efficient in optoelectronic applications.

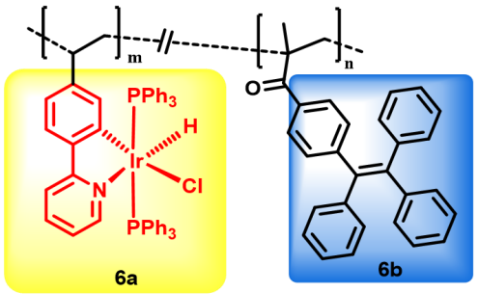

F6

Scheme 6.4 Chemical structures for white light emission tunable polymeric probe (F**6**).

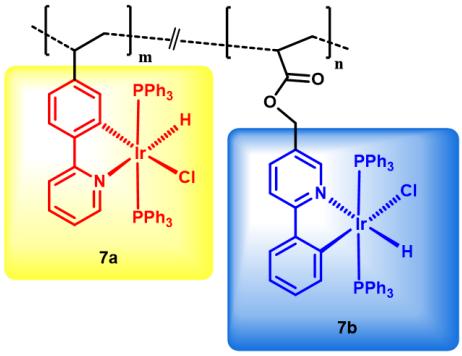

F7

Scheme 6.5 Chemical structures for white light emission tunable polymeric probe (**F7**).

6.6 References

1. P. C. Raichure, V. Kachwal, and I. R. Laskar, *Molecules*, 2022, **27**.
2. Y. Li, J. Pionteck, P. Pötschke and B. Voit, *Materials & Design*, 2019, **179**, 107897.
3. M. Liu, C. Yao, C. Liu and Y. Xu, *Scientific Reports*, 2018, **8**, 14071.
4. V. S. Mothika, A. Räupke, K. O. Brinkmann, T. Riedl, G. Brunklaus and U. Scherf, *ACS Applied Nano Materials*, 2018, **1**, 6483-6492.
5. H. Zhou, M. H. Chua, B. Z. Tang and J. Xu, *Polymer Chemistry*, 2019, **10**, 3822-3840.
6. D. Sengottuvelu, V. Kachwal, P. Raichure, T. Raghav and I. R. Laskar, *ACS Applied Materials & Interfaces*, 2020, **12**, 31875-31886.
7. A. Mohan, M. H. Al-Sayah, A. Ahmed and O. M. El-Kadri, *Sci Rep*, 2022, **12**, 2638.
8. K. Seehafer, M. Bender, and U. H. F. Bunz, *Macromolecules*, 2014, **47**, 922-927.
9. P. C. Raichure, V. Kachwal, D. Sengottuvelu and I. R. Laskar, *Macromolecules*, 2022, **55**, 10377-10384.
10. P. Alam, P. Das, C. Climent, M. Karanam, D. Casanova, A. R. Choudhury, P. Alemany, N. R. Jana and I. R. Laskar, *Journal of Materials Chemistry C*, 2014, **2**, 5615-5628.

List of Publications [A-1]

1. **Pramod C. Raichure**, Vishal Kachwal, Sengottuvelu Dineshkumar, and Inamur Rahaman Laskar, "Achieving Single Component Solid-state White Light Emission Through Polymerization-induced Phosphorescent Emission (PIPE)", *Macromolecules 2022, 55, 23, 10377-10384.*
2. **Pramod C. Raichure**, Vishal Kachwal, and Inamur Rahaman Laskar, " 'Aggregation-induced Emission' Active Mono-cyclometalated Iridium(III) Complex Mediated Efficient Vapor Phase Detection of Dichloromethane", *Molecules 2022, 27(1), 202.*
3. **Pramod C. Raichure**, Ramprasad Bhatta, Vishal Kachwal, Tirupati Chander Sharma and Inamur Rahaman Laskar, "Multi-Stimuli Distinct Responsive D-A Based Fluorogen Oligomeric Tool and Efficient Detection of TNT Vapor", *New J. Chem., 2022,46, 6560-6569.*
4. Sengottuvelu Dineshkumar, Vishal Kachwal, **Pramod Raichure**, Tarun Raghav and Inamur Rahaman Laskar, "Aggregation-induced enhanced emission (AIEE) Active Conjugated Mesoporous Oligomers (CMOs) with Improved Quantum Yield and Low-Cost Trace Nitro Aromatic Explosives Detection", *ACS Appl. Mater. Interfaces 2020, 12, 28, 31875–31886.*
5. **Pramod C. Raichure**, Bharat Kaushik, Ramprasad Bhatta, Annu, and Inamur Rahaman Laskar, "Facile and Selective Low-cost Detection of Creatinine from Human Urine by Cyclometalated Dinuclear Iridium(III) Complex Through Creatinine-triggered Emission" *(Under communication).*
6. **Pramod C. Raichure**, Bharat Kaushik, Annu, Ajit Singh, and Inamur Rahaman Laskar, "Acid-Stimuli Responsive D-A based Oligomeric Fluorogen and Application in Low-cost Detection of Lactic Acid" *(Under preparation).*
7. **Pramod C. Raichure**, Annu, Bharat Kaushik, Ajit Singh, Ramprasad Bhatta, and Inamur Rahaman Laskar, "Multi-Stimuli D-A-A based Polymeric Fluorescent Tool for Vapor Phase TNT Detection" *(Under preparation).*

List of Oral / Poster Presented in Conferences / Workshops [A-2]

- **Pramod C. Raichure**, Vishal Kachwal, Dineshkumar Sengottuvelu, and Inamur Rahaman Laskar 'Achieving Single-Component Solid-State White-Light Emission through Polymerization-Induced Phosphorescent Emission' in half-day mini-symposium being organized by department of chemistry, BITS Pilani, Rajasthan, India held on March 11, 2023 **(Poster presentation)**.
- **Pramod C. Raichure**, Vishal Kachwal, and Inamur Rahaman Laskar ''Aggregation-Induced Emission' Active Mono-Cyclometalated Iridium(III) Complex Mediated Efficient Vapor-Phase Detection of Dichloromethane' in an International Conference on 'Aggregation–Induced Emission: From Fundamental to Applications (IC-AIE-FA-2022)' held at the department of chemistry, BITS Pilani KK Birla Goa Campus, India during December 16-18, 2022 **(Oral presentation)**.
- **Pramod C. Raichure**, Ramprasad Bhatt, Vishal Kachwal, Tirupati Chander Sharmac, and Inamur Rahaman Laskar 'Multi-stimuli distinct responsive D-A based fluorogen oligomeric tool and efficient detection of TNT vapor' in one-day mini-symposium being organized by department of chemistry, BITS Pilani, Rajasthan, India on the occasion of National Science Day held on February 28, 2022 **(Poster presentation)**.
- **Pramod C. Raichure**, Vishal Kachwal, Dineshkumar Sengottuvelu, and Inamur Rahaman Laskar 'Synthesis of Aggregation-induced Emission (AIE)-active Tunable White Light Emitting Iridium(III) based polymer' in a two-day conference on 'Flexible Electronics for Electric Vehicles (FlexEV-2020)' held at Manipal University Jaipur, Rajasthan, India during March 5-6, 2020 **(Oral presentation)**.
- **Pramod C. Raichure**, Vishal Kachwal, Dineshkumar Sengottuvelu, and Inamur Rahaman Laskar 'Achieving Single-Component Solid-State White-Light Emission through Polymerization-Induced Phosphorescent Emission' at the RSCPoster Twitter international conference held entirely online on February 28 - March 1, 2023 **(Poster presentation)**.
- **Pramod C. Raichure**, Ramprasad Bhatt, Vishal Kachwal, Tirupati Chander Sharma, and Inamur Rahaman Laskar 'Multi-stimuli distinct responsive D-A based fluorogen oligomeric tool and efficient detection of TNT vapor' at the RSCPoster Twitter international conference held entirely online on March 1-2, 2022 **(Poster presentation)**.

Appendices

- Workshop on “Recent Trends on Nanostructured Thin Films and Applications” organized by the Department of Physics, BITS PILANI, Pilani Campus, Rajasthan held on 19th February 2022 (Participated).
- Workshop on ‘Analytical Instruments for Chemical and Environmental Engineers (WAICEE- 2019)’ held at BITS Pilani, Rajasthan during March 25-26, 2019 (Participated).

BRIEF BIOGRAPHY OF THE CANDIDATE [A-3]

Mr. Pramod C. Raichure is currently a Ph.D. scholar at BITS Pilani, Pilani campus Rajasthan. He obtained his Master's degree in organic chemistry from Yashwantrao Chavan Institute of Science, Satara affiliated with Shivaji University, Kolhapur, Maharashtra (INDIA) in 2016. He qualified 'Maharashtra State Eligibility Test (MH-SET)' for Assistant Professor, accredited by University Grants Commission, INDIA in January 2018. He started his Ph.D. studies at the Department of Chemistry, BITS Pilani in January 2018. He has been working on the development of luminescent-based polymer for emission tunning and small molecules for analytes detection. His professional experience includes luminescent-based hyperbranched polymeric materials for nitro-aromatic explosives sensing, mechanofluorochromism, tunable emission through polymerization, aggregation-induced emission (AIE)-active mono-cyclometalated iridium metal complex for detection of volatile organic compounds, and multi-nuclear iridium complex for biomolecules sensing. Their purpose is to provide affordable and highly sensitive tests-kit as biomarkers for kidney disease patients. He has published four research articles in peer-reviewed international journals and presented papers at six conferences/symposiums to date. Using all the resources available to do cutting-edge research to benefit humanity is his passion.

BRIEF BIOGRAPHY OF THE SUPERVISOR [A-4]

Currently, **Prof. Inamur Rahaman Laskar** has been employed as an Associate Professor at the Department of Chemistry, Birla Institute of Technology & Science, Pilani Campus, Pilani, Rajasthan, India. He received his Ph.D. in inorganic chemistry from the Indian Association for the Cultivation of Science (IACS), Kolkata, India, in 2000. From September 1999 to July 2001, he worked as a Lecturer at Ananda Mohan College, a Kolkata, India that is affiliated with the University of Calcutta. During July 2001 and February 2002, he represented as a postdoctoral associate at NTHU Taiwan. Further, he worked on post-doctoral research at Kochi University in Japan between April 2006 and March 2008 as a JSPS Postdoctoral Fellow. In August 2008, he joined and started working at the BITS Pilani Department of Chemistry. His present research is mainly concerned with the design and synthesis of new luminescent and AIE active luminescent materials. It explores the AIE mechanism, detailed study of luminescent behavior, and targets these materials in various applications such as applications in detection of analytes like volatile organic compounds, explosive/toxic from solution and vapor phase, mechanofluorochromic and organic light emitting diode, bio-imaging and cancer therapy, and so forth. His other area of interest is modeling the synthetic luminescent materials carried out to investigate their excited state features and validate them using spectroscopic data. Currently, seven Ph.D. students are working under his supervision. He received funding for many projects from various funding agencies from the Government of India: Indian Council of Medical Research, Defence R&D Organization, Department of Biotechnology, Council of Scientific & Industrial Research, and Department of Science and Technology (ongoing project 3, completed projects 3).